NASA CONTRACTOR REPORT

NASA CR-2294

NASA CR-2294

INVESTIGATION OF HIGH TEMPERATURE ANTENNAS FOR SPACE SHUTTLE

by E. A. Kuhlman

Prepared by
MCDONNELL DOUGLAS ASTRONAUTICS COMPANY-EAST
St. Louis, Mo. 63166
for Langley Research Center

NATIONAL AERONAUTICS AND SPACE ADMINISTRATION • WASHINGTON, D. C. • NOVEMBER 1973

1. Report No.	2. Government Accession No.	3. Recipient's Catalog No.
NASA CR-2294		

4. Title and Subtitle	5. Report Date
INVESTIGATION OF HIGH TEMPERATURE ANTENNAS FOR SPACE SHUTTLE	November 1973
	6. Performing Organization Code
7. Author(s)	8. Performing Organization Report No.
E. A. Kuhlman	
	10. Work Unit No.
9. Performing Organization Name and Address	
McDonnell Douglas Astronautics Company-East Saint Louis, Missouri 63166	11. Contract or Grant No. NAS1-11273
	13. Type of Report and Period Covered Contractor Report
12. Sponsoring Agency Name and Address	
National Aeronautics & Space Administration Washington, DC 20546	14. Sponsoring Agency Code

15. Supplementary Notes

This is a final report.

16. Abstract

The design and development of high temperature antennas for the Space Shuttle Orbiter are discussed. Four antenna system designs were completed which apply to three specified orbiter antenna requirements. The antenna designs were based on three antenna types,an annular slot (L-Band) a linear slot (C-Band), and a horn (C-Band). The design approach was based on combining an RF window, which provides thermal protection, with an off-the-shelf antenna. Available antenna window materials were reviewed and compared, and the materials most compatible with the design requirements were selected. Two antenna window design approaches were considered: one employed a high temperature dielectric material and a low density insulation material, and the other an insulation material usable for the orbiter thermal protection system. Preliminary designs were formulated and integrated into the orbiter structure. Simple Electrical models, with a series of window configurations, were constructed and tested. The results of these tests are given, and are used to determine the required configurations for the respective antenna designs. Structural integration studies were supported with detailed thermal and strength analyses. Layout type drawings, with detailed thermal and strength analyses. Layout type drawings, with pertinent dimensions, are given for each of the final antenna designs. The results of tests and analyses for the final antenna system designs are given and show that high temperature antenna systems consisting of off-the-shelf antennas thermally protected by RF windows can be designed for the Space Shuttle Orbiter.

17. Key Words (Suggested by Author(s))	18. Distribution Statement
Space Shuttle antennas, high temperature antennas	Unclassified - Unlimited

19. Security Classif. (of this report)	20. Security Classif. (of this page)	21. No. of Pages	22. Price*
Unclassified	Unclassified	148	Domestic, $4.50 Foreign, $7.00

*For sale by the National Technical Information Service, Springfield, Virginia 22151

CONTENTS

LIST OF FIGURES

FIGURE

FIGURE

FIGURE

FIGURE

LIST OF TABLES

LIST OF SYMBOLS

α	Attenuation constant
β	Phase constant
d_J	Thickness of dielectric sheet number J
E_1, E_J, E_N	Voltage at left surface of dielectric sheet number J
$E_{incident}$	Incident voltage
$E_{transmitted}$	Transmitted voltage
ε_1	Relative dielectric constant of air
ε_J	Complex dielectric constant
ε'_J	Relative dielectric constant of sheet number J
ε_o	Permittivity of free space
ε_r	Relative dielectric constant
f	Frequency
γ	Propagation constant in media
K_1, K_2	Numerical constants
$L_{external}$	Mechanical externally applied loads
$L_{thermal}$	Thermally induced loads
MS	Margin of safety
μ_o	Permeability of free space
N	Total number of dielectric sheets
ϕ	Angle measured from in plane antenna axis, 0° to 360°
ω	Angular frequency
ρ_N	Reflection coefficient
ΣL	Algebraic sum of loads
T	Power transmission coefficient
tan δ	Loss tangent

$\overline{t}$	Equivalent thickness
Θ	Angle measured from normal to antenna face, 0° to 180°
Θ_1	Angle of incidence
Θ_J	Angle of propagation in dielectric sheet number J
U_R	Applied stress/allowable stress in the radial direction
U_T	Applied stress/allowable stress in the tangential direction
VSWR	Voltage standing wave ratio
Z_J, Z_o	Characteristic impedance
ZI_J	Equivalent impedance at the right boundry of dielectric sheet number J

INVESTIGATION OF HIGH TEMPERATURE ANTENNAS FOR SPACE SHUTTLE

By E. A. Kuhlman

MCDONNELL DOUGLAS ASTRONAUTICS COMPANY-EAST

The purpose of this program was to examine problems associated with the design of high temperature antennas for the Space Shuttle Orbiter. The objective was to design, develop, and test three (3) different high temperature antenna installations which are compatible with Space Shuttle Orbiter requirements. It was also a goal to obtain simple designs which would: 1) allow access to the antenna and window for installation, test, and maintenance; 2) be simple to fabricate and inspect for good quality control and low costs; and 3) minimize refurbishment and maintenance costs. The three antennas studied are an L-band annular slot antenna, a C-band horn antenna, and a C-band linear slot antenna. The antenna design approach is based on the use of standard antennas (i.e., essentially off-the-shelf) thermally protected by an RF transparent antenna window. The specific antennas selected for this program correspond to Orbiter avionics system performance requirements. The thermal, strength and structural requirements were determined by nominal antenna locations on the underside of the Orbiter.

The requirements for the McDonnell Douglas Corporation (MDC) Orbiter (as proposed for the Space Shuttle Orbiter competition) were used because much of this study was conducted prior to the award of the Orbiter contract. However, the requirements used are not unique to one Orbiter design. Therefore, the study results are directly applicable to the North American Rockwell Corporation (NR) Orbiter; modifications of the design details will most probably be required prior to using the designs.

Two antenna window design approaches were considered. One employs a high temperature dielectric material and a low density insulation material and is identified as a multiple-layer window. The other employs a basic insulation material usable for the Orbiter thermal protection system (TPS) and is identified as a single-layer window. Both the multiple-layer and the single-layer window design approaches were applied to the L-band antenna, while only the single-layer window design approach was applied to the C-band horn and slot antennas.

After establishing the basic antenna system designs to pursue, the candidate window materials were reviewed and the materials most compatible with the design requirements were selected. The results of this review indicated that boron nitride (HD-0092) and Dynaquartz are the best materials for the multiple-layer window design, and LI-1500, a reusable surface insulation, is the best TPS material for the single-layer window design. Preliminary designs were then formulated and integrated into the Orbiter structure. Preliminary heat transfer calculations were made to determine window material thicknesses required for thermal protection of the antenna. Using these preliminary results as a base,

simple electrical models were constructed and tested. The physical configurations were varied to determine the window configuration(s) which resulted in the best radiation patterns and impedances and which were compatible with Orbiter system requirements. The results of these tests were then applied to the preliminary designs and more formal designs generated. Detailed thermal and strength analyses were made on these designs. The antenna system designs and electrical models were then revised (as required) and the models were tested to verify electrical performance. Layout type drawings, with all pertinent dimensions, were prepared for each of final antenna system designs.

The test results and design analyses for the L-band antenna system show that the single-layer window approach is much simpler, lower in weight, and has less effect on the antenna impedance than the multiple-layer window approach. Good results were also obtained for the C-band horn and slot antennas using the single-layer window approach.

Mr. E. A. Kuhlman, Study Manager, was responsible for overall technical direction of this study. Other members of the McDonnell Douglas engineering staff who contributed to this study are, J. C. Blome, F. R. LeTrello, P. B. Stones, V. M. Gerler, B. M. Kavanaugh, J. C. Reeder, J. M Romberg, and R. F. Sorensen. The electrical tests were supported by various members of the Antenna Laboratory.

Physical quantities defined in this report are given in both the International System of Units (SI) and the U.S. customary units.

Background

Early in the McDonnell Douglas Space Shuttle design study program the development of high temperature antennas was identified as one of the more critical design problems. The Space Shuttle mission, in addition to launch, orbital flight, and entry phases, included aeroflight and landing phases. Most of the avionics systems used for communication and navigation were programmed for use during aeroflight and landing and were similar to those used for commercial and military airplanes rather than entry vehicles. Consequently, most high temperature antennas developed for entry vehicles are not directly applicable. In addition, these high temperature antennas were designed for "one shot" operation and, therefore, probably would not meet the reusability requirements (100 missions) of the Space Shuttle. The entry times were also longer which produced a higher total heat even though the heating rates were less severe than for other entry vehicles.

Two basic technical approaches for solving the Space Shuttle high temperature antenna problem were considered in early MDC studies. One required the development of a high temperature antenna which could be mounted directly into the Orbiter surface with the radiating aperture exposed directly to high surface temperatures. The other used a low temperature antenna with a dielectric window that provided thermal protection for the antenna and good RF transmission properties for the radiated energy, while maintaining the essential characteristics

of the antenna radiation patterns. After considering the tradeoff of such things as material requirements and properties, producibility, physical integration into the Orbiter structure, and reusability, to name a few, the latter approach was selected for further study.

Early Orbiter design studies by MDC were based on a metallic thermal protection system (TPS); a coated refractory metal skin backed by a low density fibrous insulation. Using the properties of materials such as slip cast fused silica and boron nitride, thermal calculations showed that antenna windows 13.97 cm (5.5 in.) thick would be required to obtain a backface temperature of 533°K (500°F). Analysis of these results indicated several potential problems: 1) degraded antenna performance due to attenuation, reflections, and excitation of higher order modes; 2) excessive weight; and 3) availability of thick materials. To solve these problems, a multiple-layer window was devised that employed a thin outer layer of a high temperature dielectric material and inner layers of low density materials which are good thermal insulators. The advantages of this type of antenna window structure were considered to be: 1) isolation of high dielectric constant material from the antenna aperture; 2) optimization of outer layer thickness for maximum transmission at higher frequencies; 3) reduced window thickness to minimize the potential for higher order mode excitation, and reduced weight - about 85% compared to a slip cast fused silica window.

The feasibility of using a multiple-layer antenna window with a metallic TPS was investigated using an off-the-shelf L-band annular slot antenna. Results of pattern measurements for a window 8.636 cm (3.4 in.) thick and 22.86 cm (9.0 in.) in diameter showed excellent patterns (ref. 1). However, the VSWR increased from a maximum of 2:1 to about 10:1, indicating more work was required to achieve an acceptable impedance match. These test results demonstrated the basic feasibility of covering an off-the-shelf antenna with a window which could provide thermal protection.

Just prior to beginning this study, the Orbiter metallic TPS was replaced with TPS consisting of an external reusable surface insulation (RSI) covering an aluminum primary structure. This TPS approach provided a different structural environment for the antenna systems and gave rise to some new problems. For example, the RSI over the surface of Orbiter is equivalent to a dielectric sheet over a ground plane that can support surface wave propagation and could cause radiation pattern degradation. Therefore, the primary emphasis of the work described in this report is based on the design and integration of antenna systems for use with RSI TPS.

SPACE SHUTTLE REQUIREMENTS

This section gives the details of the Space Shuttle Orbiter antenna structural, thermal, and strength requirements used in this study.

Antenna Requirements

The Orbiter antenna system requirements are summarized in table I. The antenna types given were determined by the radiation pattern and frequency requirements of the respective avionics system functions. It may be noted that many of the Orbiter avionics systems are like those used on commercial and military airplanes rather than entry vehicles. These systems are used for landing communications and navigation after entry when the Orbiter is in an aeroflight mode. Consequently, most of the high temperature antennas developed for entry vehicles are not directly applicable to the Orbiter avionics systems. In addition, these antennas were designed for "one shot" operation and, therefore, do not, in general, meet the Space Shuttle requirement for reuse.

TABLE I
ANTENNA REQUIREMENTS

ANTENNA	FREQUENCY RANGE		VSWR (MAXIMUM)	RF POWER (ESTIMATE)	PATTERN (COVERAGE)	GAIN	POLARIZATION	ANTENNA TYPE SELECTED	REMARKS
	TRANSMIT (MHz)	RECEIVE (MHz)							
TACAN	1025–1087 1088–1150 (960–1220 TOTAL RANGE)	962–1024 1151–1213	2:1 TRANSMIT 5:1 RECEIVE	4 KW PK PULSE (WORST CASE)	OMNI-DIRECTIONAL IN PLANE OF AEROFLIGHT	OMNI TYPE	VERTICAL	ANNULAR SLOT	USED DURING AEROFLIGHT ONLY
AIR TRAFFIC CONTROL TRANSPONDER	1090	1030	2:1 TRANSMIT 5:1 RECEIVE	4 KW PK PULSE (WORST CASE)	OMNI-DIRECTIONAL IN PLANE OF AEROFLIGHT	OMNI TYPE	VERTICAL	ANNULAR SLOT	USED DURING AEROFLIGHT ONLY. SAME ANTENNA AS USED FOR TACAN
RADAR ALTIMETER	4210–4390	4210–4390	1.3:1	10 WATT CW (WORST CASE)	PATTERN DIRECTED PERPENDICULAR TO PLANE OF AEROFLIGHT	11 dB	LINEAR	HORN	USED DURING LANDING ONLY
VHF COMMUNICATIONS	118–136 136–138 (BACKUP)	118–136 148–150 (BACKUP)	2:1 2:1	100 WATT CW (WORST CASE)	OMNI-DIRECTIONAL IN PLANE OF AEROFLIGHT	OMNI TYPE	VERTICAL	MODIFIED PARTIAL SLEEVE	PRIMARILY USED DURING AEROFLIGHT. USED IN BACKUP VEHICLE – GROUND LINK DURING ORBITAL FLIGHT
S-BAND COMMUNICATIONS • USAF RENDEZVOUS • NASA RENDEZVOUS • USAF GROUND COMMUNICATIONS • NASA GROUND COMMUNICATIONS	 1750–1850 2020–2120 2200–2300 2200–2300	 2200–2300 2200–2300 1750–1850 2020–2120	1.5:1 TRANSMIT	20 WATT CW (WORST CASE)	3 ANTENNAS PROVIDE SPHERICAL COVERAGE	OMNI TYPE	RIGHT HAND CIRCULAR	CAVITY BACKED HELIX	USED DURING ALL MISSION PHASES
MICROWAVE LANDING SYSTEM (Ku-BAND)	N/A	15400–15700	2.0:1 RECEIVE	RECEIVE ONLY	FORWARD DIRECTED	4 dB	VERTICAL	SLOT (WAVE GUIDE CUT ON TAPER)	USED DURING FINAL FLARE AND LANDING
MICROWAVE LANDING SYSTEM (C-BAND)	5000–5060 N/A	5068–5125 5130–5250		2 KW PK (WORST CASE)			VERTICAL	SLOT	USED DURING APPROACH AND LANDING
INSTRUMENT LANDING SYSTEM, LOCALIZER	N/A	108–112	5.0:1	RECEIVE ONLY	FORWARD HEMISPHERE	3 dB (TYP)	HORIZONTAL	FOLDED MONOPOLE OR FOLDED DIPOLE	USED DURING APPROACH AND LANDING FOR FERRY FLIGHTS ONLY. ANTENNAS PROTECTED BY NOSE RADOME
INSTRUMENT LANDING SYSTEM, GLIDE SLOPE	N/A	329–336	2.0:1						

NOTES: 1. HIGH GAIN ANTENNA REQUIREMENTS NOT INCLUDED;
2. VERTICAL AND HORIZONTAL POLARIZATION IS REFERENCED TO ORBITER AEROFLIGHT ATTITUDE.

Figure 1 shows the locations selected for each of the Orbiter antennas. The respective locations were selected to obtain the best radiation pattern for the antenna types selected.

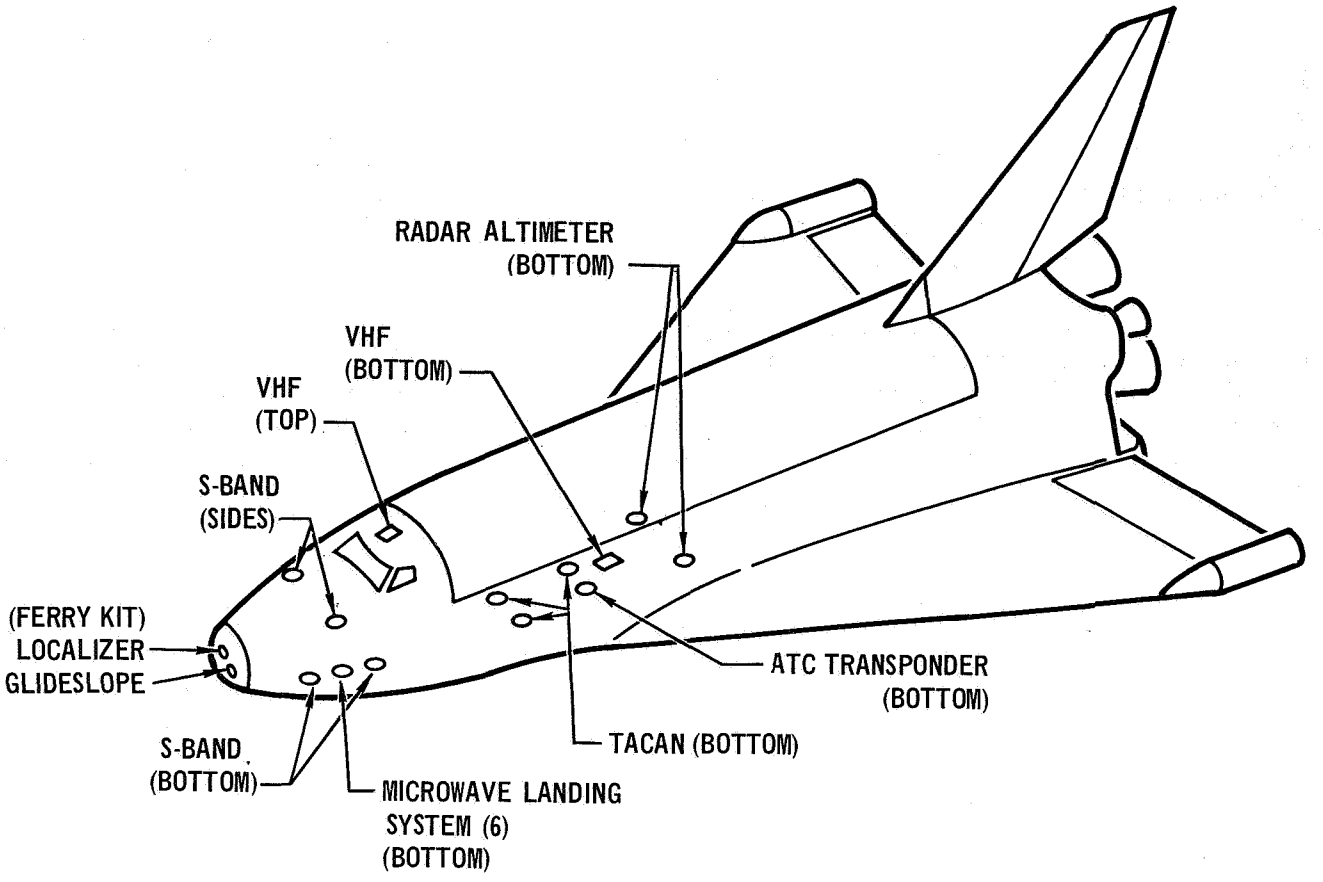

ANTENNA LOCATIONS

Figure 1

The TACAN and air traffic control transponder antennas are located on the bottom of the Orbiter. This location is preferred for best pattern coverage during aeroflight, since the Orbiter causes less RF signal shadowing for this location than for other antenna locations. No TACAN and air traffic control (ATC) transponder antennas are located on the top of the Orbiter because: 1) with an inertial system for primary navigation continuous TACAN coverage is not required during banking; and 2) the ground air traffic control radar will continue to skin track the Orbiter should air traffic control transponder RF signals be temporarily blocked due to banking of the Orbiter. The TACAN is, however, required to update the inertial system position after entry from orbit. Separate antennas are used for each TACAN and ATC transponder. With this approach, antenna switches are not required and RF isolation is achieved between each L-band set (TACAN and ATC transponder) by antenna separation.

The radar altimeter antennas are located slightly forward of the main landing gear wheels. This location allows the altitude of the main landing gear wheels to be directly and accurately determined without correcting the altitude measurement for Orbiter pitch angle. However, the antennas are spaced far enough from the main landing gears to preclude significant altitude errors due to reflections from the landing gears.

One VHF antenna is located on the top and one on the bottom of the Orbiter. The bottom antenna is in the preferred location for use during aeroflight since the Orbiter is seldom between the antenna and the ground airports and air traffic control centers. However, at the VHF frequencies the top antenna location will also provide a good coverage to the sides, forward, and 45 to 60 degrees down from the forward direction due to RF wrap around. The use of both top and bottom locations provides for better Orbiter to Earth coverage for backup VHF communications.

S-band antennas, one bottom, one upper left side, and one upper right side, provide 360° roll coverage. The placement of the S-band antennas forward on the Orbiter provides improved forward coverage for S-band rendezvous ranging with somewhat reduced coverage to the rear of the Orbiter. Two S-band antennas are located on the bottom for redundancy and to allow the simultaneous operation of two S-band sets, when required, for maximum communications capacity between the Orbiter and the Earth.

The microwave landing system (MLS) antennas are located forward, on the bottom and near the avionics bays to provide good forward coverage for landing and reduce cable and waveguide losses at the higher MLS frequencies. The Orbiter bottom is approximately ten feet from the ground. This is believed to be adequate for receiving good MLS signals for automatic rollout after landing.

Both the localizer and glide slope antennas are installed behind a nose radome, which is to be installed for ferry flights only. Landing from orbit is accomplished using the MLS System. This approach allows standard aircraft off-the-shelf glide slope and localizer antennas to be used. The forward position for the glide slope and localizer antennas provides good radiation pattern coverage. Also, investigation related to pilot cues indicated that this glide slope antenna location should provide similar pilot cues from glide slope generated displays and out-of-window viewing by the pilot. That is, this glide slope antenna location should offer safety, pilot acceptance, and proper Orbiter altitude at threshold for ferry flight landings.

The antennas selected for this study correspond to the Orbiter avionics system as follows:

Antenna Type	Avionics System	Frequency
Annular Slot	TACAN/ATC Transponder	L-band
Horn	Radar Altimeter	C-band
Linear Slot	Microwave Landing System	C-band

Structural Requirements

The Space Shuttle Orbiter structural configuration consists of an all aluminum, semi-monocoque, stiffened skin structure covered with a reusable surface insulation (RSI) which serves as the thermal protection system (TPS). A typical section through the bottom surface of the center fuselage, as shown

in figure 2a, consists of 0.051 cm (0.020 in.) thick aluminum skins riveted to fore and aft running stringers, attached between bulkheads. Stringer and bulkhead spacing are 10.16 cm (4.00 in.) and 50.80 cm (20.00 in.) respectively. A slightly different structural approach proposed for the forward fuselage section, which contains the pressurized cabin, is shown in figure 2b. In this

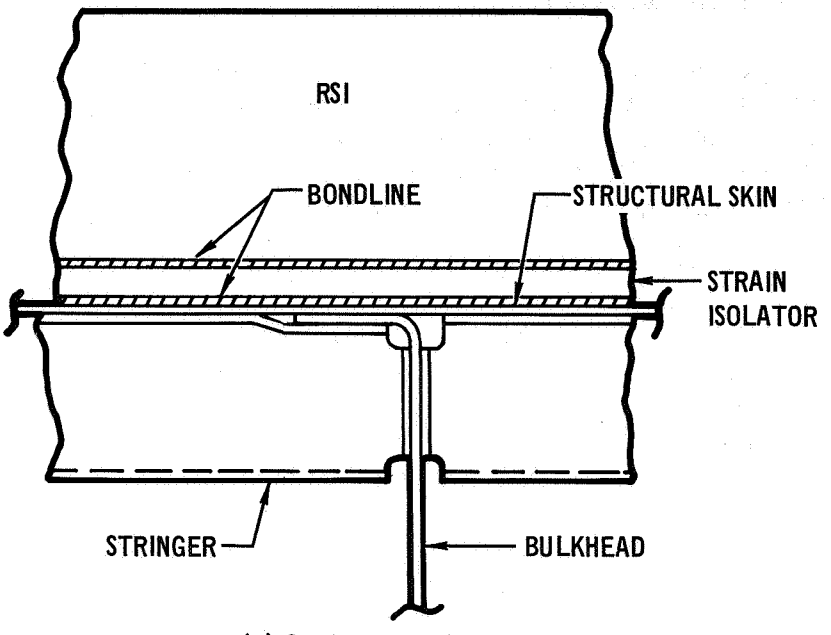

(a) Center Fuselage

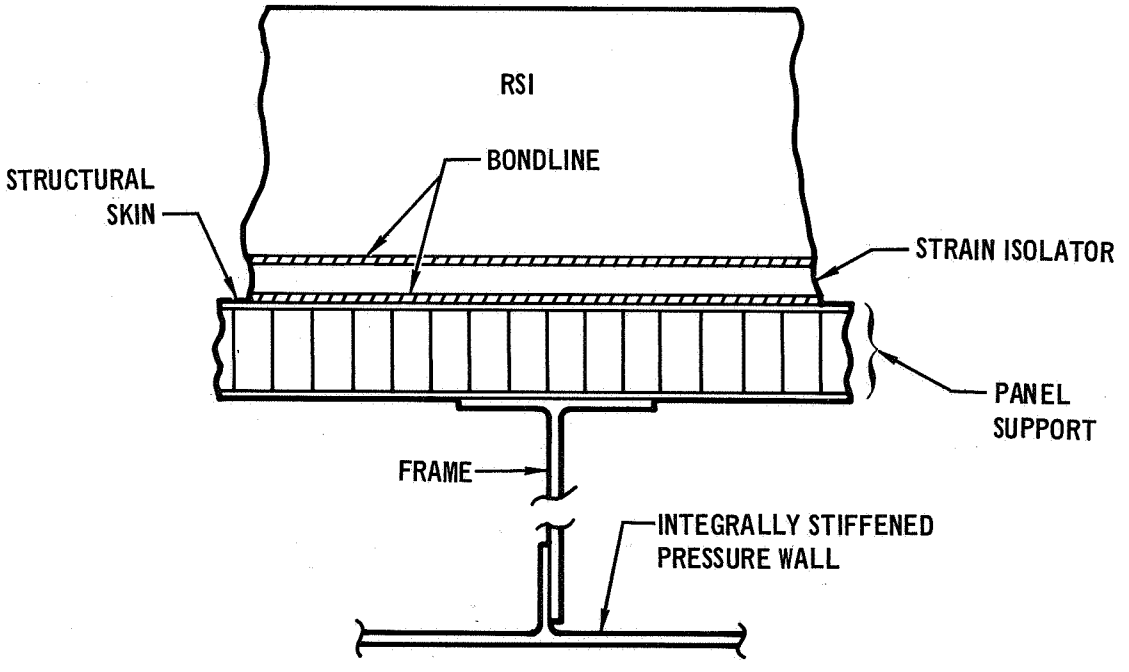

(b) Forward Fuselage

PRIMARY STRUCTURE/TPS CONCEPTS

Figure 2

area an integrally stiffened aluminum pressure wall is submerged approximately 17.78 cm (7.00 in.) inside the aerodynamic moldline. Frame members and stiffened panels are used to support the TPS. For these approaches the RSI tiles, in the form of flat or contoured surfaces, are bonded to the skin of the primary structure or to the TPS support panel by way of an intermediate silicone sponge strain isolator.

A silicone sponge, 6.35 mm (0.250 in.) average thickness, was used as a mechanical strain isolator. This permits using buckling skins and protruding head rivets for the primary structure, thereby minimizing structural weight and fabrication costs. The silicone sponge strain isolator and the RSI tiles are installed on the skin by bonding with RTV 560 adhesive. A silicone primer is applied to the aluminum surfaces and allowed to hydrolize before the adhesive is applied. The adhesive layer between both the strain isolator and the RSI tile, and the strain isolator and the skin is approximately 0.25 mm (0.010 in.) thick. Although bonding was selected for attaching the RSI tiles on the baseline Orbiter configuration it should be noted that mechanical fasteners are being studied for attaching either individual tiles or large panels. MDC is presently under contract to NASA (NAS9-12854) to study and test mechanical attachments for installing RSI to the primary structure.

The baseline TPS consists of both RSI and silicone elastomeric ablators. It was anticipated that approximately 22% of the Orbiter's surface area would be covered with ablator. These areas include the nose, leading edge of the wings and fin, and the upper surface of the wing. The ablator on the upper surface of the wings does not char since the surface temperatures are below 555^{o}K (600^{o}F). The ablator, therefore, functions as RSI. The remaining 78% of the surface area is covered with RSI. RSI is used in the Orbiter areas where antennas are installed; therefore, the study emphasis was on antenna systems for installation into a structure thermally protected by RSI.

The primary material candidates for RSI include Lockheed's LI-1500, General Electric's REI and McDonnell Douglas' HCF. The LI-1500 has a silica fiber base while the REI and HCF have a mullite base. All three materials utilize an inorganic binder and, therefore, are reusable at high temperatures. These materials are rigid and have relatively low mechanical strengths, therefore, a flexible silicone sponge is required to provide strain isolation. An inorganic, oxide based coating is applied to all the materials to provide a waterproof surface since these materials absorb water. A pigment is added to the coatings to provide a high emittance surface in order to minimize surface temperatures during entry heating.

Thermal Requirements

The thermal requirements for the Space Shuttle Orbiter antenna systems are influenced by the local TPS design and the local thermal environments. The TPS design at the various antenna locations is described in the section on Structural Requirements above.

The local thermal environment is defined by the Orbiter missions, vehicle configuration and trajectories, and specific antenna locations. The most severe thermal environment results from Orbiter Mission 3, a single-orbit delivery or retrieval of a 18 000 kg (40 000 lb) payload. Characteristics of Mission 3 include a south polar launch, a 187 km (100 n.mi.) circular orbit and return to the Western Test Range. The ascent trajectory shown in figure 3 is for insertion into a 93 x 185 km (50 x 100 n.mi.) polar transfer orbit. The entry trajectory shown in figure 4 is more severe than the ascent trajectory as it causes maximum temperatures and total heat loads. This entry trajectory provides maximum crossrange of 2037 km (1100 n.mi.) and maximum downrange maneuvering margin of 370 km (200 n.mi.). Downrange maneuvering is used to compensate for deorbit, atmosphere, guidance and navigation, and wind dispersions. Trajectory shaping optimization was used to minimize RSI TPS thickness. A final approach and landing trajectory was added to the entry trajectory shown in figure 4.

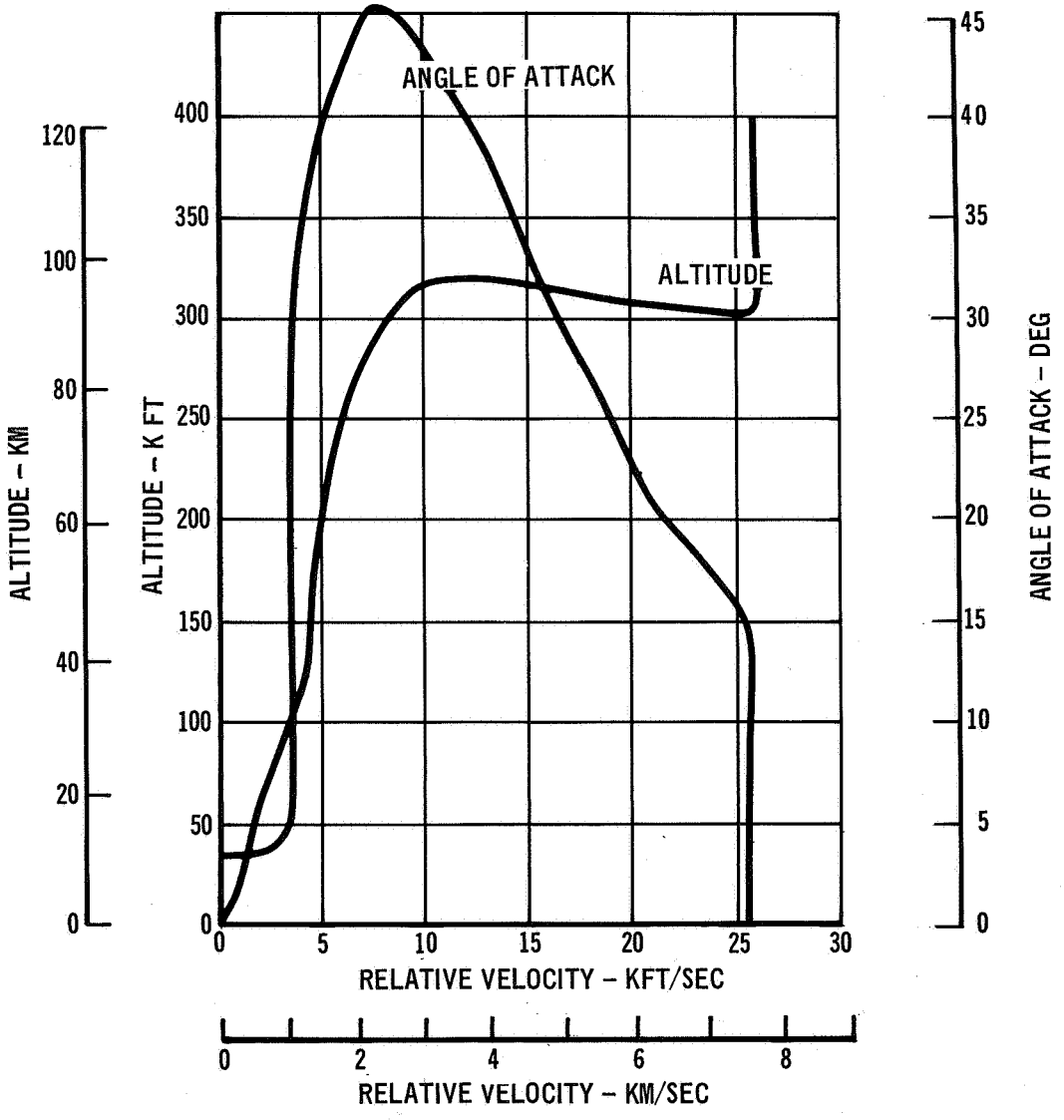

ASCENT TRAJECTORY

Figure 3

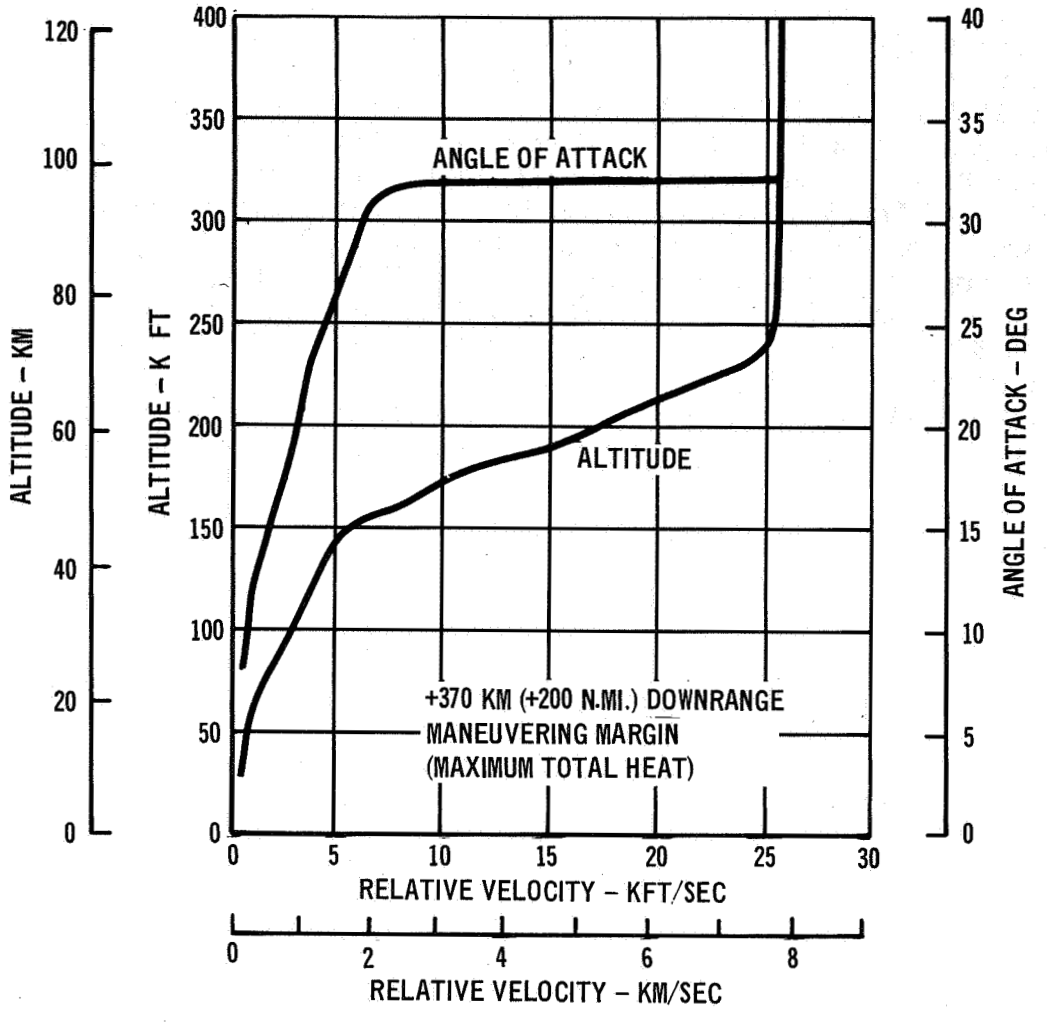

Figure 4

Orbital environments employed were 0.37 albedo (reflectivity), a solar constant of 1395 W/m^2 (444 $Btu/hr\text{-}ft^2$) and an effective earth temperature of 252°K (-6°F). Surface free convection and sky radiation to 300°K (80°F) were used for the landed environment.

The external surface temperature history during ascent is shown in figure 5. Interference heating induced by the mated external tank is included. Entry temperatures are shown in figure 6. Integrated total heat load distributions during entry for the entire vehicle and the Orbiter antenna locations are shown in figure 7. The antenna locations on the fuselage bottom have the most severe thermal environment. Thus, to assure a valid antenna design for all high temperature antennas, the local thermal environment for the rear L-band antenna was selected. The rear L-band antenna is located off centerline within the 2.16×10^8 J/m^2 (19 000 Btu/ft^2) region on the fuselage bottom. An external surface temperature history for this location is shown in figure 8. These thermal environments are based on the aerodynamic heating methodology developed by MDC during the Shuttle Phase B Study.

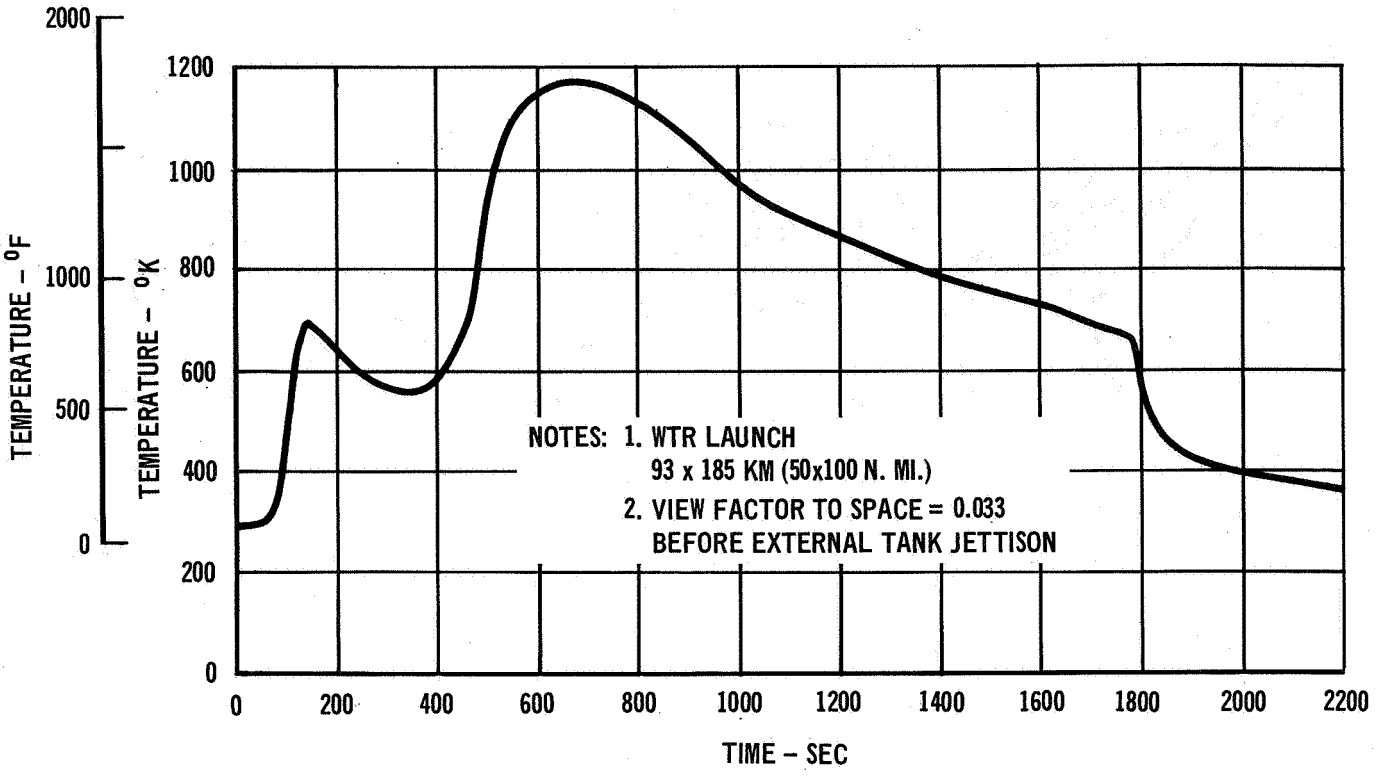

ASCENT TEMPERATURE HISTORY

Figure 5

Since thermal conductivity of RSI materials is a function of pressure as well as temperature, the local static-surface pressures (at edge of local boundary layer) are shown in figures 9 and 10 for ascent and entry, respectively.

Strength Requirements

The antenna systems were designed to withstand loads developed during the launch and entry phases of the Orbiter mission. The sources of the loads are differential pressures, fuselage bending and thermal gradients. Strength requirements imposed on the antenna systems are described in this section. A minimum factor of safety of 1.4 was applied to the sum of the expected loads. Mechanical loads and thermally induced loads were combined to determine ultimate loads according to equations, given below:

$$K_1 L_{external} + K_2 L_{thermal} \geq 1.40\,(\Sigma L)$$

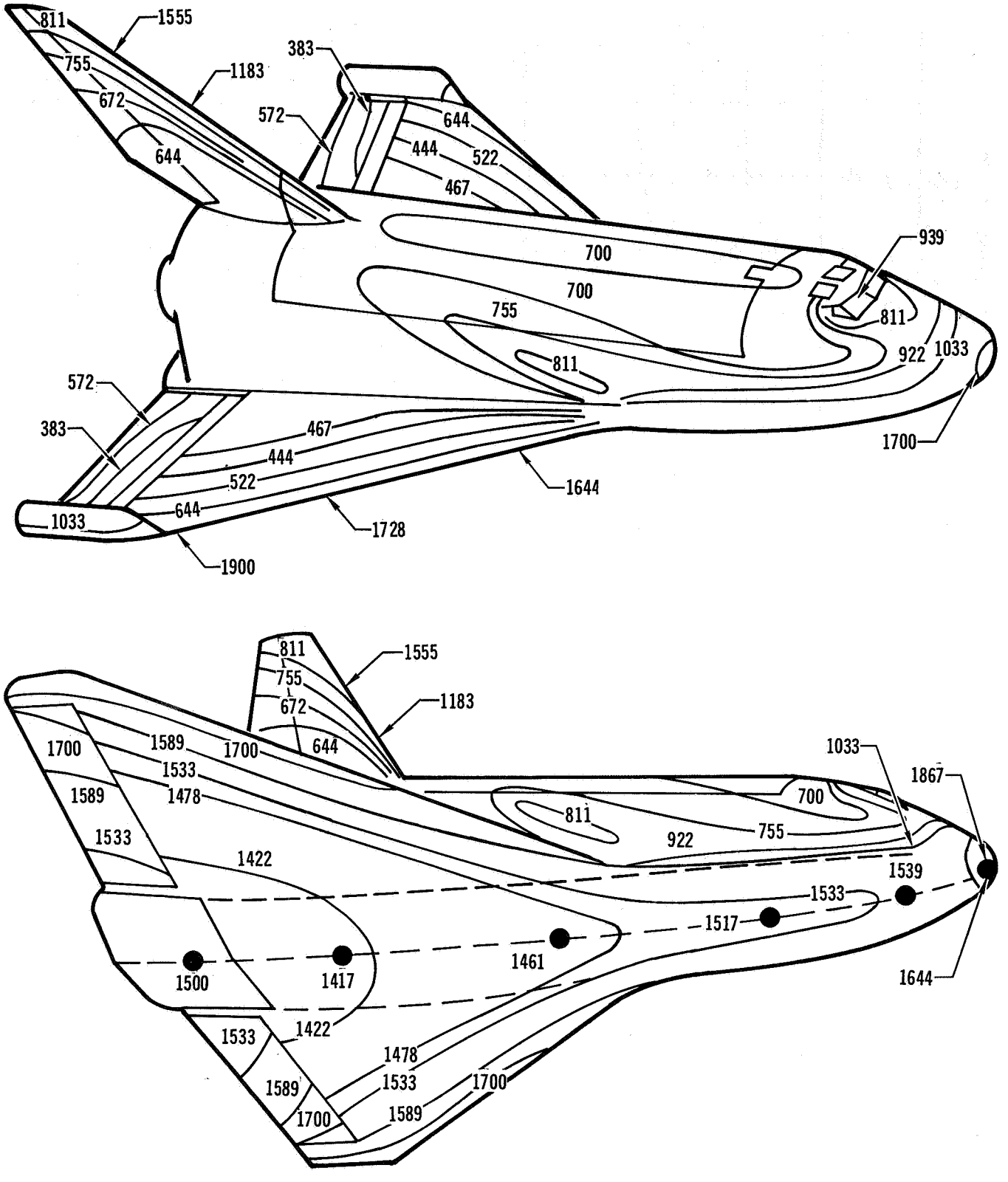

ENTRY TEMPERATURES ^{0}K

Figure 6

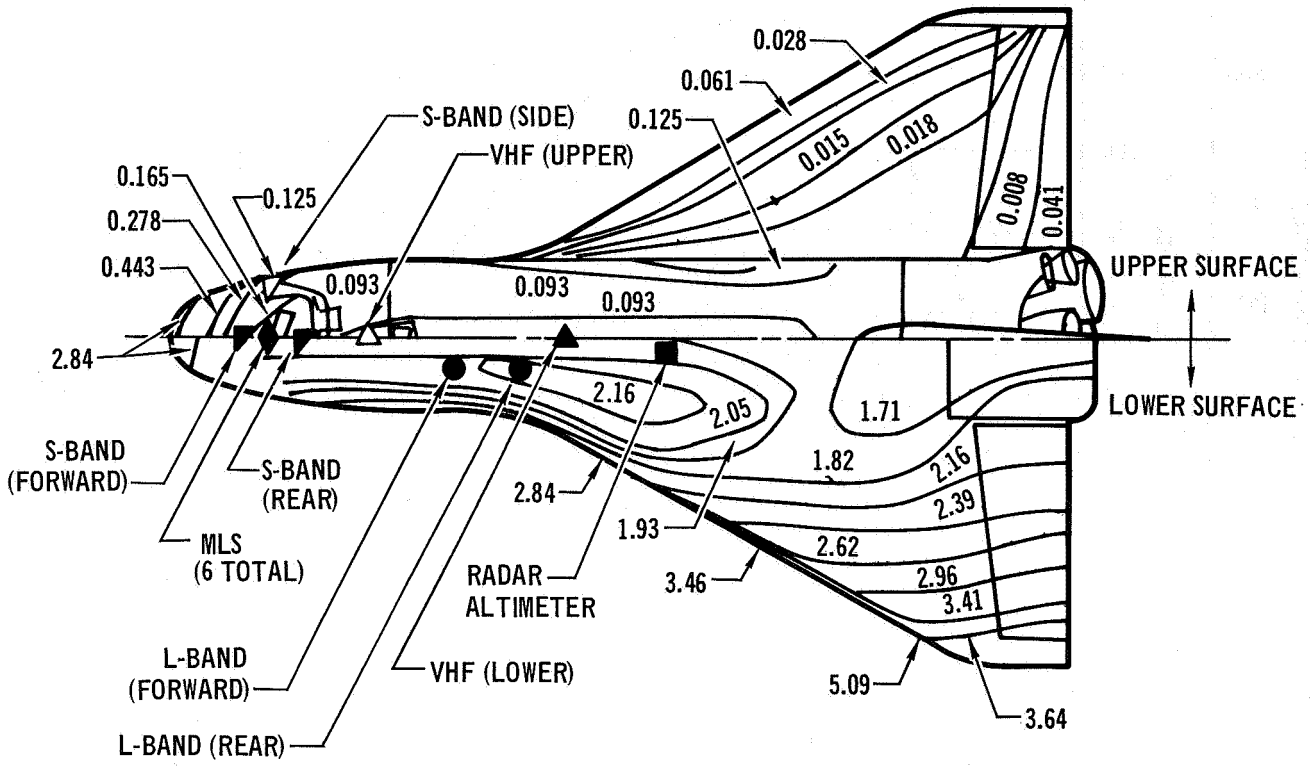

NOTES: 1. MISSION 3 MAX. DOWNRANGE TRAJECTORY
2. ALL TOTAL HEAT (Q_T) IN $J/M^2 \times 10^8$
3. $(Q_T)_{REF} = 8.1 \times 10^8$ J/M^2 (71,380 BTU/FT^2)
4. CONVERSION FACTOR: $BTU/FT^2 \times 1.137 \times 10^4 = J/M^2$
5. SHADED SYMBOLS ARE ON FUSELAGE BOTTOM

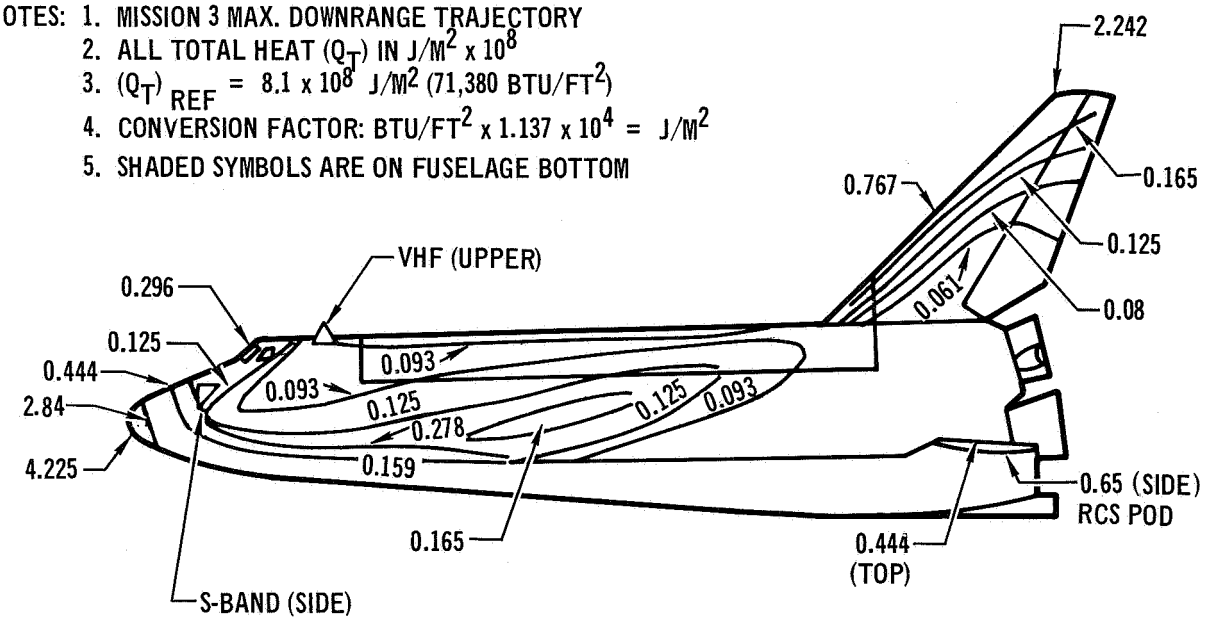

ENTRY TOTAL HEAT DISTRIBUTION

Figure 7

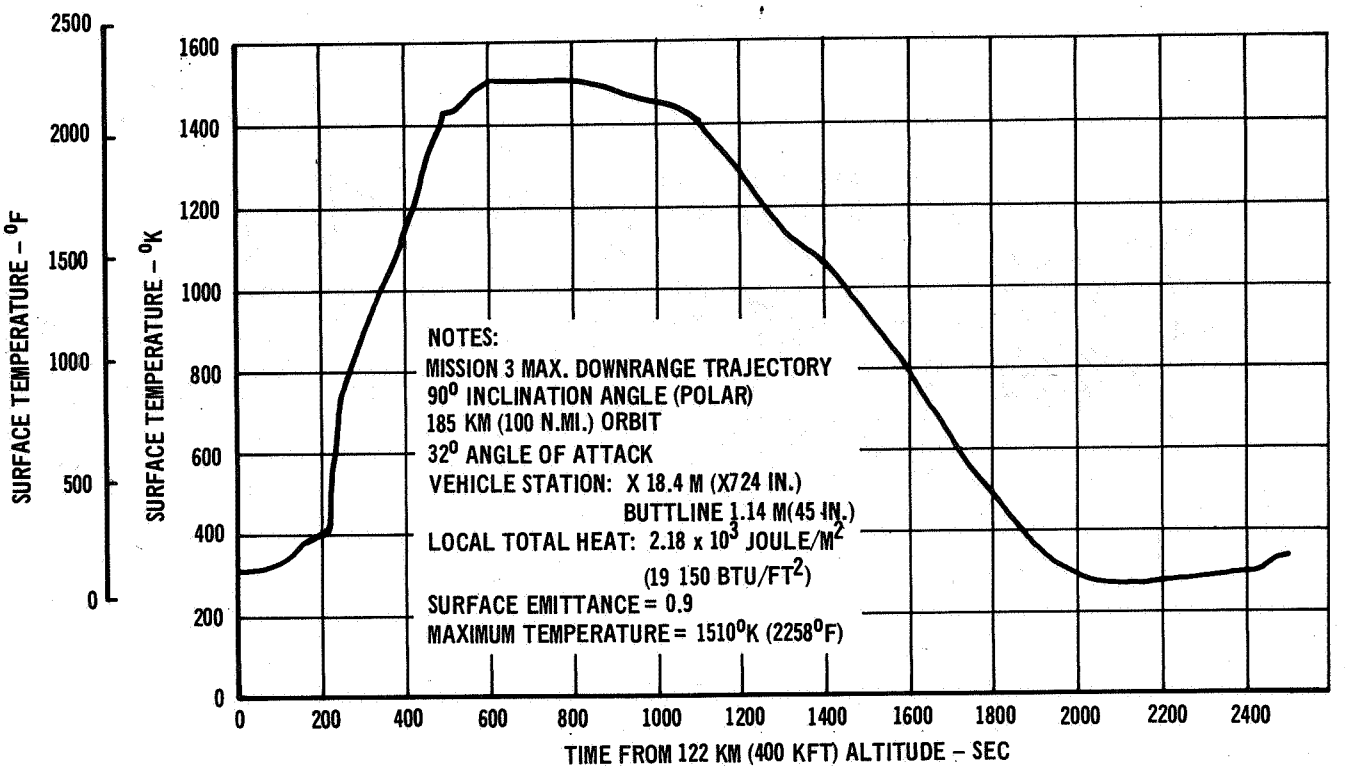

ENTRY TEMPERATURE HISTORY

Figure 8

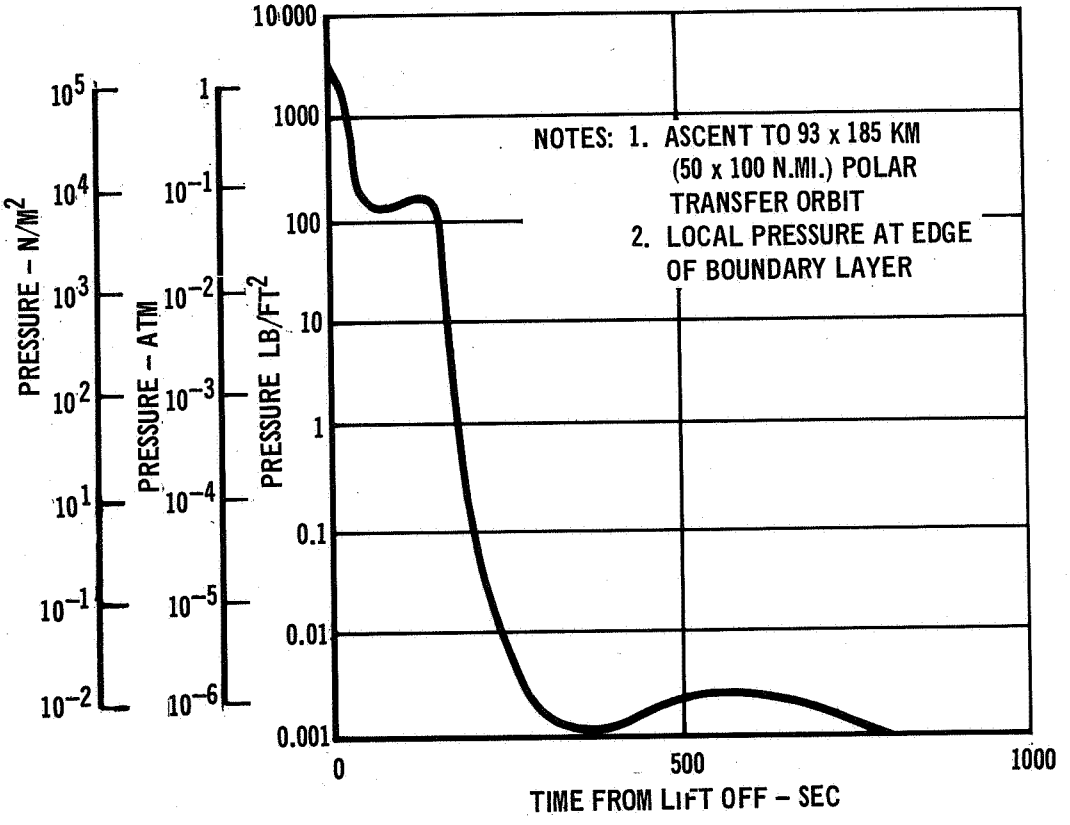

ASCENT LOCAL STATIC PRESSURE HISTORY

Figure 9

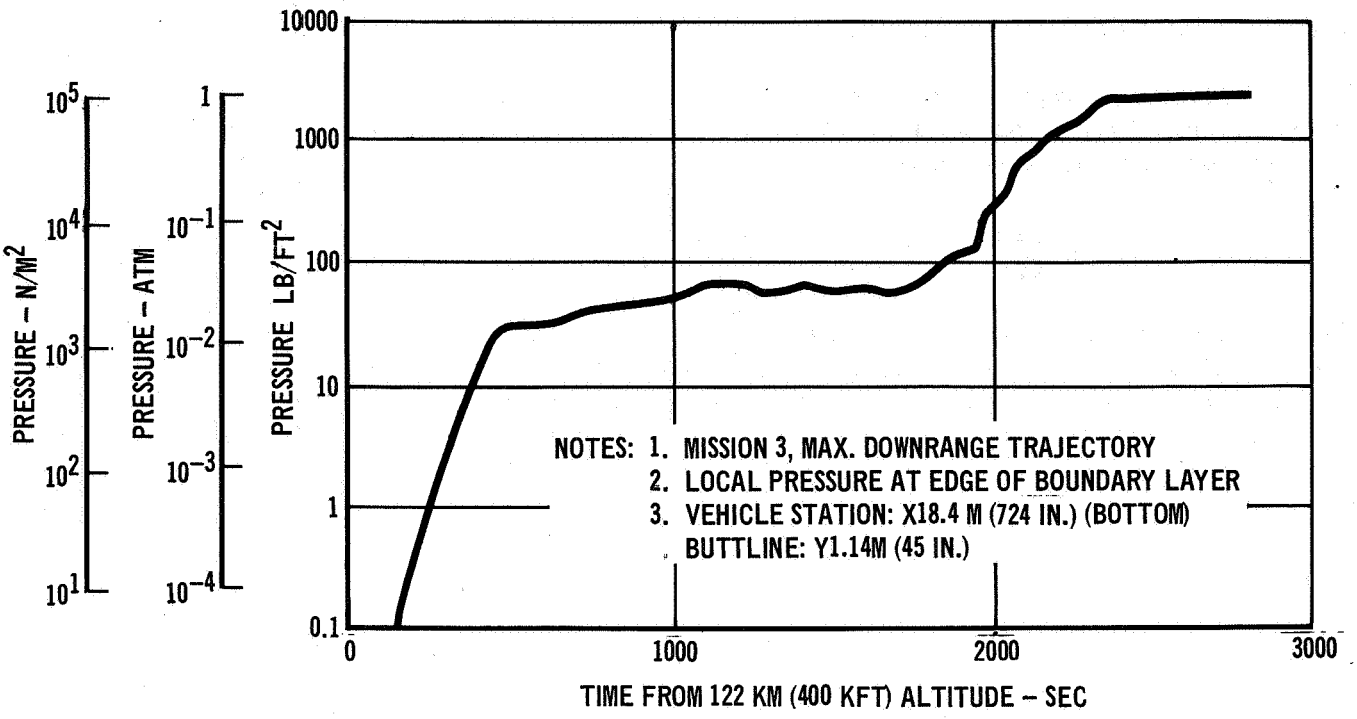

ENTRY LOCAL STATIC PRESSURE HISTORY

Figure 10

where

K_1 = 1.4 for boost conditions when the term is additive to the algebraic sum, ΣL

K_1 = 1.5 for entry, atmospheric cruise, and landing when the term is additive to the algebraic sum, ΣL

K_2 = 1.5 when the term is additive to the algebraic sum, ΣL

$L_{external}$ = mechanical externally applied loads

$L_{thermal}$ = thermally induced loads

ΣL = algebraic sum of loads

Design pressures are shown in figures 11 and 12. In order to ensure that the antennas will be structurally adequate for installation at any fuselage location, the maximal ultimate pressures were used for design and are summarized below:

Mission Phase	Pressure	Type	Factor of Safety
ASCENT	73 085 N/m^2 (10.6 psi)	Collapse	1.4
ASCENT	9 653 N/m^2 (1.40 psi)	Burst	1.4
ENTRY	4 137 N/m^2 (0.60 psi)	Collapse	1.5

These pressures were assumed to act at any time during ascent or entry.

Ultimate design loads for fuselage stringers and associated effective skin for various locations on the Shuttle are shown in figure 13. The ultimate loads chosen for antenna design are:

Tension	175 000 N/m	(1000 lb/in.)
Compression	43 700 N/m	(400 lb/in.)

These are representative of loads on the bottom surface of the Shuttle in the region of antennas and occur at room temperature. The loads are considered typical and, therefore, structure designed to withstand these loads will be representative of a typical antenna installation. Pressure loads and running loads are conditions which do not peak simultaneously.

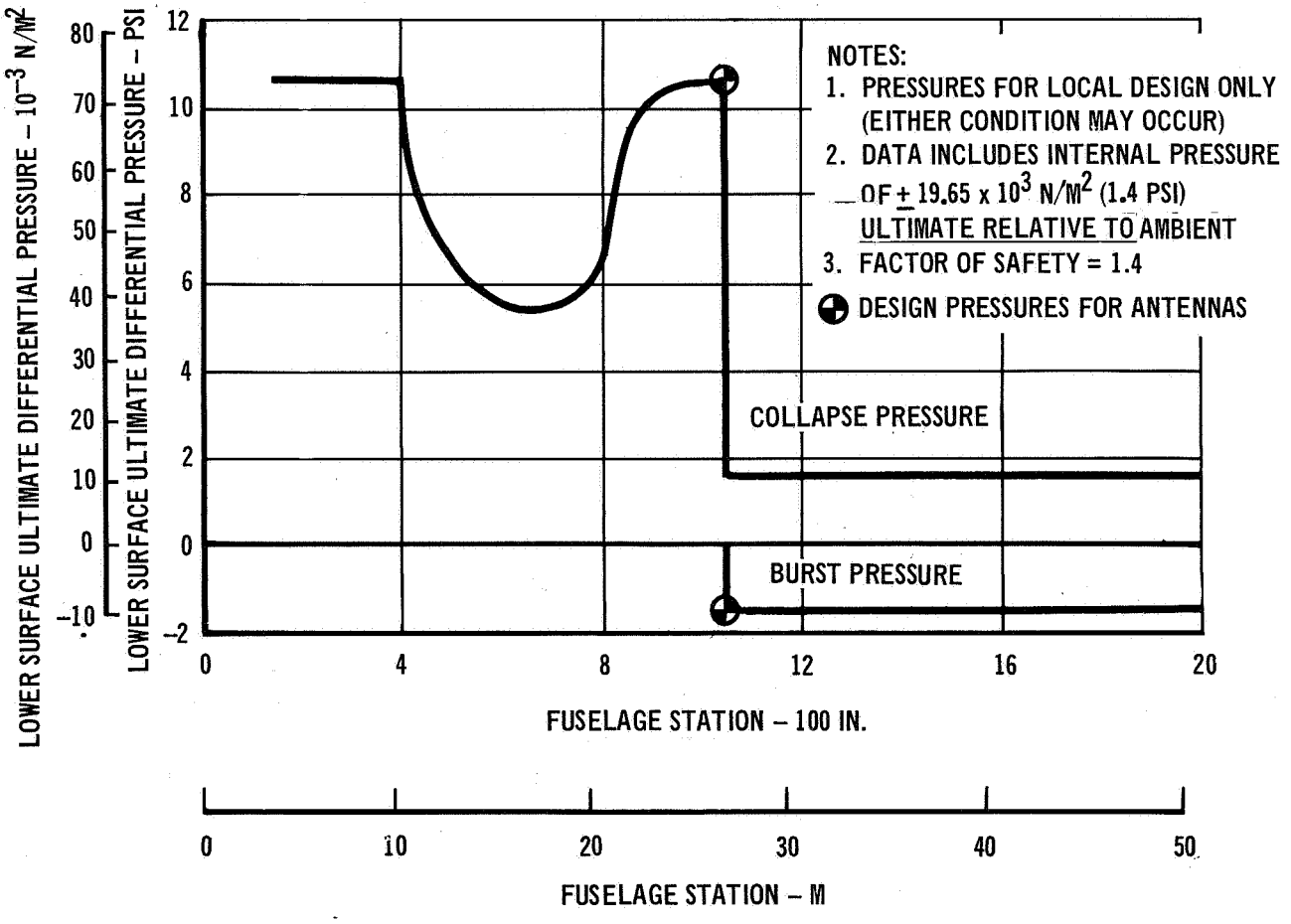

ENVELOPE OF ASCENT INTERFERENCE PRESSURES ON FUSELAGE LOWER SURFACE

Figure 11

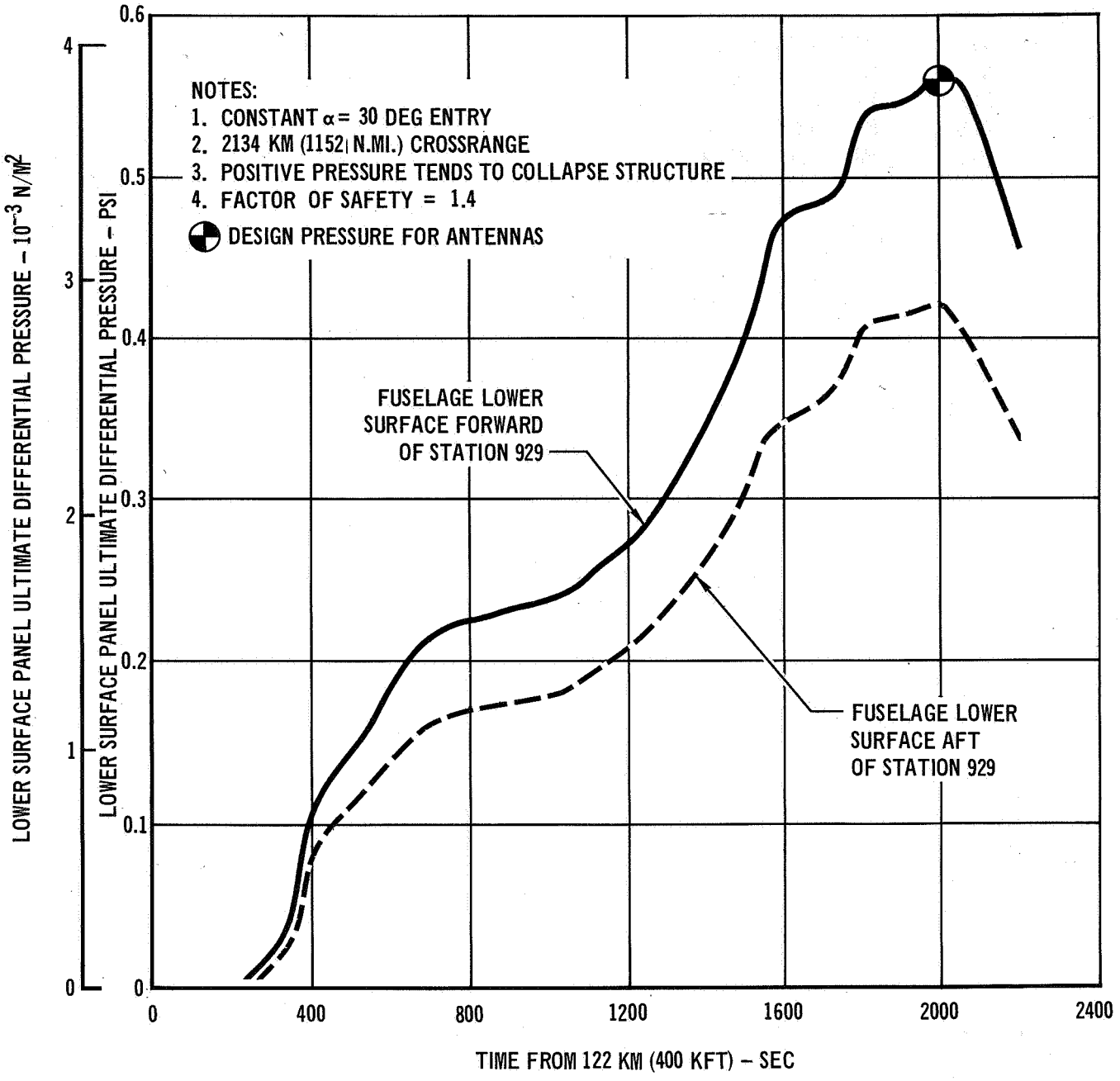

LOWER SURFACE ENTRY PRESSURE

Figure 12

HIGH TEMPERATURE ANTENNA DESIGN APPROACH

The high temperature antenna design approach used in this study combines an antenna window with a conventional antenna. Throughout this report, the antenna and antenna window, when combined, are referred to as an antenna system.

TW – MAX αq (TAILWIND)
SW – MAX β q (SIDEWIND)
MAX N_X – MAX AXIAL LOAD FACTOR
PSB – POST SRM BURNOUT
MGL – MAIN GEAR LANDING

*CRITICAL DESIGN CONDITION
(T) = TENSION
(C) = COMPRESSION

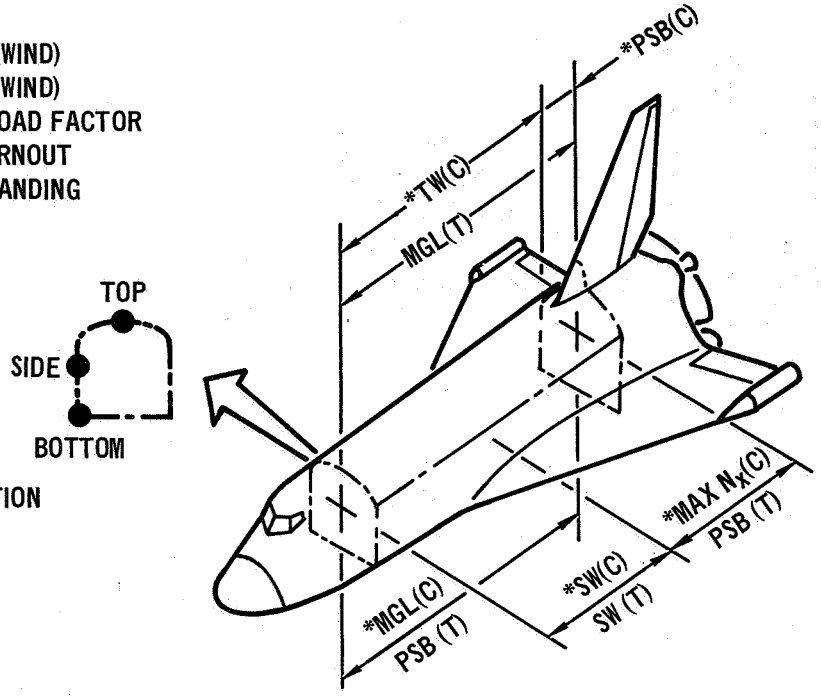

(a) Major Design Conditions

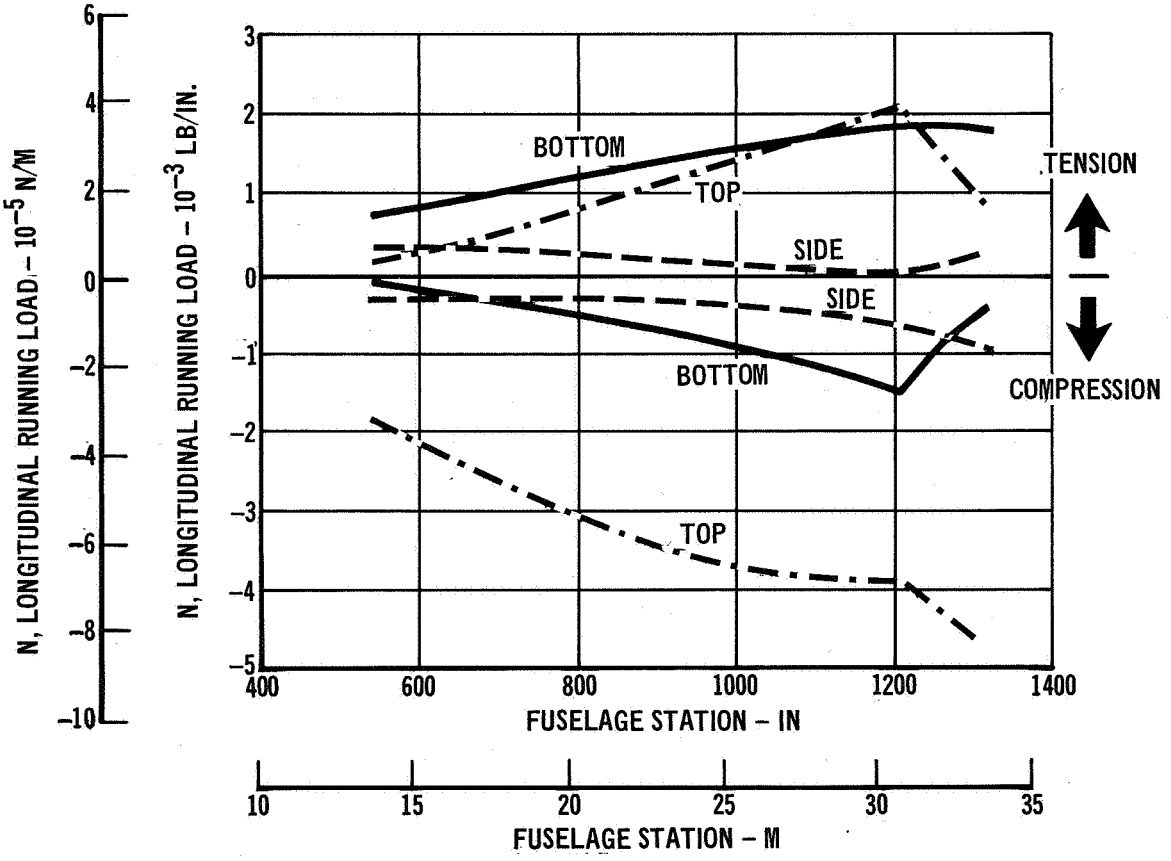

(b) Ultimate Longitudinal Running Load Envelopes

FUSELAGE LOAD INTENSITIES

Figure 13

The antenna window provides thermal protection for the antenna and a means for transmitting RF energy outside the vehicle. This approach essentially separates the high temperature problems from the electrical design problems of the antenna by limiting the antenna peak temperatures to 422°K (300°F). Therefore, the antenna is not subjected to high temperatures where dimensional changes, differential expansion, material property changes, oxidation, and similar effects occur. These effects may drastically change the performance of some antenna types and result in unacceptable system characteristics, severly limited reuse capabilities, or both. Further, the protected antennas may be fabricated using standard techniques and materials now used for commercial and military airplanes. The antenna window materials will undergo some changes in dielectric constant and loss tangent due to high temperature exposure (e.g., 533 to 1589°K (500 to 2400°F)). However, the effects of these changes on antenna system performance will be minor compared with effects due to the antennas being directly exposed to these high temperatures.

The initial approach was to provide conducting metallic window edge enclosures which provide distinct window edge boundaries. This is equivalent to terminating the antenna in a dielectrically loaded circular waveguide and extends the antenna aperture to the TPS surface. The window edge enclosure provides some radiation pattern shape control and in some cases may reduce pattern distortion by reducing surface wave excitation. Circular apertures were used because both thermal stresses and higher order mode excitation are minimized.

Two antenna window configurations were considered. One was a multiple-layer design which consisted of a thin outer layer of high temperature dielectric and an inner layer of a low density insulation material as shown in figure 14. The other was a single-layer design using the Orbiter TPS insulation material as shown in figure 15. The multiple-layer approach provides a hard outer surface which would resist rain, and runway sand and gravel errosion. The inner layer of low density insulation serves to minimize the weight and thickness of the window, since the outer layer of high temperature dielectric material, in general, will have a high density and relatively high thermal conductivity. The single-layer approach does not provide a hard outer surface, but the material has both a low density and thermal conductivity and would have mechanical properties equivalent or identical to the TPS material that is installed over most of the Orbiter skin. Both approaches were designed and tested for the L-band annular slot antenna. Only the single-layer approach was used for the two C-band antennas.

The antennas used for this study were off-the-shelf hardware with the exception of the C-band linear slot antenna, which was simulated with an open ended C-band waveguide. The L-band annular slot antenna was a AT-740/A Antenna (Transco Products, Inc. Part No. 22135) designed for operation at temperatures to 478°K (400°F). The C-band horn antenna (Transco Products, Inc. Part No. 01-34-04551) was designed for operation to 394°K (250°F). The characteristics of these antennas simply mounted in a 0.91 x 0.91 m(3 x 3 ft.) ground plane were used as the design standards or reference configurations.

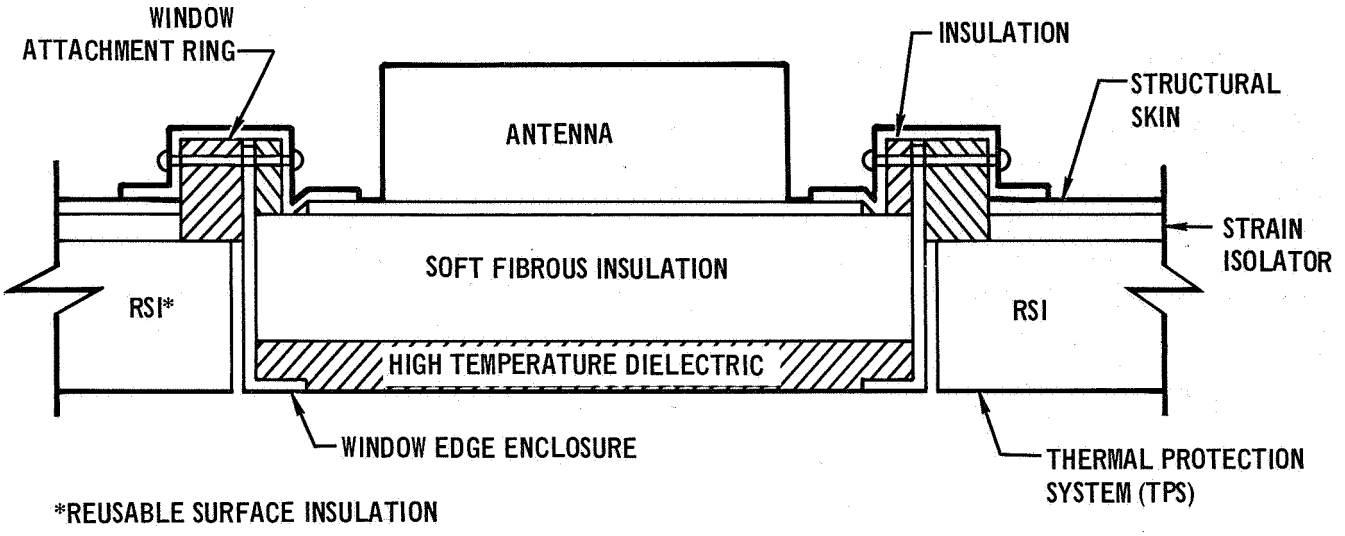

MULTIPLE-LAYER ANTENNA WINDOW CONCEPT

Figure 14

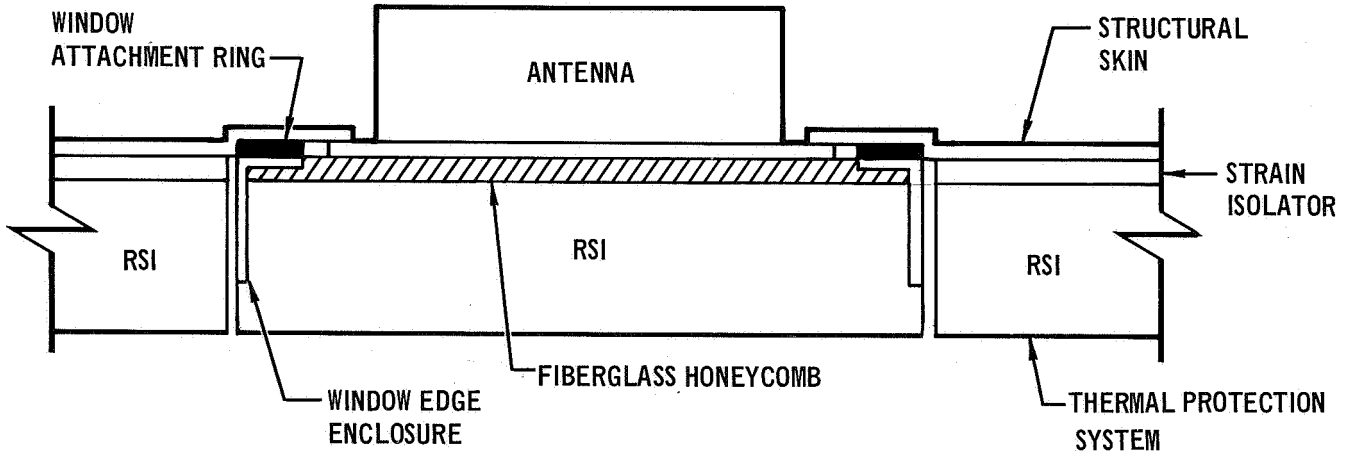

SINGLE-LAYER ANTENNA WINDOW CONCEPT

Figure 15

ANTENNA WINDOW MATERIALS SELECTION

The material requirements for Space Shuttle Orbiter antenna windows are more severe than those for previous entry vehicles, for example, (1) longer heating periods, (2) 100 mission reuses and (3) larger antenna window sizes.

As a result of longer heating periods, the antenna window must provide good thermal insulation in order to keep the thickness and weight within practical limits while limiting the window and antenna interface temperature to 422°K (300°F). This limit was used for the antennas because it is compatible with the structural aluminum skin temperature limitations as discussed in the section on Thermal Requirements. Since the longer heating times occur while the materials are in an air atmosphere, the selection of materials is further limited to those which are also oxidation resistant.

The requirement for 100 mission cycle reuse precludes the use of many antenna window materials which are adequate for one-time use. The material must survive the high temperature environment and provide thermal protection for the antennas, but must not undergo significant changes in their thermal, mechanical, or electrical properties.

Larger antenna window sizes are required because the apertures required for Orbiter avionics system antennas are, in general, larger than those of previous entry vehicles. This also restricts candidate materials because of fabrication limitations in both area and thickness.

Both high and low density window materials were studied. For the high density window material, fused silica, boron nitride, beryllia, silicon nitride, and others were considered. For the low density window materials, silica reusable surface insulation (RSI), mullite RSI, ablators, silica insulation, and silica foam materials were considered.

Tradeoff criteria for the selection of window materials included the following:

(a) High temperature recycling capability.

(b) Low temperature recycling capability.

(c) Thermal and mechanical properties at high and low temperatures.

(d) Chemical stability at high and low temperatures.

(e) Chemical stability under high vacuum.

(f) Moisture resistance.

(g) Rain and dust erosion resistance.

(h) Electrical properties at high and low temperatures (dielectric constant, loss tangent, etc.).

(i) Commercial availability.

(j) Design constraints for candidates.

(k) Compatibility with other materials.

(l) Refurbishment capabilities.

(m) Cost

Material properties were compiled to assist in the trade studies. These properties are tabulated in the following sections in order to give an overview of the properties of the candidate materials for both the high and low density windows. Many of the electrical properties listed were obtained from a Space Shuttle antenna materials test program conducted by NASA LaRC.

High Density Materials

The properties of commonly used high density, high temperature antenna window materials were tabulated and used in a tradeoff study. Table II is a summary of those properties. More detailed material properties, which were used in thermal and strength analyses, are listed in Appendix A. Since materials testing was beyond the scope of this program, the acceptability of each candidate material was based on available data. The tradeoff criteria and evaluation results are listed in table III. Some of the more important criteria which were considered are: electrical, mechanical and physical properties as a function of temperature (room temperature to 1533°K (2300°F); recycling capability; thermal shock resistance; and moisture resistance.

Selected high density material - The material selected for the high density window is hot pressed boron nitride (BN), grade HD-0092, manufactured by Union Carbide. This grade of BN has a lower oxygen content than previously available materials. The low oxygen content grade, although slightly more costly than conventional hot pressed grades, has the advantage of improved resistance to hydration and has more uniform mechanical properties. The electrical properties of HD-0092 are reasonably constant as a function of temperature. The mechanical properties at room temperature are acceptable and improve as temperature increases. The high thermal conductivity of boron nitride necessitates the use of an efficient thermal insulation between it and the antenna, which is also compatible with the electrical requirements of the antenna. The insulation for this application is discussed in the following paragraphs.

Antenna window insulation - The thermal insulation selected for use behind the BN outer window is Dynaquartz, 160 kg/m^3 (10 lb/ft^3) density, produced by Johns-Manville. Dynaquartz is a semirigid, ultra high purity, heat treated, silicon dioxide fibrous batt material that has a low thermal conductivity. It also has modest load bearing capability and is reasonably stable dimensionally to temperatures of 1533°K (2300°F) or more. The electrical properties have been determined up to 1473°K (2192°F) and are excellent. Other material properties considered are summarized in table IV, and the detailed material properties, which were used in the thermal and strength analyses, are listed in Appendix A. The commercial silica foams are suggested as possible backup materials.

All silica insulation materials are porous and are permeable to moisture. Therefore, the hygroscopic nature of these materials must be considered in an antenna design, since entrapment of moisture can affect electrical performance.

Low Density Materials

Low density thermal insulation materials considered for reusable surface insulation (RSI) were also considered for use as an antenna window, both behind the high density outer antenna window and as a single material antenna window. In both cases, good RF transmission characteristics are required. A waterproof

TABLE II
HIGH DENSITY ANTENNA WINDOW MATERIAL PROPERTIES

MATERIAL	PURITY %	DENSITY (KG/M3)	DIELECTRIC CONSTANT AND LOSS TANGENT				YOUNG'S MODULUS. N/M2 (PSI)
			DIELECTRIC CONSTANT	LOSS TANGENT	TEMPERATURE °C (°F)	FREQUENCY (MHz)	
ALUMINA (Al_2O_3) AD--99 (COORS)	99	3830	9.5 10.5	0.0002 0.0006	ROOM 1073 (1472)	10 000 10 000	3.45×10^{11} (50×10^6) 3.38×10^{11} (49×10^6) AT 810°K (1000°F)
BERYLLIA (BeO) BD--98 (COORS)	98	2850	6.6 7.6	0.0006 0.0008	ROOM 1073 (1472)	10 000 10 000	3.10×10^{11} (45×10^6)
MAGNESIA (MgO)	90--99.5	3420	9.5 10.8	0.0001 0.0001	ROOM 1283 (1850)	9375 9375	2.07×10^{11} (30×10^6) 1.72×10^{11} (25×10^6) AT 810°K (1000°F)
PYROCERAM (GLASS-CERAMIC)	NA	2600	5.5 5.5	0.00033 0.004	ROOM 973 (1292)	8500 8500	1.24×10^{11} (7×10^6)
SLIP CAST FUSED SILICA	98.5--99.5	1980	3.38 3.54	0.0006 0.003	ROOM 1473 (2192)	10 000 10 000	4.83×10^{10} (10×10^6)
CLEAR VITREOUS SILICA	>99.5	2200	3.82 4.00	0.0002 0.0003	ROOM 1673 (2552)	6100 6100	6.89×10^{10} (10×10^6)
ISOTROPIC PYROLYTIC BORON NITRIDE (IPBN)	>99.5	1220	3.01 3.01	0.0015 0.0006	ROOM 1473 (2192)	10 000 10 000	1.21×10^{10} (1.75×10^6)
ANISOTROPIC PYROLYTIC BORON NITRIDE (BORALLOY)	>99.5	2200	5.12 5.24 3.4	0.00015 0.00039 0.0001	ROOM 1673 (2552) (BOTH ⊥ TO PD) ROOM (II TO PD)	4000 4000 4000	2.07×10^{10} (3×10^6) (⊥ TO PD)
BORON NITRIDE HD0092 (UNION CARBIDE)	98.5	1990	4.08 4.24 4.04 4.20	0.00026 0.0046 0.003 0.0005	ROOM 1743 (2678) ROOM 1473 (2192)	4400 4500 10 000 10 000	4.83×10^{10} (7×10^6) (II TO PD)
SILICON NITRIDE (REACTION SINTERED)	98.0	2200 TO 2400	5.5 5.6	0.0002 0.0065	ROOM 1255 (1800)	8000 8000	1.39×10^{11} (20×10^6)
3-D SILICA COMPOSITE	98.5	1680 TO 1710	2.9 2.9	0.01 MAX 0.008	ROOM 1272 (1830)	8520 8520	1.72×10^{11} (2.5×10^6) (II AND ⊥ TO RADIALS)
			NOT DRIED BEFORE TEST				

(Table Continued on Next Page)

TABLE II (Continued)
HIGH DENSITY ANTENNA WINDOW MATERIAL PROPERTIES

MATERIAL	TENSILE STRENGTH N/M^2 (PSI)	COMPRESSIVE STRENGTH N/M^2 (PSI)	MODULUS OF RUPTURE N/M^2 (PSI)	COEFFICIENT OF THERMAL EXPANSION M/M/°K (IN./IN./°F)
ALUMINIA (Al_2O_3) AD–99 (COORS)	2.41×10^8 (35×10^3) 1.52×10^8 (22×10^3) AT 1366°K (2000°F)	2.07×10^9 (300×10^3)	3.59×10^8 (52×10^3) 1.72×10^8 (25×10^3) AT 1366°K (2000°F)	6.0×10^{-6} (3.3×10^{-6})
BERYLLIA (BeO) BD–98 (COORS)	1.17×10^8 (17×10^3) 8.27×10^5 (1.2×10^2) AT 1644°K (2500°F)	1.55×10^9 (225×10^3)	1.86×10^8 (27×10^3) 8.96×10^7 (13×10^3) AT 1366°K (2000°F)	5.8×10^{-6} (3.2×10^{-6})
MAGNESIA (MgO)	8.27×10^7 (12×10^3) TO 1089°K (1500°F) 3.45×10^7 (5×10^3) AT 1644°K (2500°F)	1.39×10^9 (200×10^3)	1.39×10^8 (20×10^3) 6.90×10^7 (10×10^3) AT 1644°K (2500°F)	14.0×10^{-6} (7.8×10^{-6})
PYROCERAM (GLASS-CERAMIC)	ND	2.07×10^9 (300×10^3) (EST)	2.41×10^8 (35×10^3) 6.89×10^7 (10×10^3) AT 1283°K (1850°F)	5.8×10^{-6} (3.2×10^{-6})
SLIP CAST FUSED SILICA	1.39×10^7 (2×10^3)	1.39×10^8 (20×10^3)	2.76×10^7 (4×10^3)	0.5×10^{-6} (0.3×10^{-6})
CLEAR VITREOUS SILICA	ND	1.03×10^9 (150×10^3)	4.83×10^7 (7×10^3) 6.89×10^7 (10×10^3) AT 1311°K (1900°F)	0.5×10^{-6} (0.3×10^{-6})
ISOTROPIC PYROLYTIC BORON NITRIDE(IPBN)	7.58×10^7 (11×10^3)	2.28×10^8 (33×10^3)	9.65×10^7 (14×10^3) 1.17×10^8 (17×10^3) AT 1978°F (3100°F)	7.2×10^{-6} (4×10^{-6})
ANISOTROPIC PYROLYTIC BORON NITRIDE (BORALLOY)	4.14×10^7 (6×10^3) (⊥ TO PD)	4.96×10^7 (72×10^3)	1.03×10^8 (15×10^3)	3.2×10^{-6} (1.8×10^{-6}) AT 373–1273°K (212–1832°F) (⊥ TO PD) 8×10^{-6} (45×10^{-6}) II TO PD
BORON NITRIDE HD0092(UNION CARBIDE)	ND	4.14×10^7 (6×10^3) II TO PD 5.17×10^7 (7.5×10^3) ⊥ TO PD	4.14×10^7 (6×10^3) 5.52×10^7 (8×10^3) AT 1473°K (2192°F)	1×10^{-6} (0.56×10^{-6})
SILICON NITRIDE (REACTION SINTERED)	1.17×10^8 (17×10^3)	4.14×10^8 (60×10^3)	1.72×10^8 (25×10^3) 1.39×10^8 (20×10^3) AT 1572°K (2370°F)	3.6×10^{-6} (2×10^{-6})
3–D SILICA COMPOSITE	ND	1.45×10^7 (2.1×10^3)	2.76×10^6 (0.4×10^3)	ND

(Table Continued on Next Page)

TABLE II (Concluded)
HIGH DENSITY ANTENNA WINDOW MATERIAL PROPERTIES

MATERIAL	THERMAL CONDUCTIVITY W/M^{0}K (BTU-IN./FT^{2}-HR-^{0}F)	SPECIFIC HEAT J/KG^{0}K (BTU/LB-^{0}F)	EMITTANCE (NORMAL)	MELTING TEMPERATURE ^{0}K (^{0}F) (3)
ALUMINA (Al_2O_3) AD-99 (COORS)	29.3 (203) 6.3 (44) AT 1073^{0}K (1472^{0}F)	8.79 x 10^{2} (0.21) AT 373^{0}K (212^{0}F)	0.79 0.5 AT 1366^{0}K (2000^{0}F)	2311 (3700)
BERYLLIA (BeO) BD-98 (COORS)	205.0 (1422) 25.1 (174) AT 1073^{0}K (1472^{0})	1.30 x 10^{3} (0.31) AT 373^{0}K (212^{0}F) 1.26 x 10^{3} (0.30) AT 373^{0}K (212^{0}F)	0.60 0.33 AT 1144^{0}K (1600^{0}F)	2839 (4650)
MAGNESIA (MgO)	43.3 (300)	1.17 x 10^{3} (0.28) AT 373^{0}K (212^{0}F)	ND	3072 (5070)
PYROCERAM (GLASS-CERAMIC)	3.3 (23)	9.76 x 10^{2} (.233)	0.85	1670 (2600)(EST)
SLIP CAST FUSED SILICA	0.58 (4)	9.21 x 10^{2} (0.22)	0.84	1978 (3100)
CLEAR VITREOUS SILICA	6.9 (48)	7.12 x 10^{2} (0.17)	0.84	1978 (3100)(EST)
ISOTROPIC PYROLYTIC BORON NITRIDE(IPBN)	18.7 (130) AT 573^{0}K (572^{0}F)	1.21 x 10^{3} (0.29)	0.80	3255 (5400) (SUBLIMES IN INERT ATMOSPHERE)
ANISOTROPIC PYROLYTIC BORON NITRIDE (BORALLOY)	1.66 (11.5) II TO PD AT 373^{0}K (212^{0}F) 62.9 (435) ⊥ TO PD AT 373^{0}K (212^{0}F)	1.00 x 10^{3} (0.24)	0.80	3255 (5400) (SUBLIMES IN INERT ATMOSPHERE)
BORON NITRIDE &D0092(UNION CARBIDE)	1.83 (127) 13.8 (96) AT 810^{0}K (1000^{0}F) 9.4 (65) AT 1366^{0}K (2000^{0}F) ALL II TO PD	1.93 x 10^{2} (0.193)	0.93	3255 (5400) (SUBLIMES IN INERT ATMOSPHERE)
SILICON NITRIDE (REACTION SINTERED)	10.1 (70) AT 1172^{0}K (1650^{0}F)	1.05 x 10^{3} (0.25)	0.75-0.80 (EST)	2172 (3450) DISSOCIATES)
3-D SILICA COMPOSITE	1.44 (10)(EST)	8.37 x10^{2} (0.20) (EST)	0.80 (EST)	1978 (3100)

NOTES:
1. ND = NO DATA
2. ALL PROPERTIES AT ROOM TEMPERATURE UNLESS OTHERWISE NOTED;
3. THE MELTING TEMPERATURE DOES NOT IMPLY MAXIMUM USE TEMPERATURE. THE MAXIMUM USE TEMPERATURE WILL BE LESS AND IS AFFECTED BY SEVERAL FACTORS SUCH AS PURITY, PROCESSING AND CONFIGURATION OF THE MATERIAL
4. EST = ESTIMATED
5. NA = NOT APPLICABLE
6. II = PARALLEL; ⊥ = PERPENDICULAR
7. PD = PRESSING DIRECTION

TABLE III
HIGH DENSITY ANTENNA WINDOW MATERIAL COMPARISONS

TRADEOFF CRITERIA	ALUMINA (Al_2O_3)	BERYLLIA (BeO)	MAGNESIA (MgO)	PYROCERAM (GLASS-CERAMIC)	SLIP CAST FUSED SILICA (SiO_2)	CLEAR FUSED SILICA (SiO_2)	ISOTROPIC PYROLYTIC BORON NITRIDE (IPBN) (BN)	ANISOTROPIC PYROLYTIC BORON NITRIDE (APBN) (BN)	HOT PRESSED BORON NITRIDE (HD0092) (BN)	SILICON NITRIDE (REACTION SINTERED Si_3N_4)	3D SILICA COMPOSITE (AS3DX) (SiO_2)
MAXIMUM TEMPERATURE RECYCLING CAPABILITY, ^0K (^0F)	> 1533 (2300)	> 1533 (2300)	> 1533 (2300)	1283 (1850)	1366 (2000)	1366 (2000)	> 1533 (2300)	> 1533 (2300)	> 1533 (2300)	> 1478 (2200) (EST)	> 1366 (2000) (EST)
THERMAL SHOCK RESISTANCE	POOR	GOOD	POOR	GOOD	EXCELLENT	EXCELLENT	GOOD	EXCELLENT	EXCELLENT	GOOD	GOOD
THERMAL PROPERTIES FOR DESIGN (CONDUCTIVITY)	MEDIUM CONDUCTIVITY	VERY HIGH CONDUCTIVITY	HIGH CONDUCTIVITY	LOW CONDUCTIVITY	VERY LOW CONDUCTIVITY	MEDIUM CONDUCTIVITY	MEDIUM CONDUCTIVITY	VERY LOW CONDUCTIVITY (C DIRECTION)	HIGH CONDUCTIVITY	LOW CONDUCTIVITY	VERY LOW CONDUCTIVITY
MECHANICAL PROPERTIES FOR DESIGN	EXCELLENT	EXCELLENT	GOOD	GOOD	GOOD	GOOD	GOOD	GOOD	FAIR	GOOD	FAIR
LOW TEMPERATURE STABILITY	ALL RATED GOOD TO EXCELLENT										
VACUUM STABILITY	ALL RATED GOOD TO EXCELLENT										
MOISTURE RESISTANCE	IMPERVIOUS	IMPERVIOUS	ABSORBS	IMPERVIOUS	ABSORBS	IMPERVIOUS	ABSORBS (VERY LOW RATE)	IMPERVIOUS	ABSORBS (LOW RATE)	IMPERVIOUS	ABSORBS
OXIDATION RESISTANCE (BELOW 1533^0K (2300^0F))	EXCELLENT	EXCELLENT	EXCELLENT	EXCELLENT	EXCELLENT	EXCELLENT	GOOD	GOOD	GOOD	GOOD	EXCELLENT
IMPACT RESISTANCE	EXCELLENT	EXCELLENT	GOOD	GOOD	FAIR	GOOD	GOOD	EXCELLENT	FAIR	GOOD	GOOD
RAIN AND DUST EROSION RESISTANCE (SUBSONIC)	EXCELLENT	EXCELLENT	FAIR	EXCELLENT	FAIR	GOOD	GOOD (EST)	EXCELLENT (EST)	FAIR (EST)	GOOD	GOOD
ELECTRICAL PROPERTIES FOR DESIGN	GOOD	GOOD	FAIR	GOOD	EXCELLENT	EXCELLENT	EXCELLENT	EXCELLENT	EXCELLENT	GOOD	FAIR
COMMERCIAL AVAILABILITY	AVAILABLE	AVAILABLE	AVAILABLE	AVAILABLE	AVAILABLE	AVAILABLE	AVAILABLE	AVAILABLE	DEVELOPMENT QUANTITIES	DEVELOPMENT QUANTITIES	DEVELOPMENT QUANTITIES
SHAPE AND DIMENSION LIMITATIONS (FOR SHUTTLE ANTENNA CONFIGURATIONS)	NONE	NONE	NONE	NONE	NONE	NONE	SURFACE AND THICKNESS DIMENSION LIMITATION	SEVERELY LIMITED IN SURFACE AND THICKNESS AVAILABLE	NONE	NONE	NONE
COST (COMPARED TO LOWEST IN THIS LINE)	LOW	LOW	LOW	LOW	LOWEST (STANDARD)	MODERATE	HIGH	VERY HIGH	HIGH	MODERATE	VERY HIGH
MACHINABILITY (STANDARD CERAMIC PROCEDURES)	GOOD	GOOD (REQUIRES SPECIAL HANDLING)	GOOD	FAIR	GOOD	GOOD	GOOD	FAIR	EXCELLENT	GOOD	FAIR
COMPATIBILITY WITH OTHER MATERIALS (NONRECEDING BELOW 1644^0K (2500^0F))	ALL CANDIDATES NONRECEDING										
SPECIAL HANDLING PROVISIONS (OTHER THAN NORMAL CERAMIC HANDLING)	NONE	REQUIRES SPECIAL HANDLING	NONE	NONE	MOISTURE ISOLATION RECOMMENDED	NONE	MOISTURE ISOLATION RECOMMENDED	NONE	MOISTURE ISOLATION RECOMMENDED	NONE	MOISTURE ISOLATION RECOMMENDED

NOTES: EST = ESTIMATED

TABLE IV
ANTENNA WINDOW/THERMAL PROTECTION SYSTEM MATERIALS PROPERTIES

MATERIAL	DENSITY KG/M^3	DIELECTRIC CONSTANT AND LOSS TANGENT				YOUNG'S MODULUS N/M^2 (PSI)
		DIELECTRIC CONSTANT	LOSS TANGENT	TEMPERATURE ^oK (^oF)	FREQUENCY (MHz)	
MULLITE-RSI (MDC MOD IIIA HCF)	240 ± 15	1.20 1.28	0.002 0.062	ROOM 1473 (2192)	10 000 10 000	5.1×10^8 (7.4×10^4) II TEN (8) 3.9×10^8 (5.6×10^4) II COMP 9.7×10^7 (1.4×10^4) ⊥ TEN 8.3×10^7 (1.2×10^4) ⊥ COMP
MULLITE-RSI (MDC MOD V HCF)	240 ± 48	1.31 1.42	0.003 0.085	ROOM 1473 (2192)	9050 9050	7.1×10^8 (10.3×10^4) II TEN 1.8×10^8 (2.6×10^4) ⊥ TEN
MULLITE-RSI (G.E. MOD IA REI)	185	1.19 1.21	0.0002 0.0066	ROOM 1473 (2192)	10 000 10 000	3.0×10^8 (4.4×10^4) II TEN (8) 3.7×10^8 (5.4×10^4) II COMP
SILICA-RSI (LOCKHEED LI-1500)	252	1.23 1.25	0.00024 0.0011	ROOM 1473 (2192)	10 000 10 000	6.9×10^8 (10×10^4) II TEN (8) 7.6×10^8 (11.1×10^4) II COMP 6.9×10^7 (1×10^4) ⊥ TEN 6.2×10^7 (0.9×10^4) ⊥ COMP
FI-600 (LOCKHEED)	96.5	1.06 (EST) 1.06 (EST)	0.0001 (EST) 0.0002 (EST)	ROOM 1473 (2192)	10 000 10 000	NA
DYNAQUARTZ (JOHNS-MANVILLE)	160	1.11 1.12 1.13	0.0006 0.003 0.007	ROOM 873 (1112) 1473 (2192)	10 000 10 000 10 000	3.4×10^5 (50) (EST)
MICROQUARTZ (JOHNS-MANVILLE)	56	1.06 (UNCOM-PRESSED)	0.0027 (UNCOMPRESSED)	ROOM	13 400	NA
SLA-561 (MARTIN)	VIRGIN 232 CHAR 128	1.30	0.0083 (VIRGIN)	ROOM	10 000	1.896×10^7 (2750)
SLA-220 (MARTIN)	VIRGIN 250 CHAR 188	1.31	0.005 (VIRGIN)	ROOM	10 000	2.027×10^7 (2940)
SILICA FOAM (GLASROCK OR NORTON)	705-800	1.70	< 0.0005	ROOM	60×10^{-6} TO 10^4	$4.8-5.5 \times 10^9$ ($0.7-0.8 \times 10^6$)
	352-448	1.40	< 0.0005	ROOM	60×10^{-6} TO 10^4	$2.1-2.8 \times 10^9$ ($0.3-0.4 \times 10^6$)

NOTES:

1. ND = NO DATA; EST = ESTIMATED; NA = NOT APPLICABLE.
2. ALL PROPERTIES AT ROOM TEMPERATURE UNLESS OTHERWISE NOTED.
3. THE MELTING TEMPERATURE DOES NOT IMPLY MAXIMUM USE TEMPERATURE. THE MAXIMUM USE TEMPERATURE WILL BE LESS AND IS AFFECTED BY SEVERAL FACTORS SUCH AS PURITY, PROCESSING AND CONFIGURATION OF THE MATERIAL.

(Table Continued on Next Page)

TABLE IV (Continued)
ANTENNA WINDOW/THERMAL PROTECTION SYSTEM MATERIALS PROPERTIES

MATERIAL	TENSILE STRENGTH N/M^2 (PSI)	COMPRESSIVE STRENGTH N/M^2 (PSI)	MODULUS OF RUPTURE N/M^2 (PSI)	COEFFICIENT OF THERMAL EXPANSION $M/M/^oK$ (IN./IN./^oF)
MULLITE-RSI (MDC MOD IIIA HCF)	6.8×10^5 (98) II (8) 2.3×10^5 (33) ⊥ (STRAIN TO FAILURE = 0.14%)	1.01×10^6 (146) II (8) 3.72×10^5 (54) ⊥	6.89×10^5 (100) (EST)	5.4×10^{-6} (3.0×10^{-6})
MULLITE-RSI (MDC MOD V HCF)	1.70×10^6 (247) II 7.31×10^5 (106) ⊥	ND	ND	5.4×10^{-6} (3.0×10^{-6}) (EST)
MULLITE-RSI (G.E. MOD IA REI)	4.0×10^5 (58) II (8) 1.7×10^5 (25) ⊥	7.79×10^5 (113) II (8) 2.55×10^5 (37) ⊥	4.14×10^5 (60) (EST)	5.2×10^{-6} (2.9×10^{-6})
SILICA-RSI (LOCKHEED LI-1500)	7.9×10^5 (115) II (8) 1.2×10^5 (18) ⊥ (STRAIN TO FAILURE = 0.12%)	1.86×10^6 (270) II (8) 3.24×10^5 (47) ⊥	7.93×10^5 (115)	0.54×10^{-6} (0.3×10^{-6})
FI-600 (LOCKHEED)	NA	NA	NA	0.54×10^{-6} (0.3×10^{-6})(EST)
DYNAQUARTZ (JOHNS-MANVILLE)	6.2×10^5 (90)	3.45×10^5 (50) (EST) WITH DEFLECTION	ND	0.54×10^{-6} (0.3×10^{-6})(EST)
MICROQUARTZ (JOHNS-MANVILLE)	NA	NA	NA	N/A
SLA-561 (MARTIN)	2.27×10^6(329) AT 133°K (-220°F) 1.86×10^5 (27) AT 366°K (+200°F)	ND	ND	29.5×10^{-6} (16.4×10^{-6})
SLA-220 (MARTIN)	5.46×10^5 (79.2)	7.58×10^5 (110)	ND	21.1×10^{-6} (11.7×10^{-6})
SILICA FOAM (GLASROCK OR NORTON)	ND	> 6.89×10^6 (1000)	$3.45-5.17 \times 10^6$ (500-750)	0.54×10^{-6} (0.3×10^{-6})
	ND	> 3.45×10^6 (500)	$1.39-2.07 \times 10^6$ (200-300)	0.54×10^{-6} (0.3×10^{-6})

NOTES CONTINUED:

4. TEN = TENSION
5. COMP = COMPRESSION
6. II = PARALLEL = NOTED STRESS APPLIED PARALLEL TO THE LONG AXES OF THE FIBERS.

(Table Continued on Next Page)

TABLE IV (Concluded)
ANTENNA WINDOW/THERMAL PROTECTION SYSTEM MATERIALS PROPERTIES

MATERIAL	THERMAL CONDUCTIVITY W/M^{0}K (BTU-IN/FT^{2}-HR-^{0}F)	SPECIFIC HEAT J/KG^{0}K (BTU/LB-^{0}F)	EMITTANCE (NORMAL)	MELTING ③ TEMP ^{0}K (^{0}F)	REMARKS
MULLITE-RSI (MDC MOD IIIA HCF)	0.384 (2.66) AT 1366^{0}K (2000^{0}F)	1.05 x 10^{3} (0.25) AT 1422^{0}K (2100^{0}F)	> 0.8	1866 (2900)	PRODUCTION MATERIAL
MULLITE-RSI (MDC MOD V HCF)	0.303 (2.1) (EST) AT 1366^{0}K (2000^{0}F)	9.63 x 10^{2} (0.23) EST	ND	1866 (2900)	IN PILOT PLANT PRODUCTION
MULLITE-RSI (G.E. MOD IA REI)	0.101 (0.7) AT 533^{0}K (500^{0}F) 0.387 (2.7) AT 1366^{0}K (2000^{0}F)	6.82 x 10^{2} (0.163) AT 255^{0}K (0^{0}F) 1.34 x 10^{3} (0.32) AT 922^{0}K (1200^{0}F)	0.65 TO 0.75	ND	–
SILICA-RSI (LOCKHEED LI-1500)	0.225 (1.56) AT 1366^{0}K (2000^{0}F)	1.34 x 10^{3} (0.32) AT 1366^{0}K (2000^{0}F)	0.85 0.95 AT 1366 (2000)	1978 (3100)	PRODUCTION MATERIAL
FI-600 (LOCKHEED)	0.120 (0.83) AT 811^{0}K (1000^{0}F)	1.34 x 10^{3} (0.32) AT 1366^{0}K (2000^{0}F)	0.8 (EST)	1978 (3100)	THIS MATERIAL IS A RESILIENT FORM OF LI-1500 USED IN TILE JOINTS
DYNAQUARTZ (JOHNS-MANVILLE)	0.095 (0.68) AT 811^{0}K (1000^{0}F)	1.13 x 10^{3} (0.27) AT 811 ^{0}K (1000) ^{0}F)	0.84	1978 (3100)	SEMIRIGID 99% SiO_2; SHRINKAGE <1% AT 1783^{0}K (2750^{0}F) FOR 24 HOURS; DEFLECTION 8% AT 1.39 x 10^{5} N/M^{2} (20 PSI)
MICROQUARTZ (JOHNS-MANVILLE)	0.098 (0.68) AT 811^{0}K (1000^{0}F)	1.13 x 10^{3} (0.27) (EST) AT 811^{0}K (1000^{0}F)	> 0.8	1978 (3100)	FELT MATERIAL. FLEXIBLE. 98.5% SiO_2. SHRINKAGE 4% AT 1089^{0}K 1500^{0}F)
SLA-561 (MARTIN)	0.063 (0.44) AT 444^{0}K (340^{0}F)	1.26 x 10^{3} (0.30) VIRGIN 1.55 x 10^{3} (0.37) CHAR	0.7 VIRGIN 0.9 CHAR	NA	A SILICONE BASED ABLATION MATERIAL.
SLA-220 (MARTIN)	0.079 (0.55) VIRGIN (EST)	1.51 x 10^{3} (0.36) VIRGIN (EST) 9.63 x 10^{3} (0.23) CHAR	0.85 VIRGIN 0.84 CHAR	NA	A SILICONE BASED ABLATION MATERIAL.
SILICA FOAM (GLASROCK OR NORTON)	0.202 (1.4) AT 811^{0}K (1000^{0}F)	9.63 x 10^{3} (0.23) AT 811^{0}K (1000^{0}F)	> 0.8	1978 (3100)	COMMERCIALLY AVAILABLE PURITY–98.5% SiO_2 (MINIMUM) POROSITY–63 TO 68%, OPEN CELL
	0.144 (1.0) AT 811^{0}K (1000^{0}F)	9.63 x 10^{3} (0.23) AT 811^{0}K (1000^{0}F)	> 0.8	1978 (3100)	COMMERCIALLY AVAILABLE PURITY–98.5% SiO_2 (MINIMUM) POROSITY–80 TO 84%, OPEN CELL

NOTES CONCLUDED:

7. ⊥ = PERPENDICULAR = NOTED STRESS APPLIED PERPENDICULAR TO THE LONG AXES OF THE FIBERS.
8. "EVALUATION OF NONMETALLIC THERMAL PROTECTION MATERIALS FOR THE MANNED SPACE SHUTTLE," VOLUME V, BATTELLE, MEMORIAL INST, 1 JUNE 1972.

coating is required to prevent the absorption of water since these low density RSI materials are highly porous and readily absorb liquids. Table IV is a list of the materials and an overview of the material properties which were considered in this study. The detailed material properties, which were used in the thermal and strength analyses, are listed in Appendix A. The trade-off criteria and evaluation results are listed in table V.

Selected low density material - The low density material selected for an RSI type antenna window is Lockheed's LI-1500. This is a silica fiber based material with an inorganic binder and a waterproof surface coating. The surface coating is a silicate material which is compatible with the low thermal expansion coefficient of the LI-1500. The RSI is fabricated into small 15.24 x 15.24 to 30.48 x 30.48 cm (6 x 6 to 12 x 12 in.) tiles and the recessed joints filled with FI-600 strips. The FI-600 is less dense and more resilient and compressible (without crushing) than the LI-1500 material. The FI-600 is also silica fiber based and is impregnated with a silicone resin for waterproofing.

The loss tangent of the LI-1500 is considerably lower at elevated temperatures than that of either of the other two RSI candidates (GE REI and MDC HCF) while the dielectric constant is comparable as shown in table IV. Therefore, LI-1500 can be expected to give the best RF Transmission characteristics.

Attachment materials - In order to attach the RSI materials to the Orbiter structure and provide an RF transparent window, additional materials are required. These include adhesives, strain isolator sponge, and an RF transparent structural panel. The RSI material (LI-1500) is a rigid material, and therefore, provision must be made to isolate it from thermally and mechanically induced strains of the structure to which it is attached. In the selected design the window back structure is a rigid, RF transparent, fiberglass-phenolic sandwich. A silicone sponge material (RL-524 type S-105) was selected as the strain isolator primarily because of its low temperature stiffening point and because of the working knowledge obtained by using it on a related program with NASA-MSC. The material properties of RL-524 are summarized in table VI

The sponge material is bonded to the RSI material and to the aluminum Orbiter structure or fiberglass-phenolic window substructure, with RTV-560, a General Electric silicone elastomeric adhesive. This silicone is iron oxide filled (red in color) for high temperature stability and uses a methyl-phenyl silicone polymer which gives it its low temperature flexibility. The RTV-560 properties are summarized in table VI.

The RF transparent structural panel is a fiberglass-phenolic honeycomb sandwich composed of a fiberglass cloth impregnated with a phenolic binder. The face sheets consisted of three layers of fiberglass cloth laminated with their warp direction oriented at 0, 30, and 60 degrees to provide uniform strength properties in all directions. These face sheets are bonded to a 56.1 kg/m^3 (3.5 lb/ft^3), 6.35 mm (0.25 in.) hexagonal cell, fiberglass-phenolic honeycomb core manufactured by the Hexcel Company. The bonding material is HT-435 (American Cynanamic Co.) which is specially formulated for RF transmission. Structural adhesives for applications such as this are usually formulated with an aluminum metal powder for high temperature strength; however,

TABLE V
ANTENNA WINDOW/INSULATION MATERIAL COMPARISON

TRADEOFF CRITERIA	SILICA FOAM (801 KG/M^3)	SILICA FOAM (400 KG/M^3)	MICROQUARTZ	DYNAQUARTZ	MULLITE-RSI (MDC MOD IIIA HCF)	SILICA-RSI (LOCKHEED LI-1500)	MULLITE --RSI (G.E. MOD IA REI)	MULLITE - RSI (MDC MOD V HCF)	SILICONE ABLATOR (MARTIN SLA-220)	FI-600 (LOCKHEED)	REMARKS
MAXIMUM TEMPERATURE RECYCLING CAPABILITY, ^{0}K (^{0}F)	1255 (1800)	1255 (1800)	1255 (1800)	1255 (1800)	1644 (2500)	1533 (2300)	1644 (2500)	1644 (2500)	644 (700)	589 (600)	BASED ON ONE SIDE, TRAJECTORY SIMULATION HEATING
THERMAL SHOCK RESISTANCE	ALL GOOD TO EXCELLENT										BASED ON THERMAL CONDUCTIVITY
THERMAL PROPERTIES FOR DESIGN	ALL GOOD TO EXCELLENT										
MECHANICAL PROPERTIES FOR DESIGN	VERY GOOD	GOOD	POOR	GOOD	GOOD	GOOD	GOOD	GOOD	BEST	POOR	AS A LOAD BEARING INSULATOR
LOW TEMPERATURE STABILITY	ALL GOOD TO EXCELLENT										
VACUUM STABILITY	ALL GOOD TO EXCELLENT										
MOISTURE RESISTANCE	FAIR TO POOR								GOOD	GOOD	
OXIDATION RESISTANCE (BELOW 1533^{0}K (2300^{0}F))	GOOD TO EXCELLENT								POOR TO GOOD	GOOD TO EXCELLENT	
IMPACT RESISTANCE	ALL FAIR TO POOR										
RAIN AND DUST EROSION RESISTANCE (SUBSONIC)	ALL POOR										
ELECTRICAL PROPERTIES FOR DESIGN	EXCELLENT	EXCELLENT	GOOD TO EXCELLENT (ESTIMATE)	GOOD TO EXCELLENT	GOOD--ROOM TEMPERATURE THRU 589^{0}K (600^{0}F) FAIR 589^{0}K (600^{0}F) THRU 1366^{0}K (2000^{0}F)	EXCELLENT	GOOD--ROOM TEMPERATURE THRU 589^{0}K (600^{0}F) FAIR 589^{0}K (600^{0}F) THRU 1366^{0}K (2000^{0}F)	GOOD--ROOM TEMPERATURE THRU 589^{0}K (600^{0}F) FAIR 589^{0}K (600^{0}F) THRU 1366^{0}K (2000^{0}F)	EXCELLENT BEFORE CHARRING; FAIR AFTER CHARRING	CARBON FROM SILICONE IMPREGNANT COULD CAUSE PROBLEMS	ROOM TEMPERATURES THRU 1366^{0}K (2000^{0}F)
COMMERCIAL AVAILABILITY	AVAILABLE	AVAILABLE	AVAILABLE	AVAILABLE	DEVELOPMENT QUANTITIES	DEVELOPMENT QUANTITIES	DEVELOPMENT QUANTITIES	DEVELOPMENT QUANTITIES	AVAILABLE	DEVELOPMENT QUANTITIES	
SHAPE AND DIMENSION LIMITATION (FOR SHUTTLE ANTENNA CONFIGURATIONS)	NONE	NONE	NONE	NONE	NONE	NONE	NONE	NONE	NONE	NONE	
COST(COMPARED TO LOW COST SILICA FOAM)	LOWEST (STANDARD)	LOWEST (STANDARD)	LOW	MODERATE	HIGH	HIGH	HIGH	HIGH	MODERATE	HIGH	
MACHINABILITY OR CUT-ABILITY (STANDARD CERAMIC PROCEDURES	GOOD	GOOD	NOT APPLICABLE	GOOD	GOOD	GOOD	GOOD	GOOD	GOOD	GOOD	
COMPATIBILITY WITH OTHER MATERIALS (BELOW 1255^{0}K (1800^{0}F))	FULLY COMPATIBLE WITH ANTENNA WINDOW MATERIALS										
SPECIAL HANDLING PROVISIONS (OTHER THAN NORMAL CERAMIC HANDLING)	REQUIRE ISOLATION FROM MOISTURE BEARING ENVIRONMENTS								NONE	NONE	

no aluminum is used HT-435 in order to permit RF transmission. The properites of these materials are summarized in table VI.

ANTENNA WINDOW DESIGN

Antenna window designs for this program were developed using conceptual design and structural integration studies in conjunction with electrical design tests. First sketches were prepared to show details which were incorporated to meet the expected structural integration, thermal and electrical requirements. These preliminary designs were supported by a one-dimensional thermal analysis to establish thickness requirements for both the antenna windows and surrounding TPS. Electrical mock-ups were then constructed using these designs as baseline configurations. Radiation pattern and impedance measurements were made for suitable antennas covered with the antenna windows to evaluate the electrical performance of each antenna window configuration. These measurement results were compared with those of the same antenna mounted in a ground plane without window or simulated TPS. The window diameters, window thickness and TPS thickness were varied to determine both the optimum antenna window configuration and the limitation of each antenna window approach. One of the primary goals was to obtain a antenna window configuration which yielded both acceptable antenna system radiation patterns and input impedances over the operating frequency bands.

Additional analyses and measurements were made to characterize antenna window transmission loss, antenna transfer characteristics, and antenna system impedance matching.

Description of Antenna Window Configurations

Preliminary designs were made to evaluate the antenna window approach. These designs were based on an L-band annular slot antenna, and are generally applicable to the C-band horn and slot antennas; however, the window area and shape for those configurations would be determined from their particular radiating apertures.

Single-layer RSI window. - Preliminary designs for two (2) antenna window configurations using a single-layer of RSI are shown in figures 16 and 17.

Figure 16 shows a large RSI window, including a window edge enclosure concept. In this design the attachment provisions are placed inside the window edge enclosure boundry. Figure 17 shows a minimum size RSI window with a window edge enclosure and attachment provisions external to the enclosure. The RSI is based on Lockheed's LI-1500 (see section on ANTENNA WINDOW MATERIALS SELECTION) which is bonded to a fiberglass phenolic honeycomb panel with RTV-560. The honeycomb panel provides: 1) structural support for the LI-1500; 2) a means for attaching the window to the Orbiter structure; 3) low RF transmission losses (see section Antenna Window Transmission Losses); and 4) can be used to temperatures of 533°K (500°F) without degradation.

TABLE VI
STRAIN ISOLATOR FOAMS, ADHESIVES, & RF TRANSPARENT STRUCTURE

MATERIAL	DENSITY KG/M^3	DIELECTRIC CONSTANT	LOSS TANGENT	TENSILE STRENGTH N/M^2 (PSI)	COEFFICIENT OF THERMAL EXPANSION $M/M/^oK$ (IN./IN./^oF)	THERMAL CONDUCTIVITY W/M^oK (BTU-IN. FT^2-HR-^oF)	SPECIFIC HEAT WS/KG ^oK (BTU/LB-^oF)	LOW TEMPERATURE STIFFENING POINT ^oK (^oF)	DEGRADATION TEMPERATURE ^oK (^oF)	REMARKS
PD-200	450	ND	ND	1.21×10^6 (175) AT 339°K (-150°F) 1.09×10^5 (15.8) AT 422°K (300°F) 6.07×10^4 (8.8) AT 616°K (650°F)	360×10^{-6} (200×10^{-6})	0.124 (0.86)	9.63×10^2 (0.23) AT 144°K (-200°F) 1.67×10^3 (0.4) AT 700°K (800°F)	164 (-165) (EST)	533 (500)	GENERAL ELECTRIC'S STRAIN ISOLATOR
RL-524; COMPOUND NO. S-105 (RAYBESTOS MANHATTAN)	480 ± 80	1.69 AT 323°K (122°F) 1.61 AT 429°K (312°F)	0.013 AT 323°K (122°F) 0.003 AT 429°K (312°F)	5.31×10^5 (77)	229×10^{-6} (127×10^{-6})	0.208 (1.44)	1.34×10^3 (0.32)	164 (-165)	533 (500)	MDC'S BASELINE STRAIN ISOLATOR; A LOW STIFFENING POINT SILICONE
RTV-560 (GENERAL ELECTRIC)	1420	4.4 AT 60 Hz 4.2 AT 10^5 Hz	0.006 AT 60 HZ 0.001 AT 10^5 Hz	4.90×10^6 (710)	205×10^{-6} (114×10^{-6})	0.311 (2.16)	1.34×10^3 (0.32)	164 (-165)	533 (500)	A FLEXIBLE, IRON OXIDE FILLED, SILICONE ADHESIVE
HONEYCOMB: FIBERGLASS - PHENOLIC	56	1.1 (EST)	0.001 (EST)	NA	ND	0.173 (1.2)	9.63×10^2 (0.23)	NA	533 (500)	1/4 INCH HEXAGONAL CELLS
FACE SHEETS: FIBERGLASS - PHENOLIC	2500	5 (EST)	0.02 (EST)	2.76×10^8 (4×10^4) IN PLANE	8.1×10^{-6} (4.5×10^{-6}) IN PLANE	0.173 (1.2)	9.63×10^2 (0.23)	NA	533 (500)	USED ON GEMINI HEAT SHIELD
HT-435 STRUCTURAL ADHESIVE	2500 (EST)	4 (EST)	0.02 (EST)	NA	ND	0.173 (1.2) (EST)	9.63×10^2 (0.23)	NA	478 (400)	HT424 FILM WITHOUT ALUMINUM FILLER FOR ELECTRICAL TRANSPARENCY

NOTES:

1 ND = NO DATA

2 ALL PROPERTIES AT ROOM TEMPERATURE UNLESS OTHERWISE NOTED

3 (EST) = ESTIMATED

4 NA = NOT APPLICABLE

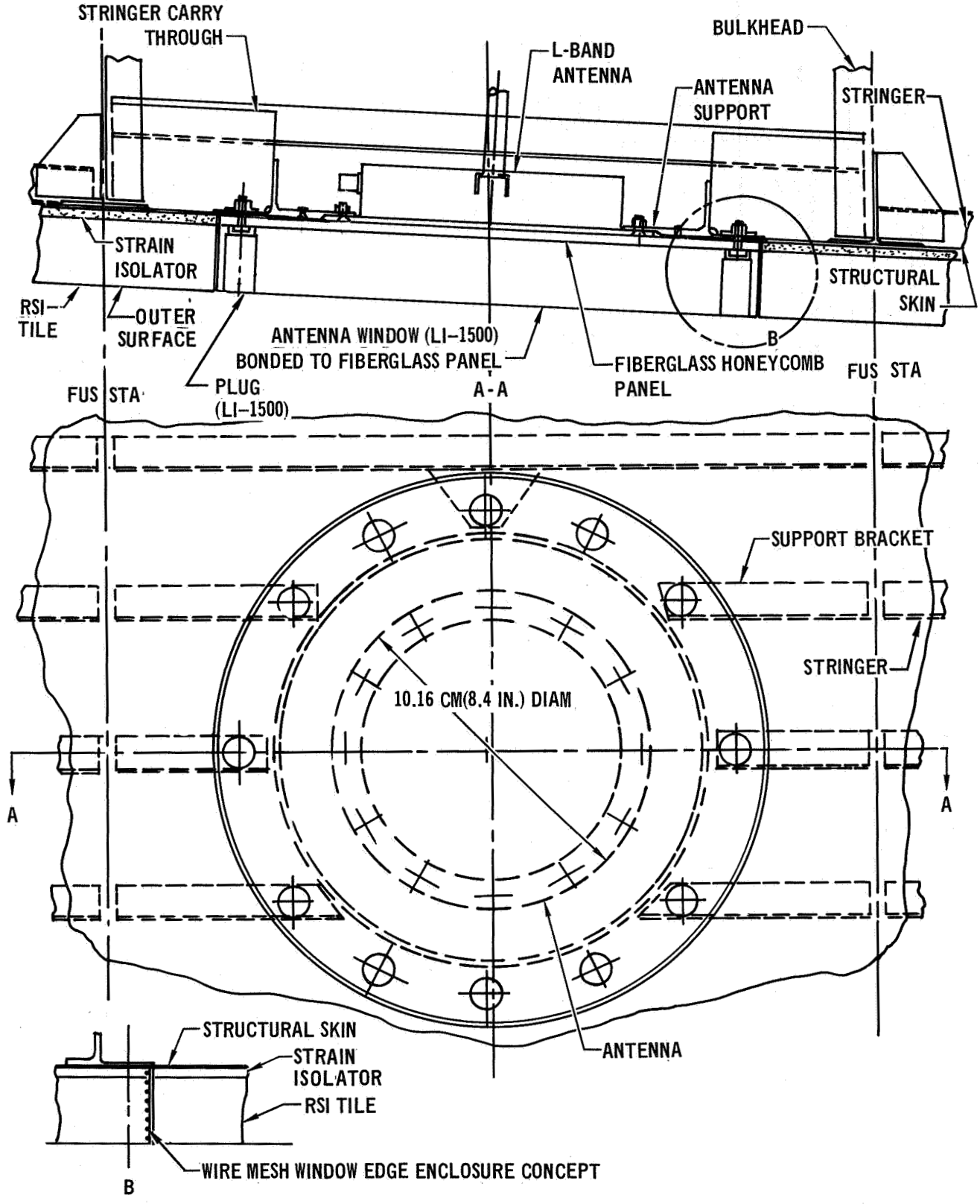

SINGLE-LAYER RSI ANTENNA WINDOW DESIGN – LARGE WINDOW SIZE

Figure 16

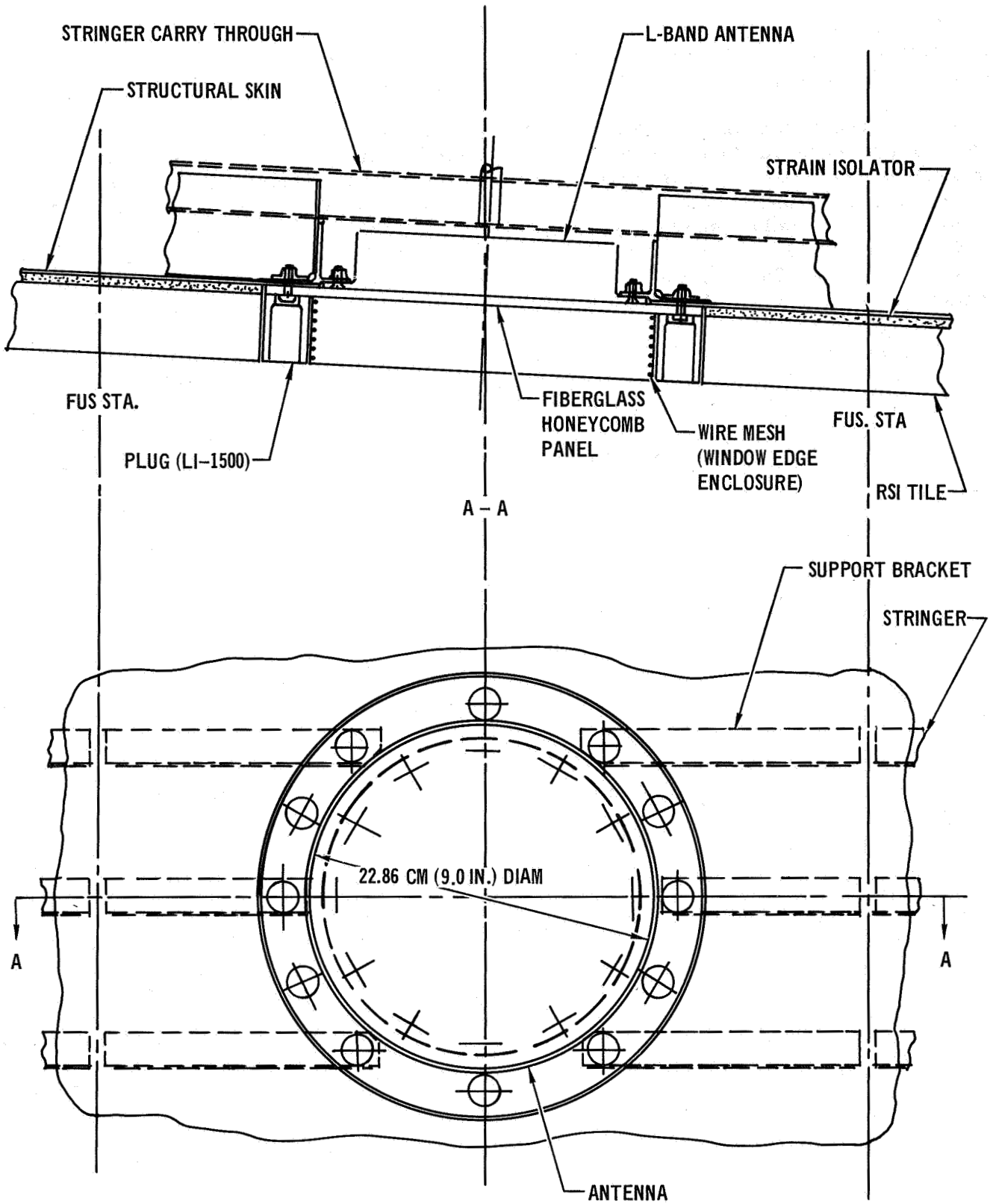

SINGLE-LAYER RSI ANTENNA WINDOW DESIGN – MINIMUM WINDOW SIZE

Figure 17

The LI-1500 plugs close a hole used for mounting the antenna window over the antenna. To gain access to the antenna, the plugs can be removed and replaced with new plugs when the window is replaced.

An analysis was made to size the honeycomb configuration to withstand the external pressure loads and support the LI-1500 over the antenna and eliminate transfering any loads to the antenna. A panel 30.48 cm (12 in.) in diameter with a line of support 24.4 cm (10.8 in.) in diameter was used for this analysis. The results showed that the honeycomb panel skins should be 0.3048 mm (0.012 in.) thick (three layers of cloth), and the core 7.112 mm (0.28 in.) thick (6.35 mm (0.25 in.) cell size, 56.1 kg/m^3 (3.5 lb/ft^3) density). Under maximum load, 7.3×10^4 N/m^2 (10.6 psi), the maximum honeycomb deflection is 2.692 mm (0.106 in.). With 5.08 cm (2.0 in.) thick LI-1500 bonded to the honeycomb, the deflection is reduced to 0.965 mm (0.038 in.). The calculated stresses developed in the LI-1500 for this deflection were within the allowable stress limits. With 2.54 mm (0.10 in.) of sponge rubber strain isolation material bonded between the LI-1500 and the honeycomb, the deflection of the composite was reduce to 0.254 mm (0.01 in.).

Multiple-layer window. - Preliminary designs of two (2) antenna window configurations using the multiple-layer approach are shown in figures 18 and 19. Figure 18 shows a maximum diameter window version and figure 19 shows a minimum diameter version. The window edge enclosure provides a means for holding the high temperature dielectric material (HD-0092) in place. The window edge enclosure is a coated columbium cylinder, since it is subjected to the high Orbiter surface temperatures. The columbium retainer ring, in addition to holding the HD-0092 in place, provides a means for removing the window and access to the antenna for either installation or removal. The load bearing insulation is used to obtain thermal isolation between the window edge enclosure and the antenna. The insulation on the outside of the edge enclosure was provided to obtain thermal isolation to the surrounding TPS substructure. Index pins are provided to prevent the HD-0092 from rotating within its retaining structure due to mechanical or acoustical vibration.

The maximum window diameter is determined by the fabrication limitations of the materials selected for the high temperature dielectric. For HD-0092, current production capabilities are limited to finished pieces approximately 34.3 cm (13.5 in.) in diameter (or square) and 1.3 cm (0.5 in.) thick. The minimum window diameter is limited by the antenna aperture size and the cutoff characteristics of the circular waveguide formed by the edge enclosure. The dielectric constant of the window material will also affect the cutoff characteristics of the edge enclosure.

Preliminary Thermal Sizing Analyses

Preliminary thermal sizing analyses were conducted to determine the antenna window thickness. This was done for the single-layer and the multiple-layer window. The heat short effects were not considered in this analyses but were deferred for the more detailed analysis discussed in the section on ANTENNA SYSTEM DESIGN AND INTEGRATION.

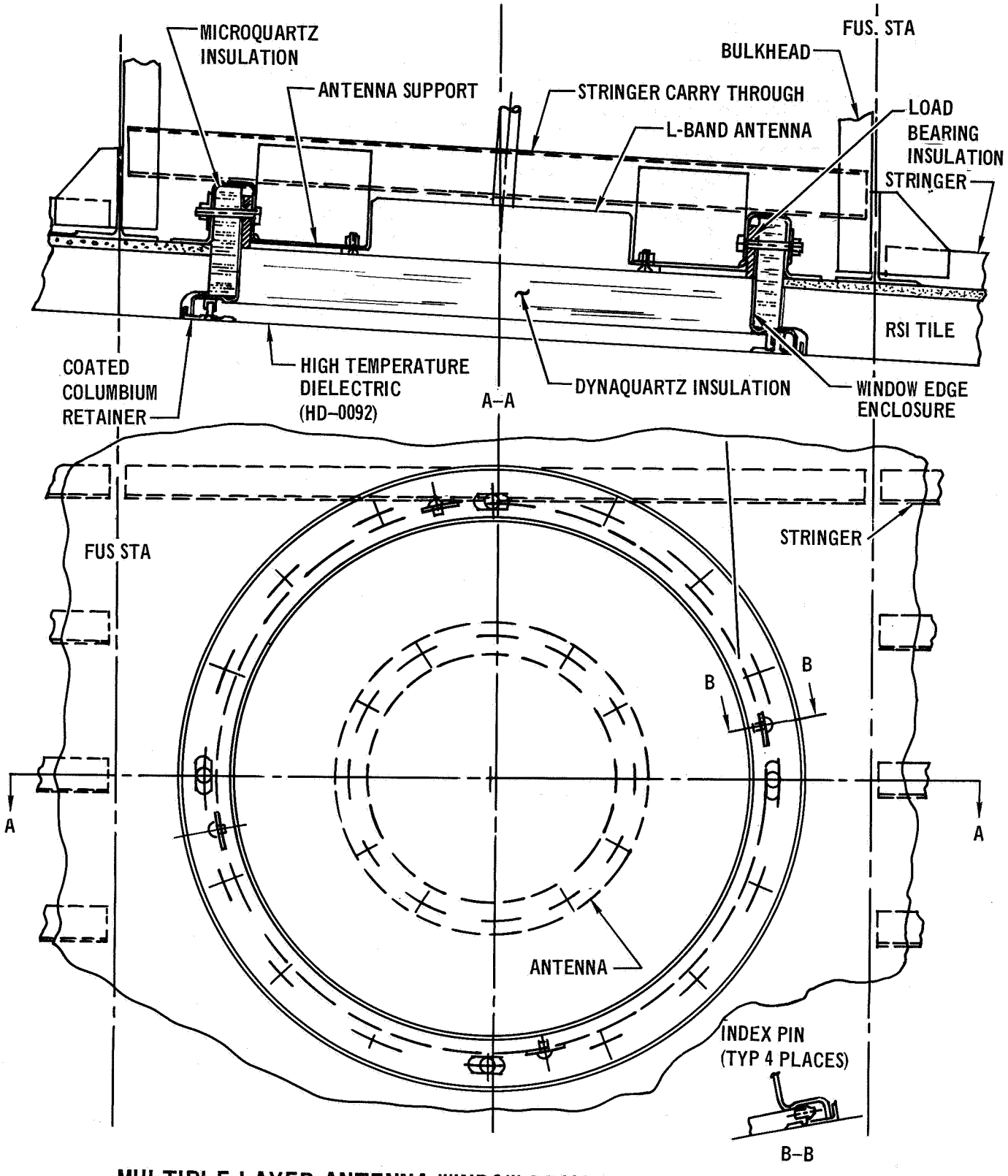

MULTIPLE-LAYER ANTENNA WINDOW DESIGN – MAXIMUM WINDOW SIZE

Figure 18

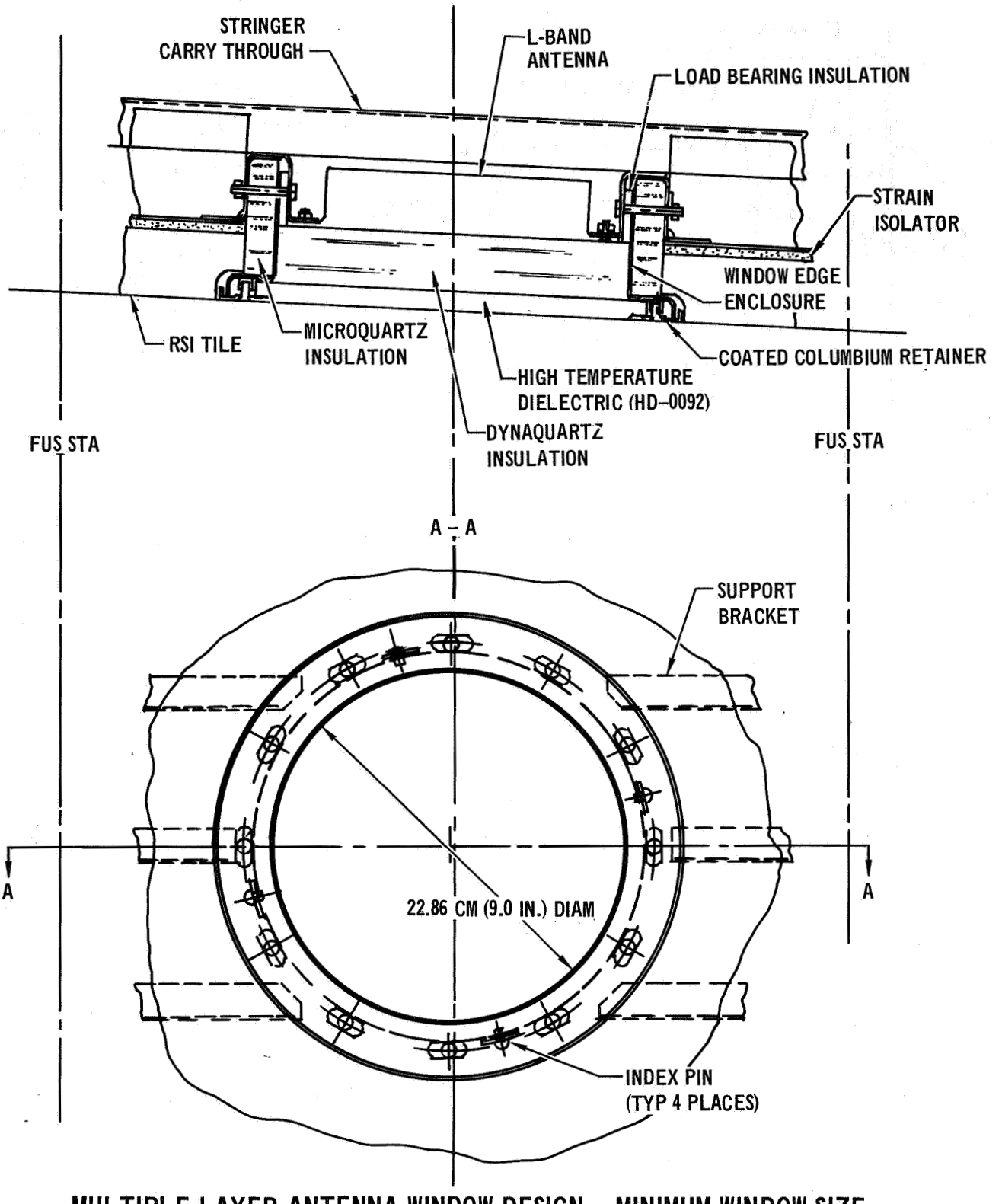

MULTIPLE-LAYER ANTENNA WINDOW DESIGN – MINIMUM WINDOW SIZE

Figure 19

Environmental factors. - The required antenna window thickness is governed by the thermal environments and the particular antenna window concept. The critical thermal environment occurs during entry. Other factors of primary importance in antenna system thermal design include: 1) the initial and maximum allowable temperature; 2) the surface emittance and solar absorptance of the antenna window surface material; 3) the local pressure environment of the insulation; 4) the mass or heat capacitance of the antenna/primary-structure; and 5) the heat transfer boundary condition on the inboard side of the antenna/primary-structure. The thermal analyses utilized the following environmental factors:

(a) maximum and minimum pre-entry initial temperature design values of 311°K (100°F) and 161°K (-170°F) were determined considering solar absorptance and emittance, vehicle location and a number of shuttle mission variables. Minimum pre-entry temperatures were used to provide temperature data for thermal stress calculations.

(b) maximum allowable antenna/primary-structure temperature of 422°K (300°F) is based on repeated exposure of aluminum alloy material.

(c) constant 0.9 surface emittance and 0.76 solar absorptance for LI-1500 coating; variable surface emittance for HD-0092 boron nitride.

(d) local static surface pressure used to determine LI-1500 thermal conductivity.

(e) an equivalent thickness ($\bar{t}$) of aluminum primary structure of 1.525 mm (0.06 in.).

(f) inboard heat transfer from primary structure included.

Thermal models. - One-dimensional thermal analyses and MDC's General Heat Transfer Program (Heatran Code) were used to determine the antenna window thicknesses required to maintain the antenna to a 422°K (300°F) maximum temperature. The computer program is a "block type" thermal analyzer in which the physical properties, geometry and linkage relationships are input to the program which then calculates lumped thermal capacitance and conductance terms. Aerothermodynamic heat transfer coefficients and recovery temperatures were fed in also. Backward finite difference techniques were used to obtain transient solutions.

The one-dimensional thermal models used for the single-layer LI-1500 window and the multiple-layer window design concepts are shown in figure 20. The single-layer antenna window was divided into 22 nodes; the multiple-layer window was divided into 35 nodes and the adjacent TPS model was divided into 37 nodes, as shown. Thermal property data used for thermal analyses are tabulated in Appendix A. Coating, adhesive, strain isolator and honeycomb face-sheet and core thicknesses were modeled. No inboard forced convection cooling was used.

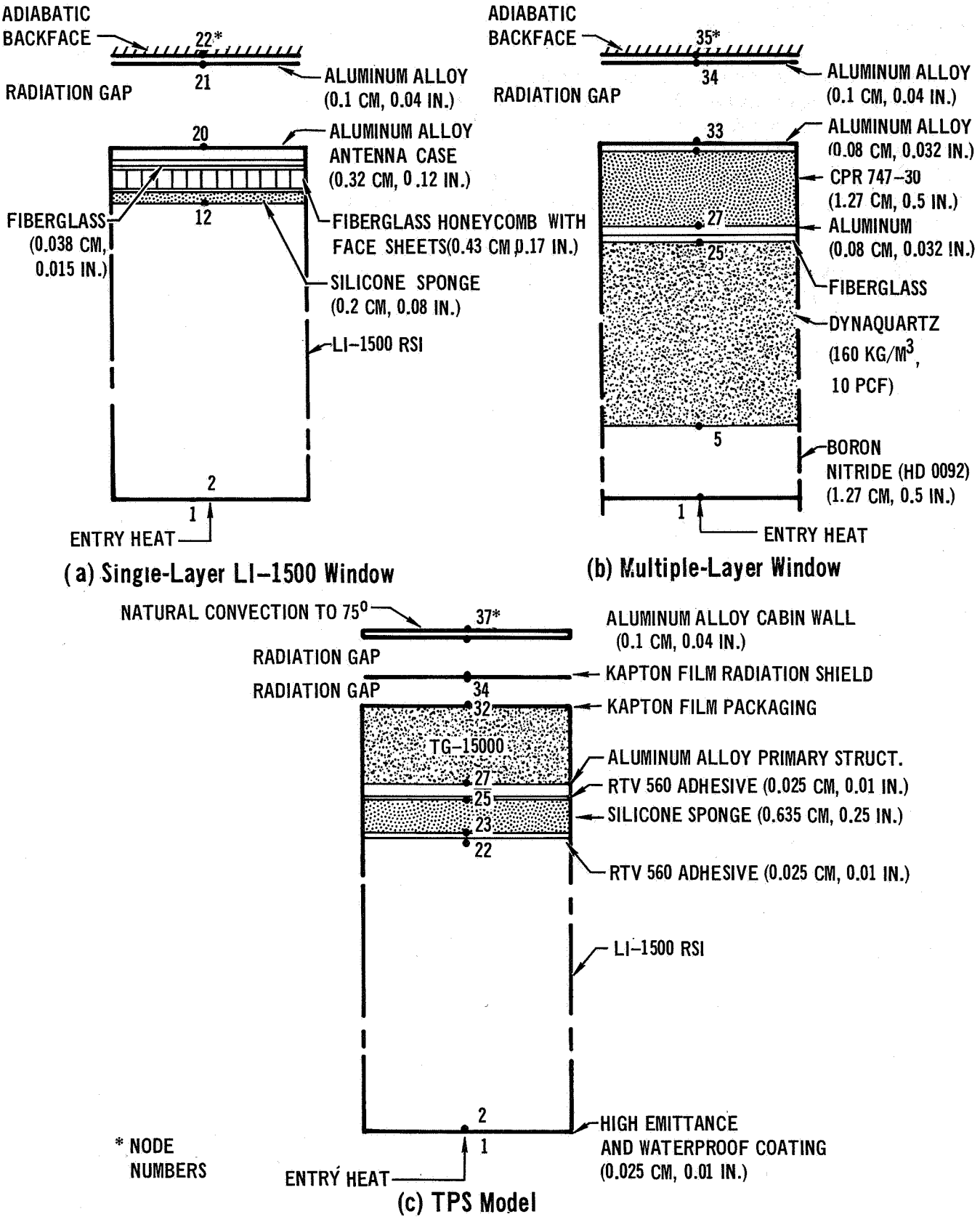

THERMAL MODELS FOR ANTENNA WINDOW SIZING

Figure 20

Results. - Thermal sizing cross plots of maximum antenna face temperature versus window thicknesses are shown in figure 21 for the particular window concepts considered in this study: the single-layer LI-1500 window and multiple-layer window. The single-layer LI-1500 thickness is 5.08 cm (2.0 in.) and the multiple-layer window Dynaquartz thickness is 4.57 cm (1.8 in.) or 3.18 cm (1.25 in.) depending on the pressure environment (i.e. whether or not the edge enclosure seals the antenna from the local static pressure environment).

Electrical Design Tests

Electrical design tests were conducted to determine the best window configurations, for each of the antenna systems, which meet the Orbiter requirements. Mock-ups were fabricated for each window configuration and radiation pattern and impedance measurements made. This section describes the test configurations, techniques, and results for the test configurations considered important in arriving at the recommended final designs.

Test configurations. - All measurements were taken with the antennas flush mounted in a ground plane. A 91.44 cm (3 ft) square ground plane was used with all three antennas. Two additional ground plane sizes were used, a 76.2 cm (30.0 in.) square with the C-band slot antenna and a 1.83m (6.0 ft) diameter with the L-band antenna.

Conducting window edge enclosures were made from sheet aluminum and filled with styrofoam. The styrofoam added rigidity and helped to maintain the circularity of the enclosure. The window edge enclosures were centered over the antenna and bonded to the ground plane with conductive metal tape. This configuration was used to size window edge enclosures which could be used with the antennas. Styrofoam was used because its dielectric constant is low (1.01 to 1.05) and, therefore, changes in radiation pattern or impedance would be due to the window edge enclosure. Other antenna window configurations were simulated using the following materials; Emerson Cummings Inc. Stycast HiK (ε_r = 4.0), Eccofoam PS (ε_r = 1.2), and Dynaquartz (ε_r = 1.1). Stycast HiK simulated HD-0094 boron nitride and Eccofoam simulated LI-1500 RSI.

Two RSI thicknesses were simulated, 2.54 cm (1.0 in.) and 5.08 cm (2.0 in.), since these thicknesses should bracket the expected RSI thickness. Both were also used when simulating the TPS on the ground plane. The RSI was simulated with Eccofoam PS and RTV-524 type S-105 elastomer sponge was used as the strain isolator. Therefore, these simulations duplicated both the dimensions and the dielectric constants of the materials specified for the TPS.

Test techniques. - Radiation pattern and swept frequency impedance measurements were used to evaluate the effects of the different antenna window configurations in relation to reference data taken with the antenna flush mounted in a bare ground plane. The coordinate system shown in figure 22, was used for the radiation patterns. Unless identified, all radiation patterns presented in this report are oriented with $\theta = 0°$ toward the top of the page. The orientation of the respective ground planes and antenna systems were held fixed relative

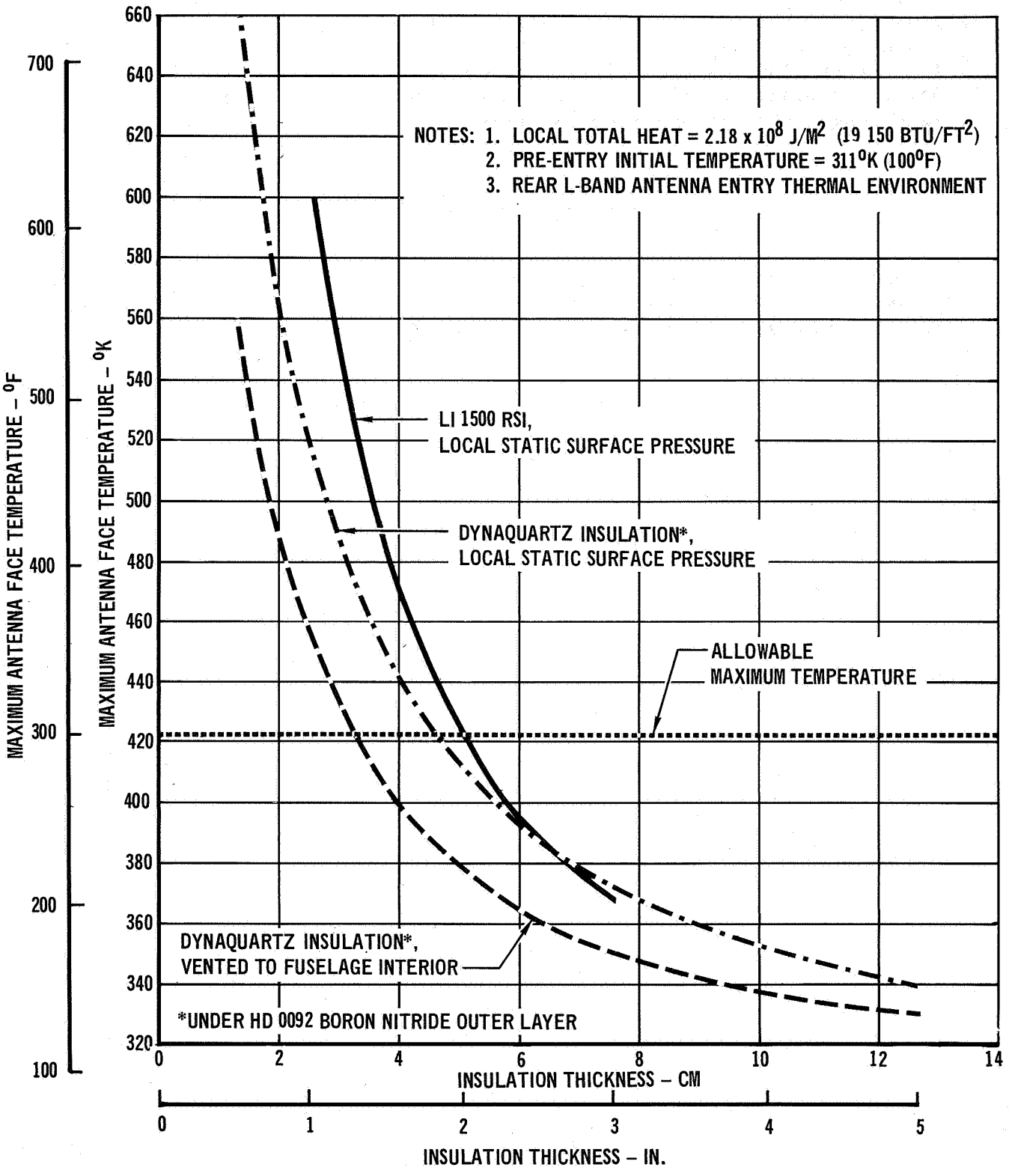

THERMAL SIZING RESULTS

Figure 21

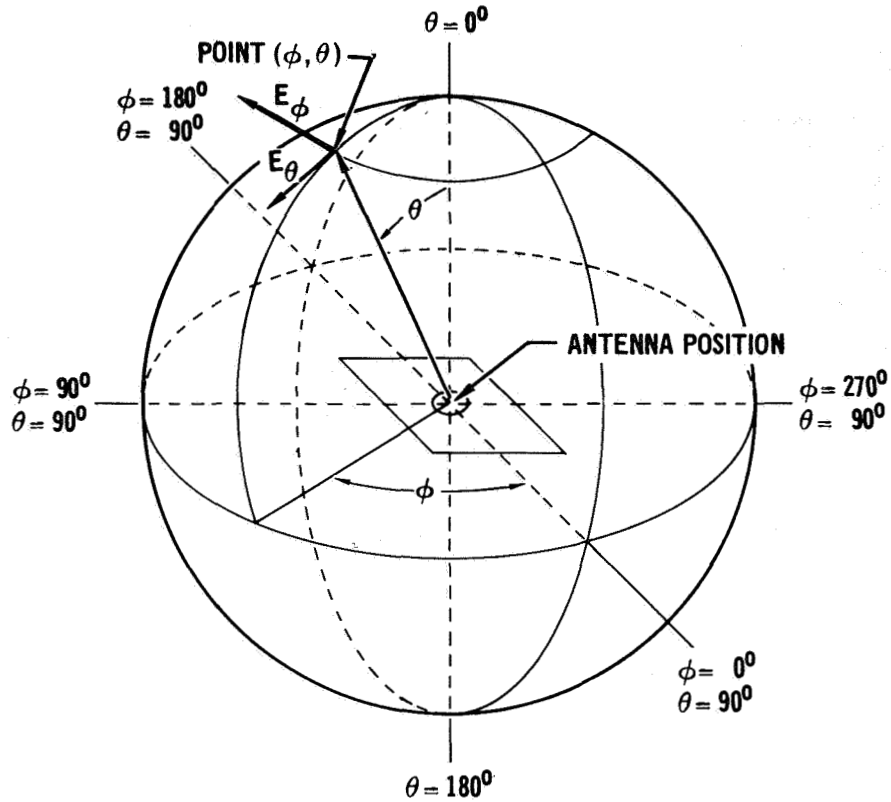

ANTENNA COORDINATE SYSTEM

Figure 22

to the coordinate system. A standard polar plot having a 40 dB amplitude range is used for all pattern plots.

Reference measurements were used to facilitate the comparison of the pattern magnitude measured for the different configurations within each frequency run. A small log periodic antenna was placed on a tripod in the corner of the anechoic chamber to obtain a constant signal level at each of the L-band frequencies. Standard gain horns were used for the two C-band antennas. Figure 23 is a block diagram depicting the typical anechoic chamber test set-up.

Transmission distances used were 12.19m (40 ft), 27.43m (90 ft) and 152.4m (500 ft). L-band patterns were initially made at 27.43m (90 ft) then changed to 12.19 (40 ft) to obtain better symmetry. The 152.4m (500 ft) distance was used on an outdoor range during investigation of cross-polarization levels on the L-band antenna. All C-band patterns were made in the anechoic chamber with a 27.43m (90 ft) transmission distance.

Impedance plots of the various configurations were taken with a Hewlett-Packard Model 8410A Network Analyzer System. Figure 24 shows a typical set-up for swept frequency impedance measurements.

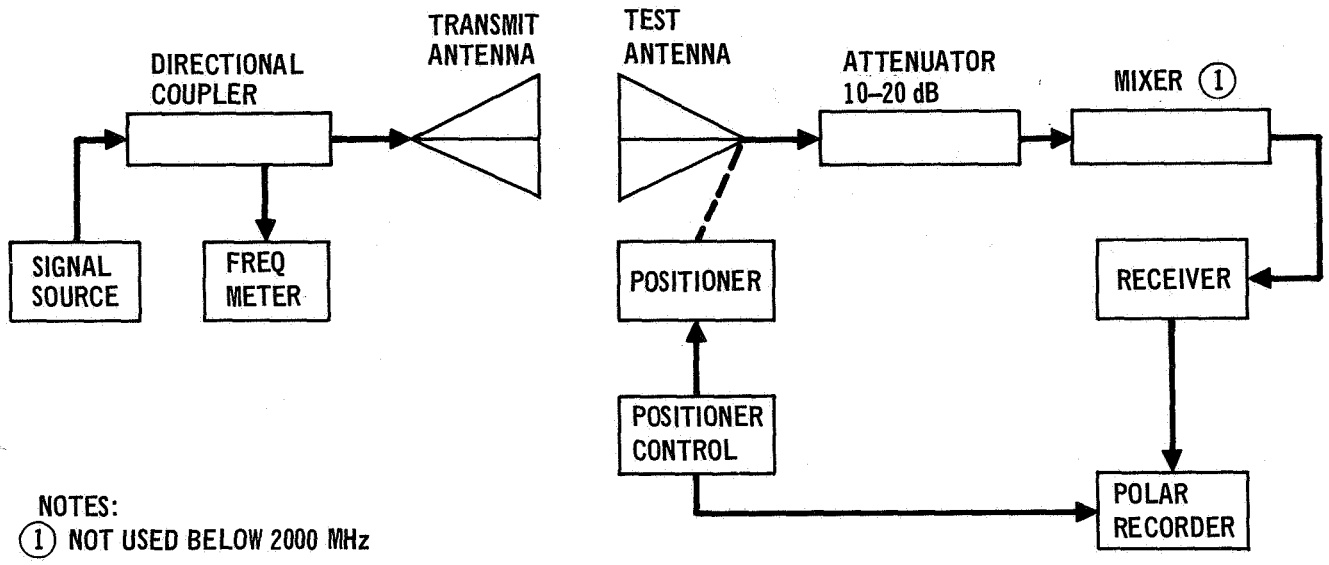

ANECHOIC CHAMBER TEST SET–UP BLOCK DIAGRAM

Figure 23

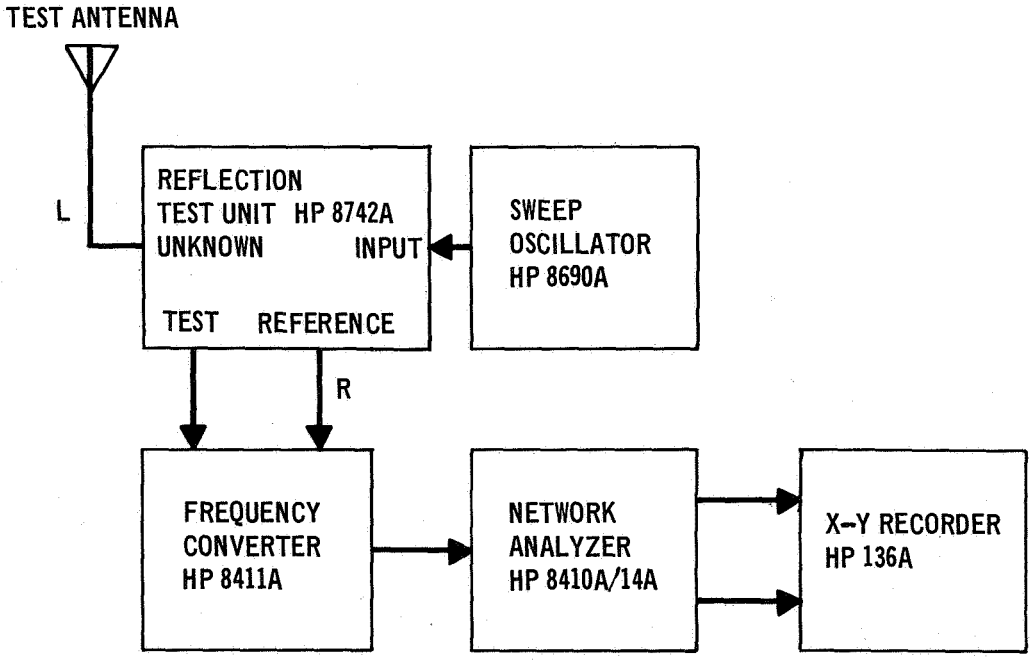

LENGTH R MUST EQUAL 2L OVER SWEEP RANGE.

IMPEDANCE TEST SET–UP BLOCK DIAGRAM

Figure 24

Test results. - The results of radiation patterns and impedance measurements for the antenna system configurations tested are presented in this section. Selected data is shown to illustrate the effects of the different configurations. A more complete set of data is presented for the final configurations.

L-band annular slot antenna: Radiation patterns for the L-band annular slot antenna flush mounted in a ground plane are shown in figure 25. These patterns serve as a reference or standard for comparison with the patterns measured for the various window configurations considered in the design study. Patterns were measured at frequencies of 960, 1090, and 1220 MHz.

The initial L-band antenna system tests were made to determine the effects of a window edge enclosure on the antenna, with the enclosure extending above the ground plane. In the testing performed prior to this study (see section on Background) where the ground plane was located at the surface of the TPS, it was essential to enclose the window edges with a conductor in order to obtain acceptable patterns.

The window edge enclosures consisted of sheet metal cylinders 2.54 and 5.08 cm (1.0 and 2.0 in.) long with diameters of 22.86 cm (9.0 in.), 27.94 cm (11.0 in.) and 31.76 cm (12.5 in.). These cylinders were filled with styrofoam for good dimensional control and attached to the ground plane with a metal conductive tape. Since the dielectric constant of styrofoam is very low (1.01 to 1.05), the test results basically show the effects of the conducting cylinder, or the effects of terminating the antenna aperture in a circular waveguide. Radiation patterns for these configurations are shown in figures 26 through 28. The patterns show a variation in shape with the variation in window edge enclosure length (window thickness) and diameter. Figure 26 shows the patterns for the 22.86 cm (9.0 in.) diameter windows. For the 5.08 cm (2.0 in.) thick window, the pattern distortion is similar to that found in LaRC measurements (ref. 3) of a horn antenna feeding a 10.6 cm (4.0 in.) and 15.24 cm (6.0 in.) square cavity 5.08 cm (2.0 in.) deep and terminated in a ground plane. This effect did not occur in the patterns measured with a 22.86 cm (9.0 in.) window diameter terminated in a ground plane (ref. 1). The pattern distortion is greatly reduced as the window diameter is increased to 27.94 cm (11.0 in.) as shown in figure 27, and virtually disappears when the window diameter is increased to 31.75 cm (12.5 in.) as shown by figure 28. It may be noted that the pattern distortion occured at different test frequencies for different window diameters or thicknesses. In all cases, however, the pattern is changed very little in the region of primary interest, $\theta = 60°$ to $\theta = 100°$. The best overall radiation pattern results were obtained with the 31.75 cm (12.5 in.) diameter window as shown by figure 28.

The results of the impedance measurements for the above window configurations is shown in figures 29 thru 32. Figure 29 shows the impedance of the antenna mounted in the ground plane (reference configuration). Figure 30 shows the impedance of the antenna with a 22.86 cm (9.0 in.) diameter window. It is obvious that the increase in window thickness has a significant effect on the antenna impedance (VSWR). An increase in the antenna window diameter to 27.94 cm (11.0 in.) resulted in a significant improvement in VSWR for both window

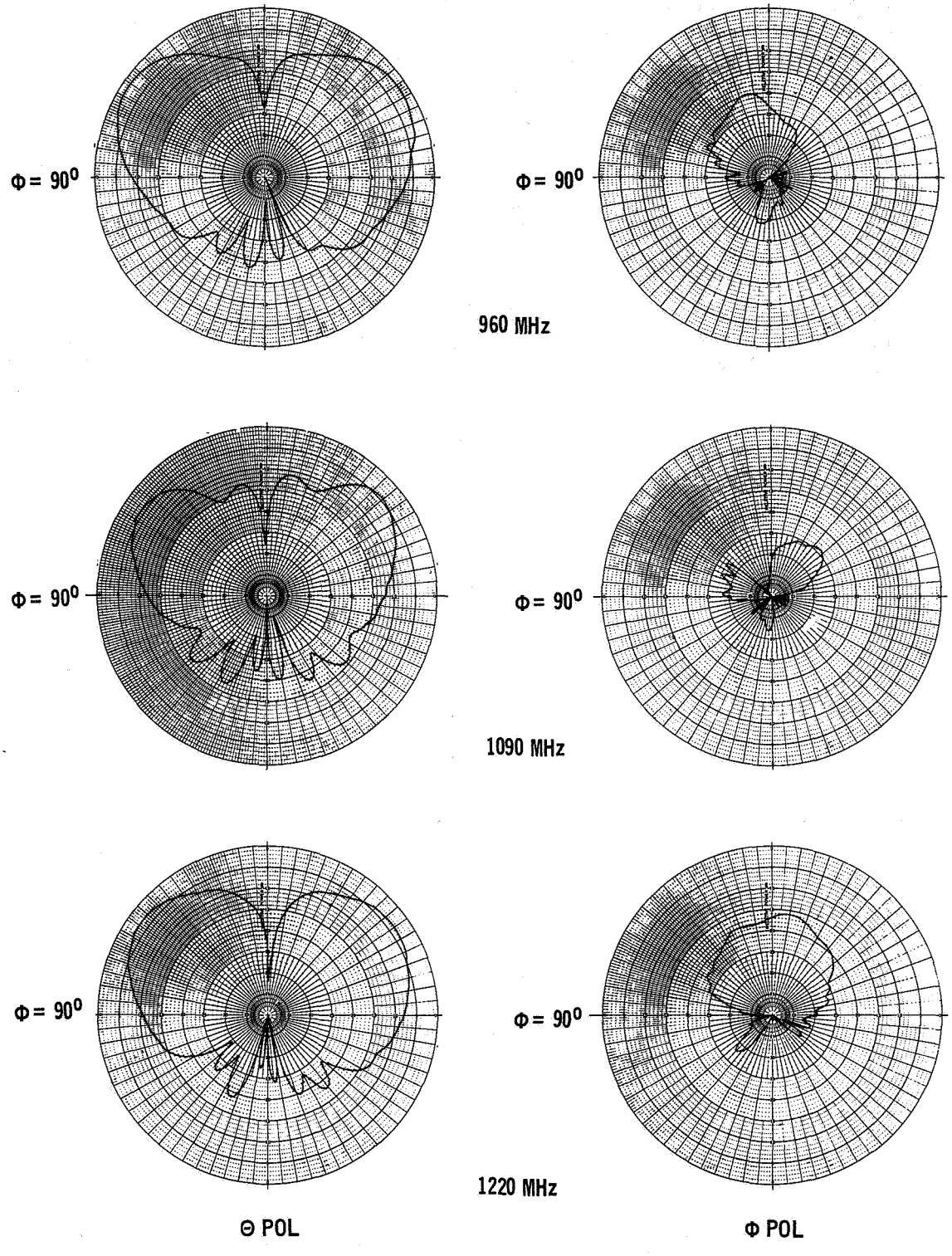

L-BAND REFERENCE PATTERNS – 27.43M (90 FT) TRANSMIT DISTANCE

Figure 25

(Figure Continued on Next Page)

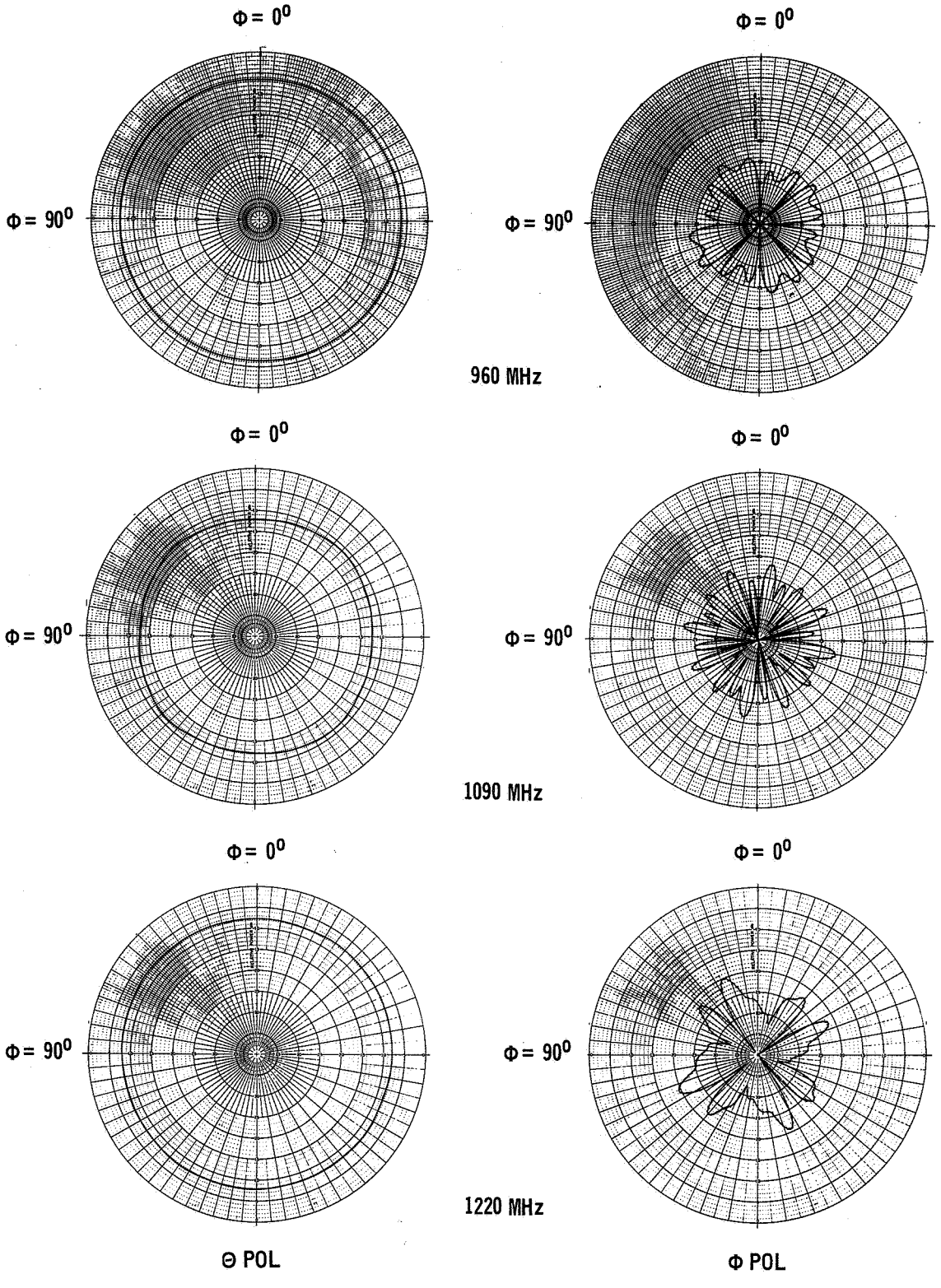

L-BAND REFERENCE – 27.43 M (90 FT)
(Concluded)

Figure 25

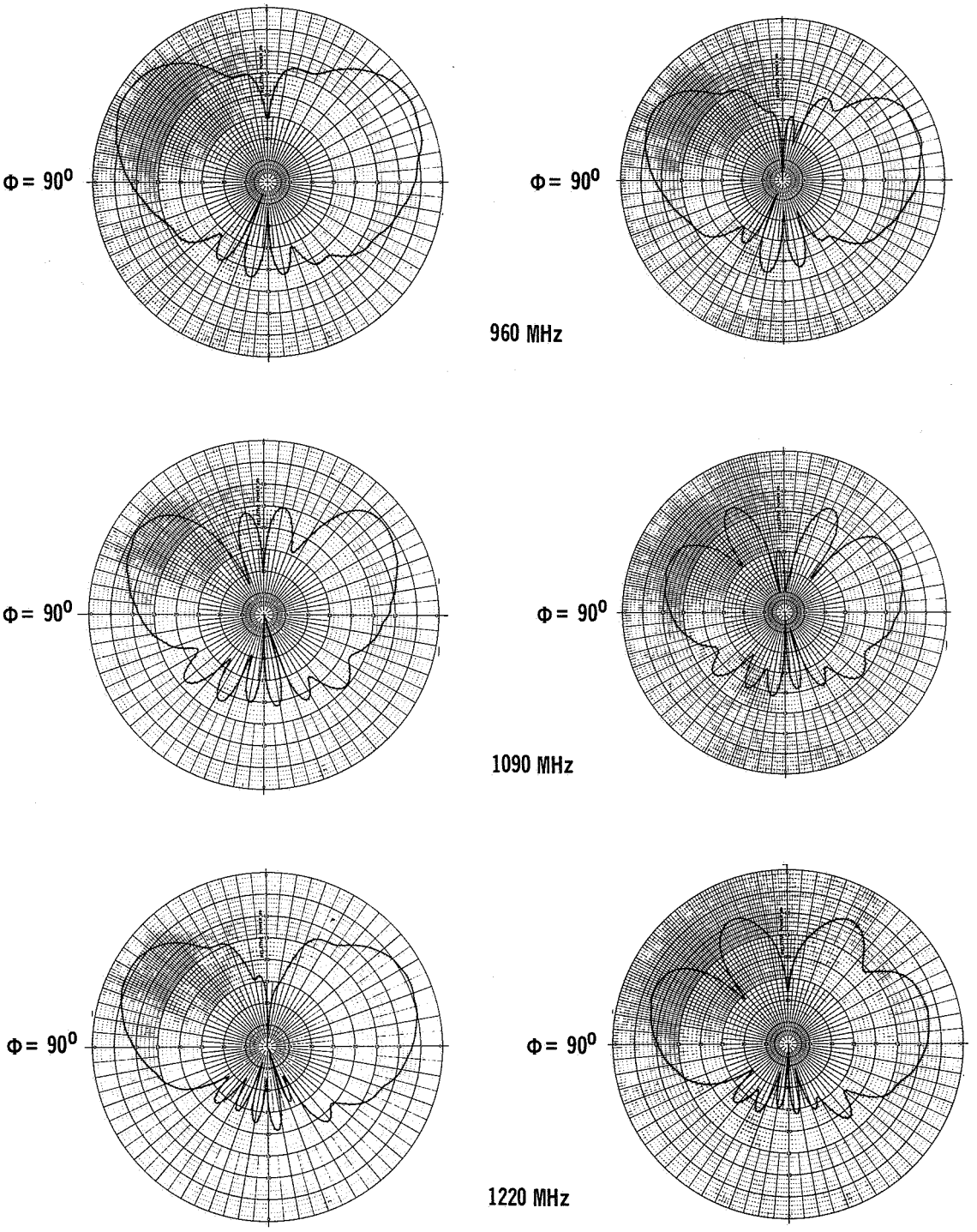

L-BAND PATTERNS – 22.86 CM (9.0 IN.) DIAMETER WINDOW

Figure 26

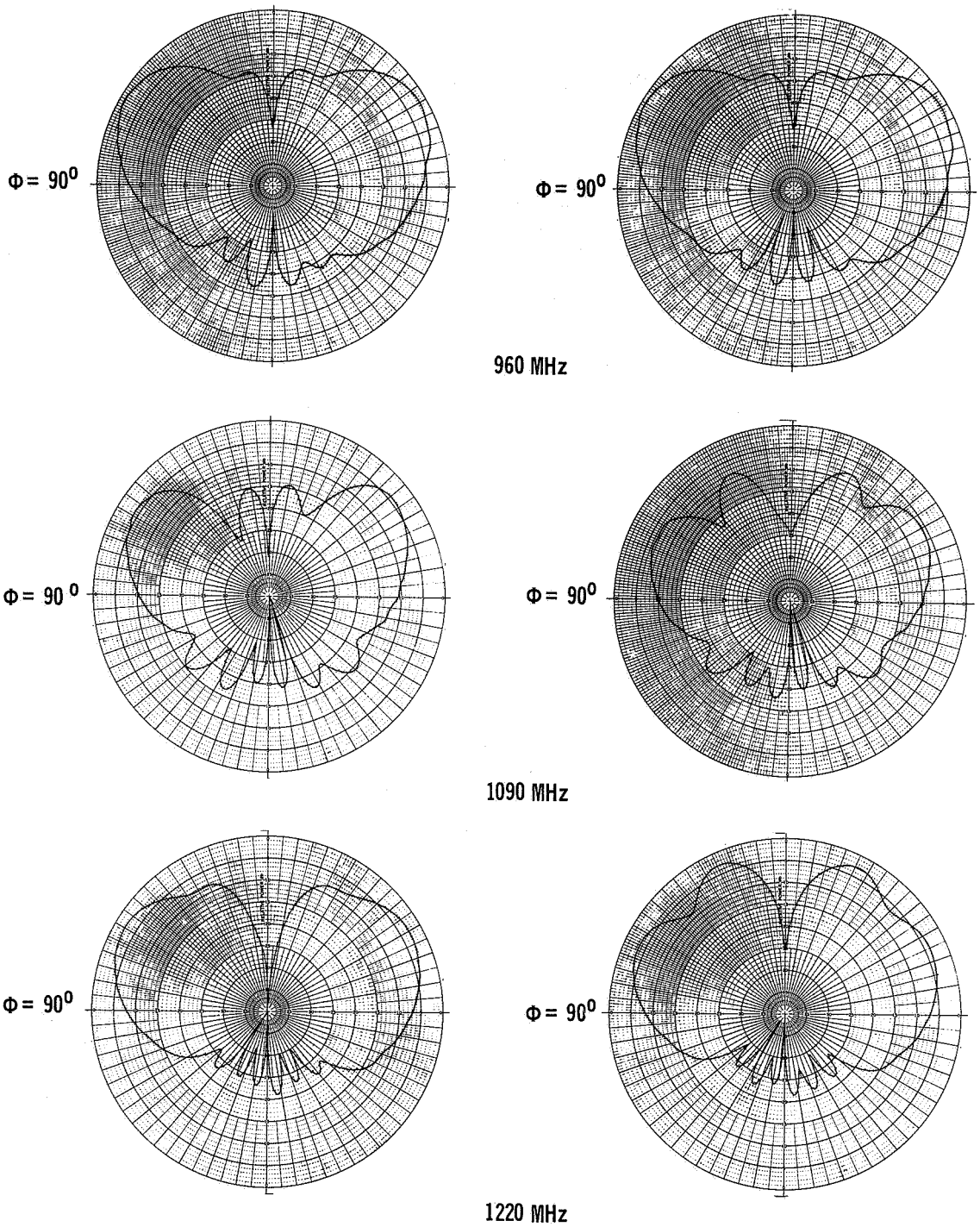

L-BAND PATTERNS – 27.94 CM (11.0 IN.) DIAMETER WINDOW

Figure 27

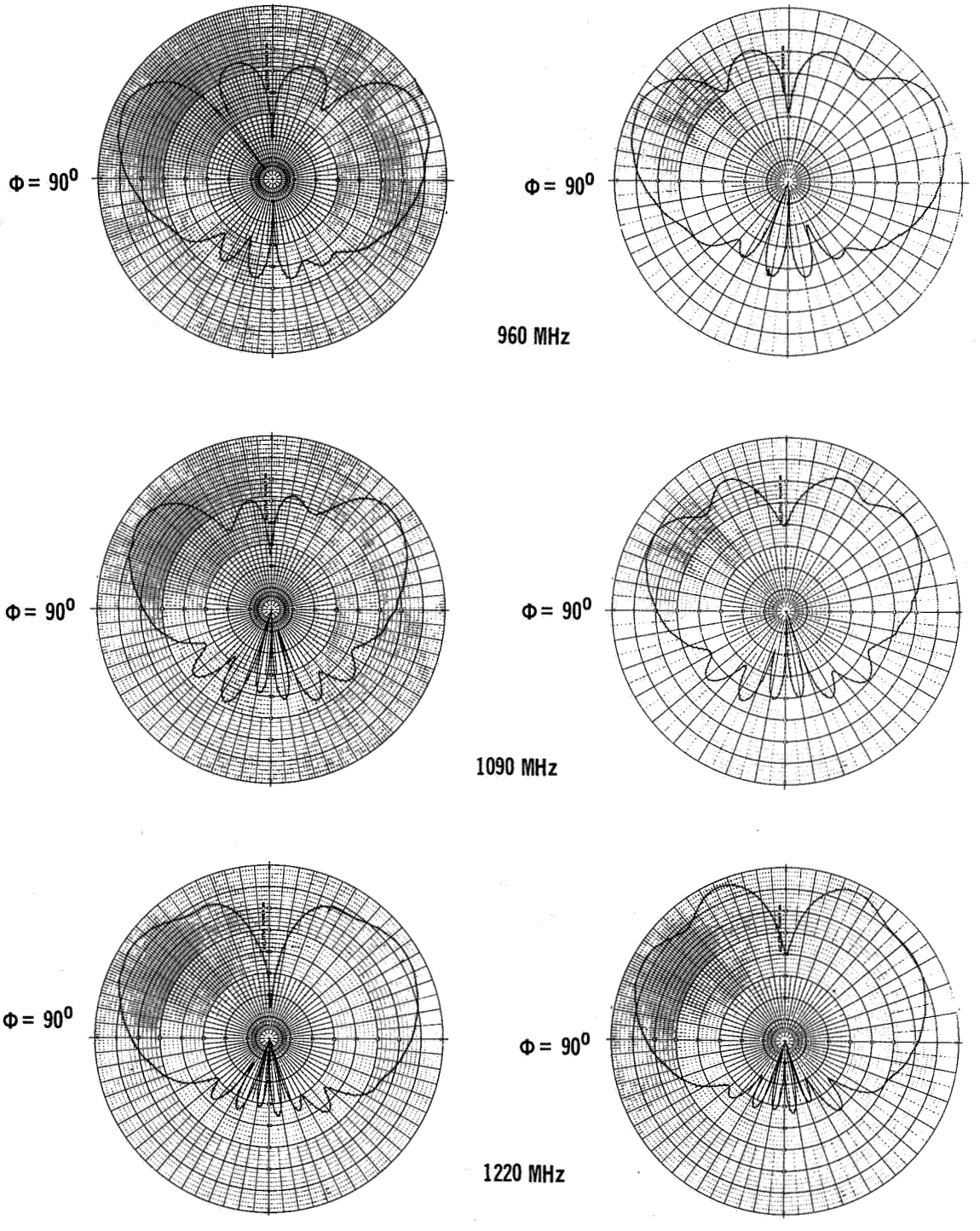

L-BAND PATTERNS – 31.75 CM (12.5 IN.) DIAMETER WINDOW

Figure 28

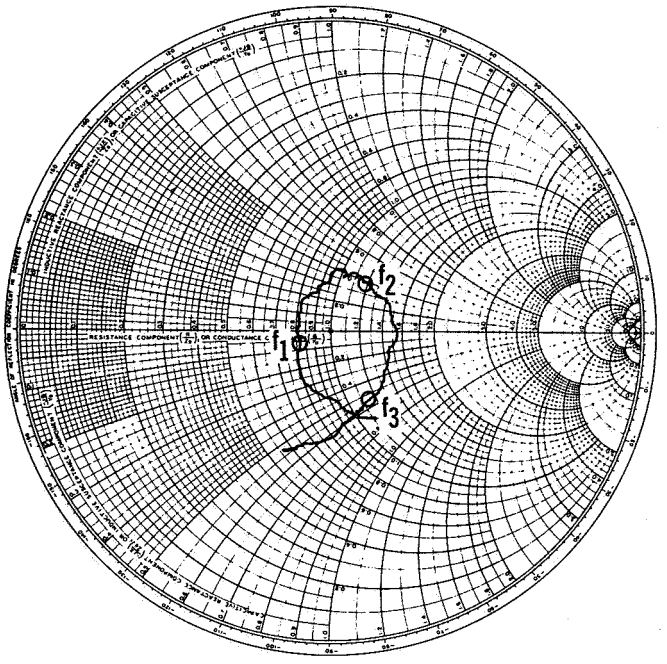

Z_0 = 50Ω
f_1 = 960 MHz
f_2 = 1090 MHz
f_3 = 1220 MHz

SWEEP RANGE
900 MHz TO 1300 MHz

L-BAND REFERENCE IMPEDANCE

Figure 29

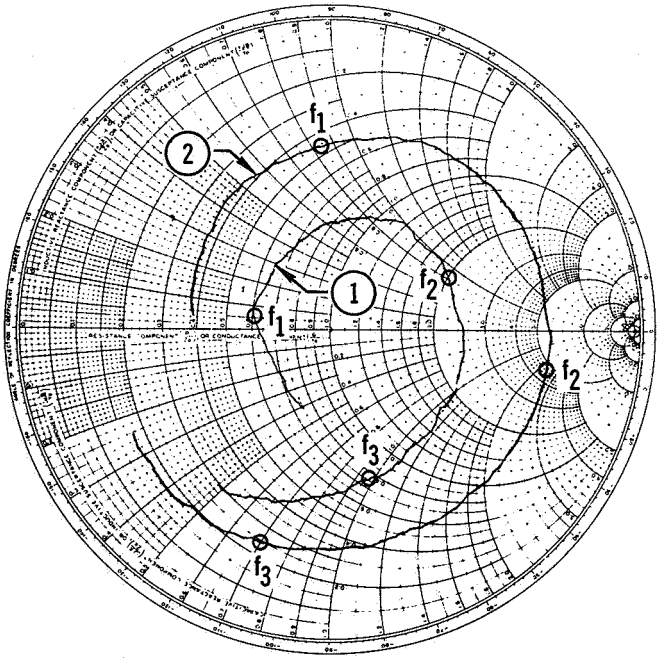

① 2.54 CM (1.0 IN.)
② 5.08 CM (2.0 IN.)
Z_0 = 50Ω
f_1 = 960 MHz
f_2 = 1090 MHz
f_3 = 1220 MHz

SWEEP RANGE
900 MHz TO 1300 MHz

L-BAND IMPEDANCE – 22.86 CM (9.0 IN.) DIAMETER WINDOW

Figure 30

thicknesses as shown by figure 31. The maximum VSWR is less than 3.0:1 and may be acceptable for operational use. A further increase in window diameter to 31.75 cm (12.5 in.) resulted in even more improvement in the antenna VSWR as shown by figure 32. The VSWR for the 2.54 cm (1.0 in.) window is better than the reference configuration while the VSWR for the 5.08 cm (2.0 in.) window is increased only slightly above the reference configuration. The latter should be acceptable for an operational system without additional matching, since the VSWR exceeds 2.0:1 only slightly at the low end of the L-band frequency range which is used for receive only. These test results show that the L-band annular slot antenna impedance is sensitive to both the diameter and thickness of the antenna window. However, the changes in antenna impedance are caused primarily by the window edge enclosure, since the window material for these tests was styrofoam.

Based on the results for the 31.75 cm (12.5 in.) diameter window, this size was selected for the multiple-layer window design. This selection was also consistent with the limitations for the boron nitride (HD-0092) plate diameter discussed in the section on Description of Antenna Window Configurations (Multiple-layer window).

Tests were conducted to determine the cause of the dissymmetry and shallow nulls in some of the L-band antenna patterns (figures 26 through 28) discussed above. The symmetry was improved by moving the transmitting horn antenna closer to the test antenna, from 27.43 cm (90 ft) to 12.18m (40 ft). However, there still was a slight difference (<1 dB) in the right lobe (reference to page orientation) of the θ plane patterns and the ϕ plane ($\theta = 90°$) pattern at the cross-over point. This condition applies to the left lobe if the antenna faces the opposite wall of the anechoic chamber when measuring the ϕ plane pattern. The difference is small and is attributable to the facility. Therefore, no additional effort was made to get exact correspondence in the cross-over points.

The null depth variation found in some patterns results from the basic pattern null being canted away from the aperture normal several degrees. Figure 33 shows typical results for $\theta = 0°$ and $\theta = 2.5°$. The null direction appears to change slightly with frequency. For a perfect null on the aperture normal, the $\theta = 2.5°$ pattern should be a circular pattern 15 to 20 dB below the pattern peak. Therefore, two selected orthogonal θ plane patterns may not have deep nulls on the antenna aperture normal. This is attributed to a slight dissymmetry in the annular slot aperture resulting from manufacturing tolerances. However, a slight shift in the null axis will not affect operational performance, because the direction of the null has no functional requirement in the TACAN or ATC operations.

Since the pattern symmetry improved at the 12.19m (40 ft) transmitting distance, reference patterns were remeasured. These patterns are shown in figure 34. The ϕ polarization level was about 7 dB higher at 1220 MHz than at 960 MHz and 1090 MHz, and only about 10 dB below the θ polarization pattern peak. To determine if the high cross polarization level was due to the anechoic chamber, patterns were measured on MDC's outdoor antenna range. Figure 35 shows the results for the L-band antenna mounted on a ground plane (reference con-

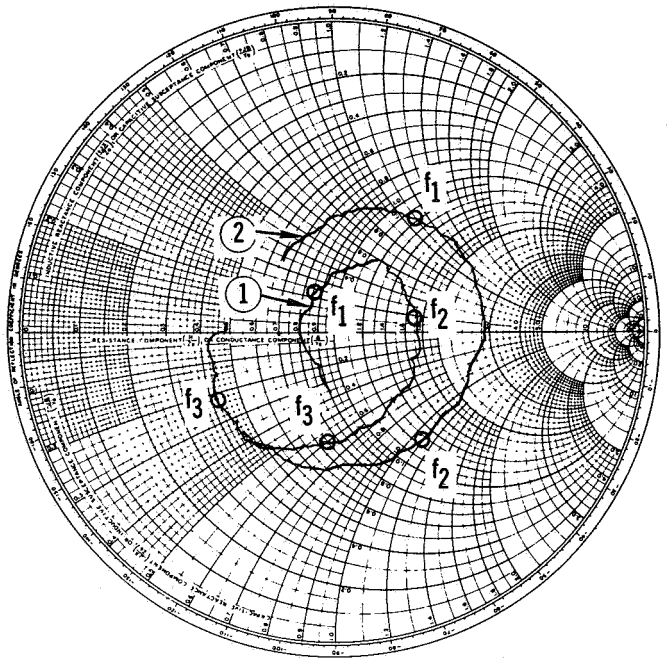

① 2.54 CM(1.0 IN.)
② 5.08 CM (2.0 IN.)

Z_0 = 50Ω
f_1 = 960 MHz
f_2 = 1090 MHz
f_3 = 1220 MHz
SWEEP RANGE
900 MHz TO 1300 MHz

L-BAND IMPEDANCE – 27.94 CM (11.0 IN.) DIAMETER WINDOW

Figure 31

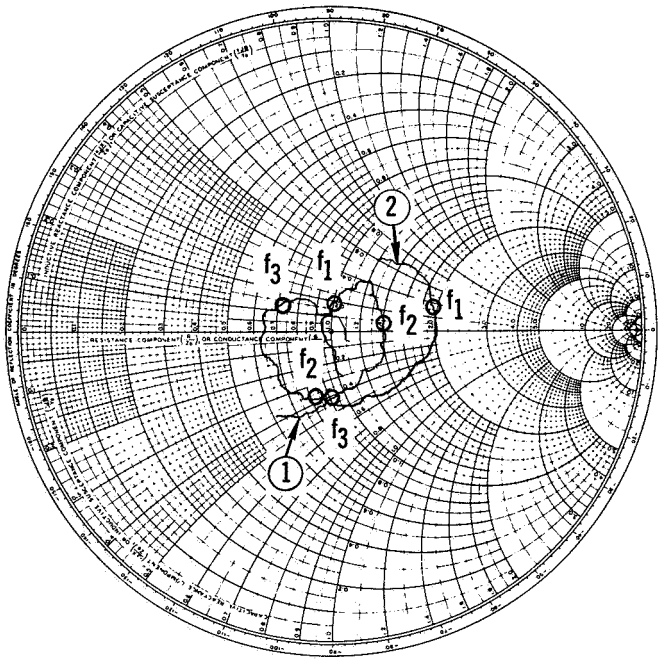

① 2.54 CM (1.0 IN.)
② 5.08 CM (2.0 IN.)

Z_0 = 50Ω
f_1 = 960 MHz
f_2 = 1090 MHz
f_3 = 1220 MHz
SWEEP RANGE
900 MHz TO 1300 MHz

L-BAND IMPEDANCE – 31.75 CM (12.5 IN.) DIAMETER WINDOW

Figure 32

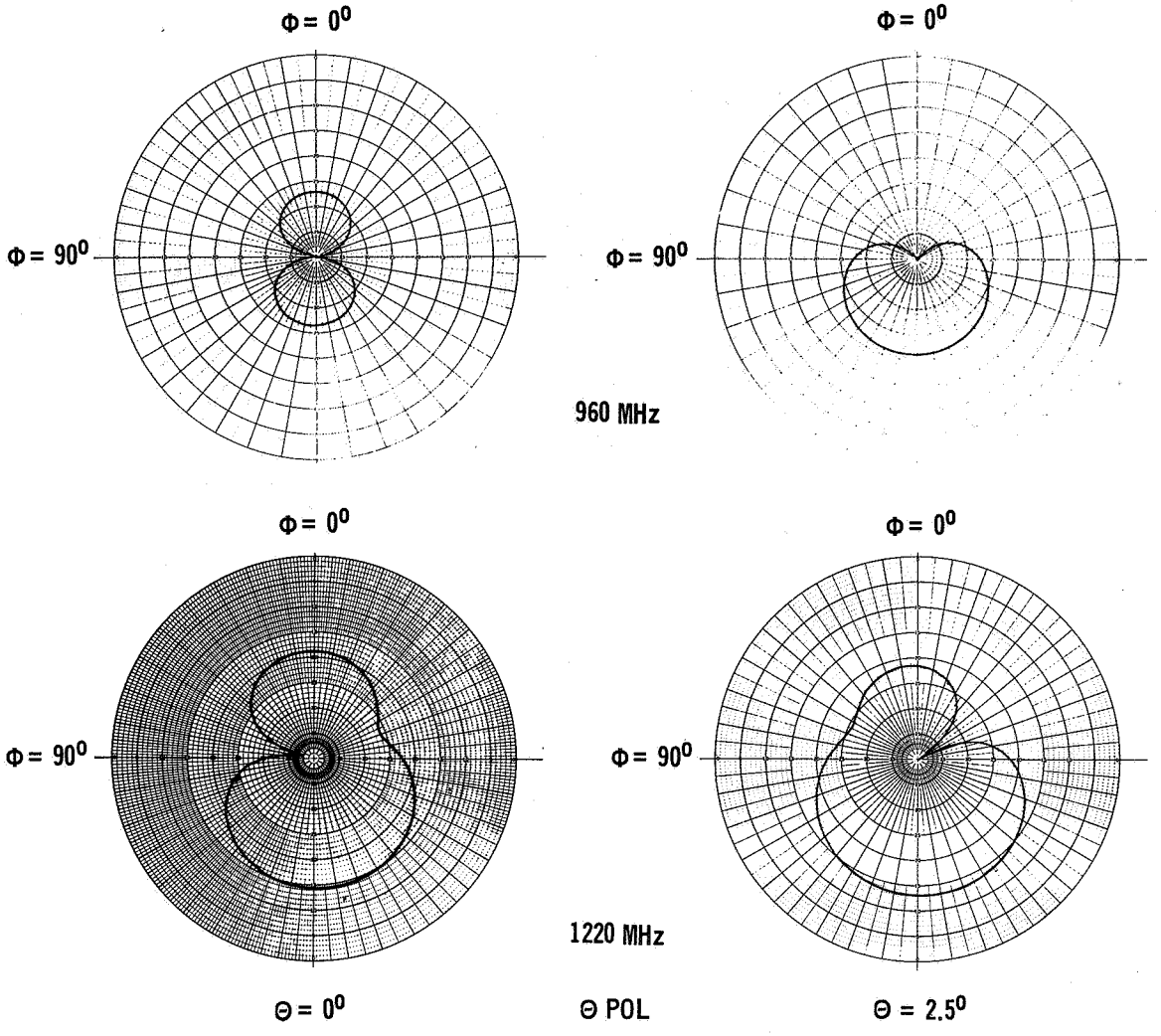

L-BAND PATTERNS – NULL ORIENTATION

Figure 33

figuration) at a 152.4 m (500 ft.) transmitting distance. The ϕ polarization is about 15 dB below the peak radiation level at 1220 MHz, an improvement of about 6 to 1. The improvement was even greater at 960 MHz and 1090 MHz. The shapes of the θ polarization patterns were essentially the same as those obtained in the anechoic chamber. Therefore, the high cross polarization levels obtained in the pattern measured at the 12.19m (40 ft.) distance are attributed to reflections from the anechoic chamber walls.

Patterns were measured with the ground plane covered with simulated TPS. The results are shown in figure 36 for 5.08 cm (2.0 in.) thick Eccofoam and 6.35 mm (0.25 in.) thick sponge, covering a 76.2 x 76.2 cm (30 x 30 in.) area. The peak gain is reduced less than 1 dB and a slight dip in the pattern magnitude can be seen at about $\theta = 35°$. The pattern magnitude $\theta = 90°$ increased 0.25 to 1.5 dB at the test frequencies. The results with a 2.54 cm (1.0 in.) thick Eccofoam were essentially the same. Patterns with the sponge only showed a decrease in peak pattern gain of about 1 dB at 1220 MHz. This could be attributed in part to an increase in the VSWR of the antenna.

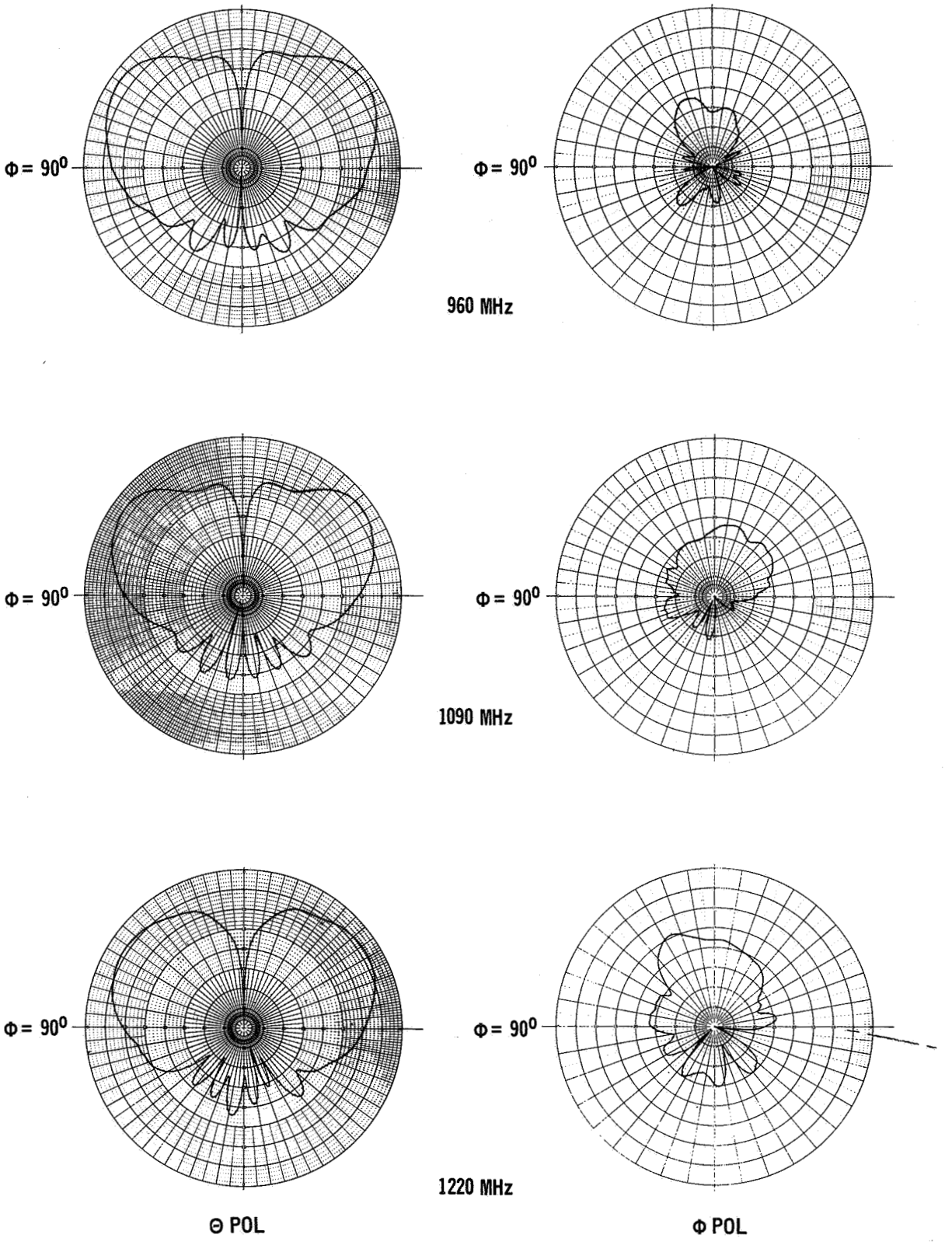

L-BAND REFERENCE PATTERNS – 12.9 M (40 FT) TRANSMIT DISTANCE

Figure 34

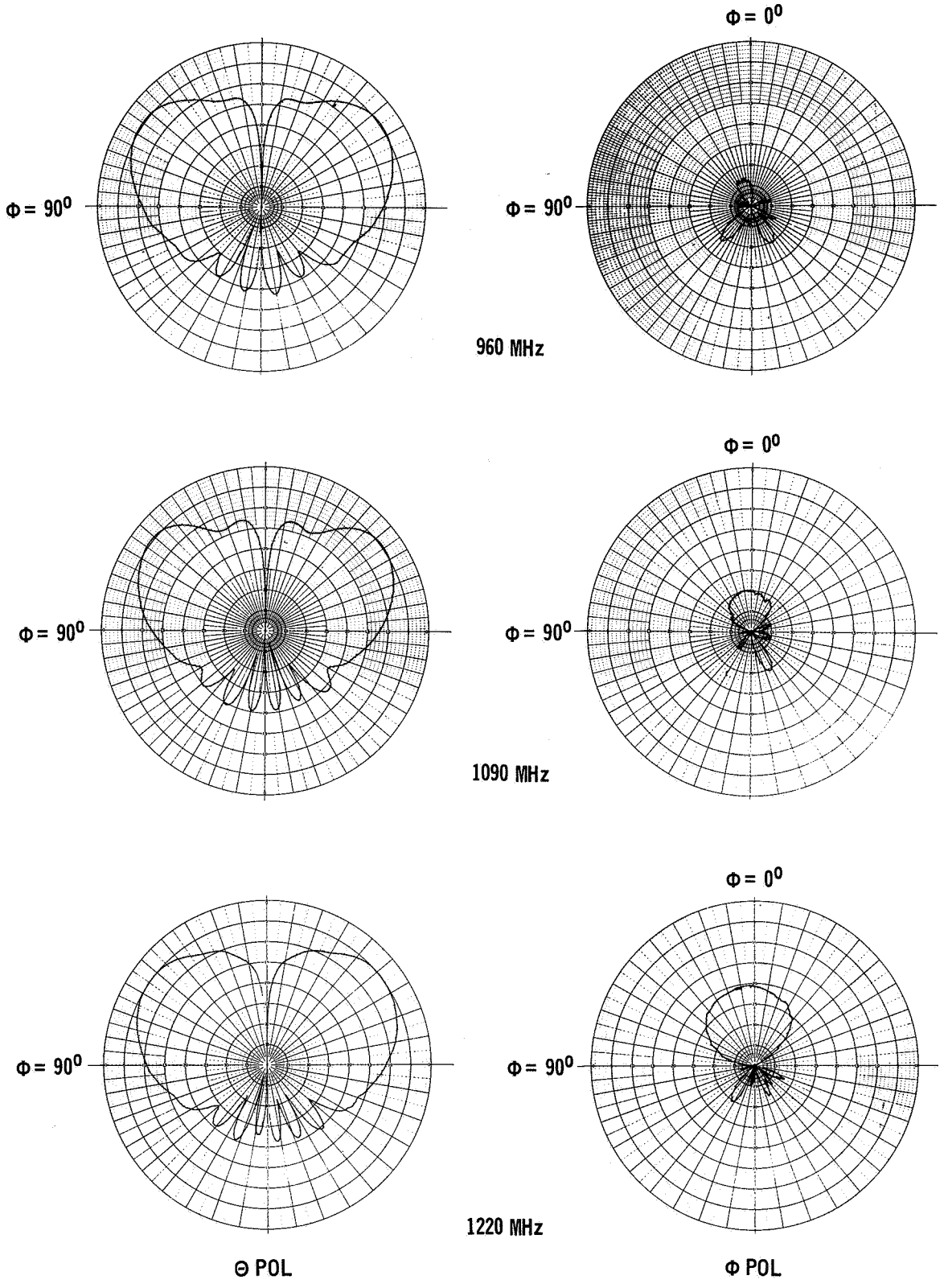

L-BAND REFERENCE PATTERNS – OUTDOOR RANGE, 152.4M (500 FT) TRANSMIT DISTANCE

Figure 35

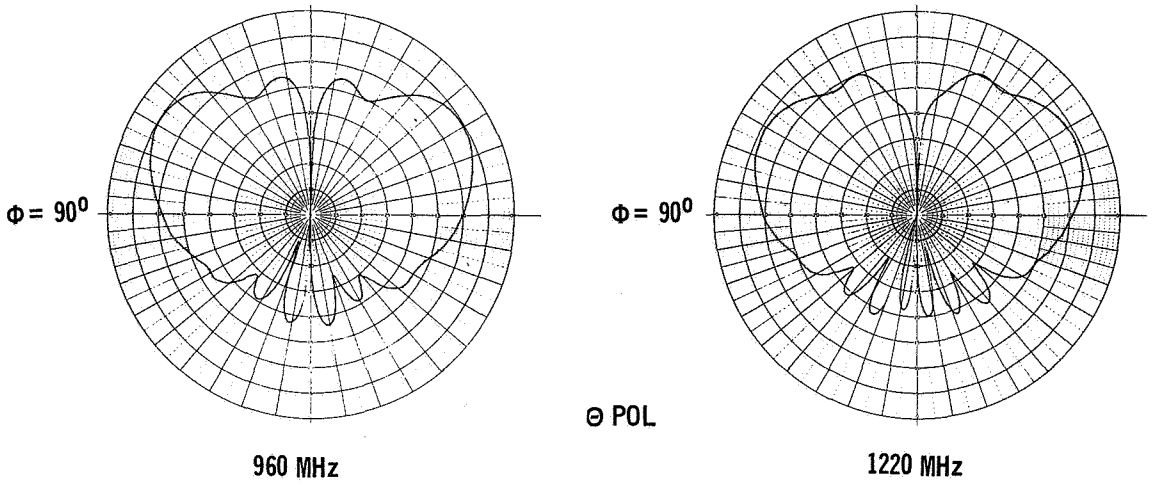

L-BAND PATTERNS WITH SIMULATED TPS – 5.08 CM (2.0 IN.) THICK

Figure 36

The results of impedance measurements for the simulated 5.08 cm (2.0 in.) TPS configuration are shown in figure 37. The VSWR is about 2:1 up to 1150 MHz and increases to 3:1 at 1220 MHz. The frequencies above 1150 MHz are used for receive only. The results with the 2.54 cm (1.0 in.) TPS were essentially the same. The results of measurements with the sponge only covering the ground plane and antenna, figure 38, show that the sponge has the major affect on the antenna impedance. However, in the preliminary L-band antenna system design, figure 16, the sponge is replaced by a honeycomb panel.

Radiation patterns were made with a 1.588 mm (0.0625 in.) gap in the Eccofoam both centered over the antenna and offset 2.54 cm (1.0 in.). There was no discernable difference between the patterns for this configuration and the configuration without a gap ; therefore, the patterns are not shown.

Measurements were made with the L-band antenna on a ground plane 1.83m (6 ft) in diameter to better assess the effects of surface waves on the radiation patterns. Figure 39 shows patterns of the antenna covered with 5.08 cm (2.0 in.) thick Eccofoam over an area 76.2 x 76.x cm (30 x 30 in.) centered over the antenna. The effect is relatively small, increasing the gain about 1.0 dB at $\theta = 90°$ compared to that without the Eccofoam. A strip 30.48 x 76.2 x 5.08 cm (12 x 30 x 2 in.) was added along one radial. The principal effect, as shown by the radiation patterns in figure 40, is an increase in the gain along the ground plane in the direction of the added material. This can be considered an improvement for operational purposes, since an increase in gain is desirable in that region. However, a ground plane size comparable to that of the Orbiter surface, covered with the appropriate dielectric layer is required to accurately assess the effects of surface waves.

A review of the above results indicated that a window edge enclosure is not necessary for a single-layer RSI window. The patterns without an edge enclosure are superior to those with an enclosure. Therefore, the L-band single-layer window design was made without a window edge enclosure.

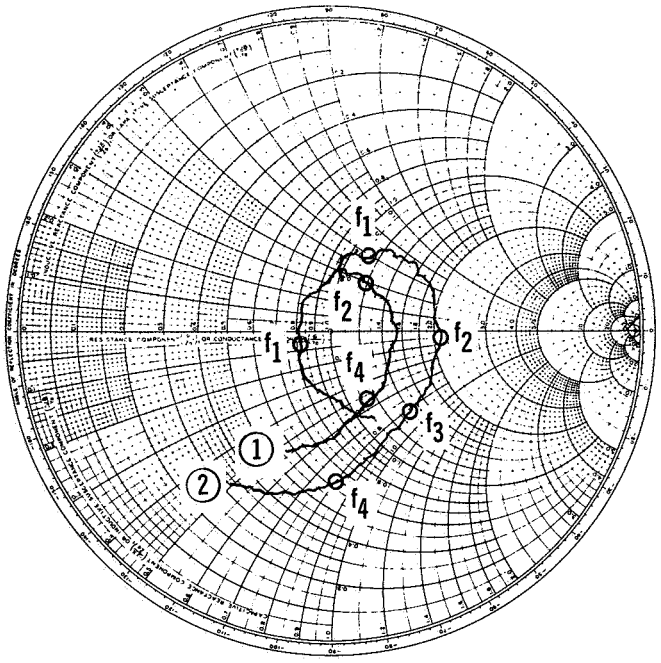

① REFERENCE
② 5.08 CM (2.0 IN.) TPS
Z_0 = 50Ω
f_1 = 960 MHz
f_2 = 1090 MHz
f_3 = 1150 MHz
f_4 = 1220 MHz
SWEEP RANGE
900 MHz TO 1300 MHz

L-BAND IMPEDANCE WITH SIMULATED TPS – 5.08 CM (2.0 IN.) THICK

Figure 37

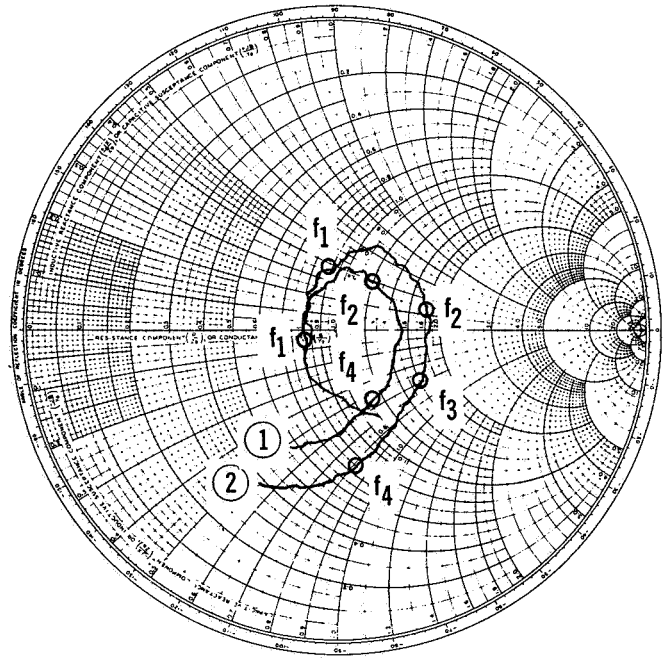

① REFERENCE
② 6.35 MM (0.25 IN.) SPONGE
Z_0 = 50Ω
f_1 = 960 MHz
f_2 = 1090 MHz
f_3 = 1220 MHz
f_4 = 1220 MHz
SWEEP RANGE
900 MHz TO 1300 MHz

L-BAND IMPEDANCE – 6.35 MM (0.25 IN.) SPONGE ONLY

Figure 38

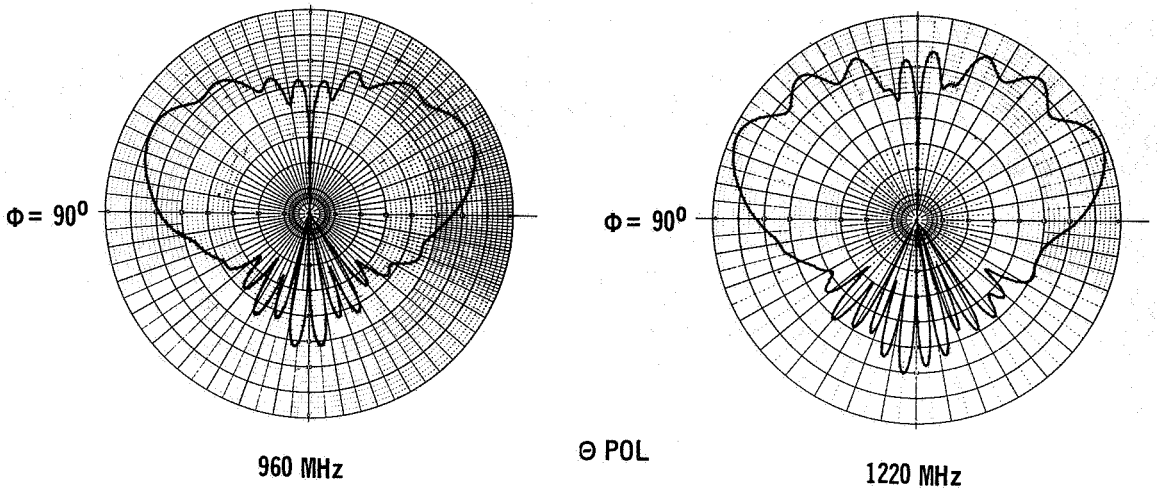

L-BAND PATTERNS WITH SIMULATED RSI–1.83M (6 FT) DIAMETER GROUND PLANE

Figure 39

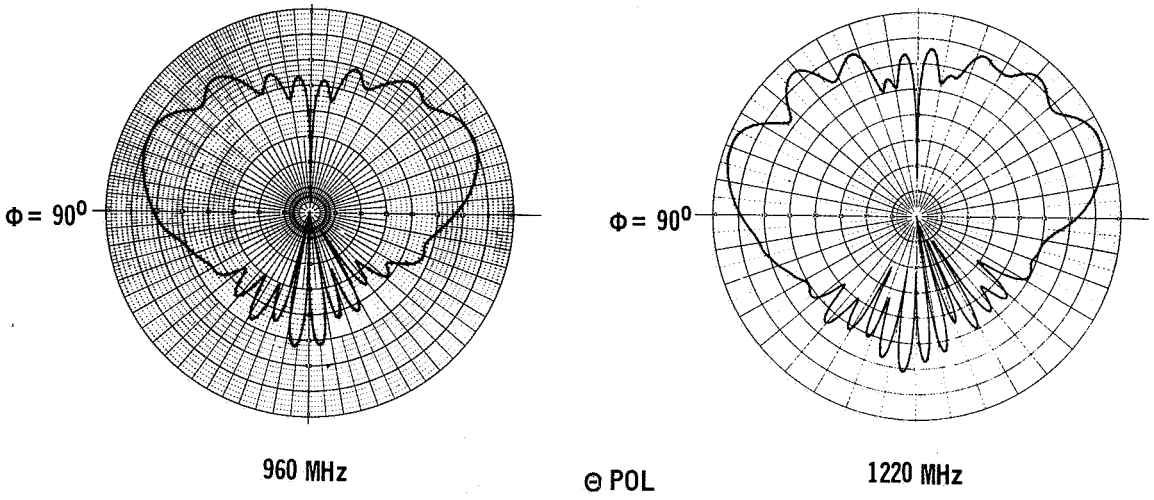

L-BAND PATTERNS WITH SIMULATED RSI RADIAL–1.83M (6 FT) DIAMETER GROUND PLANE

Figure 40

The final L-band single-layer antenna window configuration tested is described in the section on ANTENNA SYSTEM DESIGN AND INTEGRATION, figure 85. This configuration consists of a fiberglass honeycomb panel with a layer of sponge between the antenna aperture and the Eccofoam. Figure 41 shows a photo of the test set-up. Figure 42 shows the radiation patterns for this configuration. These patterns compare very closely to the reference patterns shown in figure 43. (Note: new reference patterns were measured because of refurbishment and material changes in the anechoic chamber.) The results of impedance measurements are shown in figure 44. The VSWR is less than 2.2:1 up to 1150 MHz and less than 2.7:1 at 1220 MHz.

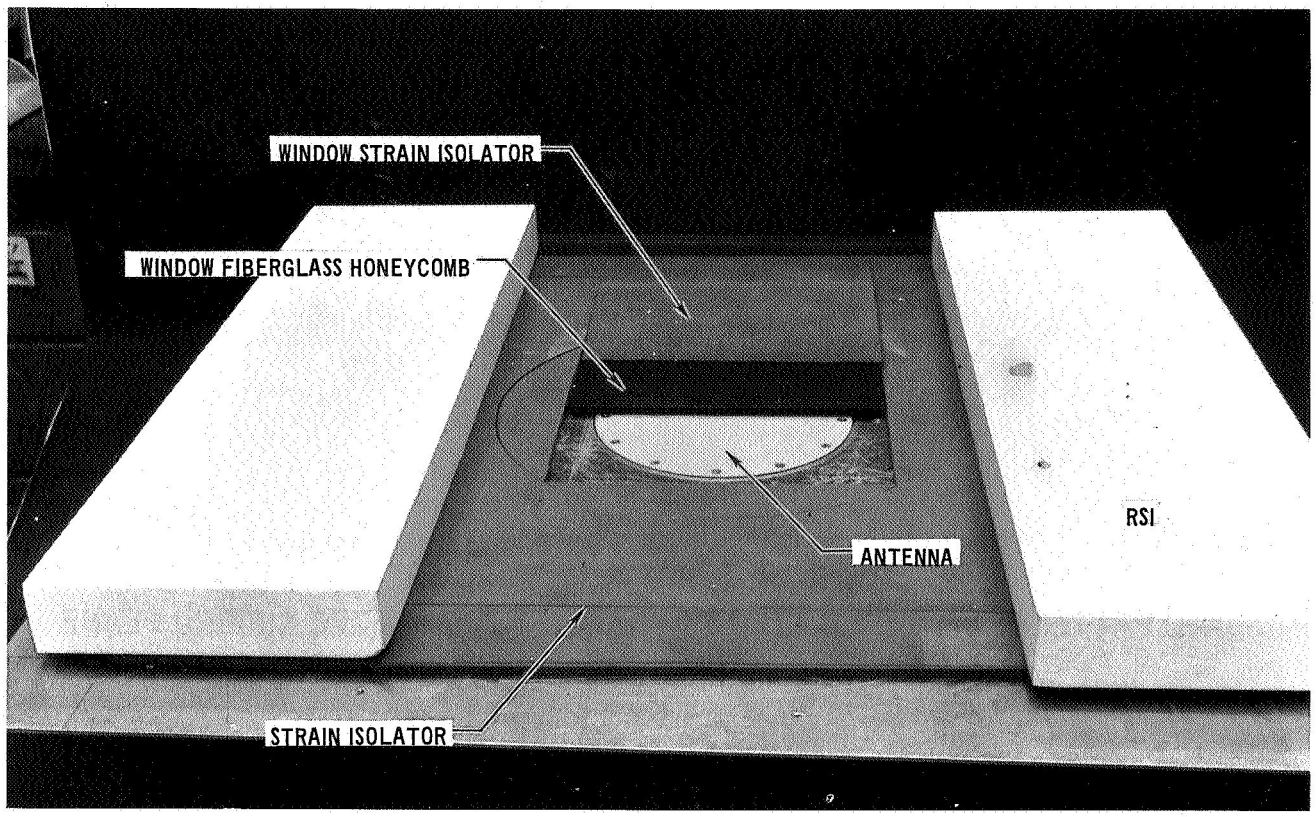

L-BAND ANTENNA SYSTEM – SINGLE-LAYER WINDOW SIMULATION

Figure 41

The L-band multiple-layer antenna window configuration tested is equivalent to that described in the section on ANTENNA SYSTEM DESIGN AND INTEGRATION, figure 86. This configuration consists of a layer of Stycast HiK, simulating boron nitride (HD-0092), and a layer of Dynaquartz. Figure 45 shows a photo of this configuration. Figure 46 shows the radiation patterns for a 32.40 cm (12.6 in.) diameter multiple-layer window. These patterns differ considerably from those measured for a 31.75 cm (12.5 in.) window diameter, figure 28. The pattern magnitude is increased in the region of $\theta = 10°$ to $\theta = 30°$ and is reduced about 5 dB at $\theta = 90°$. The changes are attributed to the difference in the dielectric constant of the Stycast HiK outer window layer and that of the Styrofoam used in the earlier measurements. The changes noted in these patterns, figure 46, were compared with calculated patterns (ref. 4) assuming a 31.75 cm (12.5 in.) circular waveguide aperture filled with a material having a dielectric constant of 4, a TM_{01} aperture distribution, and terminated in a ground plane of like size. The calculated patterns show the same general trends in the beam shape as the measured patterns.

The results of the impedance measurements, figure 47, on the multiple-layer antenna window show a increase in VSWR and a distinct rotation of the impedance plot compared to those obtained for the simple 31.75 cm (12.5 in.) window diameter (figure 32). At the transmit frequencies, 1090 to 1150 MHz, the

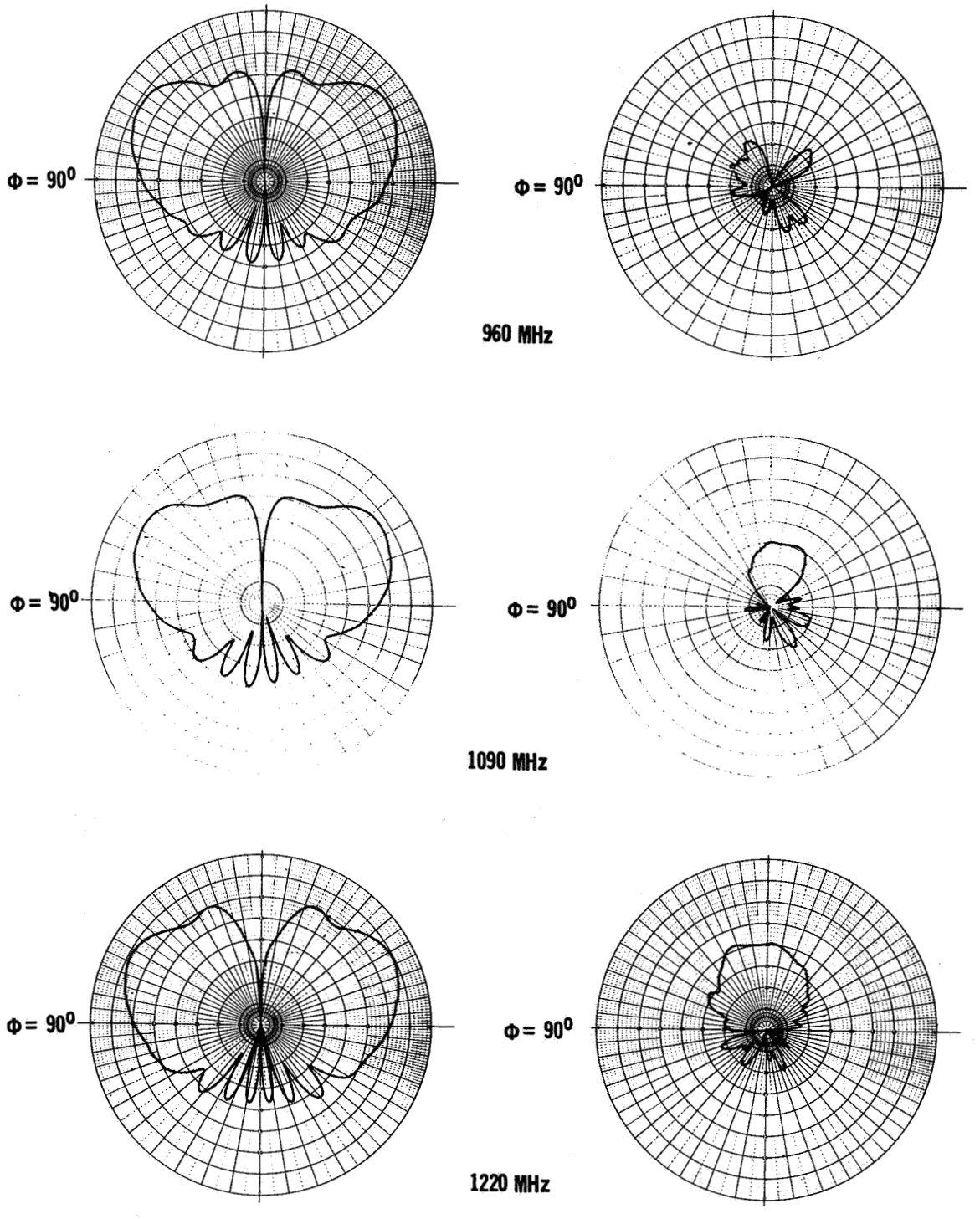

L-BAND PATTERNS – SINGLE-LAYER RSI WINDOW AND SIMULATED TPS

Figure 42

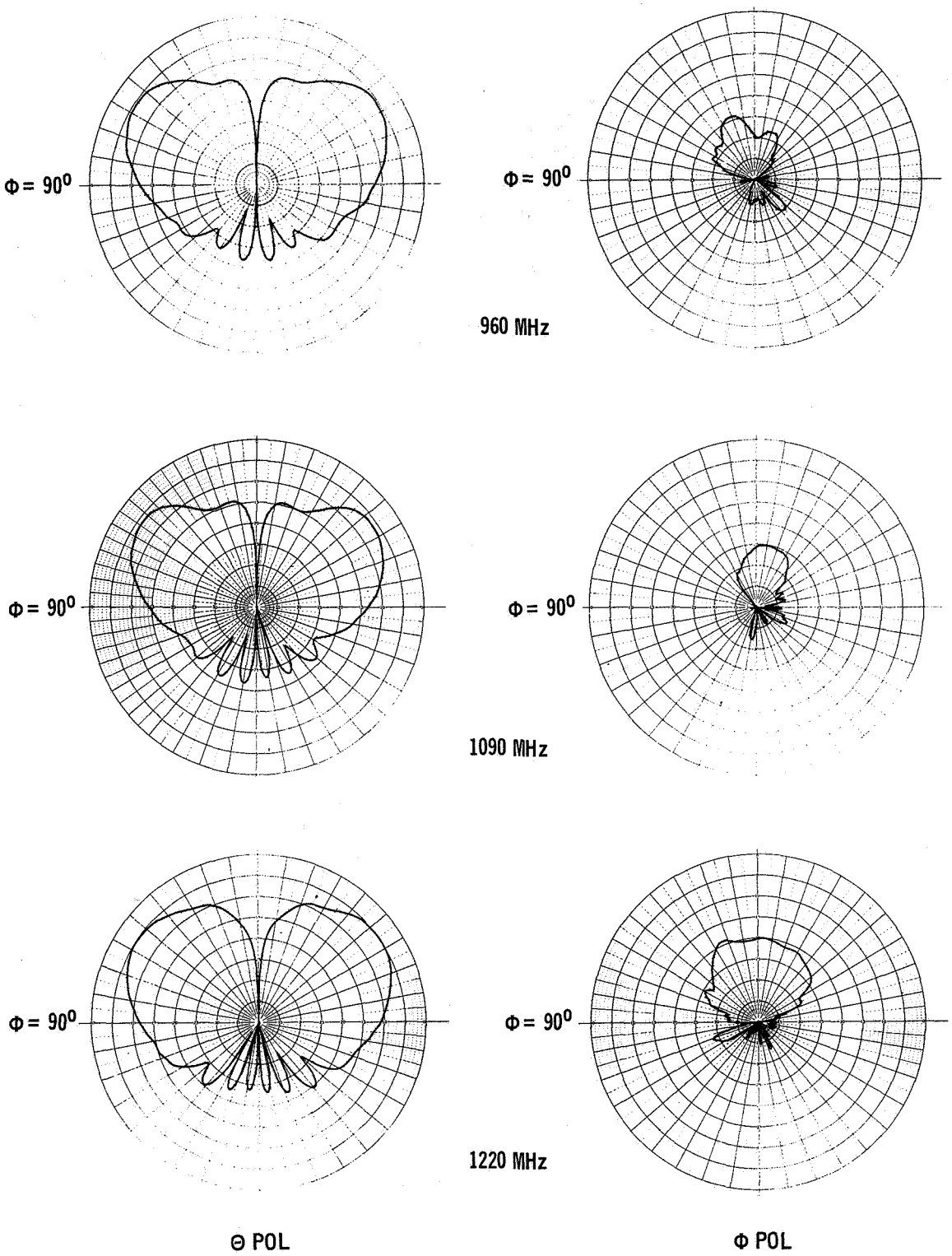

L-BAND REFERENCE PATTERNS – FINAL CONFIGURATIONS

Figure 43

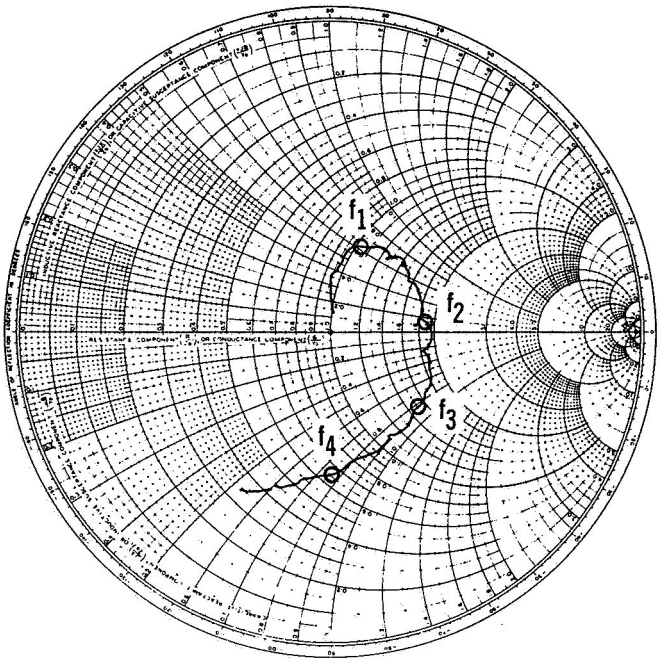

Z_0 = 50Ω
f_1 = 960 MHz
f_2 = 1090 MHz
f_3 = 1150 MHz
f_4 = 1220 MHz
SWEEP RANGE
900 MHz TO 1330 MHz

L-BAND IMPEDANCE–SINGLE-LAYER WINDOW

Figure 44

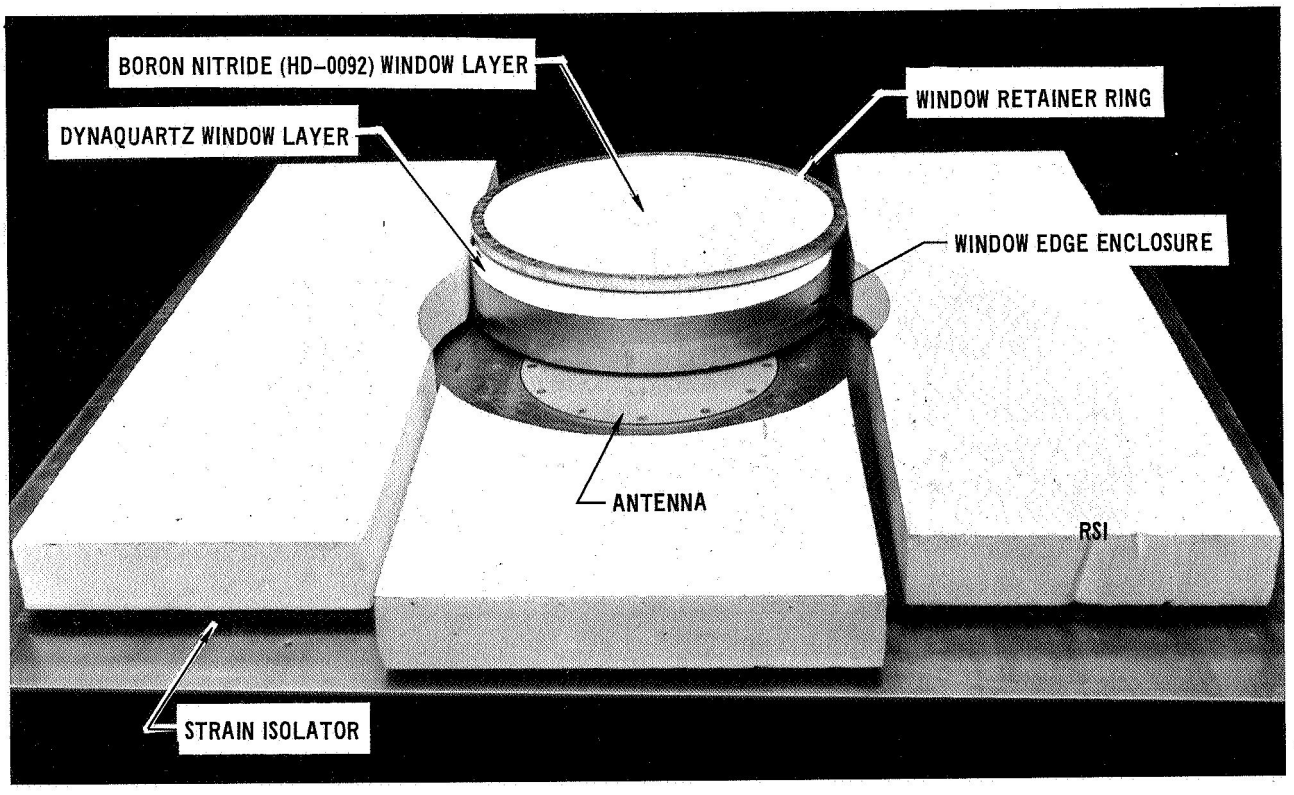

L-BAND ANTENNA SYSTEM – MULTIPLE-LAYER WINDOW SIMULATION

Figure 45

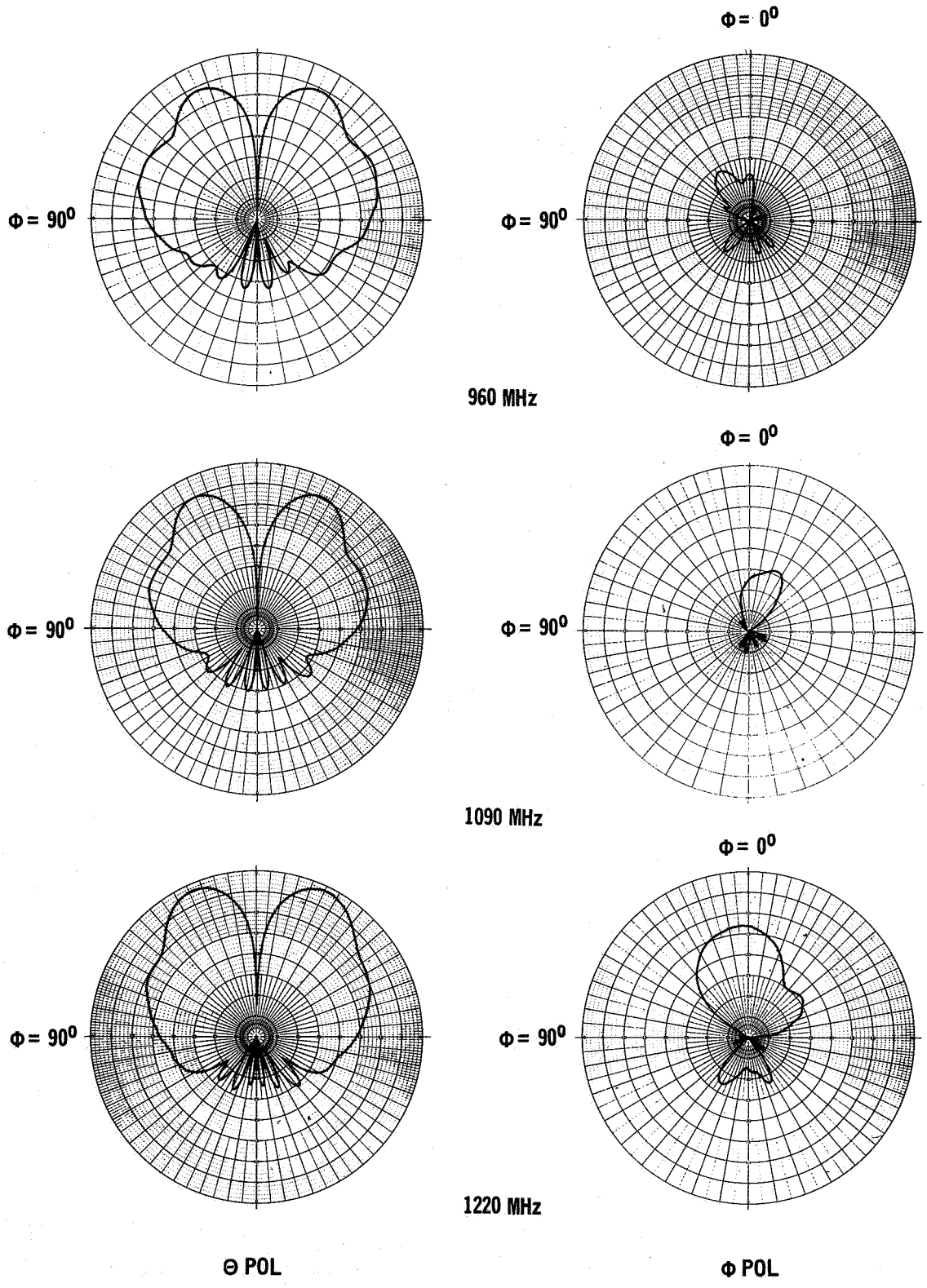

L-BAND PATTERNS – MULTIPLE-LAYER WINDOW AND SIMULATED TPS

Figure 46

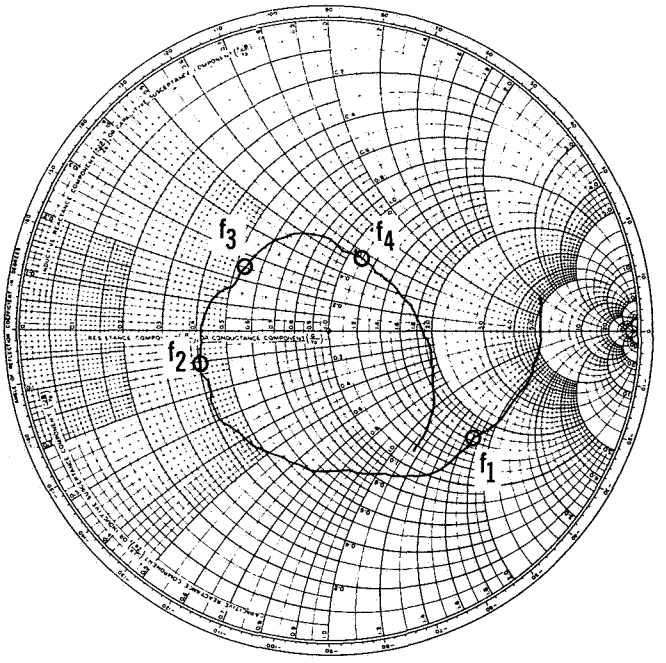

Z_0 = 50Ω
f_1 = 960 MHz
f_2 = 1090 MHz
f_3 = 1150 MHz
f_4 = 1220 MHz
SWEEP RANGE
900 MHz TO 1330 MHz

L-BAND IMPEDANCE – MULIPLE-LAYER WINDOW

Figure 47

VSWR varies from 2.5:1 to 2:1. At the receive frequencies the VSWR is less than 4:1. With the Stycast HiK layer removed, the impedance plot (figure 48) was essentially the same as that shown in figure 32 for the simple window case. These results indicate that the outer layer of the multiple-layer window configuration has a considerable effect on the L-band antenna impedance. An attempt to improve the impedance match by placing an "iris" in the window area resulted in a general increase in the VSWR at all frequencies of interest.

C-band horn antenna: Radiation patterns for the C-band horn antenna flush mounted in a square ground plane are shown in figure 49. These patterns serve as a reference for comparison with the patterns measured for the window configurations considered in the C-band horn design study. Patterns were measured at 4300 MHz only, because of the narrow operating frequency band requirements. The impedance was measured from 4250 to 4350 MHz.

The initial tests were made to determine the effect of a window edge enclosure extending above the ground plane. The window edge enclosures consisted of sheet metal cylinders 2.54 and 5.08 cm (1.0 and 2.0 in.) long with diameters of 11.43 cm (4.5 in.), 15.24 cm (6.0 in.), 20.32 cm (8.0 in.), 22.86 cm (9.0 in.), and 27.94 cm (11.0 in.). These cylinders were filled with Styrofoam for good dimensional control and attached to the ground plane with a metal conductive tape. As in the case of the L-band antenna system measurement, the cylinder had the affect of terminating the antenna aperture in a circular waveguide. Radiation patterns for these configurations are shown in figures 50 through 53. Side lobes develop and disappear as the window diameter and thickness are varied. The best results were obtained for the 15.24 cm (6.0 in.) and

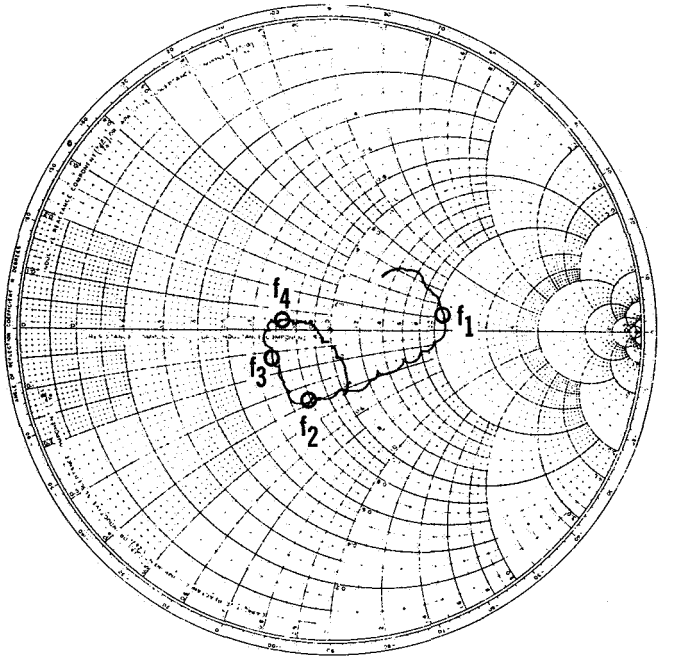

Z_0 = 50Ω
f_1 = 960 MHz
f_2 = 1090 MHz
f_3 = 1150 MHz
f_4 = 1220 MHz
SWEEP RANGE
900 MHz TO 1300 MHz

L-BAND IMPEDANCE – STYCAST WINDOW LAYER REMOVED

Figure 48

20.32 cm (8.0 in.) window diameters. In general the results of these measurements were similar to the LaRC measurements (ref. 3) discussed in the section on L-band annular slot antenna system. It appears that good patterns can be obtained by selecting the proper window dimensions.

The impedance of the C-band horn antenna was generally shifted to a lower value by the different window configurations. Figure 54 shows the impedance for the reference configuration. Figure 55 shows the impedance for the 15.24 cm (6.0 in.) diameter window, 2.54 cm (1.0 in.) thick. The VSWR is increased but is still less than 2:1. This result is also typical of the magnitude of change for the other window configurations tested.

Measurements were made with the ground plane and antenna aperture covered with 2.54 cm (1.0 in.) and 5.08 cm (2.0 in.) thick Eccofoam covering an area 76.2 x 76.2 cm (30 x 30 in.). The patterns are shown in figure 56. Side lobes developed in the E-plane for both thicknesses and in the H-plane for the 5.08 cm (2.0 in.) Eccofoam thickness. The impedance of the antenna was virtually unaffected as shown in figure 57 for the 5.08 cm (2.0 in.) Eccofoam thickness.

The TPS simulation was improved by adding a 6.35 mm (0.25 in.) thick strain isolator sponge to the 5.08 cm (2.0 in.) thick Eccofoam. Figure 58 shows the patterns for this configuration. The E-plane pattern side lobes are increased and both the E- and H-plane patterns show more pronounced effects of surface wave excitation. These results show that the sponge has a strong effect on the

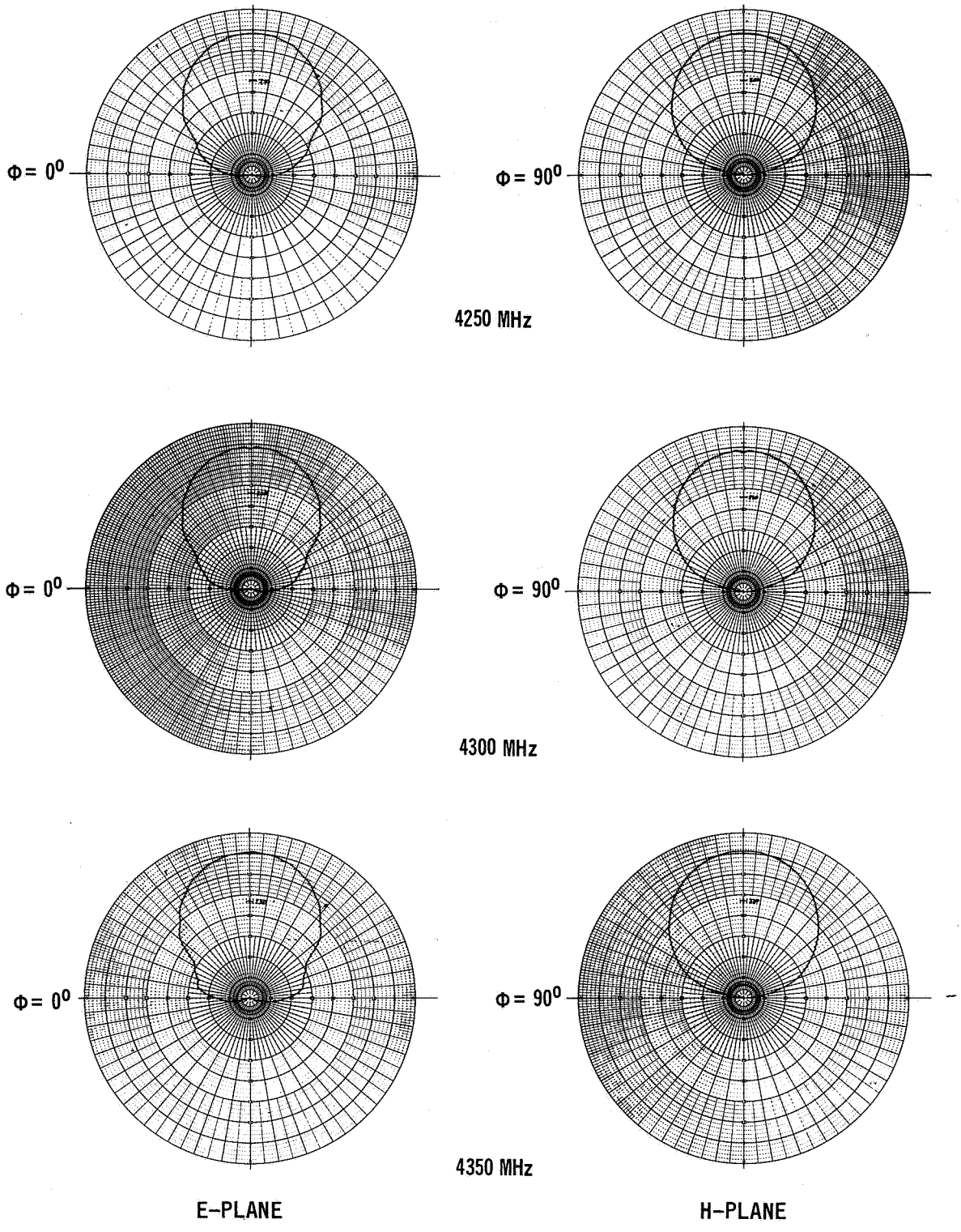

C-BAND HORN REFERENCE PATTERNS

Figure 49

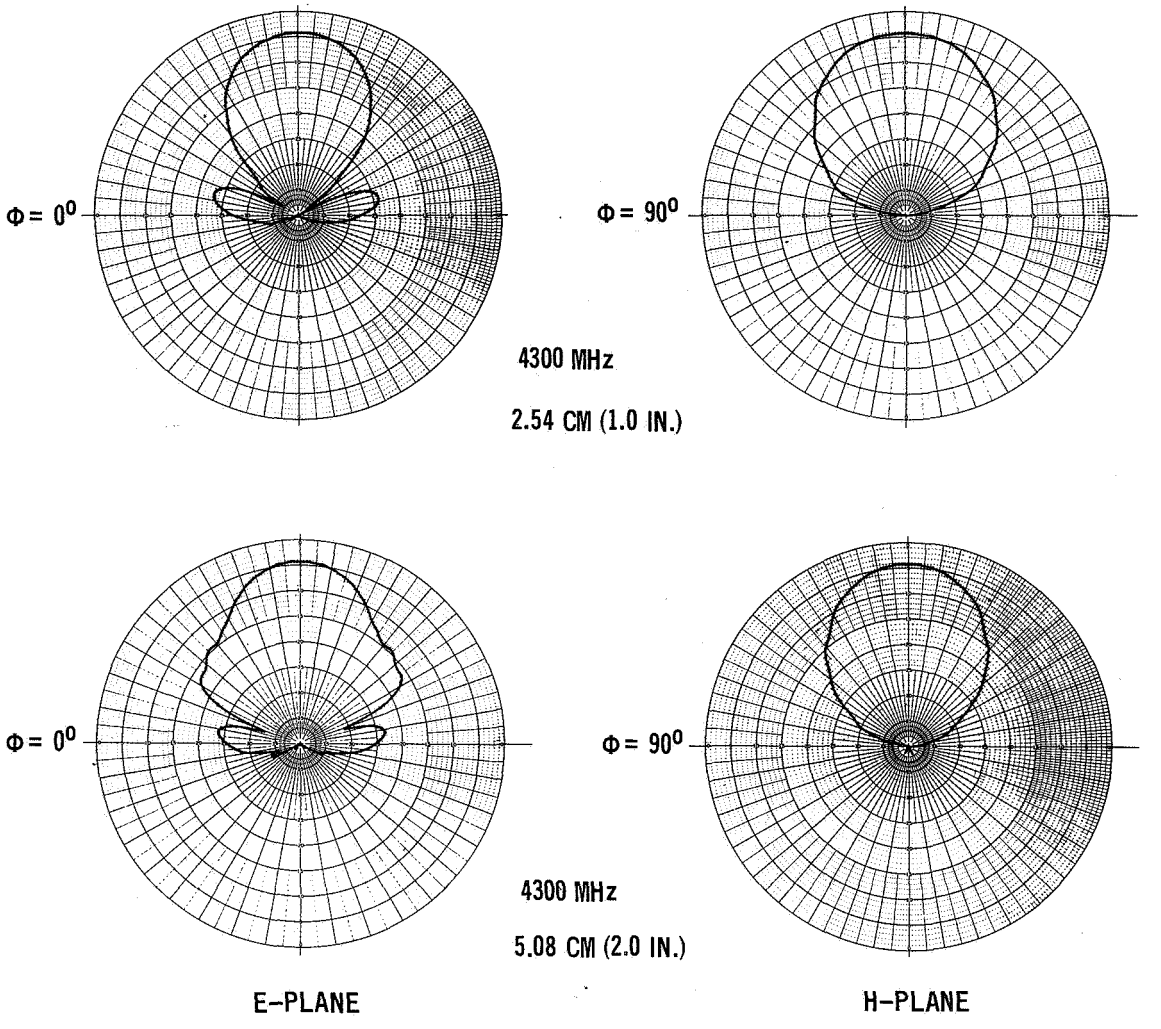

C-BAND HORN PATTERNS – 11.43 CM (4.5 IN.) DIAMETER WINDOW

Figure 50

level of surface wave excitation. Based on these results, the 15.24 cm (6.0 in.) diameter window was selected for further design efforts based on the single-layer antenna window.

Initial test results indicated that the 15.24 cm (6.0 in.) diameter window had to be reduced to 13.97 cm (5.5 in.) to account for the difference in the dielectric constant of Eccofoam and Styrofoam. The window edge enclosure was reduced from 5.08 cm (2.0 in.) in height to 2.54 cm (1.0 in.) to reduce its heat short effect as discussed in the section on Thermal Analysis. Figure 59 shows the patterns with the ground plane covered with 5.08 cm (2.0 in.) Eccofoam and the window edge enclosure extending 2.54 cm (1.0 in.) in to the Eccofoam. The E-plane pattern side lobes are essentially eliminated, but the H-plane pattern side lobes are increased about 4 dB compared to those measured without a window edge enclosure shown in figure 56. An unsuccessful attempt was made to reduce the H-plane side lobes by adding a choke type structure around the window edge enclosure.

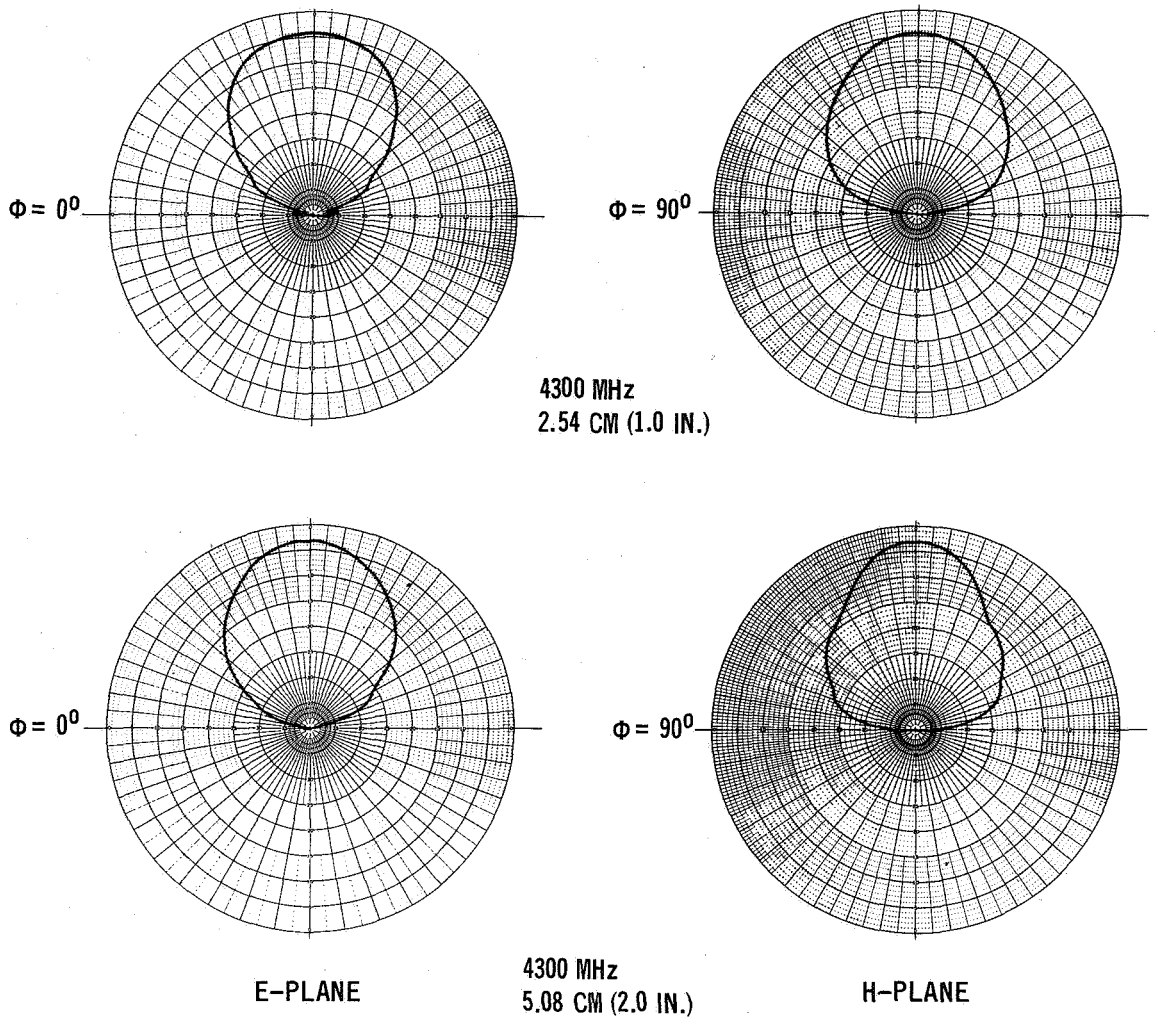

C-BAND HORN PATTERNS – 15.24 CM (6.0 IN.) DIAMETER WINDOW

Figure 51

Measurements were made to establish the quality of the final C-band horn antenna system design described in the section on ANTENNA SYSTEM DESIGN AND INTEGRATION, figure 87. Figure 60 shows a photo of the test set-up. Figure 61 shows the radiation patterns of the final configuration. The H-plane side lobes occur at $\theta = 80°$ and are 15 dB below the pattern peak. The results of the impedance measurements are shown in figure 62. The VSWR increases with this window configuration, but is still less than 2:1. It appears that a change in the impedance matching network of the C-band horn antenna could easily reduce the VSWR to less than 1.5:1.

C-band slot antenna: A tunable C-band slot antenna was fabricated for use in these tests in lieu of using an off-the-shelf antenna. A photo of this antenna is shown in figure 63. Radiation patterns for the C-band slot antenna flush mounted in a ground plane are shown in figure 64. These patterns serve as a reference for comparison with the patterns measured for the various C-band slot designs. Patterns were measured at 5125 MHz only because of the narrow

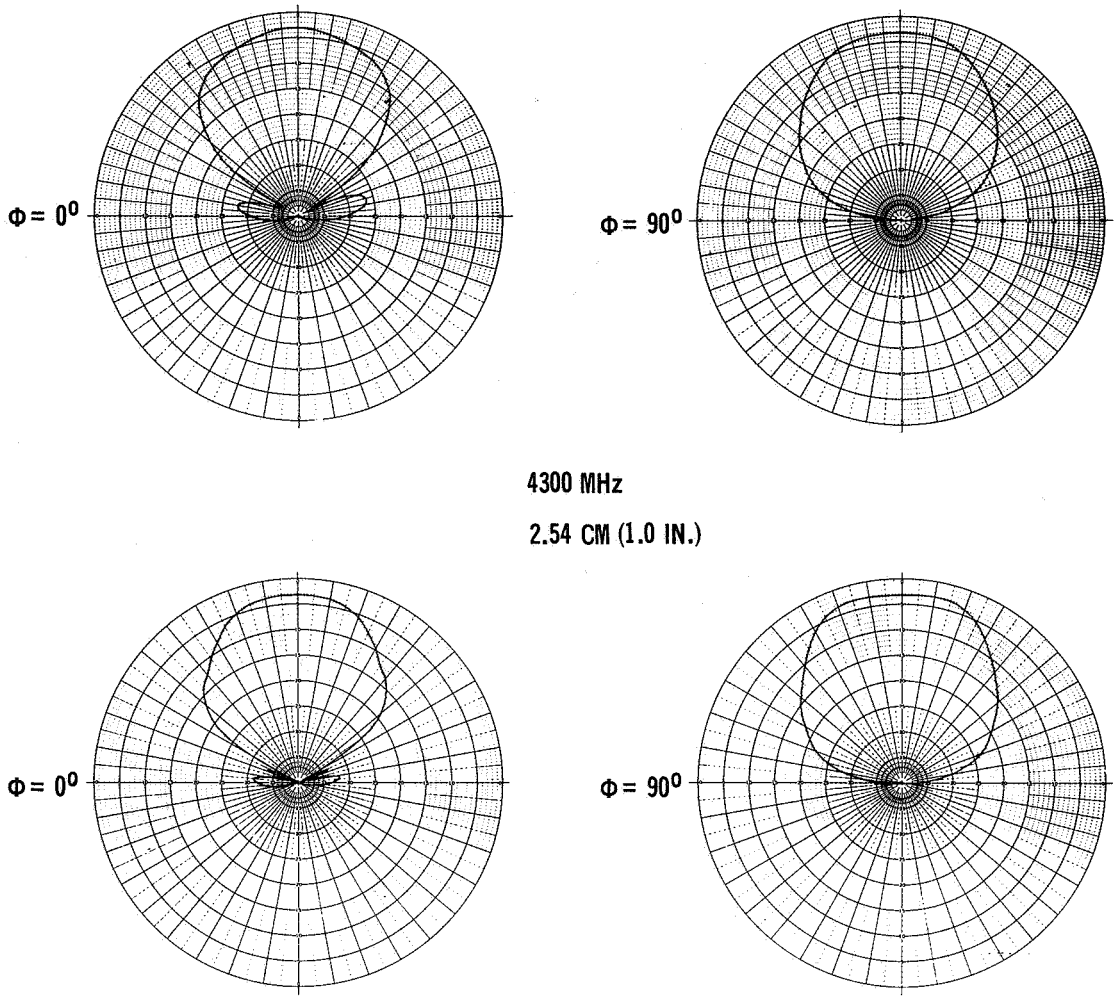

C-BAND HORN PATTERNS – 22.86 CM (9.0 IN.) DIAMETER WINDOW

Figure 52

operating frequency band requirements. The impedance was measured from 5000 to 5250 MHz. Tuning was required for each window configuration. This was accomplished with the tuning screws showin in figure 63 and aperture "irises". In general, the antenna could be tuned to a VSWR of less than 1.5:1. The one exception was a 6.35 cm (2.5 in.) diameter window edge enclosure. Therefore, the measured impedance will only be shown for this configuration and the final design configuration.

The initial tests were to determine the effect of a window edge enclosure extending above the ground plane. The window edge enclosures consisted of sheet metal cylinders. No attempt was made to provide a smooth transition from the antenna aperture to the window edge enclosure for any of the window configurations.

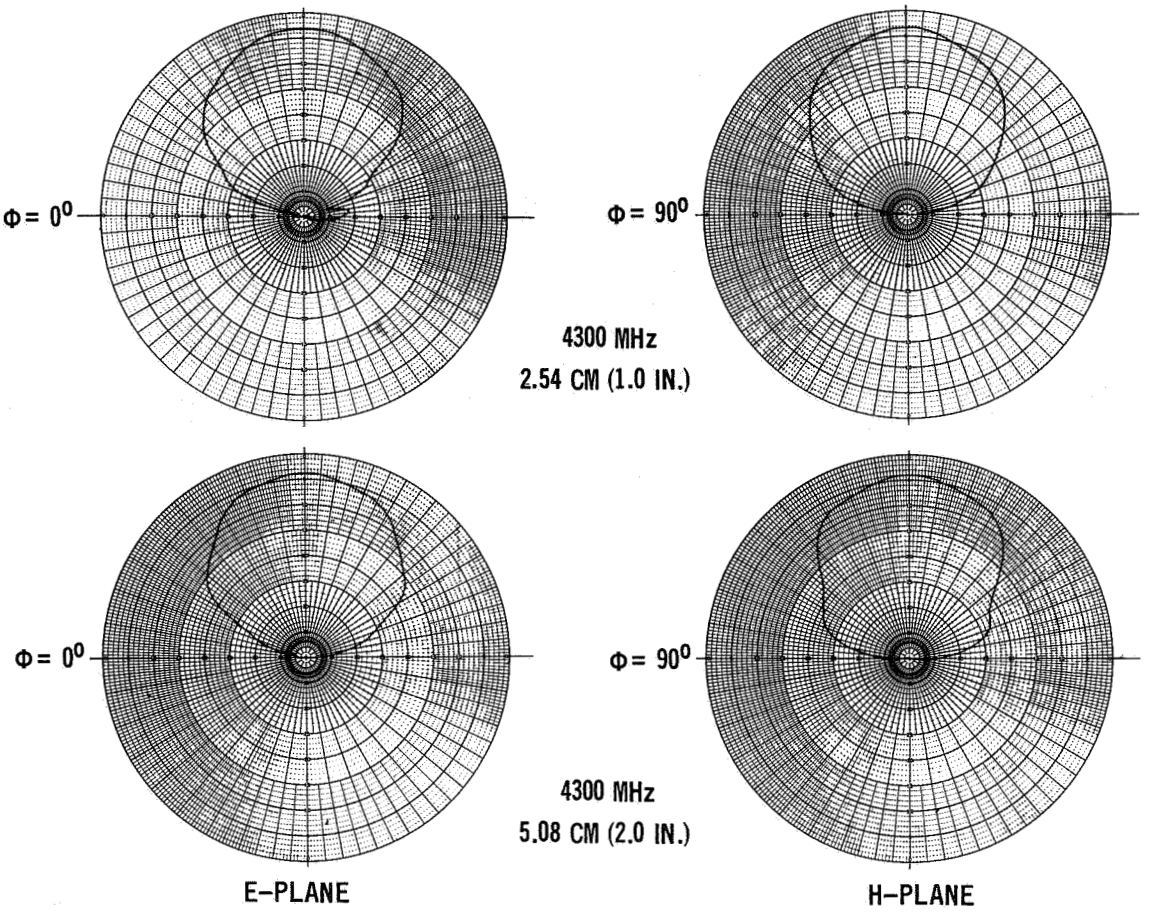

C-BAND HORN PATTERNS – 27.94 CM (11.0 IN.) DIAMETER WINDOW

Figure 53

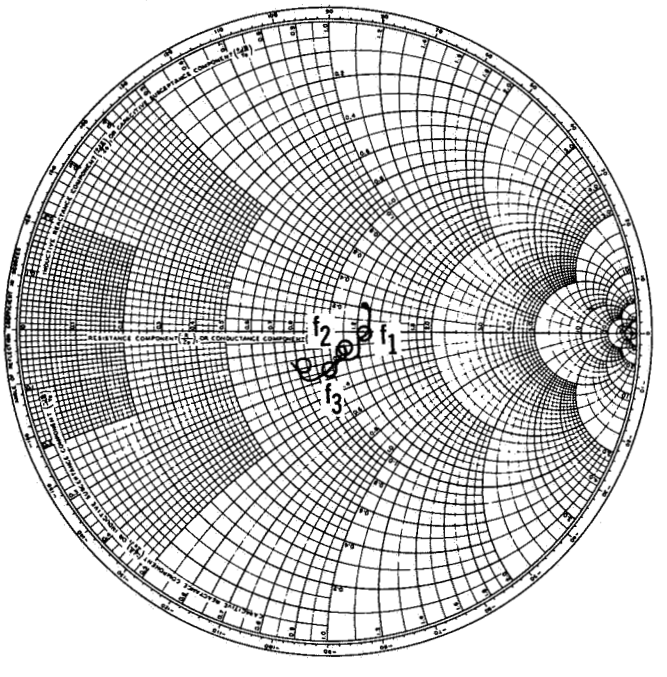

Z_0 = 50Ω
f_1 = 4250 MHz
f_2 = 4300 MHz
f_3 = 4350 MHz
SWEEP RANGE
4200 MHz TO 4400 MHz

C-BAND HORN REFERENCE IMPEDANCE

Figure 54

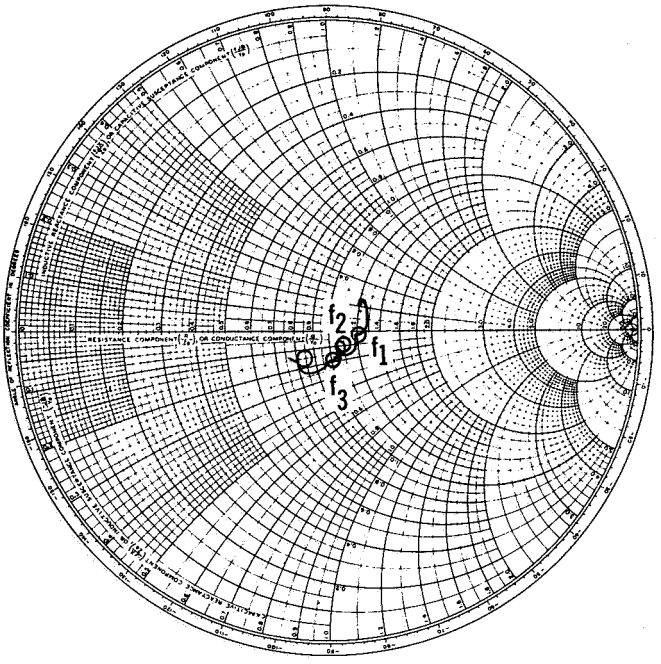

Z_0 = 50Ω
f_1 = 4250 MHz
f_2 = 4300 MHz
f_3 = 4350 MHz
SWEEP RANGE
4200 MHz TO 4400 MHz

C-BAND HORN IMPEDANCE – 15.24 CM (6.0 IN.) DIAMETER WINDOW

Figure 55

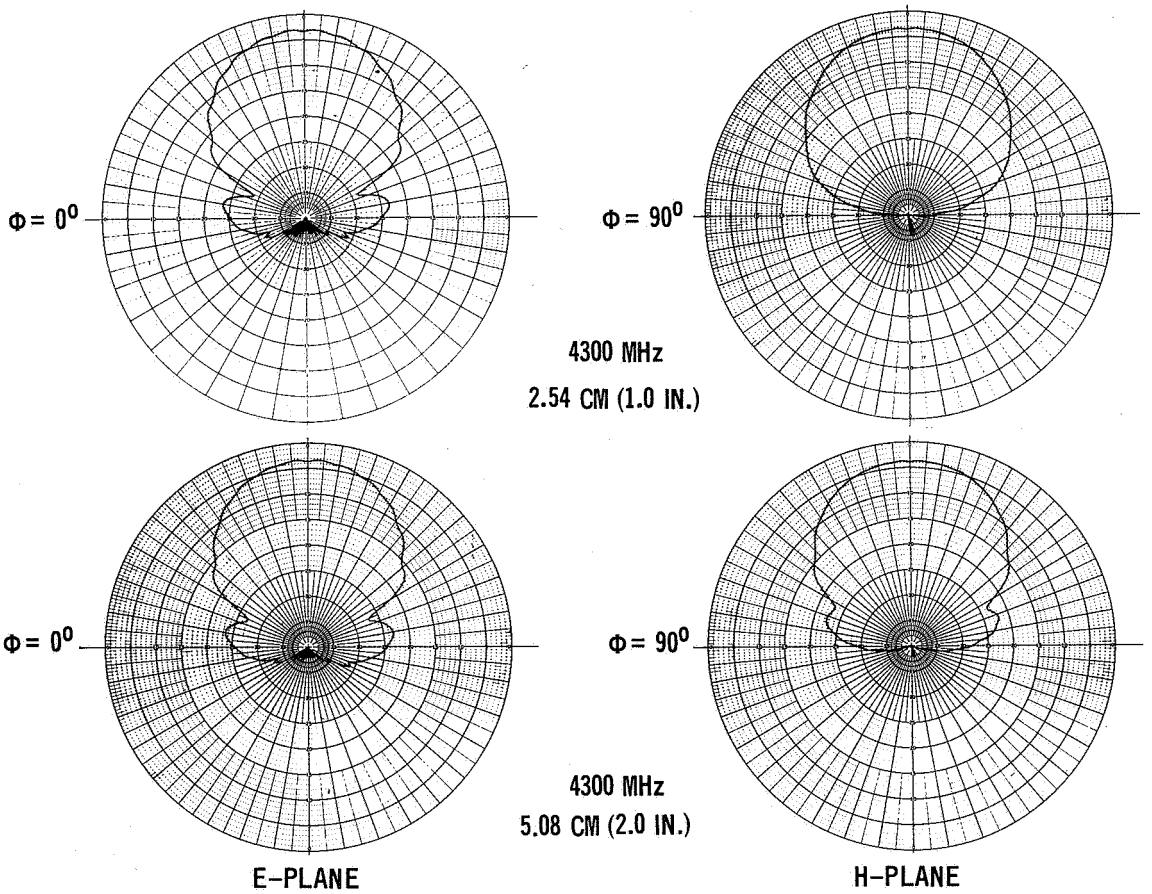

C-BAND HORN PATTERNS WITH SIMULATED RSI – 2.54 CM (1.0 IN.) AND 5.08 CM (2.0 IN.) THICK

Figure 56

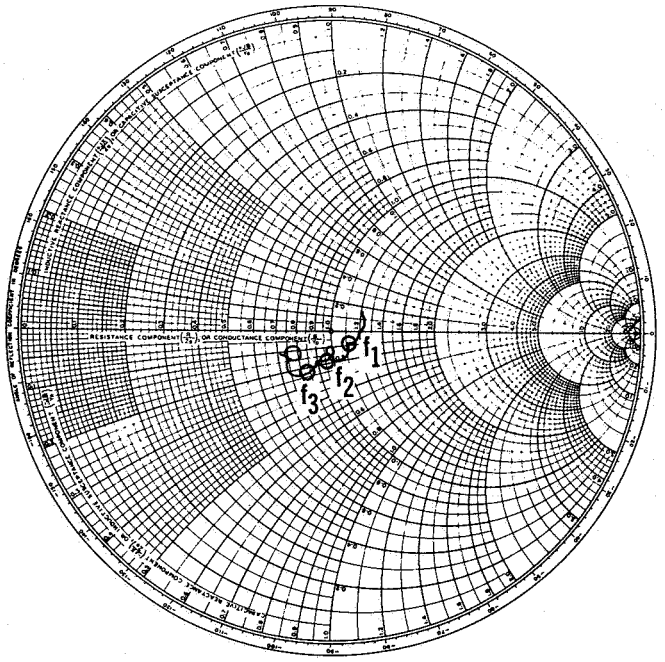

Z_0 = 50 Ω
f_1 = 4250 MHz
f_2 = 4300 MHz
f_3 = 4350 MHz

SWEEP RANGE
4200 MHz TO 4400 MHz

C-BAND HORN IMPEDANCE WITH SIMULATED RSI – 5.08 CM (2.0 IN.) THICK

Figure 57

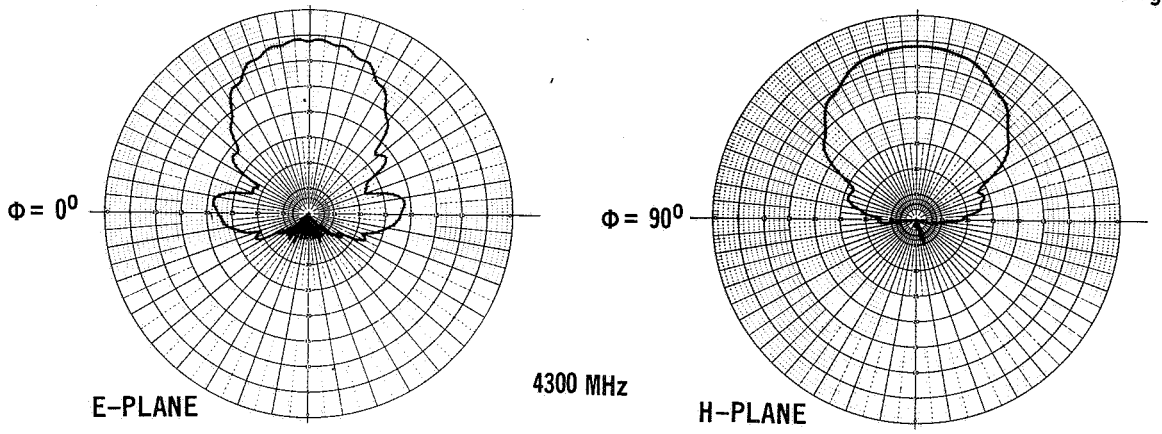

C-BAND HORN PATTERNS WITH SIMULATED TPS – 5.08 CM (2.0 IN.) THICK

Figure 58

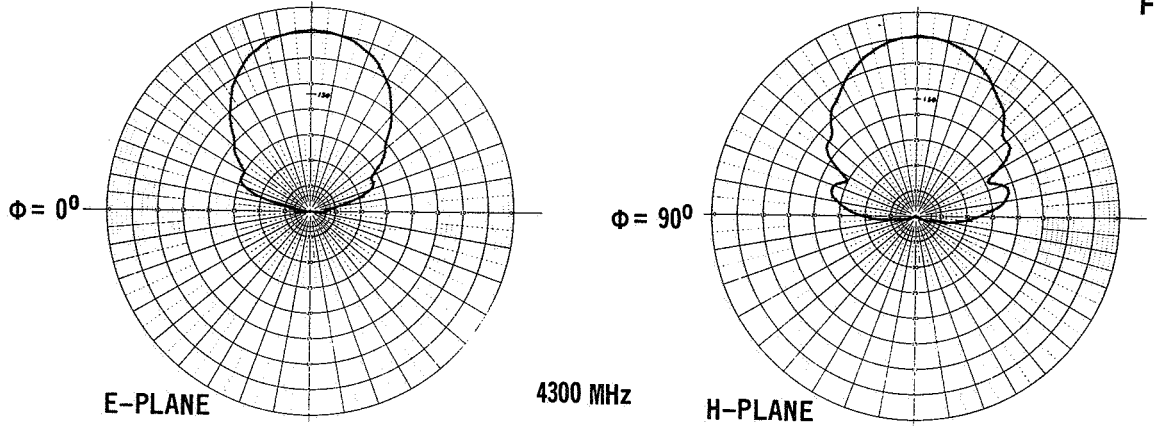

C-BAND HORN PATTERNS – 15.24 CM (6.0 IN.) DIAMETER WINDOW AND 5.08 CM (2.0 IN.) SIMULATED RSI

Figure 59

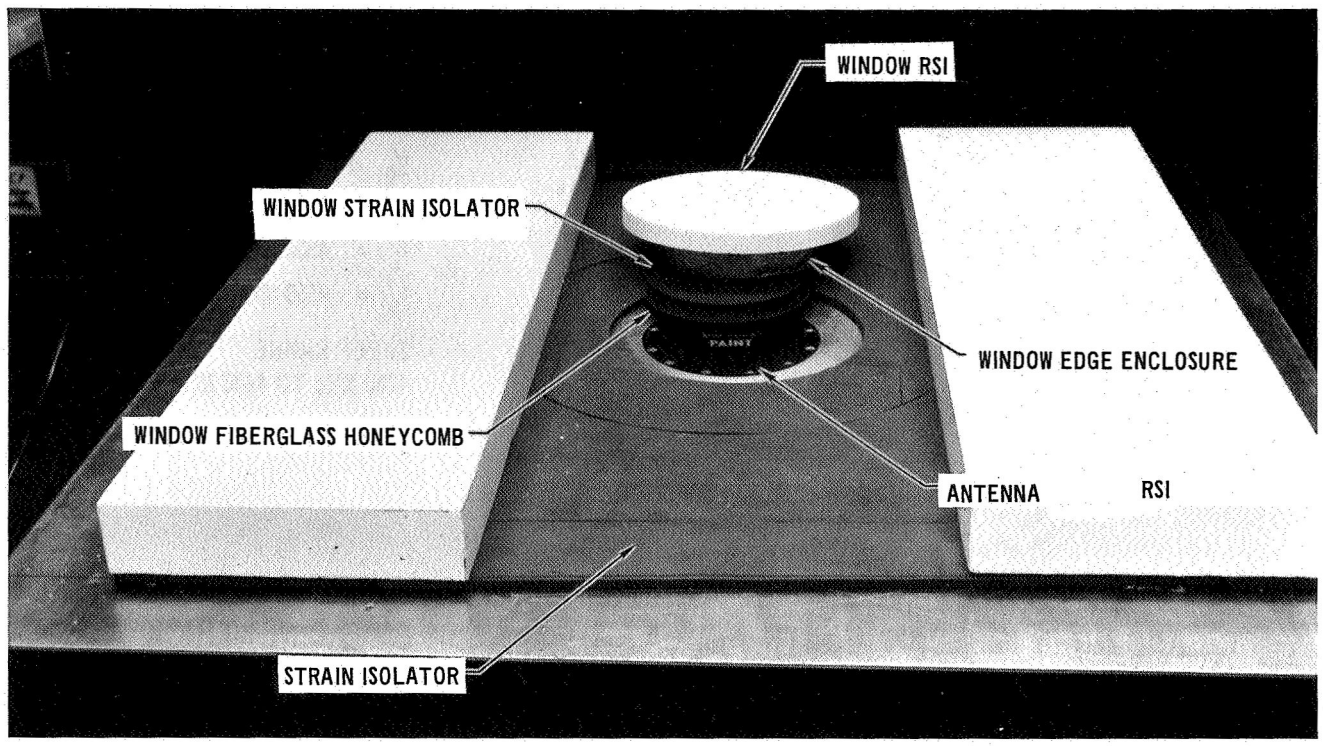

C-BAND HORN ANTENNA SYSTEM – FINAL CONFIGURATION SIMULATION

Figure 60

Figure 65 shows the patterns for a cylinder, filled with Eccofoam, 3.81 cm (1.5 in.) in diameter extending 2.54 cm (1.0 in.) above the ground plane. The E-plane pattern is narrower with apparent side lobes while the H-plane pattern appears to broaden. Patterns with the same cylinder, but with the Eccofoam removed were nearly identical. Figure 66 shows the patterns for an air filled cylinder 6.35 cm (2.5 in.) in diameter and extending 3.81 cm (1.5 in.) above the ground plane. The E-plane pattern is even narrower than that for the 3.81 cm (1.5 in.) window diameter, while the H-plane pattern is about the same as the reference configuration, figure 64. The E- and H-plane pattern beamwidths are nearly equal. This condition may be expected when the cylinder diameter is 1.22 wavelengths. These patterns demonstrate the pattern control which can be obtained by a variation in the window diameter.

The impedance for this configuration is shown in figure 67. This represents the best overall impedance characteristic obtainable. The VSWR could, however, be tuned to a very low value at any selected frequency.

Patterns measured for two (2) thicknesses of simulated TPS, covering the ground plane over a 76.2 x 76.2 cm (30 x 30 in.) area, are shown in figure 68. These patterns show the thickness of the TPS has considerable effect on the pattern shape from $\theta = 60°$ to $\theta = 90°$.

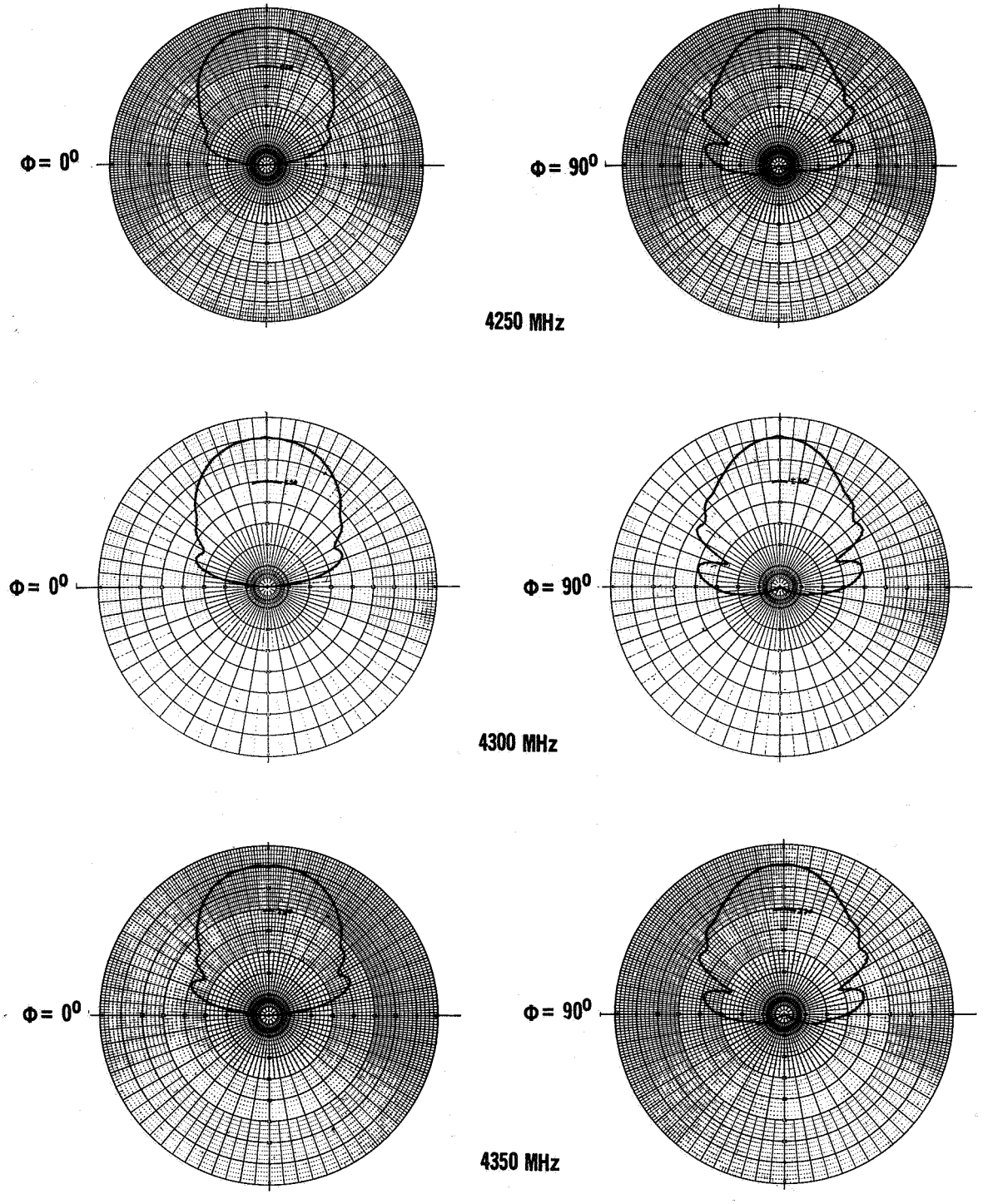

C-BAND HORN PATTERNS – FINAL CONFIGURATION

Figure 61

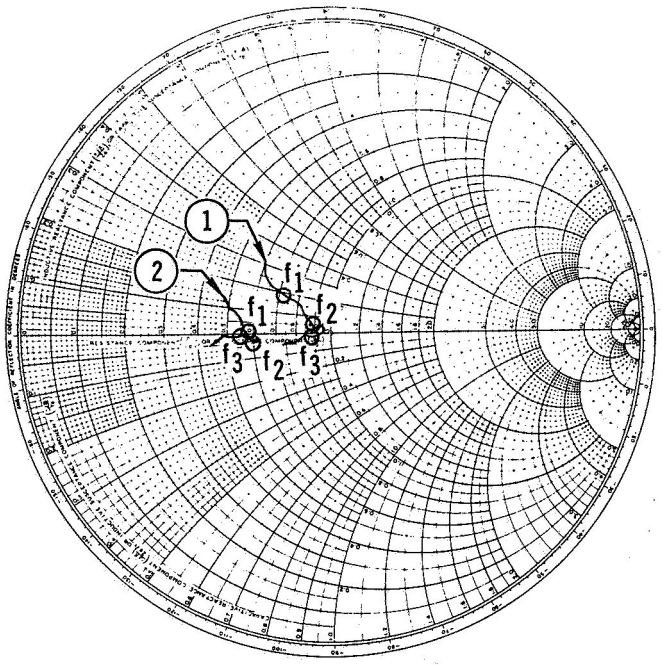

① REFERENCE
② FINAL CONFIGURATION
Z_0 = 50Ω
f_1 = 4250 MHz
f_2 = 4300 MHz
f_3 = 4350 MHz
SWEEP RANGE
4200 MHz TO 4400 MHz

C-BAND HORN IMPEDANCE – FINAL CONFIGURATION

Figure 62

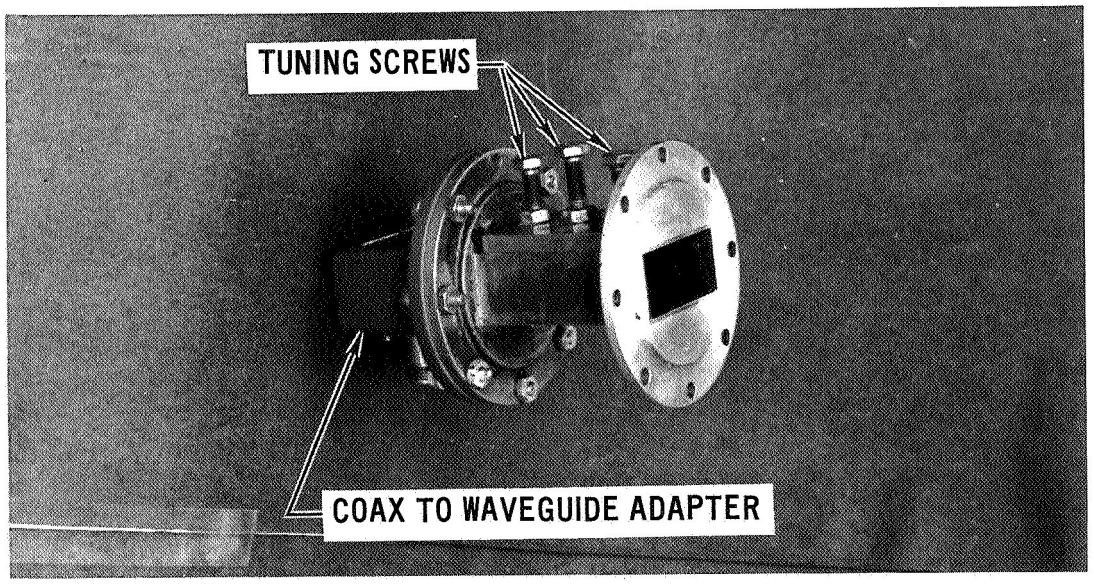

C-BAND SLOT ANTENNA

Figure 63

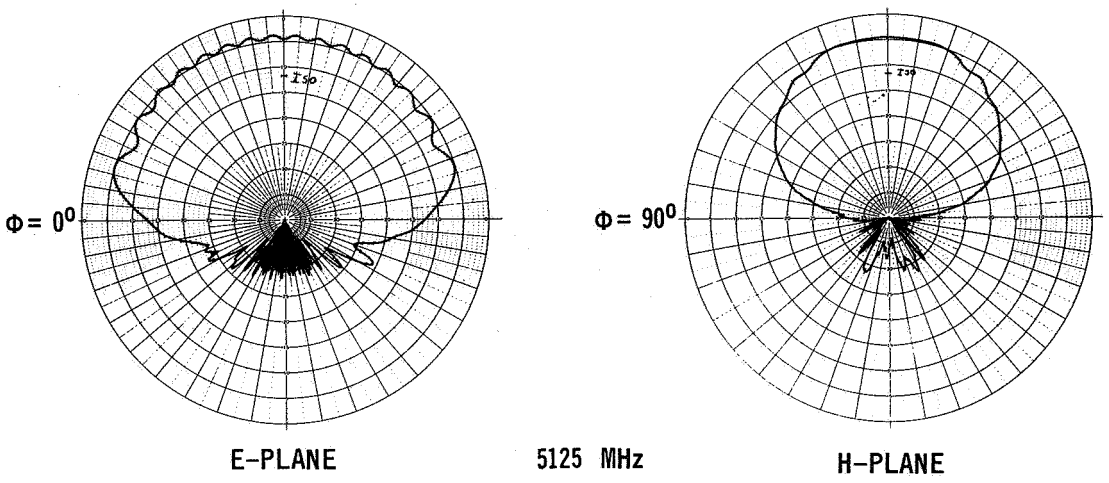

C-BAND SLOT REFERENCE PATTERNS

Figure 64

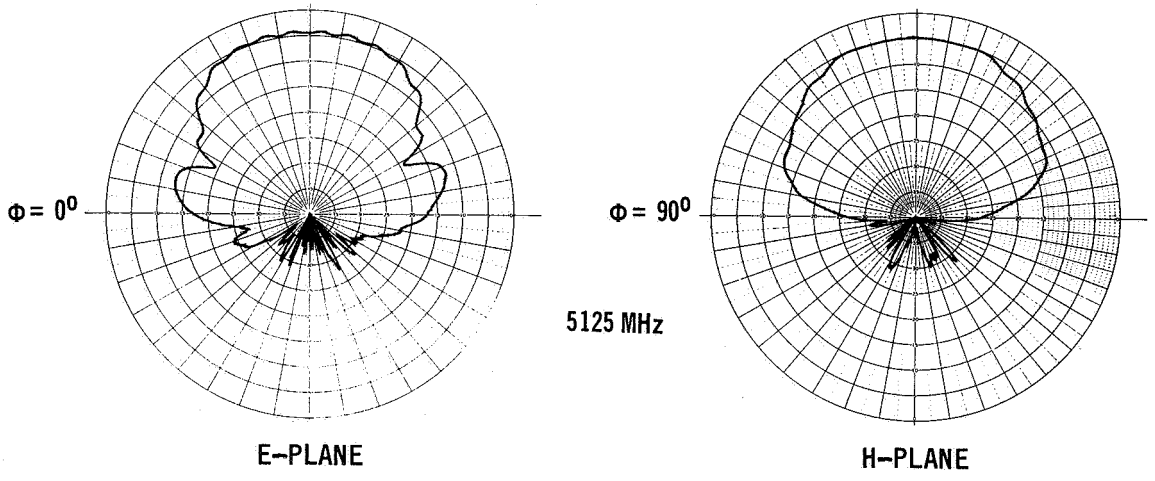

C-BAND SLOT PATTERNS – 3.81 CM (1.5 IN.) DIAMETER RSI WINDOW

Figure 65

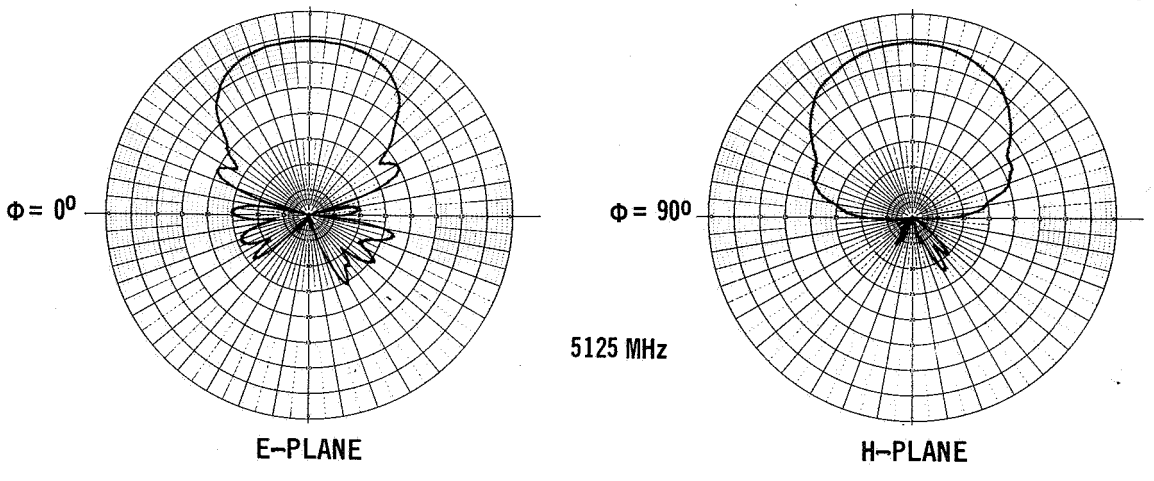

C-BAND SLOT PATTERNS – 6.35 CM (2.5 IN.) DIAMETER AIR FILLED WINDOW

Figure 66

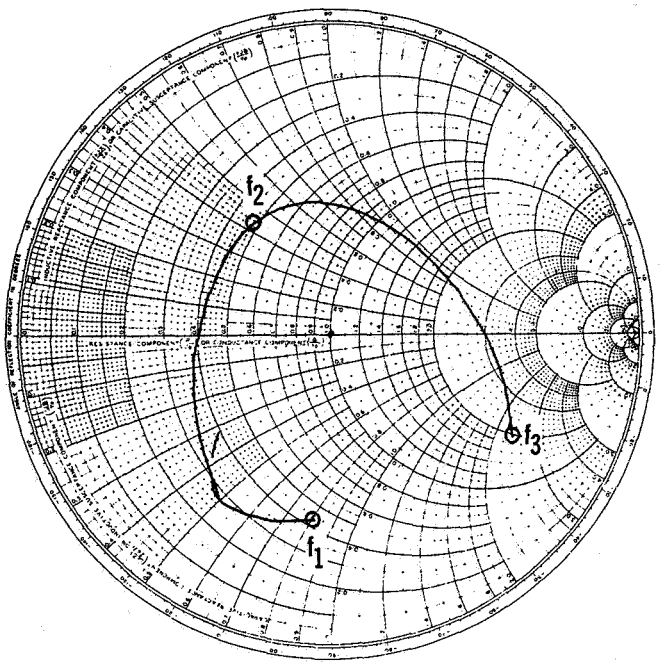

Z_0 = 50Ω
f_1 = 5000 MHz
f_2 = 5125 MHz
f_3 = 5250 MHz

C-BAND SLOT IMPEDANCE – 6.35 CM (2.5 IN.) DIAMETER WINDOW

Figure 67

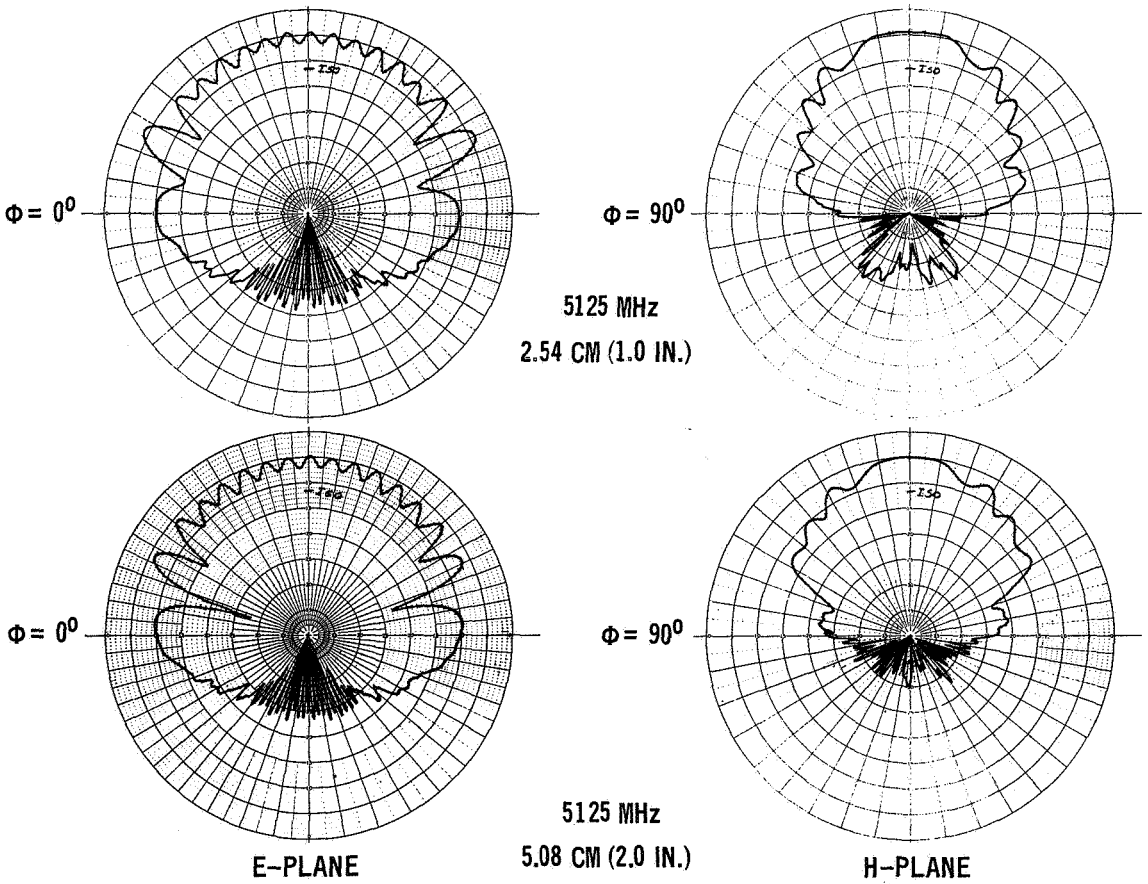

C-BAND SLOT PATTERNS WITH SIMULATED TPS – 2.54 CM(1.0 IN.) AND 5.08 CM (2.0 IN.) THICK

Figure 68

The ground plane was reduced to 76.2 x 76.2 cm (30 x 30 in.) to make the ground plane edges corresond to the TPS boundaries. This was done to obtain a condition for which theoretical patterns could be calculated. Figure 69 shows the patterns for this reference configuration. Figure 70 shows the patterns with the ground plane covered with 5.08 cm (2.0 in.) thick Eccofoam. These patterns compare very closely with patterns calculated by NASA - Langley Research Center, which are shown in Appendix B.

Patterns with the ground plane covered with the 5.08 cm (2.0 in.) thick simulated TPS, but with the sponge removed from a 6.35 cm (2.5 in.) diameter area centered over the antenna aperture, are shown in figure 71. The sponge appears to increase the surface wave excitation magnitude as evidenced by the deeper nulls in E-plane patterns, compared to the pattern without sponge shown in figure 70.

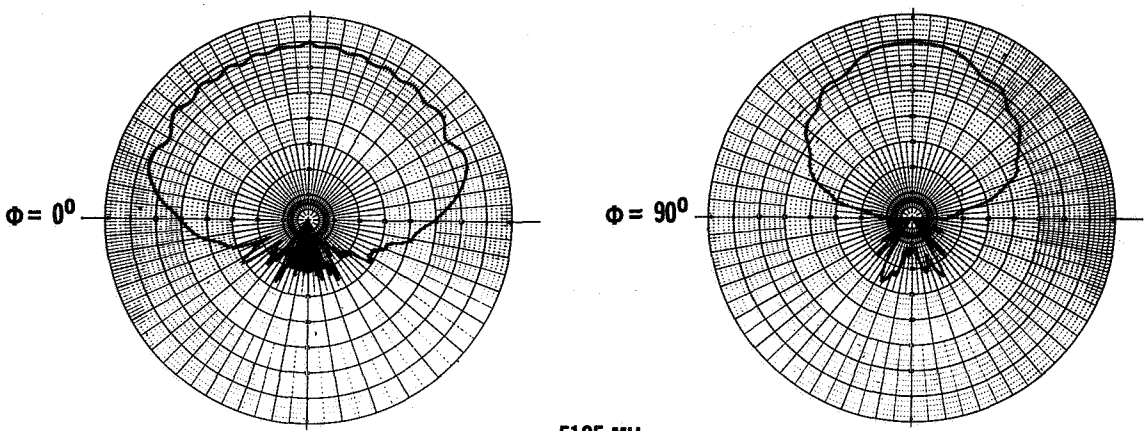

C-BAND SLOT REFERENCE PATTERNS – 76.2 x 76.2 CM (30.0 x 30.0 IN.) GROUND PLANE

Figure 69

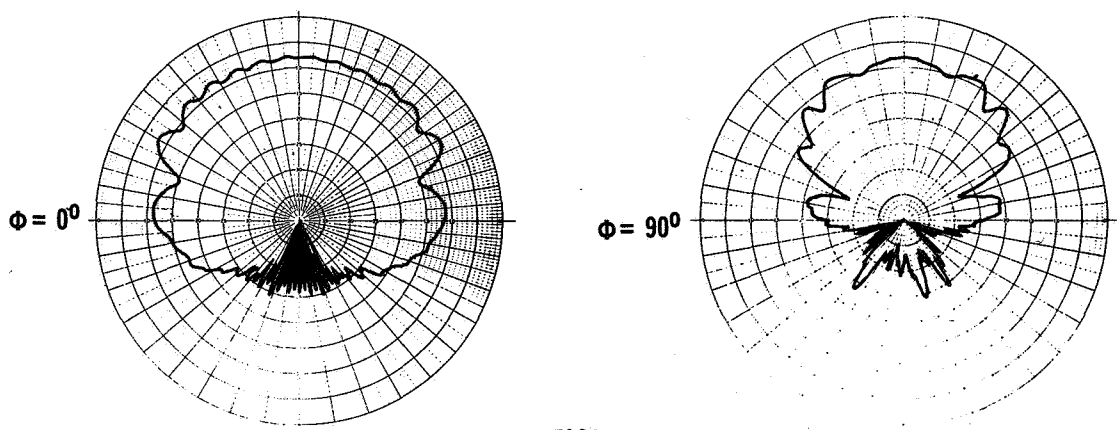

C-BAND SLOT PATTERNS WITH SIMULATED RSI – 5.08 CM (2.0 IN.) THICK

Figure 70

Measurements were made with window edge enclosures 3.81 cm (1.5 in.) and 5.08 cm (2.0 in.) in diameter extending into the simulated TPS 3.81 cm (1.5 in.). The strain isolator sponge was removed from within the window area and replaced with Eccofoam. The patterns are shown in figure 72. Good E-plane pattern coverage is provided normal to the ground plane from $\theta = 0°$ to $\theta = 70°$. The E-plane pattern magnitudes at $\theta = 90°$ are reduced about 20 dB below the pattern peaks. The H-plane patterns show considerable surface wave excitation. The H-plane magnitudes are increased to within ±3 dB of the 0 dB gain level at $\theta = 90°$. The changes in the H-plane pattern shapes are such that they take on the appearance of E-plane patterns.

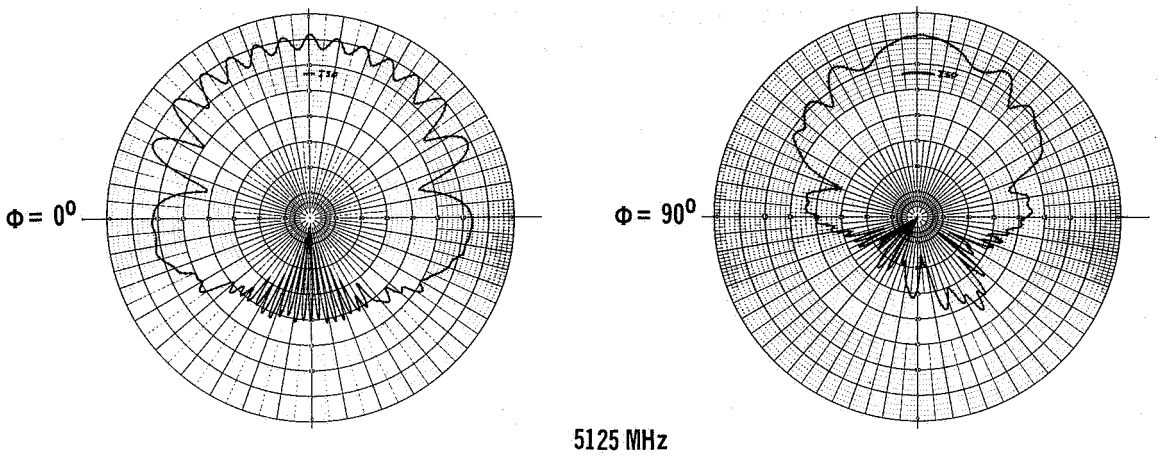

C-BAND SLOT PATTERNS WITH SIMULATED TPS–WITHOUT STRAIN ISOLATOR OVER ANTENNA

Figure 71

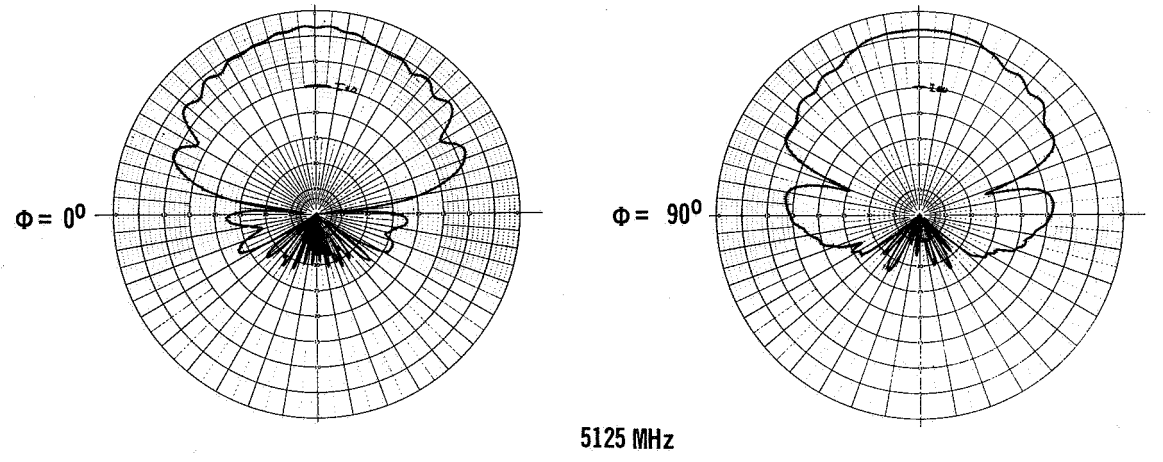

C-BAND SLOT PATTERNS WITH SIMULATED TPS–5.08 CM (2.0 IN.) DIAMETER WINDOW

Figure 72

Measurements were made to establish the quality of the final C-band slot antenna system design described in the section on ANTENNA SYSTEM DESIGN AND INTEGRATION, figure 88. Figure 73 shows a photo of the test configuration. The window edge enclosure is 4.45 cm (1.75 in.) in diameter and extends above the ground plane 3.05 cm (1.2 in.). Figure 74 shows the radiation pattern of this configuration taken at 5125 MHz. The patterns at 5000 and 5250 MHz are nearly identical to these patterns and are not shown. The E- and H-plane patterns are nearly equal from $\theta = 0°$ to $\theta = 55°$. The H-plane pattern magnitude at $\theta = 90°$ exceeds that of E-plane patterns about 8 dB, a reversal of the relation shown by the reference patterns, figure 69. It may be noted that the H-plane pattern takes on the appearance of an E-plane pattern more so than does the E-plane pattern. The results of the impedance measurements are shown in figure 75. The VSWR is less than 1.3:1 from 5000 to 5250 MHz.

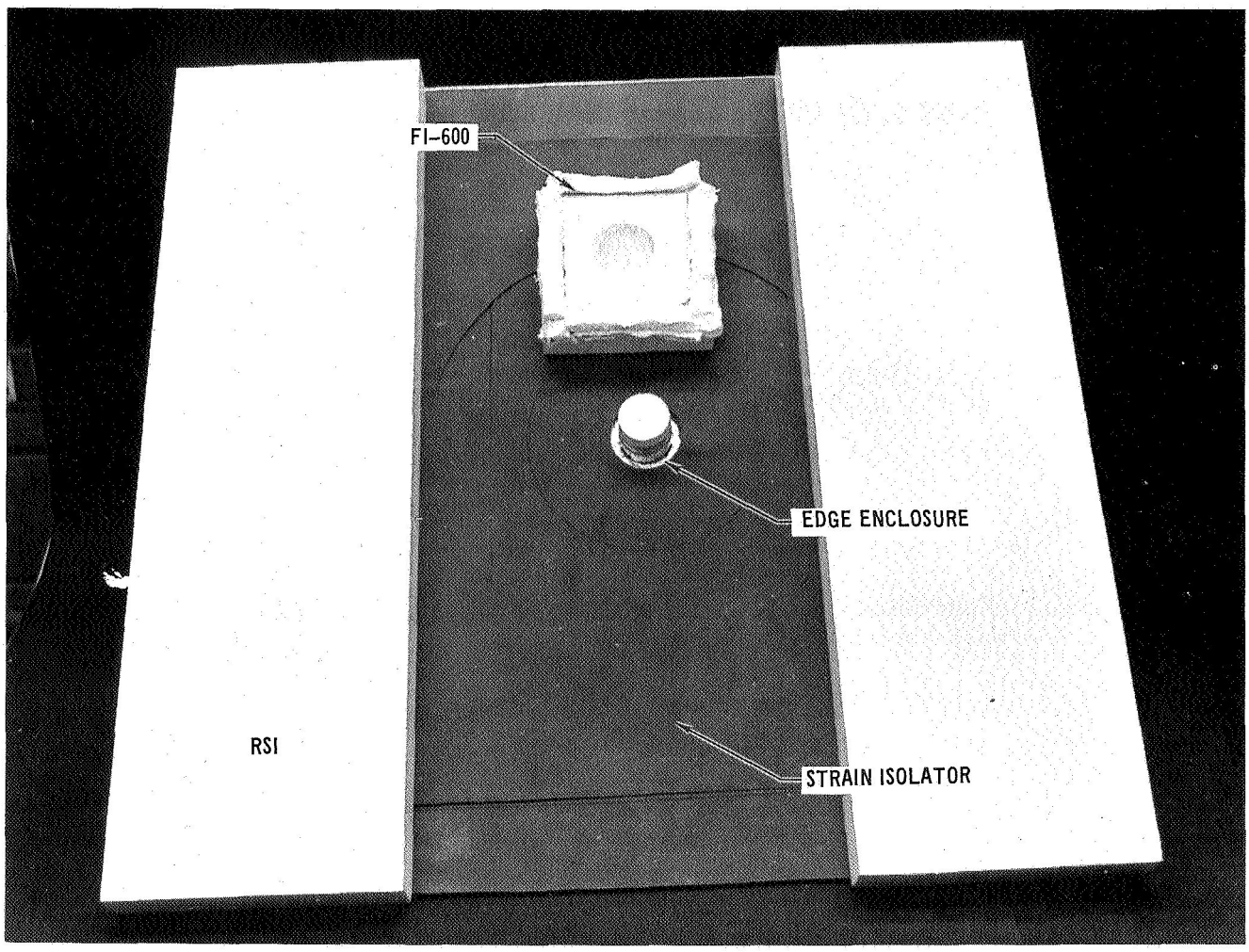

C-BAND SLOT ANTENNA SYSTEM – FINAL CONFIGURATION SIMULATION

Figure 73

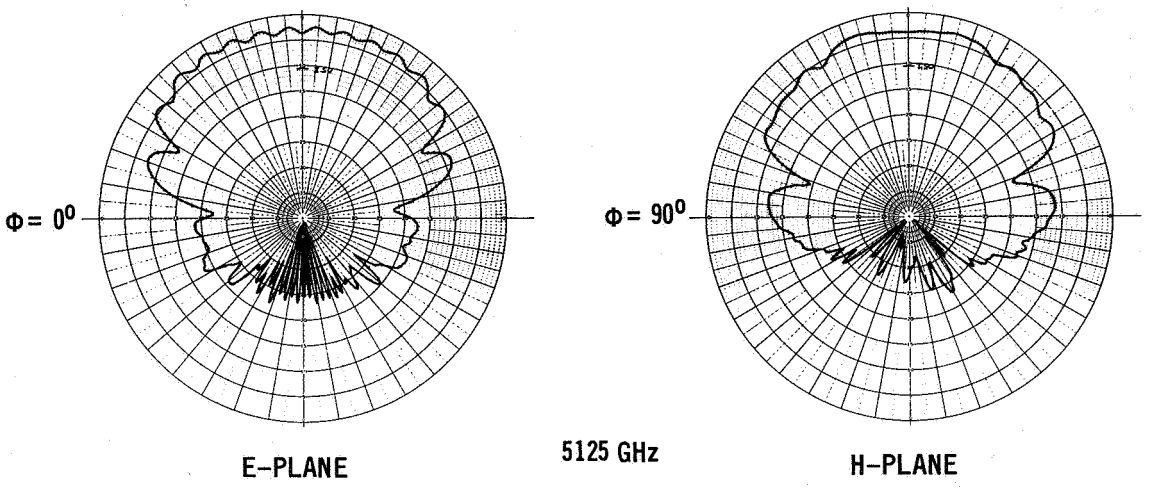

C-BAND SLOT PATTERNS – FINAL CONFIGURATION

Figure 74

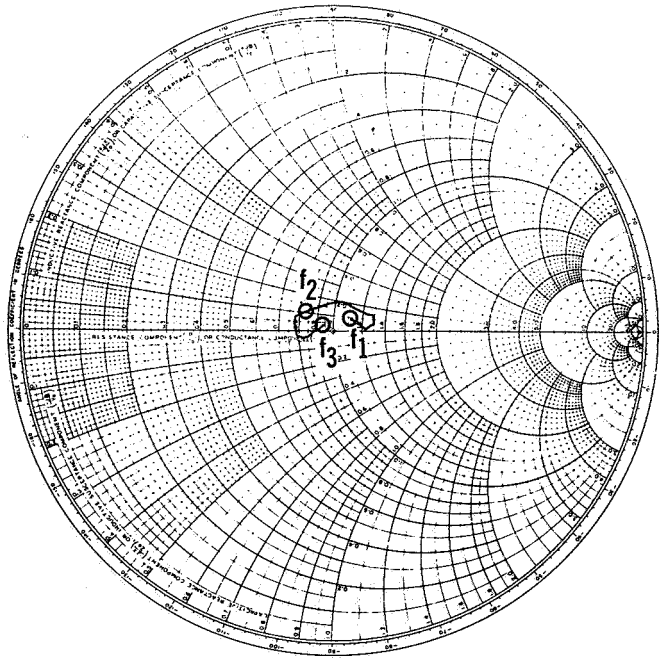

Z_0 = 50Ω
f_1 = 5000 MHz
f_2 = 5125 MHz
f_3 = 5250 MHz

C-BAND SLOT IMPEDANCE – FINAL CONFIGURATION

Figure 75

Antenna Window Transmission Loss

The transmission characteristics of several antenna window configurations were analyzed using plane wave techniques. Each layer of material was considered a section of transmission line with the characteristic impedance dependent upon the dielectric constant and loss tangent of the layer. The expressions given in Appendix C were programmed on a Hewlett-Packard 9100A calculator with a 1901A Extended Memory. The program was written to accommodate 20 layers but could be extended to about 50 without difficulty. The program was validated by comparing results for a single layer with results obtained using formulas given in Jasik (ref. 5). There was agreement to eight (8) decimal places in transmission coefficient for a loss tangent of zero and two (2) decimal places for a loss tangent of 0.18, a difference in transmission of about 0.02 dB. A deviation in results is expected for higher values of loss tangent since the formulas given in Jasik ignore squared terms of loss tangent.

Table VII gives the details of antenna window configurations which employ reusable surface insulation (RSI) as the principal window material. The primary RSI material considered was LI-1500 as discussed in the section on ANTENNA WINDOW MATERIALS SELECTION. Although these configurations are considered to be a single layer approach, in reality they consist of a number of different materials. The additional materials consist of a bonding material (RTV−560), sponge rubber strain isolator, and/or fiberglass-phenolic honeycomb support structure and the LI-1500 coating.

Table VIII gives the details of the multiple-layer antenna window configurations considered. The primary difference in these configurations is in the thickness of the outer layer of boron nitride (HD-0092). The dielectric constant of HD-0092 is about 4 and is the major contributor to the transmission loss. The dielectric constant and loss tangent of the Dynaquartz layer are both low over the applicable temperature range and have only a small effect on the transmission loss. A nominal thickness of 1.27 cm (0.5 in.) was selected initially for the HD-0092 antenna window layer based on a preliminary thermal-stress analysis. At the two C-band frequency ranges, the 1.07 and 1.27 cm (0.42 and 0.5 in.) HD-0092 layer thicknesses are near 0.25 wavelengths, where maximum transmission loss will occur. By increasing the thickness of the HD-0092 layer to 0.5 wavelength, the transmission loss can be minimized as shown by the calculated results. However, a 0.5 wavelength antenna window is not considered practical at the L-band frequencies since the window would be about 6.985 cm (2.75 in.) thick and about 7 times heavier than the 1.07 cm (0.42 in.) window.

The transmission loss for the RSI window configurations is shown in figures 76 and 77. For reference, transmission loss is shown for LI-1500 5.08 cm (2.0 in.) thick without coating or bonding materials. For this case the transmission loss is less than 0.1 dB at the highest frequency considered. The addition of a 0.254 mm (0.01 in.) coating to the LI-1500 increases the transmission loss a small amount; less than 0.05 dB at the C-band frequencies and about 0.01 dB at the L-band frequencies. Figures 76 and 77 show that the fiberglass honeycomb and/or the sponge rubber increase the transmission loss

0.03 dB or less at the L-band frequencies and less than 0.36 dB at the C-band frequencies. The maximum transmission losses were 0.08 dB at the L-band frequencies and 0.45 dB at the C-band frequencies.

TABLE VII

SINGLE-LAYER RSI ANTENNA WINDOW CONFIGURATIONS

CONFIGURATION	LAYER NO.	THICKNESS (IN.)	DIELECTRIC CONSTANT	LOSS TANGENT	MATERIAL
NO. S1 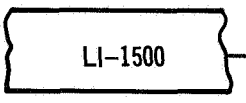	1	2	1.2	0.0016	LI-1500
NO. S2 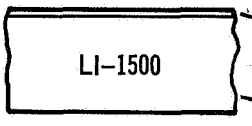	1	0.01	4	0.1	COATING
	2	2	1.2	0.0016	LI-1500
NO. S3 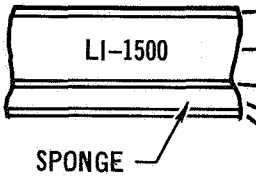	1	0.01	4	0.1	COATING
	2	2	1.2	0.0016	LI-1500
	3	0.01	4	0.005	RTV-560
	4	0.25	1.64	0.0134	SPONGE
	5	0.010	4	0.005	RTV-560
NO. S4 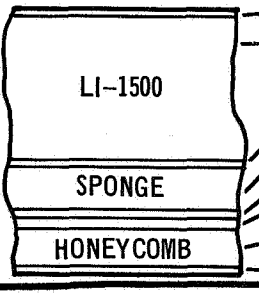	1	0.01	4	0.1	COATING
	2	2	1.2	0.0016	LI-1500
	3	0.010	4	0.005	RTV-560
	4	0.080	1.64	0.0134	SPONGE
	5	0.010	4	0.005	RTV-560
	6	0.012	5	0.02	FACE SHEET
	7	0.146	1.1	0.001	CORE
	8	0.012	5	0.02	FACE SHEET
NO. S5 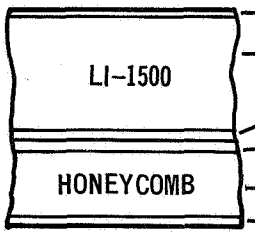	1	0.01	4	0.1	COATING
	2	2	1.2	0.0016	LI-1500
	3	0.010	4	0.005	RTV-560
	4	0.012	5	0.02	FACE SHEET
	5	0.280	1.1	0.001	CORE
	6	0.012	5	0.02	FACE SHEET

TABLE VIII

MULTIPLE-LAYER ANTENNA WINDOW CONFIGURATIONS

CONFIGURATION		LAYER 2			
		NO.	THICKNESS (IN.)	DIELECTRIC CONSTANT	LOSS TANGENT
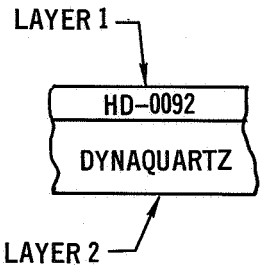	M1	1	0.5	4	0.005
		2	1.75	1.15	0.00012
	M2	1	0.42	4	0.005
		2	0.78	1.15	0.00012
	M3	1	0.687*	4	0.005
		2	1.75	1.15	0.00012
	M4	1	0.5**	4	0.005
		2	1.75	1.15	0.00012

NOTES: * $\lambda/2$ AT 4300 MHz
** $\lambda/2$ AT 5125 MHz

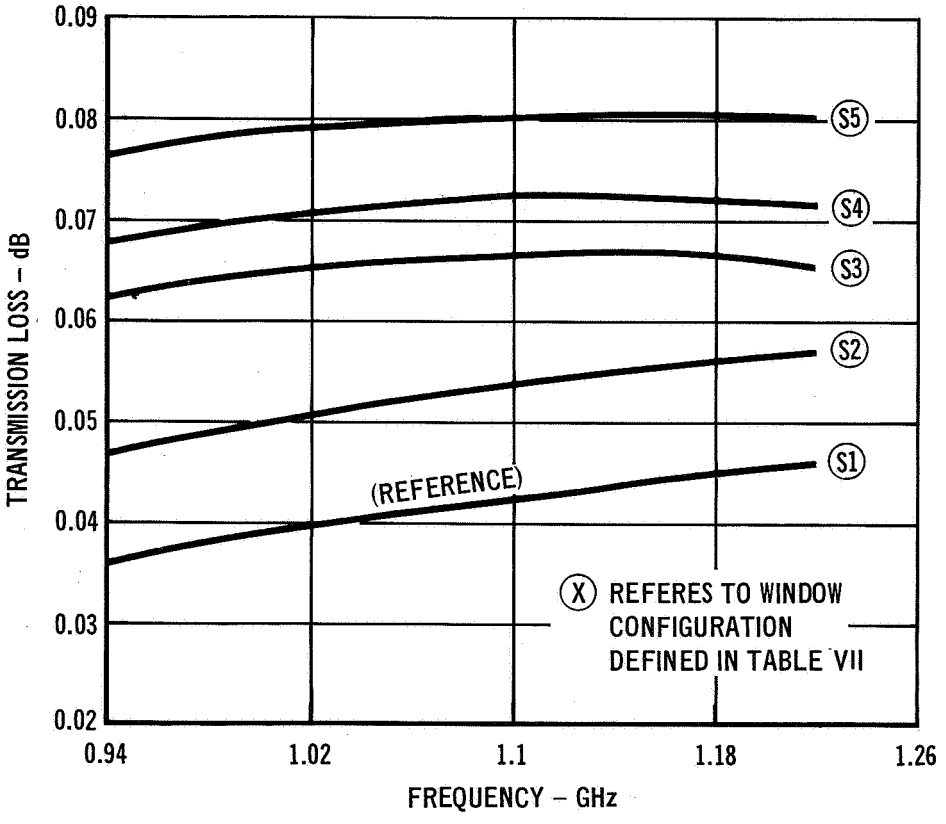

TRANSMISSION LOSS THRU SINGLE-LAYER ANTENNA WINDOWS AT L-BAND

Figure 76

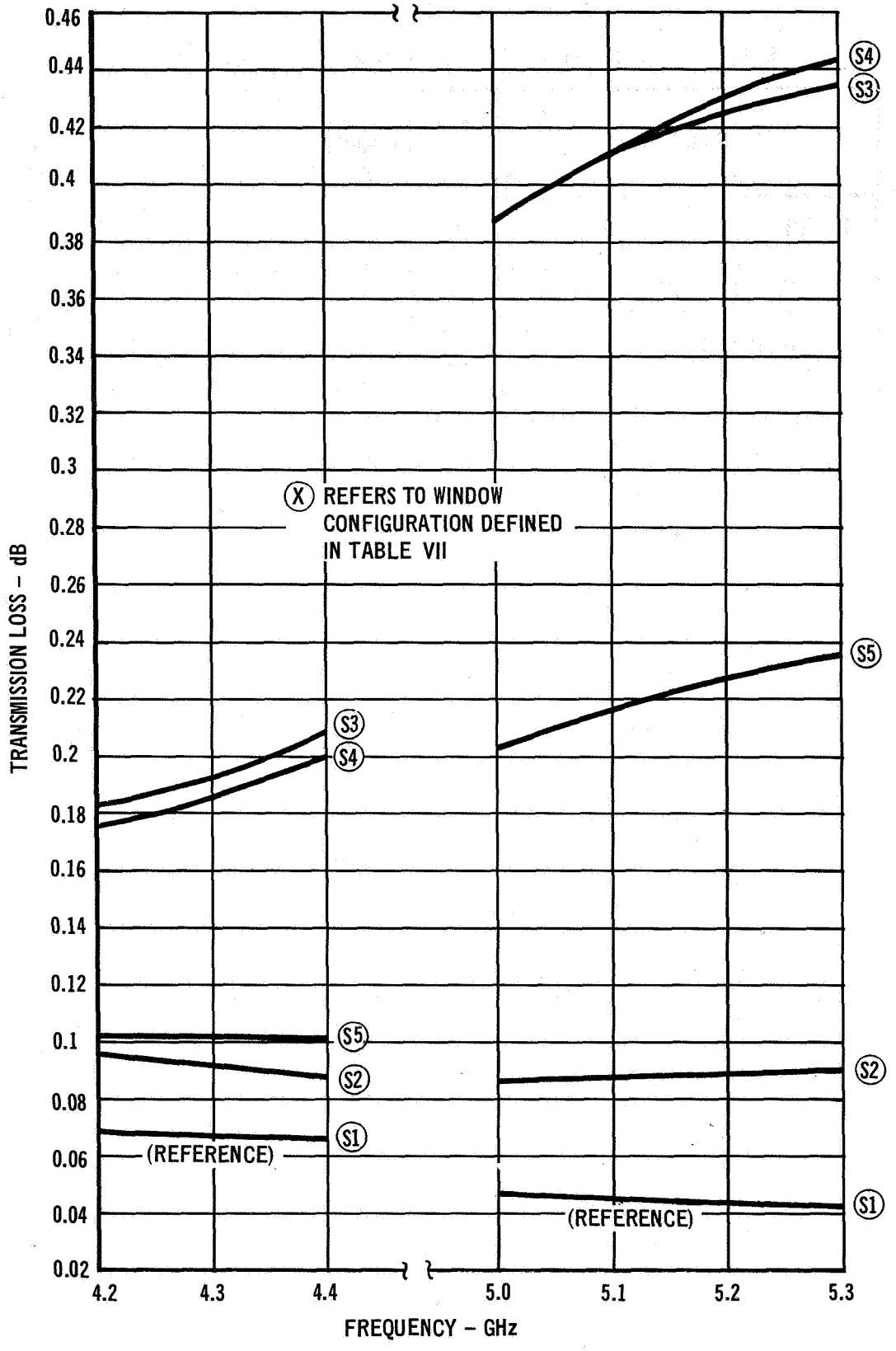

TRANSMISSION LOSS THRU SINGLE-LAYER ANTENNA WINDOWS AT C-BAND

Figure 77

The transmission loss for the multiple-layer antenna window configurations is shown in figures 78 and 79. At the L-band frequencies, figure 78 shows that the minimum transmission loss is achieved with the minimum thickness of HD-0092. For the 1.067 cm (0.42 in.) HD-0092 window layer thickness the maximum transmission loss is less than 0.6 dB. At the C-band frequencies figure 79 shows that the HD-0092 window-layer thickness of 0.5 wavelengths results in a transmission loss less then 1.0 dB, where as a 0.42 in. thickness results in a transmission of about 1.0 to 1.5 dB.

A comparison of the two antenna window design approaches clearly shows that the use of the LI-1500 RSI material results in the lowest transmission losses at both the L- and C-band frequencies. The dielectric constant of the HD-0092 boron nitride is significantly higher than that of LI-1500 and, therefore, the transmissions loss is more sensitive to HD-0092 thickness because of greater interface reflections.

Antenna Transfer Characteristics

The antenna transfer characteristics may be determined from the proper manipulation of the scattering parameters (ref. 6). The reflection coefficient at the aperture plane may then be referred to the antenna input terminal reference plane. If the aperture is covered with materials other than air or terminated in an antenna window, the effect on the aperture plane impedances (admittances) can be calculated and referred to the antenna input using the scattering parameters. This is a useful tool to look at the effects of system or environmental changes without actually testing the specific configurations.

The scattering parameters were obtained using Deschamps' method (refs. 7 and 8). The antenna is terminated in a coax or waveguide which matches the antenna aperture. A movable short in the coax or waveguide section then provides the means for obtaining the necessary data.

The L-band annular slot antenna and coaxial termination with a movable short is shown in figure 80. A Hewlett-Packard Model 8410A Network Analyzer System was used to measure the reflection coefficients at the antenna input. The output of the Network Analyzer was fed into a rectangular recorder and the data plotted directly on a Smith Chart. The Network Analyzer was calibrated with a short-circuit in place of the antenna to establish the input impedance reference plane. The antenna aperture reference plane was established by shorting the antenna aperture with metalic tape, because the movable short did not provide an adequate means for shorting the antenna aperture directly. The antenna input reflection coefficients were then measured and plotted at frequencies of 960 MHz, 1090 MHz, 1150 MHz and 1220 MHz. This data was required both to determine the scattering parameter phases and to establish an equivalent reference position of the movable short.

After the reference data were obtained the coaxial termination was attached to antenna aperture. The position of the movable short, which duplicated the aperture short-circuit reference data, nearest to the antenna aperture, was established. A half-wavelength displacement was then obtained by moving the

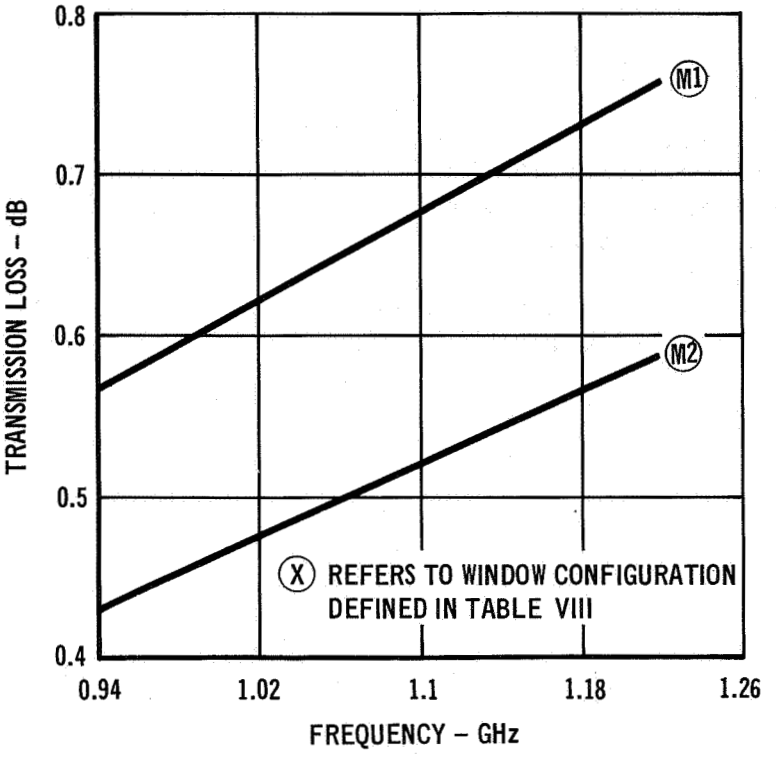

TRANSMISSION LOSS THRU MULTIPLE–LAYER ANTENNA WINDOWS AT L-BAND

Figure 78

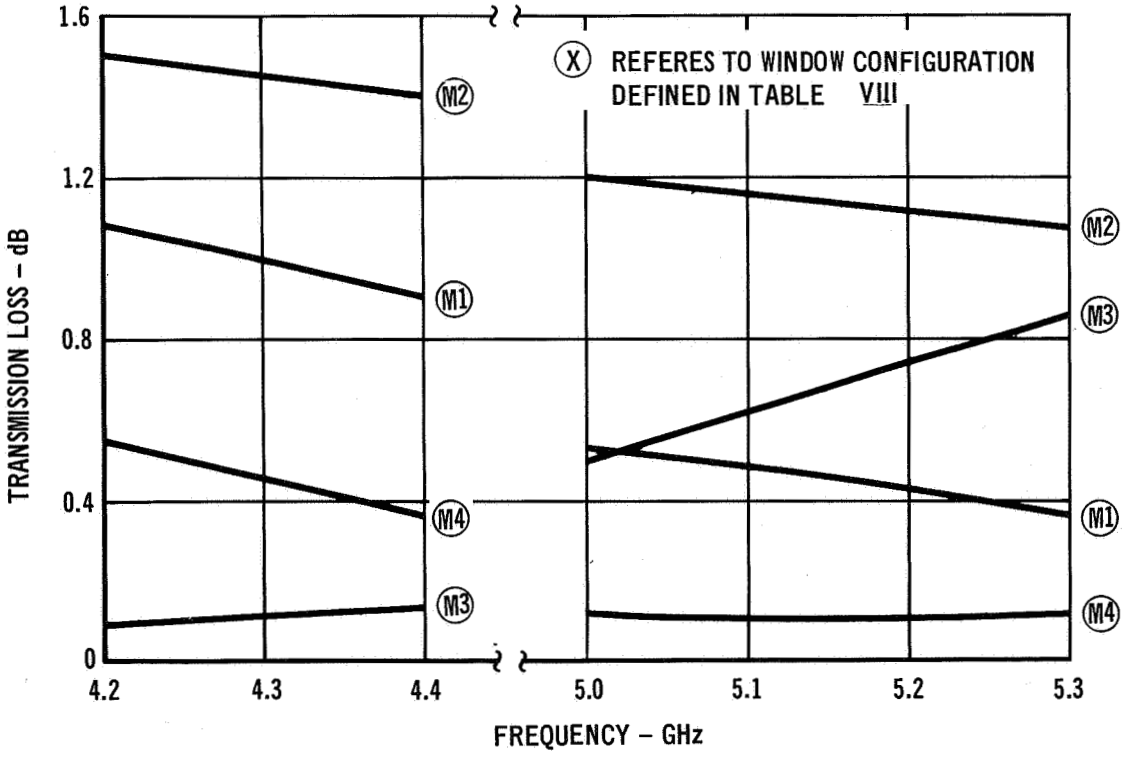

TRANSMISSION LOSS THRU MULTIPLE-LAYER ANTENNA WINDOWS AT C-BAND

Figure 79

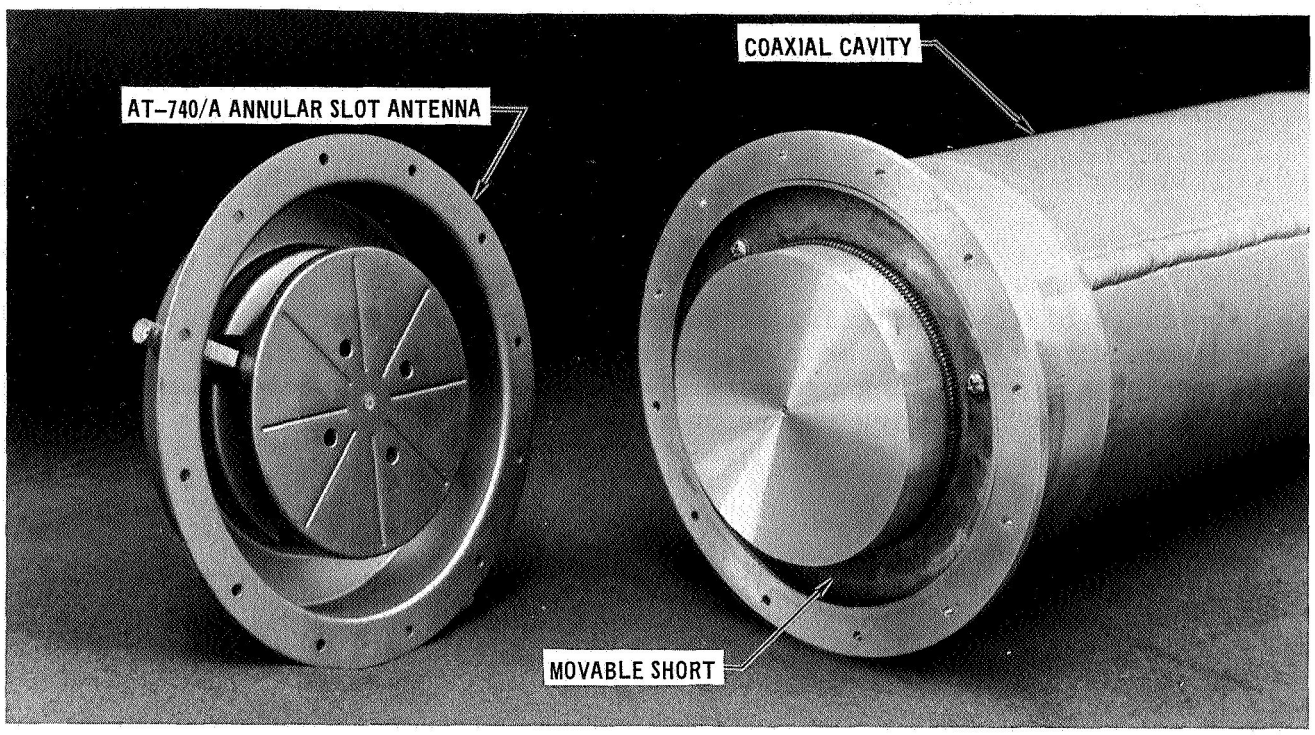

L-BAND ANTENNA AND MOVABLE SHORT CIRCUIT

Figure 80

short away from the antenna aperture until the reflection coefficient loci traversed one revolution on the Smith Chart. The displacement length was measured and divided into eight equal increments to obtain the intermediate short positions required for the scattering parameter measurements. Measured half wavelengths were within 2.0 mm (0.079 in.) of the freespace values. Figure 81 is a plot of the reflection coefficients of the L-band annular slot antenna, for 960 MHz, measured at eight equally spaced short positions. An indication of the validity of the data is shown by the well-behaved nature of the plot; there are no stray points and a circle is produced. A plot of the original reflection coefficient phases versus the transformed reflection coefficient phases approximated a straight line with a 45-degree slope (ref. 7), indicating the absence of systematic errors.

The coefficients determined are defined as S_{11}, the reflection coefficient at the input when the output is matched; S_{22}, the reflection coefficient at the output when the input is matched; and S_{12}, the transmission coefficient from the input to the output. The scattering parameters obtained for the L-band

annular slot antenna are given below.

Frequency	S_{11}	S_{22}	S_{12}
960 MHz	0.676 /-13.5°	0.684 /113°	0.680 /62.5°
1090 MHz	0.664 /-65°	0.605 /111°	0.737 /89°
1150 MHz	0.667 /-87.2°	0.656 /117.5°	0.712 /101.5°
1220 MHz	0.624 /-108.5°	0.625 /119°	0.730 /112.5°

The magnitudes of the scattering parameters are taken and/or calculated from measurements directly from the plot, with the Smith Chart radius equal to unity. The phases of the scattering parameters are found by a transformation of point P' to point P" and measuring the respective angles.

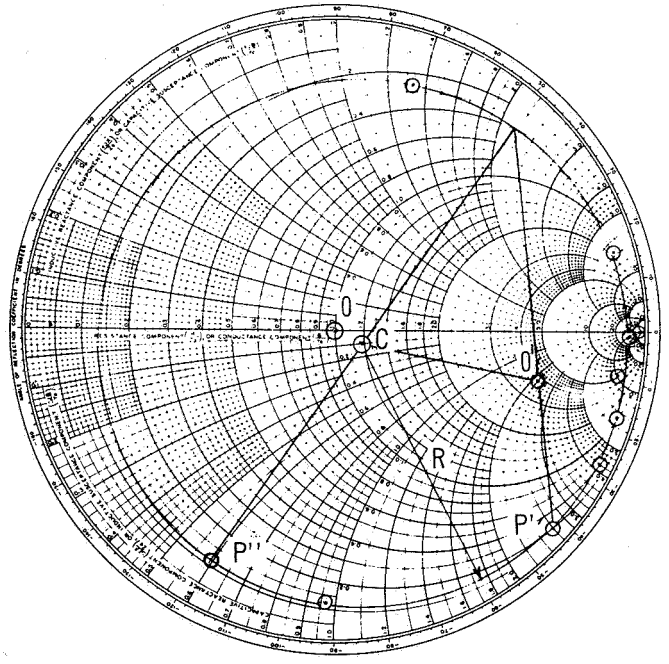

f = 960 MHz

TYPICAL L-BAND ANTENNA SCATTERING MATRIX MEASUREMENT DATA

Figure 81

The same method was utilized to determine the scattering parameters of the C-band slot antenna. The antenna was tuned for best VSWR when flush mounted in a 76.2 cm x 76.2 cm (30 in. x 30 in.) ground plane with a 6.35 mm (0.25 in.) thick by 76.2 cm (30 in.) square sheet of RL-524 sponge rubber with a 6.35 cm (2.5 in.) diameter cut-out over the antenna and a 5.08 cm (2 in.) thick by

76.2 cm (30 in.) square sheet of Eccofoam PS centered over it. Figure 82 is the data taken at 5.125 GHz. The scattering parameters are:

Frequency	S_{11}	S_{22}	S_{12}
5.0 GHz	0.430 /113.5°	0.419 /135.5°	0.900 /11°
5.125 GHz	0.304 /53°	0.297 /294°	0.945 /64°
5.25 GHz	0.245 /12°	0.235 /340°	0.953 /74.5°

The measured half-wavelength was less than 1.0 mm (0.039 in.) of the calculated waveguide values.

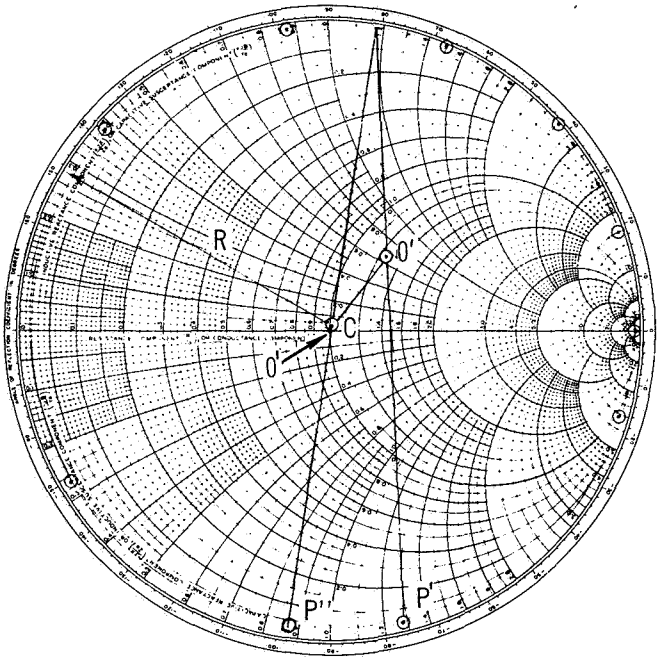

f = 5125 MHz

TYPICAL C-BAND SLOT ANTENNA SCATTERING MATRIX MEASUREMENT DATA

Figure 82

Impedance Matching Considerations

The results of the impedance measurements show that the antennas selected for this study could be used without additional improvement. However, if further avionics system analysis shows that lower VSWR's are required, it appears that the VSWR of each of the antennas tested can be improved by internally matching the antennas with the particular window configuration over the antenna. The one exception is the L-band antenna system with the multiple-layer window,

which is not a prime candidate for further development. The VSWR is between 2:1 and 2.6:1 over part of the transmit band (1090 to 1150 MHz) and should probably be improved if this design approach becomes a serious candidate. Attempts were made to place circular "irises" in the region of the aperture to improve the VSWR. This approach, however, produced the opposite effect. Therefore, it appears that the most effective means of improvement would be to alter the matching network inside the antenna.

ANTENNA SYSTEM DESIGN AND INTEGRATION

Antenna systems for L-band annular slot, C-band horn, and C-band linear slot antennas were designed and integrated into typical Space Shuttle Orbiter structure and thermal protection system (TPS). The results of the electrical measurements, described in the preceding section, and the detailed thermal and strength analyses were used to modify and complete the designs.

Structural Integration

Structural integration is one of the important considerations in achieving a satisfactory high temperature antenna system design for the Space Shuttle Orbiter. Not only must the antenna system provide the required radiation pattern and impedance characteristics, but it must do so in a structural environment which includes a TPS in addition to the load carrying members. Particular attention was paid to the installation attachment and removal factors, such that these items can be accomplished with relative ease. In accomplishing these goals it is necessary to preserve the TPS so that heat transfer to the bondline in the antenna area is equal to or less than that in the surrounding structure.

Two basic installation/replacement concepts were investigated for integrating the antenna systems into the baseline orbiter configuration. These two concepts are identified as:

(a) Component Installation/Replacement

(b) Modular Installation/Replacement

Both of these concepts, illustrated in figure 83, allow the antennas to be installed/removed from the outside of the orbiter.

For the component installation/replacement concept the design permits the antenna window assembly, consisting of the RSI tile, strain isolator and tile support to be fabricated and installed as a unit. As shown in figure 83 the antenna is attached to an antenna support ring, while the antenna window is attached to the primary structure. This allows the antenna window assembly to be removed without removing the antenna and breaking the electrical connection or destroying the RSI window material or adjacent RSI tiles attached to primary structure of the orbiter. Upon removal of the antenna window assembly

the antenna can be readily removed for refurbishment or replacement.

For the modular installation/replacement concept the antenna is attached to the inner surface of the RSI tile support. Thus, the antenna window and antenna are assembled to the primary structure of the Orbiter as a module. Damage to either the RSI window material or the antenna requires removal of the entire module for replacement or repair.

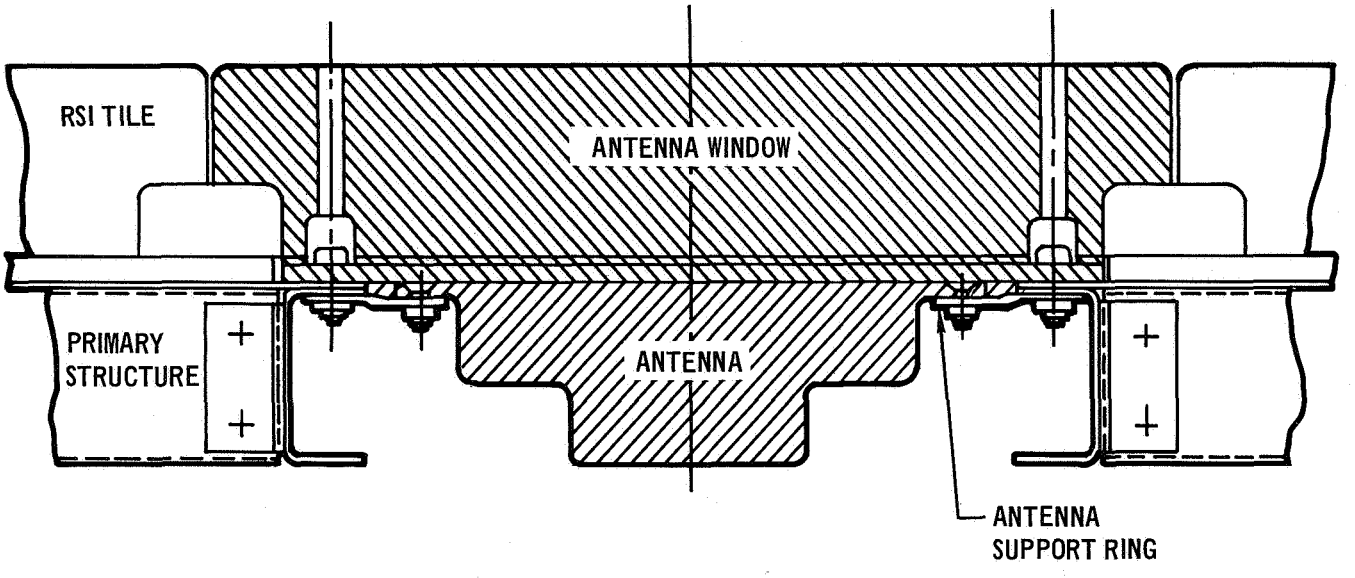

(a) Component Installation/Replacement

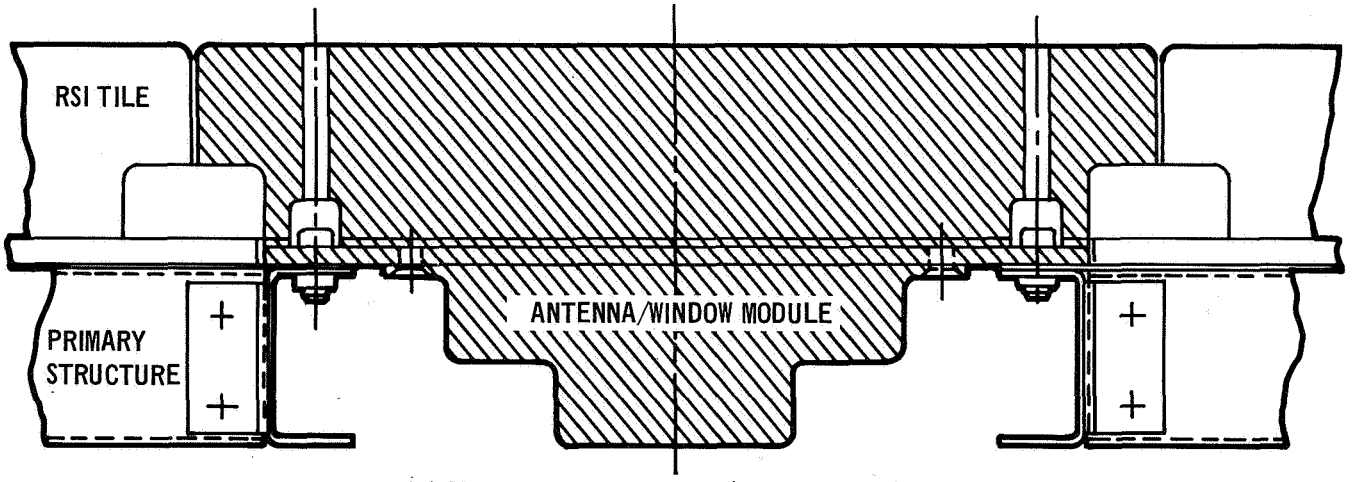

(b) Modular Installation/Replacement

ANTENNA INSTALLATION/REPLACEMENT CONCEPTS

Figure 83

The component installation/replacement concept is incorporated in the antenna system designs described in the subsequent paragraphs.

Antenna system designs.- Four antenna window concepts were selected as feasible candidates for integration into the baseline orbiter configuration. These four concepts are:

(a) L-band antenna installation - RSI window

(b) L-band antenna installation - multiple-layer window

(c) C-band horn antenna installation - RSI window

(d) C-band linear slot antenna installation - RSI window

The basic geometric data associated with these antenna configurations are shown in figure 84.

Layout type drawings for each of the above concepts were prepared in sufficient detail to show the principal design features applicable to each antenna window configuration. The primary Orbiter structure in the areas of the antenna locations consists of a 0.051 cm (0.020 in.) aluminum skin, stiffened by fore and aft running stringers that are positioned between 50.80 cm (20.0 in.) spaced bulkheads. Nominal stringer spacing is 10.16 cm (4.0 in.). Stringer spacing in the antenna window areas was allowed to vary locally depending on the antenna configuration. Three of the antenna window assembly concepts use Lockheed's LI-1500 RSI as the basic window material while the fourth concept use an outer layer of boron nitride, and an inner layer of Dynaquartz. The LI-1500 is coated with an organic surface sealer and high emittance coating. In addition the LI-1500 is impregnated with silicone to provide rain and moisture protection. For each concept studied a 5.08 cm (2.00 in.) RSI tile thickness was used. Adding 0.635 cm (0.25 in.) thick strain relief isolation pad (sponge rubber) and 0.051 cm (0.020 in.) for RTV-560 bonding thickness, the total TPS thickness is 5.766 cm (2.270 in.).

The three concepts using LI-1500 for the antenna window material are designed as a three piece antenna window assembly, consisting of the RSI material, a 0.203 cm (0.08 in.) thick RL-524 type S-105 silicone sponge strain isolator and a 0.430 cm (0.17 in.) thick fiberglass-phenolic honeycomb subpanel with the basic configuration described in the section on Description of Antenna Window Configuration. The strain isolator pad is bonded to the RSI tile and the subpanel with RTV-560 adhesive. High density laminated phenolic inserts are provided where the fasteners attach the honeycomb panel to the primary structure. These inserts match the thermal expansion of the panel.

Three of the concepts also have a super-alloy foil window enclosure. This enclosure does not extend to the outer surface of the RSI, but stops at a level where the temperature maximum is approximately 600°K (800°F).

L-band antenna installation - RSI window: The modifications required for installing the L-band antenna, shown in figure 84, is shown in figure 85.

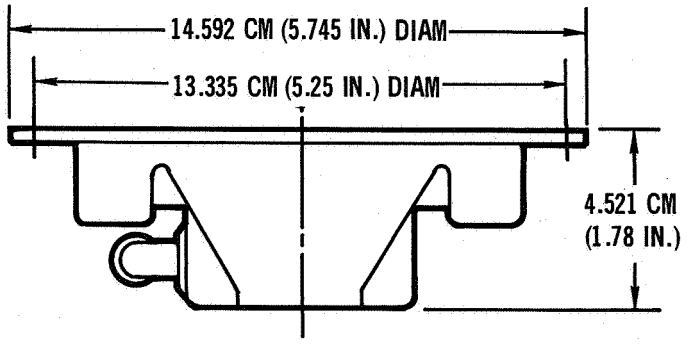

C-Band Horn Antenna

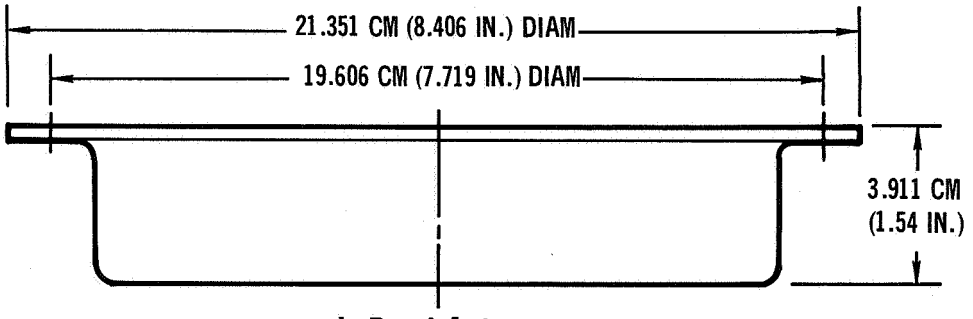

L-Band Antenna

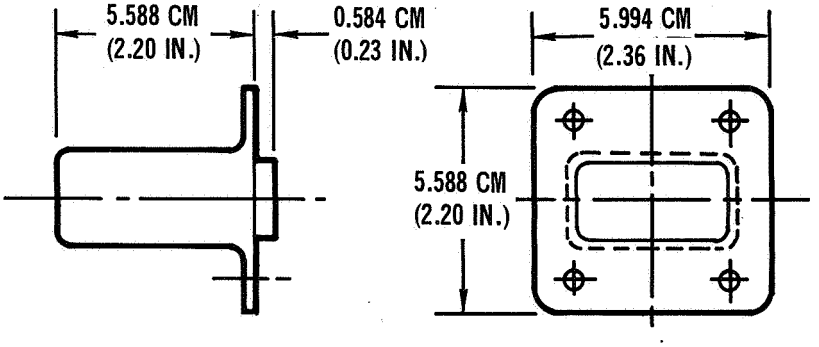

C-Band Linear Slot Antenna

ANTENNA CONFIGURATIONS

Figure 84

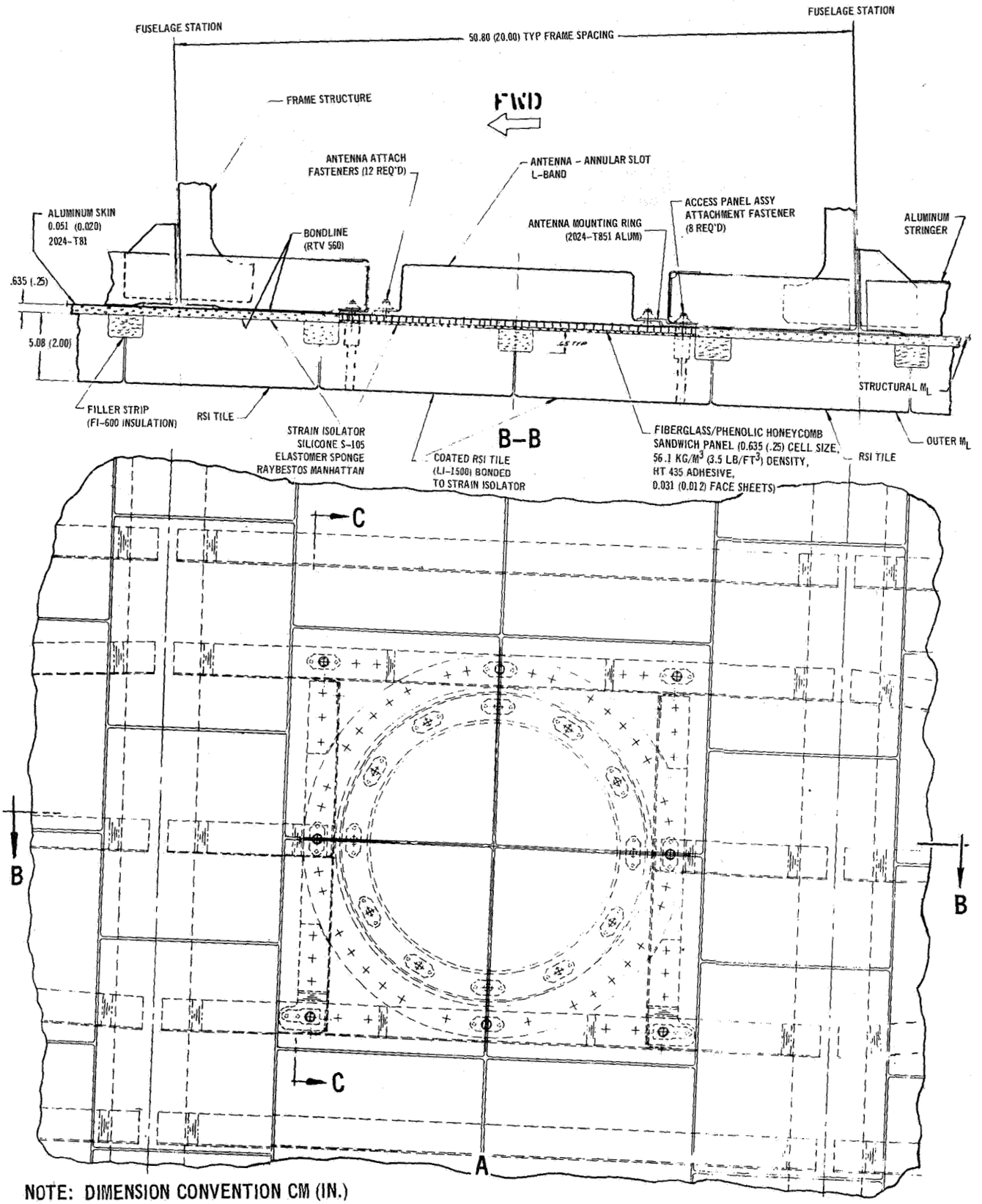

NOTE: DIMENSION CONVENTION CM (IN.)

L-BAND ANTENNA SYSTEM INSTALLATION – SINGLE-LAYER RSI WINDOW

Figure 85

(Figure Continued on Next Page)

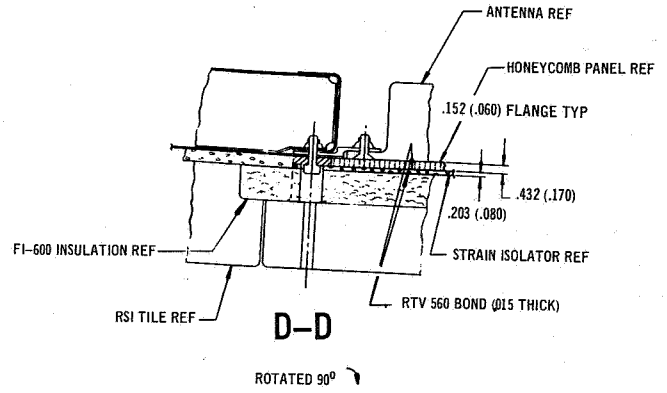

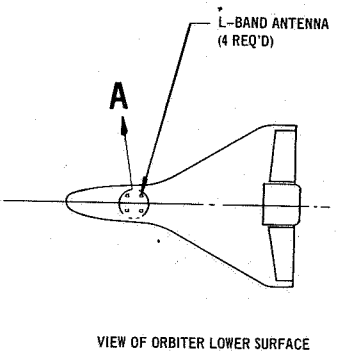

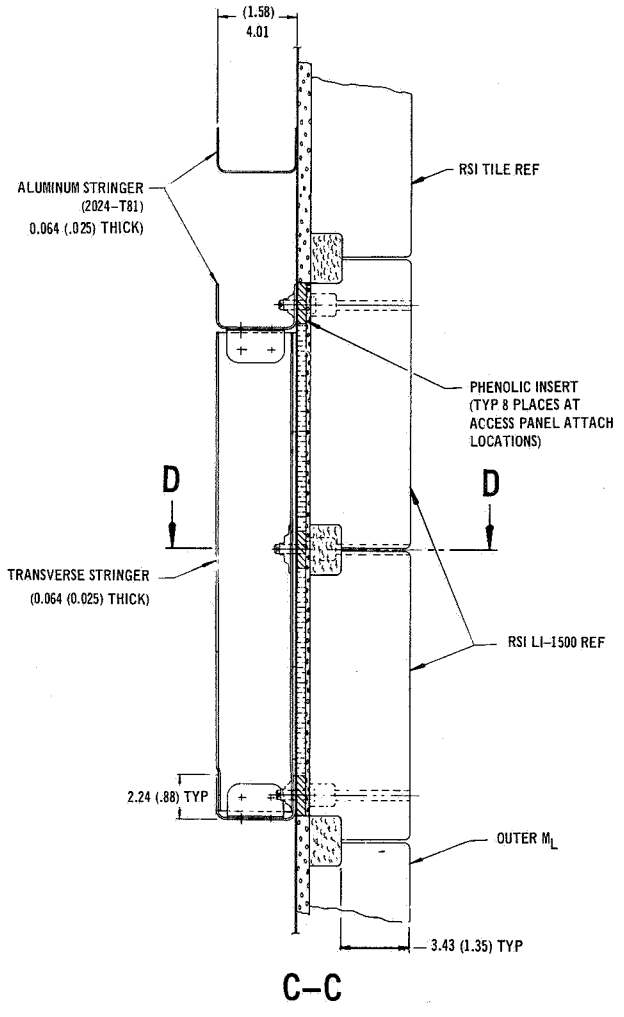

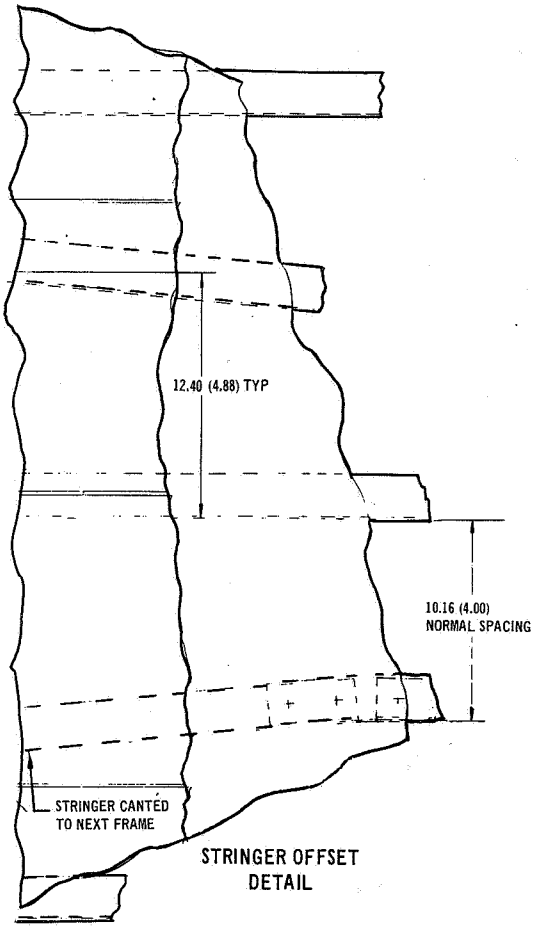

NOTE: DIMENSION CONVENTION CM (IN.)

L-BAND ANTENNA SYSTEM INSTALLATION – SINGLE-LAYER RSI WINDOW

Figure 85 (Concluded)

As shown the airframe structure in this area consists of 0.081 cm (0.032 in.) thick aluminum sheet metal stringers running fore and aft, connected to the fuselage frames. The size of the antenna requires interrupting one stringer and canting the outer stringers, locally, by 2.235 cm (0.88 in.). A frame, consisting of two transverse stringers and a sheet metal ring are added to provide the continuity in the area of the interrupted stringer. A machined, aluminum ring, attached to the sheet metal ring, provides the sill for attaching the antenna from the outside of the vehicle. The antenna window assembly, consisting of four (4) LI-1500 tiles bonded to a strain isolator covered honeycomb subpanel is attached with eight (8) cap screw fasteners. Access to these fasteners, which are trapped in the window assembly, is obtained through holes in the tiles (see section on Thermal Analysis below). The window assembly (and the C-band LI-1500 window assemblies) is attached with allen head recessed cap screws. Experience gained through a MDC RSI mechanical attachment study being conducted for NASA (NAS9-12854) indicated that the RSI tiles are less prone to damage and simpler to install using an allen head shaped tool instead of a screw driver.

L-band antenna installation - multiple-layer window: This antenna window design consists of two layers of high temperature material as shown in figure 86. The outer layer is boron nitride (HD-0092) and the inner layer is Dynaquartz. The two layers are positioned with a window edge enclosure sheet metal ring made of FS85 columbium with a Sylvania R512E coating. The Dynaquartz layer is under a slight compression to improve its resistance to acoustical vibration. This ring is attached to the base with eight (8) bolts and thermally isolated with load bearing insulation. The boron nitride layer is held in place by a coated columbium retainer ring which is attached with 12 columbium fasteners. Access to the antenna, for either installation or removal is achieved by removing the retainer ring and the multiple-layer window. A thick aluminum ring is required for dissipating the heat conducted through the window enclosure ring (see following section on Thermal Analysis). As shown in figure 86, a sheet metal ring, supported by four brackets and attached to the Orbiter aluminum skin, is used to support the L-band antenna behind the window.

The structure modification required for accommodating this antenna installation concept consists of installing five off-set aluminum stringers, 0.081 cm (0.032 in.) thick, beneath the antenna. The depth of the adjacent stringers are increased locally to provide continuity with the off-set stringers. The mounting structure (excluding the window material) for this antenna window installation design is approximately sixteen times heavier than the LI-1500 antenna window design discussed above.

C-band horn antenna installation - RSI window: The C-band horn antenna installation, shown in figure 87, is similar to the L-band antenna with the LI-1500 antenna window. However, instead of interrupting one of the stringers the smaller size antenna permits canting two adjacent stringers, allowing the antenna to fit between the stringers. The stringer spacing is increased from 10.16 cm (4.00 in.) to 15.49 cm (6.10 in.) in the area of the antenna. Two transverse stringers are added to form a box frame that cradles the antenna mounting ring. The antenna is attached to the mounting ring with twelve flush fasteners. The mounting ring in turn is attached with six (6) flush fasteners.

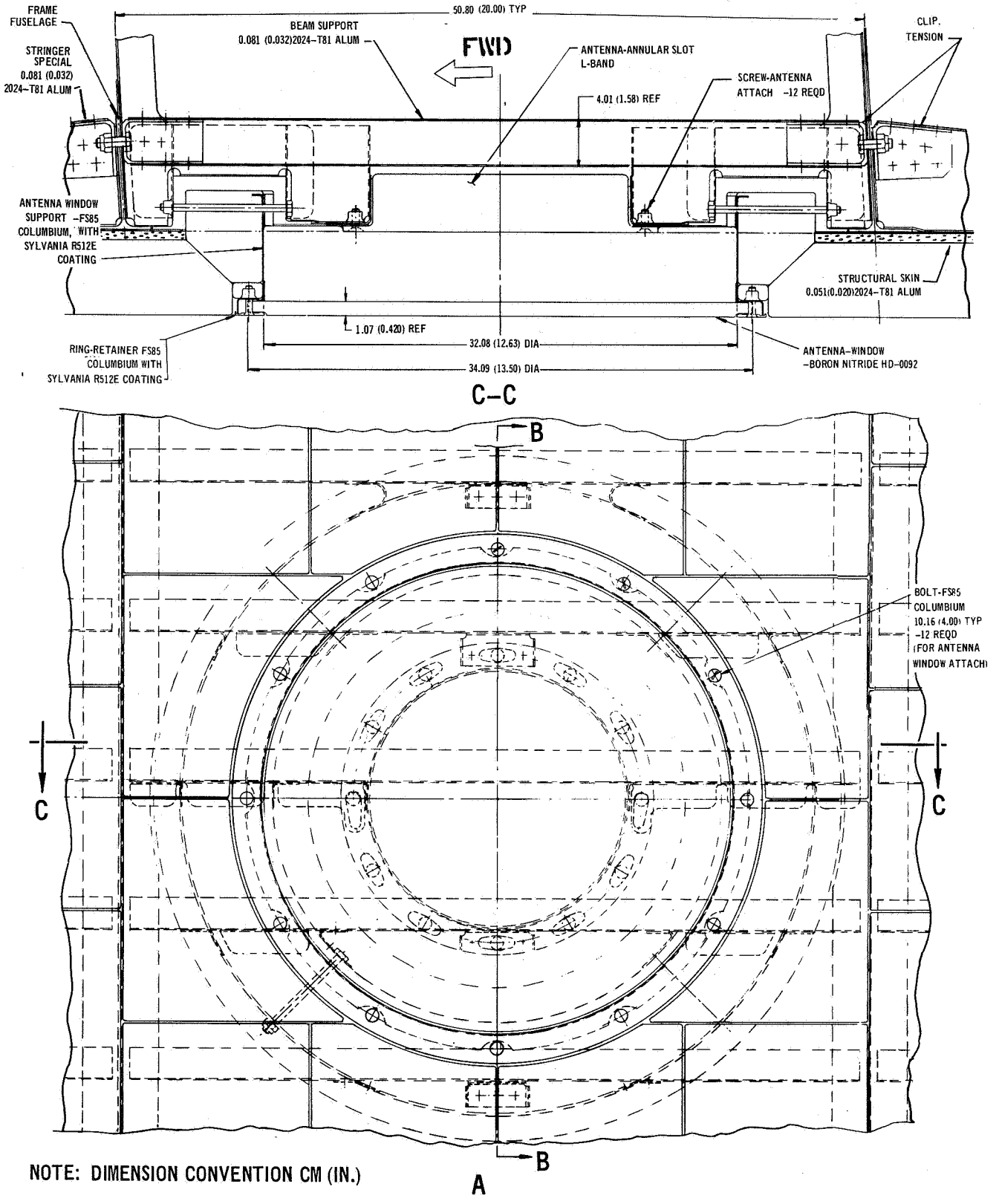

NOTE: DIMENSION CONVENTION CM (IN.)

L-BAND ANTENNA SYSTEM INSTALLATION – MULTIPLE-LAYER WINDOW

(Figure Continued on Next Page)

Figure 86

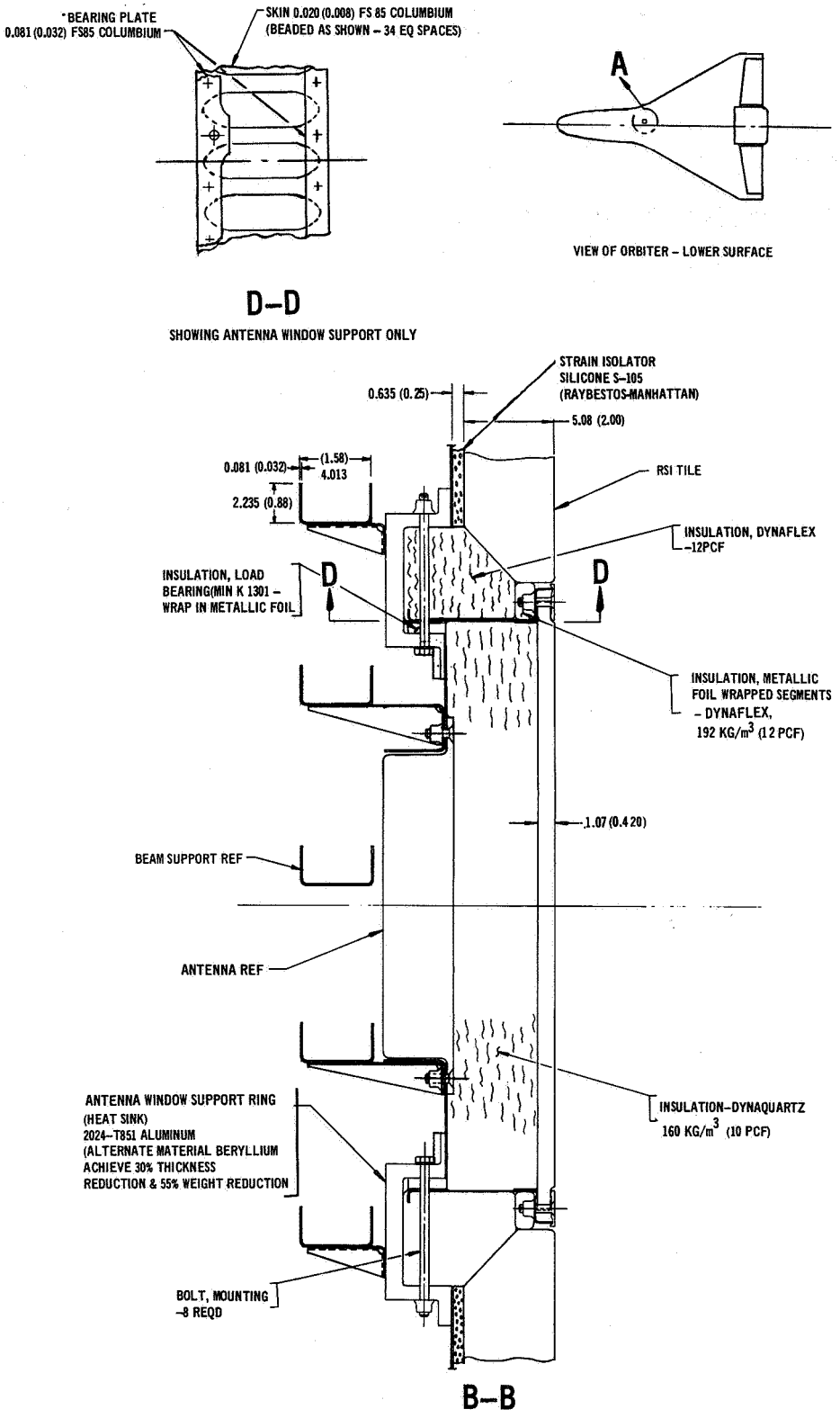

NOTE: DIMENSION CONVENTION CM (IN.)

L-BAND ANTENNA SYSTEM INSTALLATION – MULTIPLE-LAYER WINDOW

Figure 86 (Concluded)

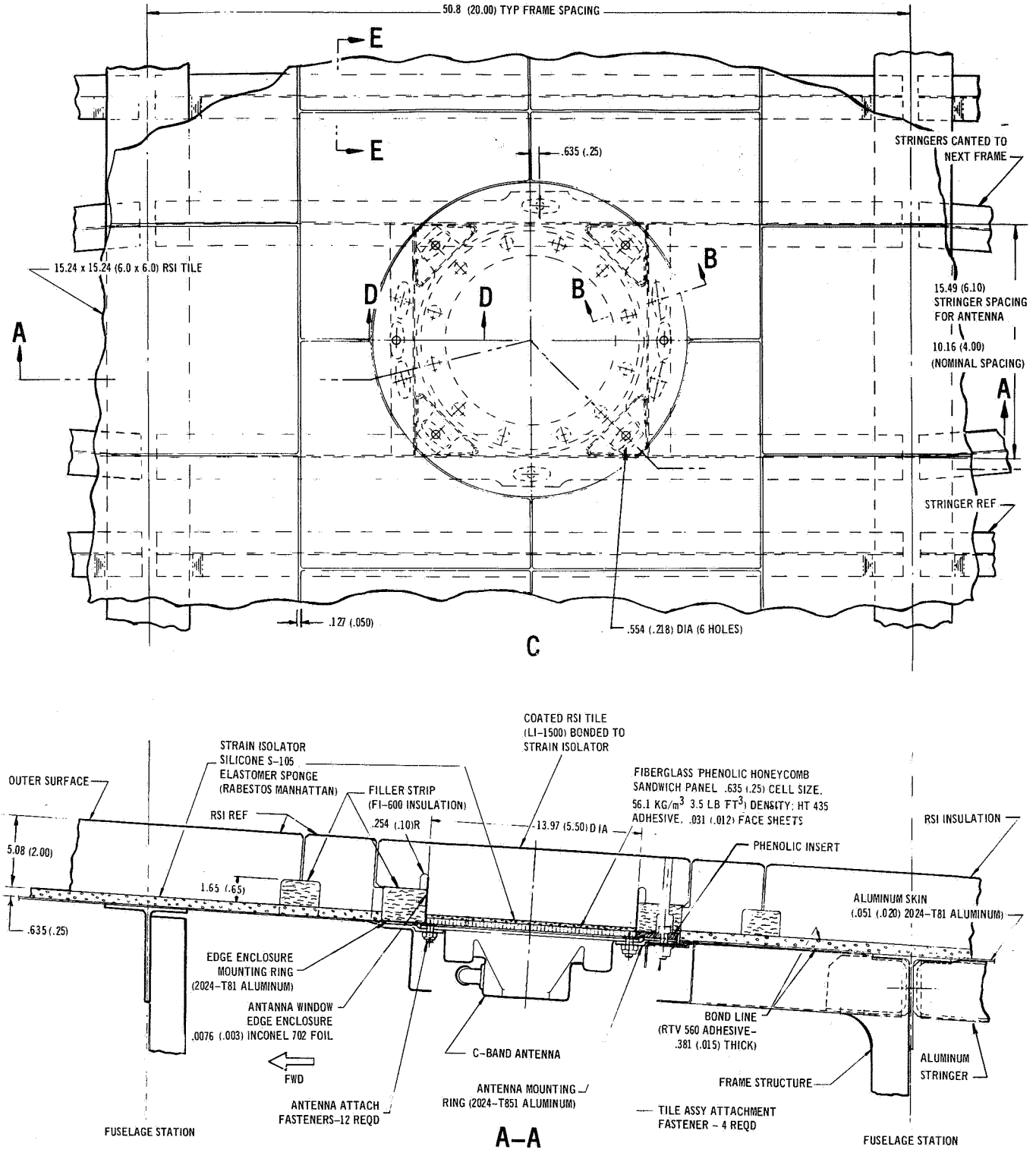

NOTE: DIMENSION CONVENTION CM (IN.)

C-BAND HORN ANTENNA SYSTEM INSTALLATION

(Figure Continued on Next Page)

Figure 87

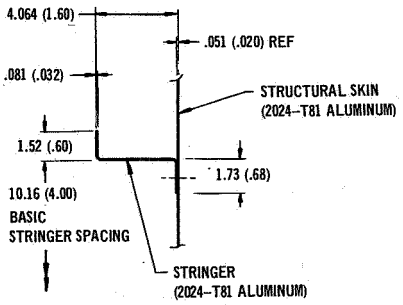

E–E
(TPS OMITTED FOR CLARITY)

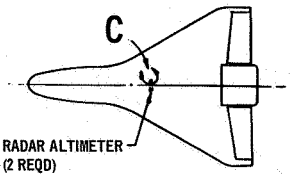

VIEW OF ORBITER LOWER SURFACE

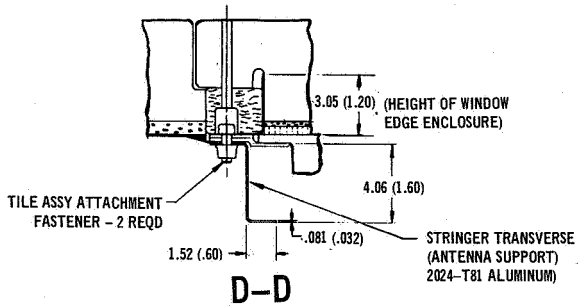

D–D

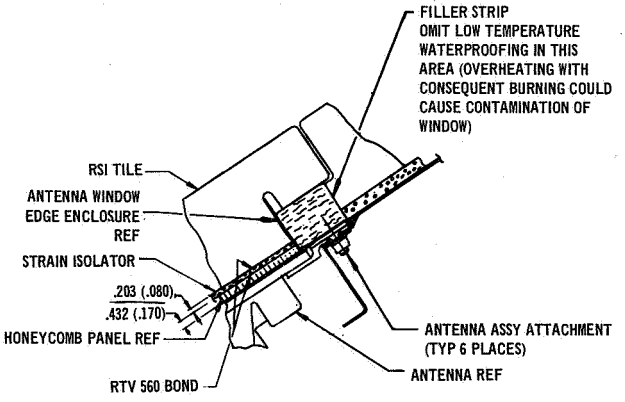

B–B

NOTE: DIMENSION CONVENTION CM (IN.)

C-BAND HORN ANTENNA SYSTEM INSTALLATION

Figure 87 (Concluded)

The antenna window assembly includes a one piece LI-1500 tile, a strain isolator, fiberglass honeycomb subpanel, antenna window edge enclosure, fibrous insulation filler strips and an aluminum mounting ring. As shown in figure 87, the strain isolator is sandwiched between the tile and honeycomb subpanel. The aluminum mounting ring, which is bonded to the tabs on the subpanel retains the donut shaped filler strip and the antenna window edge enclosure. This assembly is attached to the support structure with six (6) allen recessed cap screws.

C-band slot antenna installation - RSI window: Modification to the primary orbiter structure for this antenna installation is very minimal. The size of this antenna, as specified in figure 84, permits installing it between adjacent stringers without changing the nominal 10.16 cm (4.00 in.) spacing. An aluminum mounting ring is riveted to the structural skin as shown in figure 88. This mounting ring is used for supporting both the antenna and the antenna window assembly. A circular groove is machined in the LI-1500 antenna window to allow the window edge enclosure member to penetrate up into the tile. A spacer is required for eliminating the wide air gap and to retain the shape of the thin enclosure member. This spacer, however, could be eliminated if future vibration testing proves that a very narrow gap with square corners is not detrimental to the tile. The antenna window assembly is attached with four (4) fasteners. It should be noted that the size and shape of the LI-1500 antenna window is identical to the adjacent RSI tiles.

Thermal Analysis

Temperature distributions were calculated for each of the L-band annular slot, C-band horn and C-band slot antenna system installations considered in this study. The primary concern was to ensure that adequate thermal protection for the antenna was provided to survive the entry environment, since these antennas operate after entry peak heating. This section describes the analysis procedures, a description of each thermal model, and the thermal response results.

Analysis procedures. - The thermal response of the antenna systems were calculated using MDC's General Heat Transfer Computer Program (HEATRAN Code). Two-dimensional finite-difference thermal models were used.

The thermal analysis procedure was to first size the antenna window insulation thicknesses; then minimize the heat short aspects of the integrated antenna system design; and finally, to size the heat sink to absorb heat from the short, if required. Insulation thicknesses were based on one-dimensional thermal sizing discussed in section on Preliminary Thermal Sizing Analysis. Most antennas have more heat capacitance than local skin structure; therefore, an insulation thickness less than or equal to that over adjacent Orbiter skin structure was needed over the antennas. A total window thickness equal to surrounding TPS was used for simplicity of mounting antennas to the primary structure. Only the antenna face covers and cases were incorporated into the thermal model because maximum temperatures of the antennas (i.e. 422°K (300°F)) were less than the thermal capabilities of existing antennas. This precluded the need for modeling the complex internal configurations of the antennas. Additional assumptions used

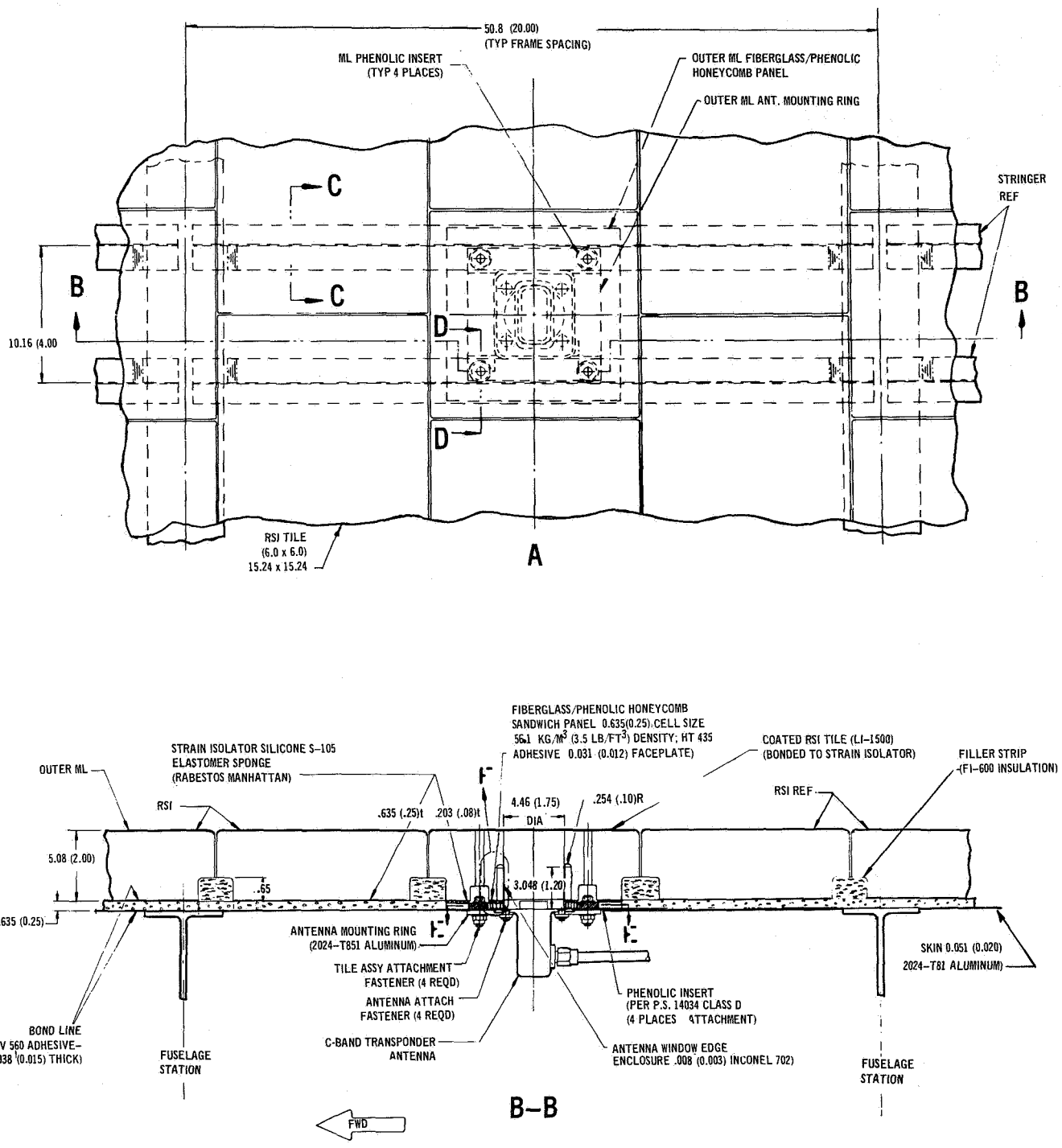

NOTE: DIMENSION CONVENTION CM (IN.)

C-BAND LINEAR SLOT ANTENNA SYSTEM INSTALLATION

(Figure Continued on Next Page)

Figure 88

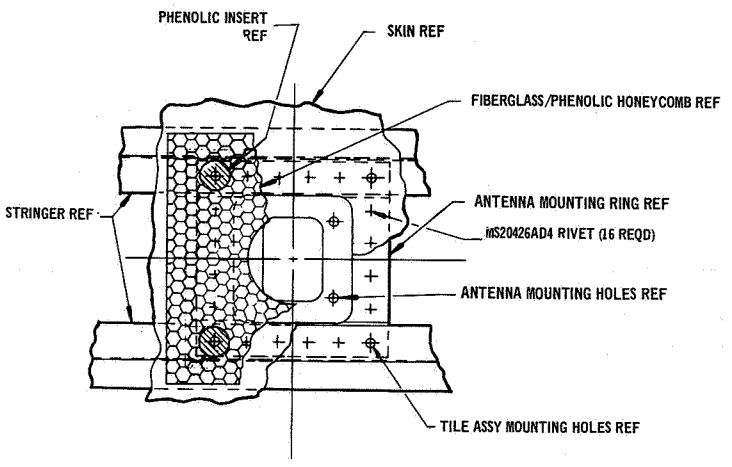

E–E

(ANTENNA AND WINDOW EDGE ENCLOSURE RING OMITTED FOR CLARITY)

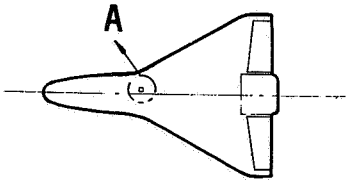

VIEW OF ORBITER – LOWER SURFACE

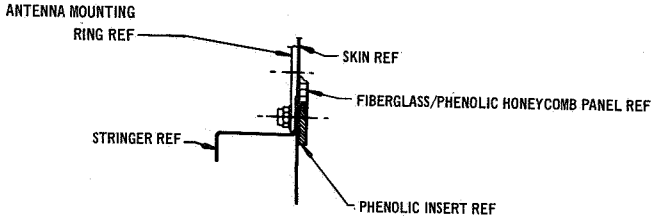

D–D

(TPS OMITTED FOR CLARITY)

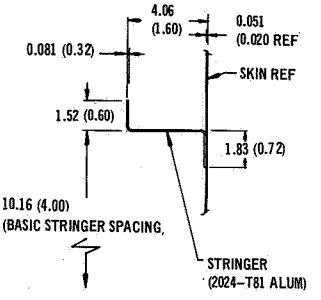

C–C

(TPS OMITTED FOR CLARITY)

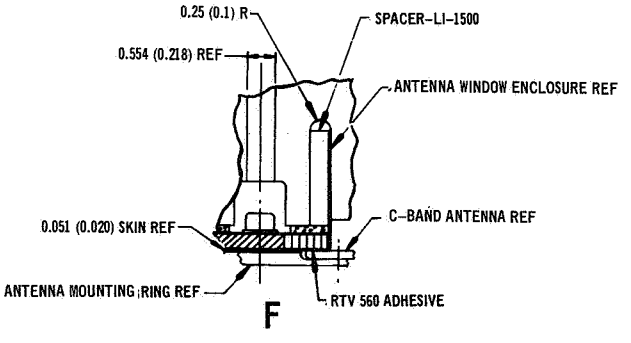

F

NOTE: DIMENSION CONVENTION CM (IN.)

C-BAND LINEAR SLOT ANTENNA SYSTEM INSTALLATION

Figure 88 (Concluded)

for the thermal analysis were: 1) boron nitride, LI-1500 and LI-1500 coatings are opaque to thermal radiation; 2) internal heat energy generated in the antenna is negligible; and 3) good thermal contact exists at all metal joints and between interfacing materials.

L-band antenna system results.- Two antenna window concepts, a single-layer LI-1500 window and a multiple-layer window, were considered for the L-band antenna.

Single-layer antenna window: The L-band antenna system with a single-layer window is shown in Figure 85. Important thermal aspects include: 1) rectangular four-tile intersection over the center axis of the cylindrical antenna; 2) double-lap strip joints between tiles; 3) FI-600 fibrous insulation strips under the joint-gaps prevent boundary layer gas heating from reaching the bondline; 4) a high emittance coating covers the FI-600 strips in the region under the joint-gaps; and 5) fastener-access holes through the RSI tiles for the antenna window assembly attachment and removal. Measured data from MDC's Contract NAS9-12854, Development and Design Application of Rigidized Reusable Surface Insulation Thermal Protection System, has shown no increase in local bondline temperature for dead-end holes with diameters of 0.475 cm (0.1875 in.). Also, plasma arc tunnel testing of Gemini ablative heat shield indicated no significant charring for heat shield holes of 0.635 cm (0.25 in.) diameter. Therefore, 0.554 cm (0.218 in.) holes through the RSI are considered acceptable for attachment and removal of the antenna window assemblies.

The thermal model for the L-band antenna with single-layer window is shown in figure 89 and has 179 nodes and 320 connectors. Convective heating distributions for the tile joint; and radiation between joint-faces and to space were simulated in the thermal model.

Transient temperatures for the L-band single-layer RSI window are shown in figure 90. The antenna face reaches a maximum temperature about 40 minutes after landing. The maximum temperature at any point in the LI-1500 window material at start of antenna operation, 45.7 km (150 kft) altitude is about 1011°K (1360°F).

Multiple-layer antenna window: The multiple-layer window concept (originally designed for a metallic TPS) was integrated into an RSI TPS. Small and large diameter antenna windows were considered, using a boron nitride (HD-0092 outer layer over a Dynaquartz insulation layer.

Thermal models were constructed for the small and large diameter L-band multiple-layer antenna windows. The nonisotropic thermal conductance properties of the boron nitride were simulated. Available HD-0092 data indicated that the thermal conductivity parallel to the outer moldline was 1.9 times the perpendicular value. A free stream flight ambient pressure was assumed for the Dynaquartz layer because it was considered sealed off from the local static surface pressure by the continuous edge enclosure. A flight ambient free stream pressure environment conservatively simulates antenna venting to the fuselage interior that is vented to leeward, or base area, which is lower than free stream pressure. The columbium window edge enclosure was found to be a significant heat short.

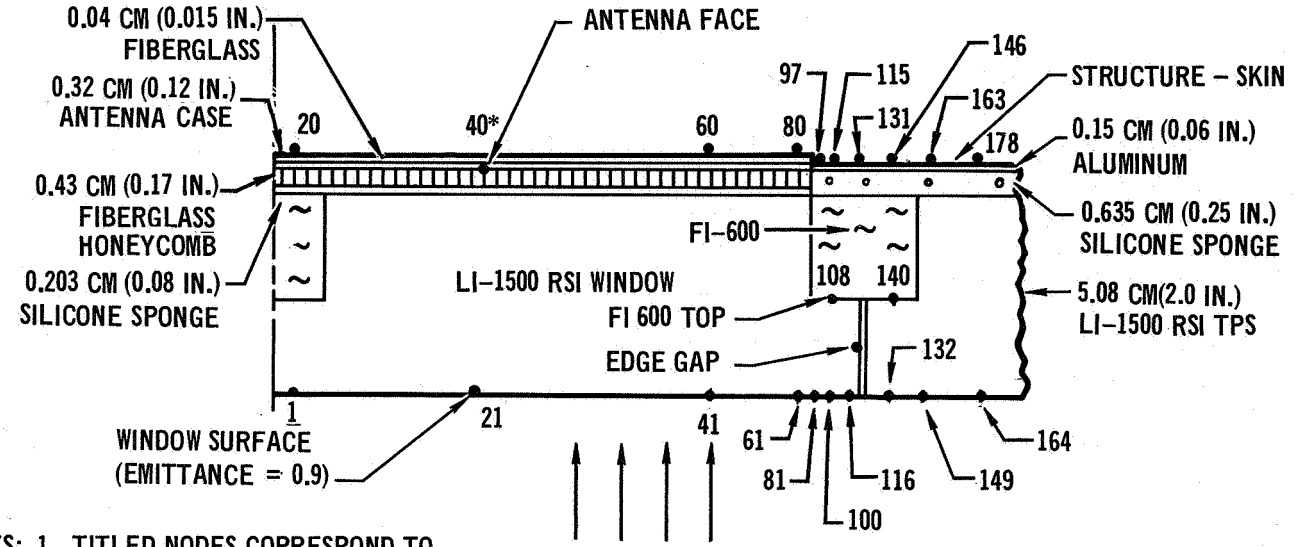

NOTES: 1. TITLED NODES CORRESPOND TO PLOTTED CURVES ON THERMAL RESPONSE TEMPERATURE HISTORY
2. *DESIGNATES NODE NUMBERS

L-BAND ANTENNA SYSTEM THERMAL MODEL – SINGLE-LAYER WINDOW

Figure 89

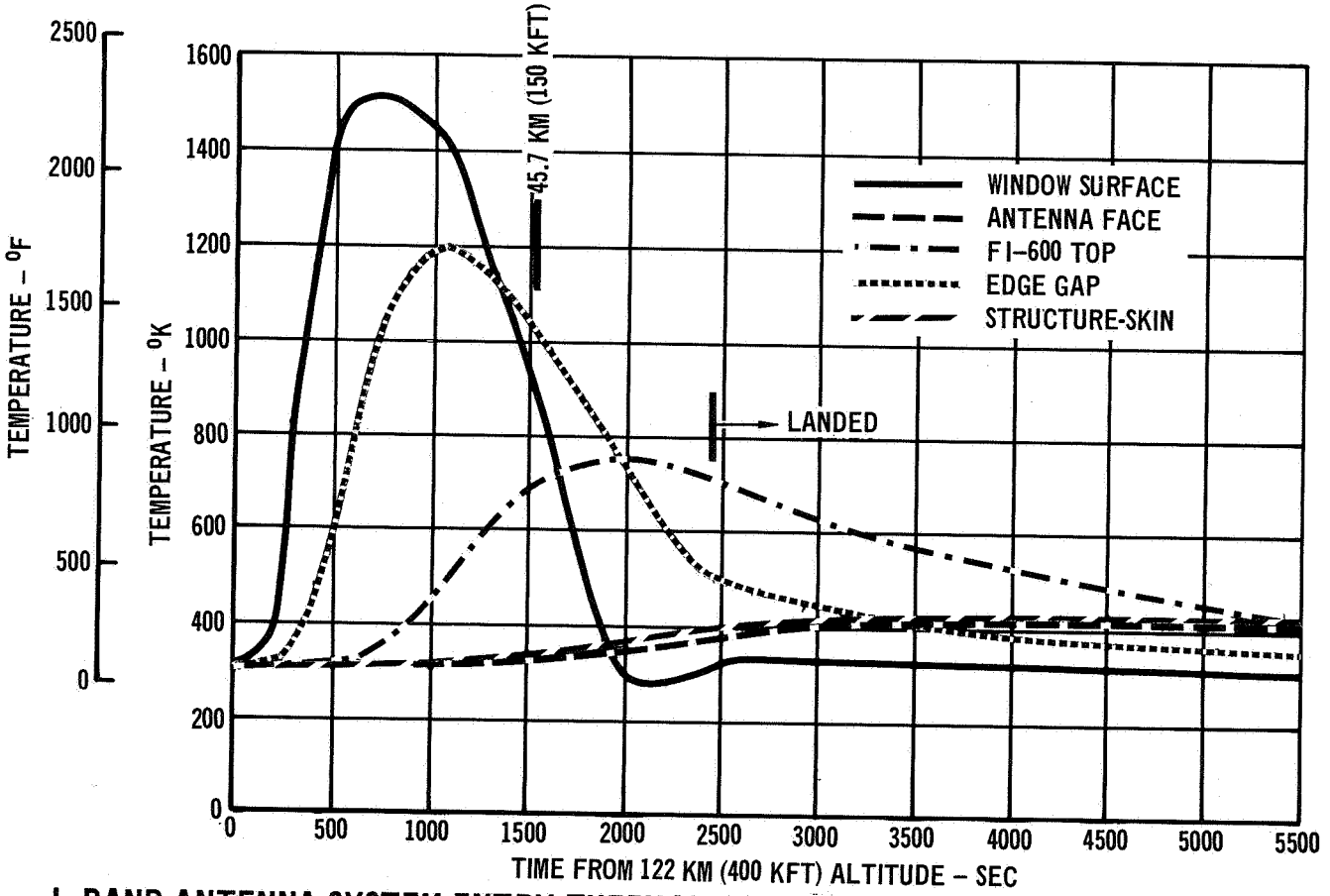

L-BAND ANTENNA SYSTEM ENTRY THERMAL RESPONSE – SINGLE-LAYER WINDOW

Figure 90

The maximum size multiple-layer antenna window system, 0.32 meter (12.6 in.) diameter, is shown in figure 86. The thermal model, shown in figure 91, consists of 145 nodes and 267 connectors.

Transient temperatures for ascent are shown in figure 92. Ascent temperatures were calculated because of concern over the edge enclosure heat short effect on skin structure temperatures at ascent maximum dynamic-pressure loading, about 70 seconds after launch. The temperature of the antenna face and primary structure skin remained at the initial temperature of 294°K (70°F) until 500 and 1000 seconds respectively after launch. Therefore, mechanical material properties at room temperatures may be used in stress analysis for ascent maximum dynamic-pressure loading.

Transient temperatures for entry are shown in figure 93. The calculated maximum temperature of the antenna is about 405°K (270°) and occurs 5160 seconds after the 122 km (400 kft) altitude entry interface. Only a 3.18 cm (1.25 in.) thickness of Dynaquartz was needed for the temperature-pressure environment; however, a 4.58 cm (1.8 in.) thickness was provided. With this thickness and the boron nitride layer of 1.07 cm (0.42 in.) the desirable feature of having the antenna window total thickness about the same as adjacent TPS was achieved. The maximum temperature at any point in the window materials at start of antenna operation, 45.7 km (150 kft) altitude is about 1137°K (1586°F).

The minimum size, multiple-layer window configuration (0.23 m (9.0 in.) diameter window) is shown in figure 19. The thermal model, shown in figure 94, consists of 130 nodes and 247 connectors. Both the boron nitride/Dynaquartz and adjacent LI-1500 were sized to 422°K (300°F). Using this model, a number of design changes were examined to find the most effective method of thermally isolating the window edge enclosure from the antenna and Orbiter skin. The relative influence of: 1) changing the fibrous insulation material between the edge enclosure and TPS; 2) changing the load bearing insulation material; 3) heat sinking the U-shaped internal mounting ring (i.e. making this section thicker); 4) reducing the edge enclosure thickness; and 5) the local effect of the the mounting attachment bolt were examined. The effects of these changes on selected temperature nodes are summarized in table IX. Table IX shows that heat sinking the mounting ring is the most effective method. The heat sink thickness required was 0.76 cm (0.3 in.) as shown in figure 95.

C-band horn antenna system results. - The C-band horn antenna system is shown in figure 87. The C-band horn antenna window installation has a cylindrical Inconel 702 foil window edge enclosure. The design has a cylindrical tile with a single lap joint and a FI-600 strip filler. The thermal model used for analysis, shown in figure 96, consists of 186 modes and 333 connectors. Cylindrical tile joint convective heating characteristics were not known so rectangular tile joint data was used. The design originally considered foil extending 3.81 cm (1.50 in.) above the ground plane of the antenna with only 1.75 cm (0.69 in.) of LI-1500 above it. This design required a filler strip of FI-600 not impregnated with silicone oil because of the potential ignition of the oil near the surface. Although this edge enclosure height was preferred for best radiation pattern characteristics, preliminary analyses indicated that the foil, that near the TPS surface, caused excessive temperature at the face

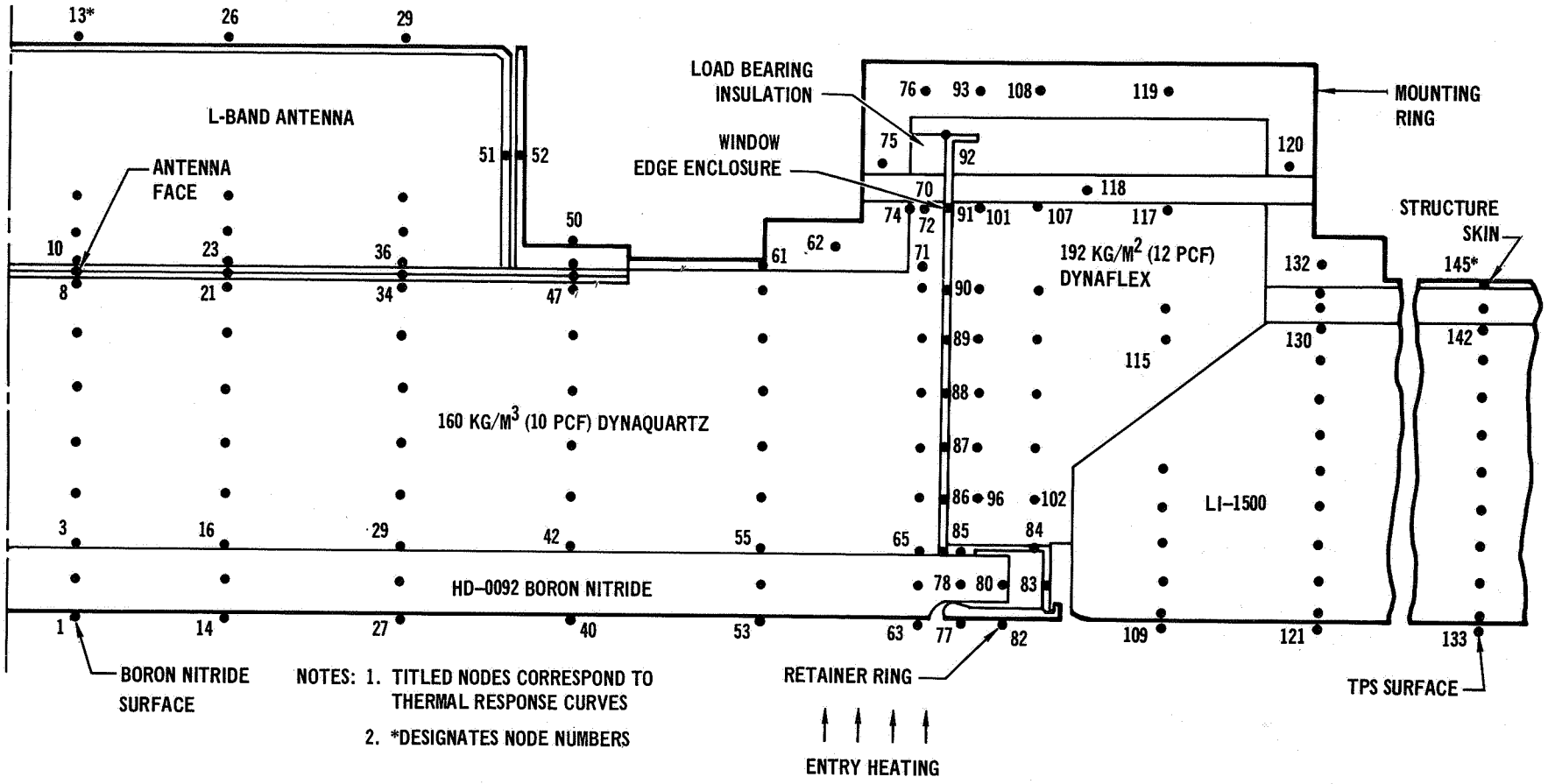

L-BAND ANTENNA SYSTEM THERMAL MODEL – MAXIMUM SIZE MULTIPLE-LAYER WINDOW

Figure 91

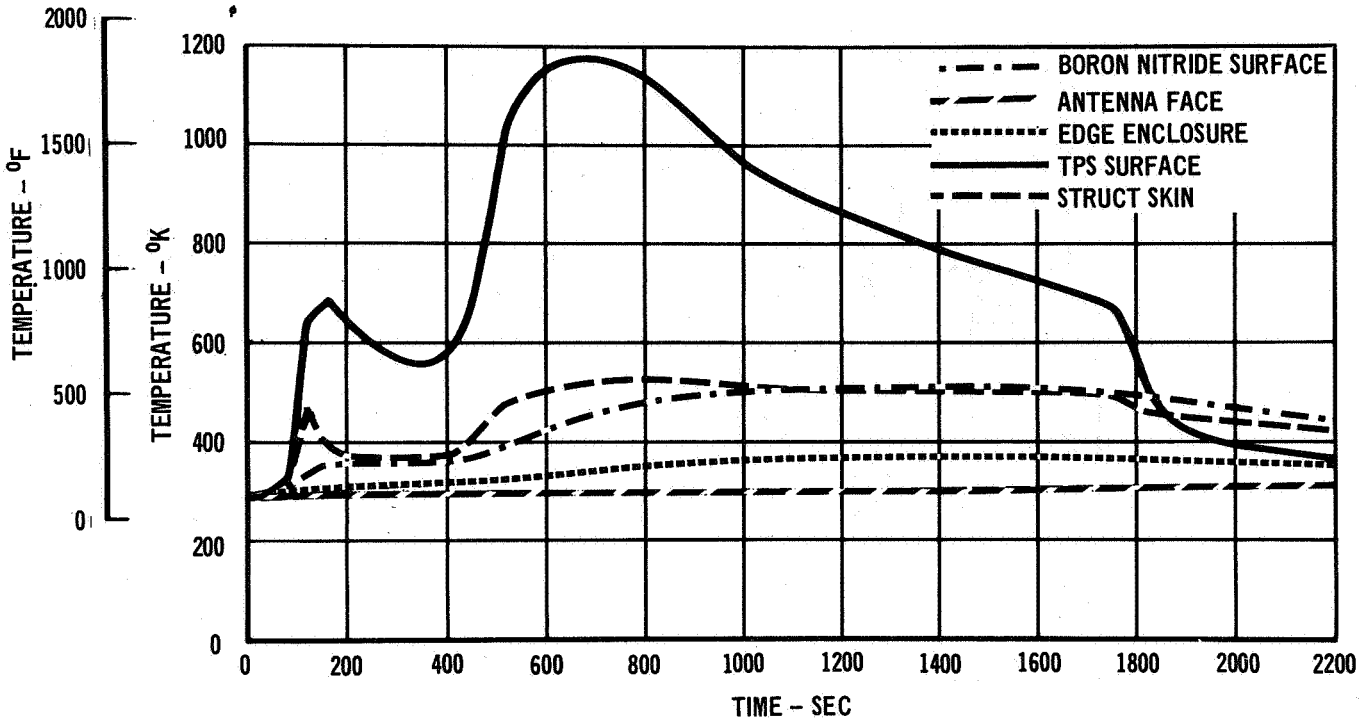

MAXIMUM SIZE MULTIPLE-LAYER WINDOW ANTENNA SYSTEM ASCENT THERMAL RESPONSE

Figure 92

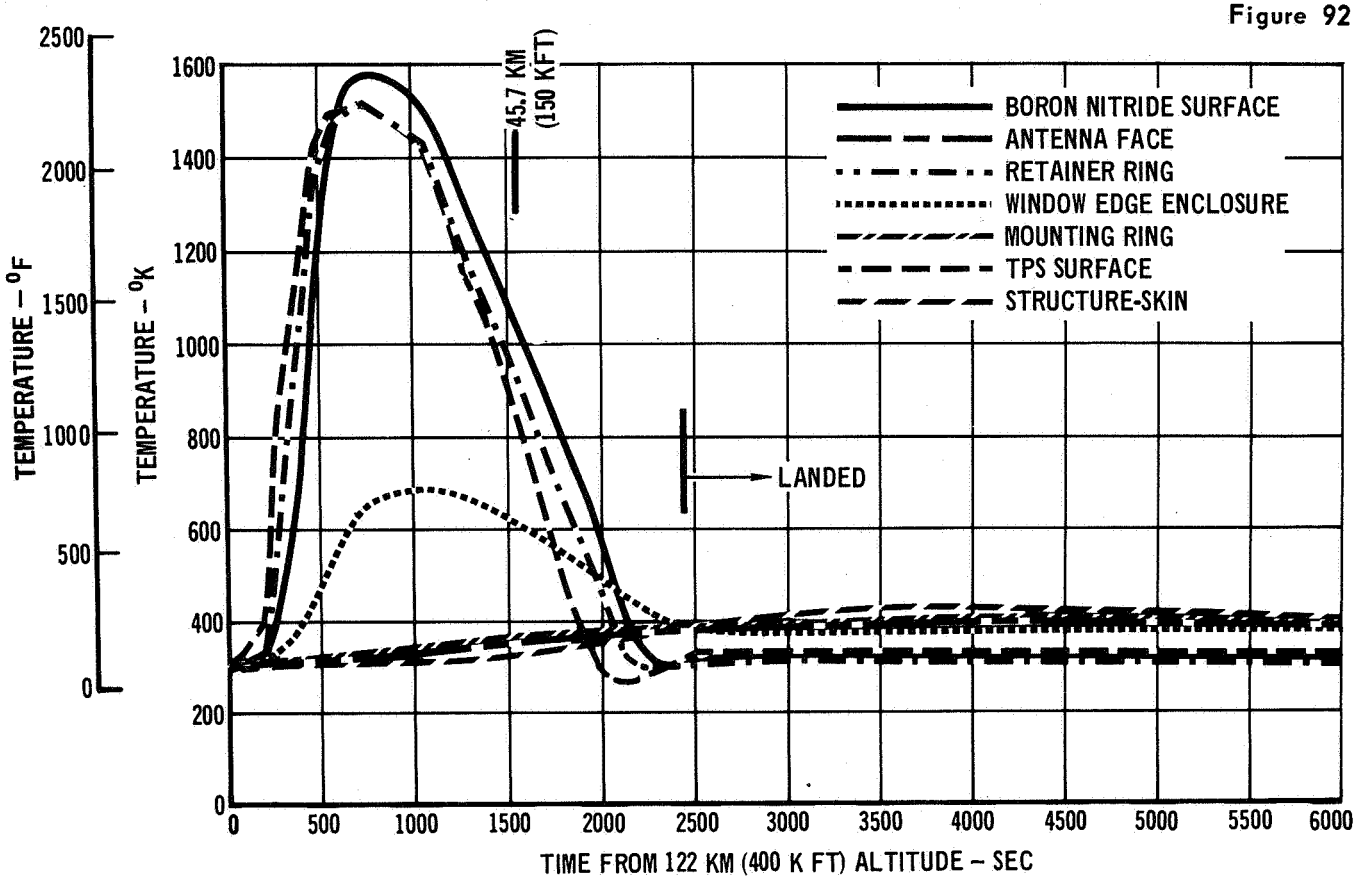

L-BAND ANTENNA SYSTEM ENTRY THERMAL RESPONSE – MAXIMUM SIZE MULTIPLE-LAYER WINDOW

Figure 93

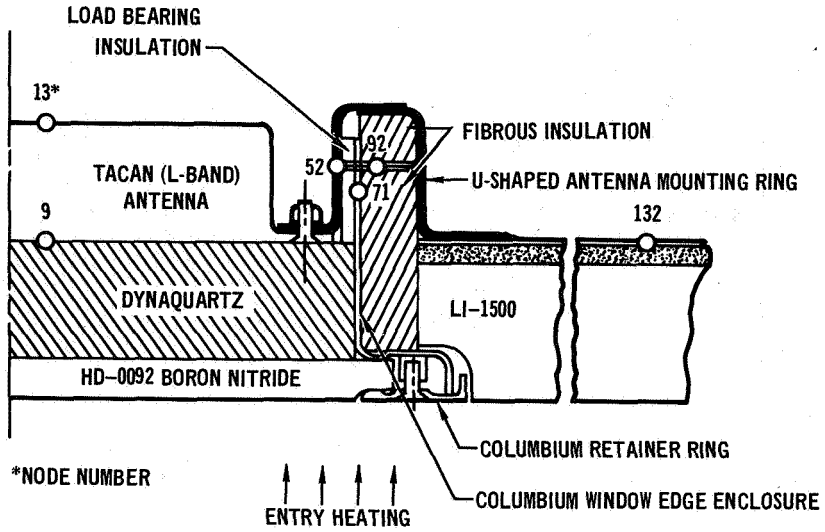

L-BAND ANTENNA SYSTEM THERMAL MODEL – MINIMUM SIZE MULTIPLE-LAYER WINDOW

Figure 94

TABLE IX

MINIMUM SIZE MULTIPLE-LAYER ANTENNA TEMPERATURE SUMMARY

CONFIGURATION	MAXIMUM TEMPERATURE ^{o}K (^{o}F)			
	ANTENNA WINDOW EDGE ENCLOSURE (FS 85 Cb) NODE NO. 71	INTERNAL MOUNTING FOR ANTENNA (2024T ALUM) NODE NO. 75	ANTENNA CASE (6061–0 ALUM) NODE NO. 13 OR NODE NO. 19	PRIMARY STRUCTURAL (2024T–81 ALUM) SKIN (UNDER TPS, 0.3M (12 IN. FROM ANTENNA) NODE NO. 132
1. BASIC*	624 (663)	456 (361)	459 (367)	459 (367)
2. INCREASED DENSITY INSUL. RING (TO 240 KG/M^3) BETWEEN WINDOW EDGE ENCL. AND TPS	604 (627)	450 (351)	454 (357)	458 (365)
3. REDUCE THERMAL CONDUCTIVITY OF LOAD BEARING INSUL. (TO 0.0398 W/M^{o}K (0.023 BTU/FT HR ^{o}F))	925 (1205)	441 (334)	440 (333)	449 (349)
4. HEAT SINK ENTIRE U-SHAPED INTERNAL MOUNTING RING TO 0.71 CM (0.28 IN.) THICKNESS	910 (1178)	422 (300)	422 (299)	427 (309)
5. CONNECT ATTACHMENT BOLT (NODE 92); REDUCE EDGE ENCLOSURE THICKNESS TO 0.355 MM (0.014 IN.); SLIGHTLY INCREASE HEAT SINK 0.507 MM (0.02 IN.)	712 (821)	422 (299)	422 (300)	422 (309)

*BASIC CONFIGURATION

1. INSULATION RING BETWEEN EDGE-ENCLOSURE AND TPS: MICROQUARTZ 56 KG/M^3 (3.5 LB/FT^3).
2. LOAD BEARING INSULATION: CS–1000, 0.693 W/M^{o}K (0.4 BTU/FT HR ^{o}F).
3. TPS (LI–1500 RSI) AND ANTENNA WINDOW INSULATION: DYNAQUARTZ, 160 KG/M^3 (10 LB/FT^3)
4. COLUMBIUM WINDOW EDGE-ENCLOSURE THICKNESS: 0.507 MM (0.02 IN.)
5. NO ATTACHMENT BOLT.

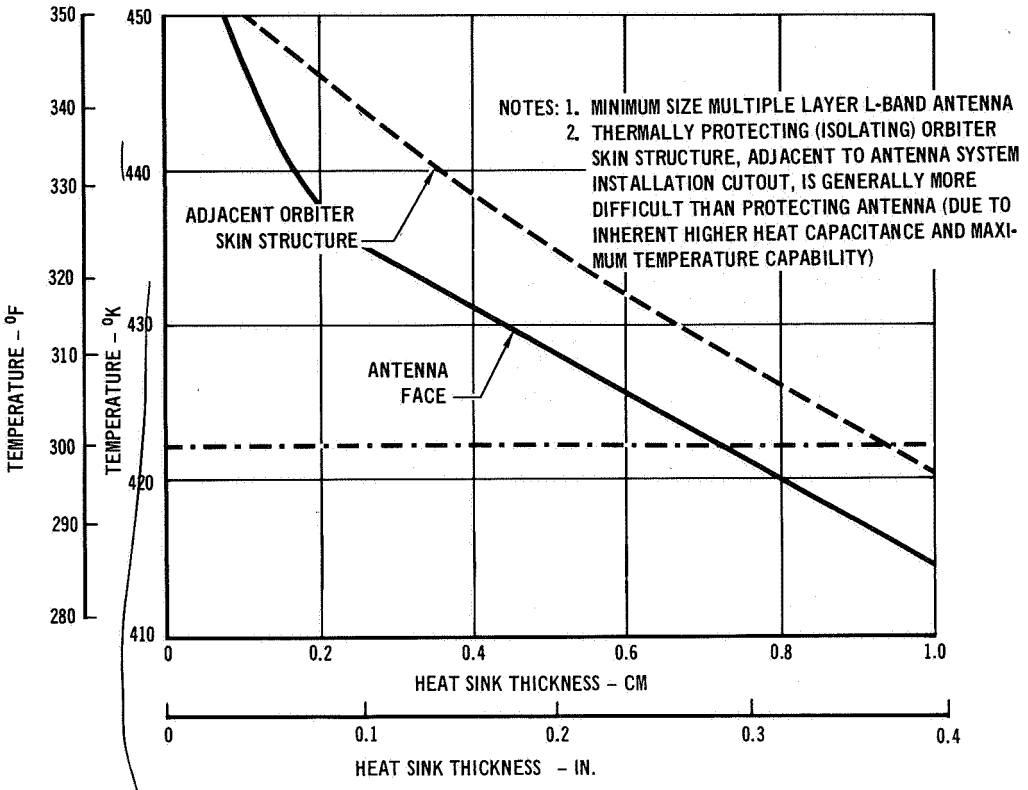

EFFECTS OF MOUNTING RING HEAT SINK THICKNESS ON MAXIMUM ANTENNA TEMPERATURE

Figure 95

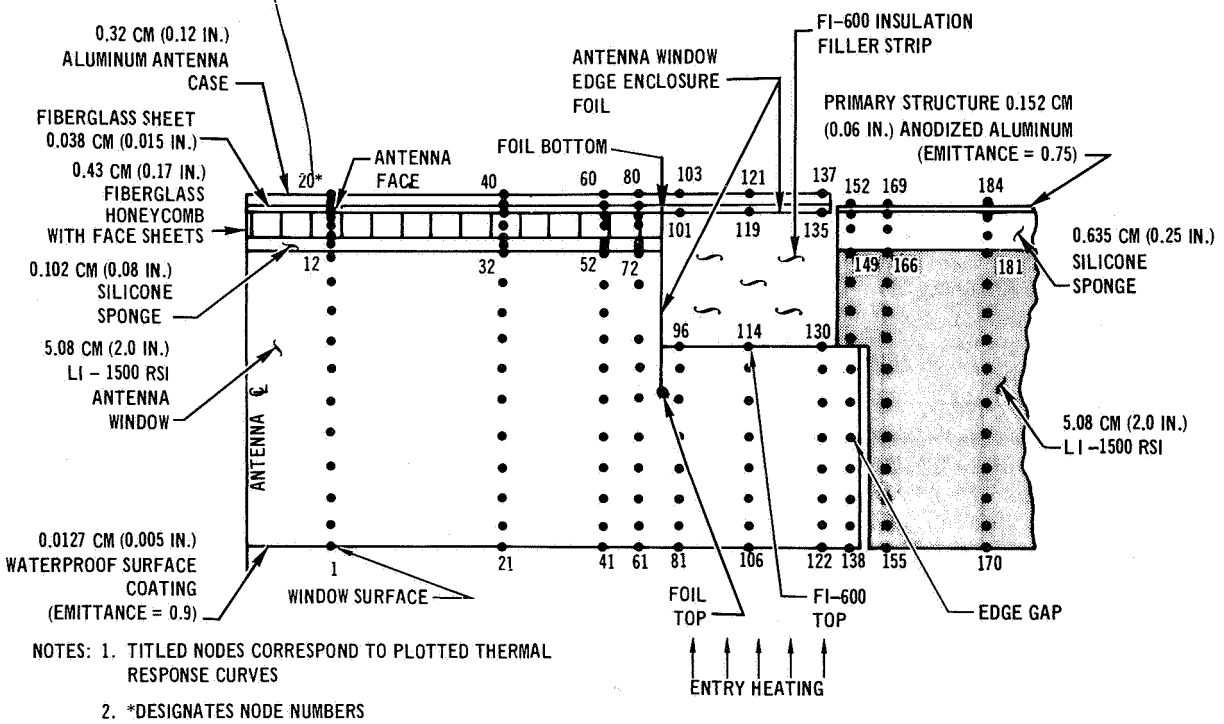

NOTES: 1. TITLED NODES CORRESPOND TO PLOTTED THERMAL RESPONSE CURVES

2. *DESIGNATES NODE NUMBERS

C-BAND HORN ANTENNA SYSTEM THERMAL MODEL

Figure 96

of the antenna. Therefore, the window edge enclosure height was reduced to 3.04 cm (1.20 in.). This achieved a simpler design, allowed for conventional FI-600 waterproofing, provided safer thickness of LI-1500 above the foil, and still allowed some edge enclosure for radiation pattern control.

Transient entry temperatures for the C-band horn antenna system are shown in figure 97. The maximum temperature at the outboard tip of the foil was about 700°K (800°F). The heat short created by the foil caused a local cool spot in LI-1500 at the foil tip. The maximum temperature of the antenna face was 420°K (296°F).

C-band slot antenna system results. - The C-band slot antenna system is shown in figure 88. An Inconel 702 foil edge enclosure buried in a rectangular RSI tile window is also incorporated in the C-band slot antenna system installation. This design has a double-lap strip joint design using a FI-600 filler strip. The foil edge enclosure in this design differs from that in the C-band horn, because it lacks the benefit of cooler temperatures beneath the FI-600 filler strip. The C-band slot thermal model, shown in figure 98 has 182 nodes and 207 connectors. The thermal mass of the antenna was more completely simulated in this thermal model than in the others. Entry temperatures for the C-band slot antenna system are shown in Figure 99.

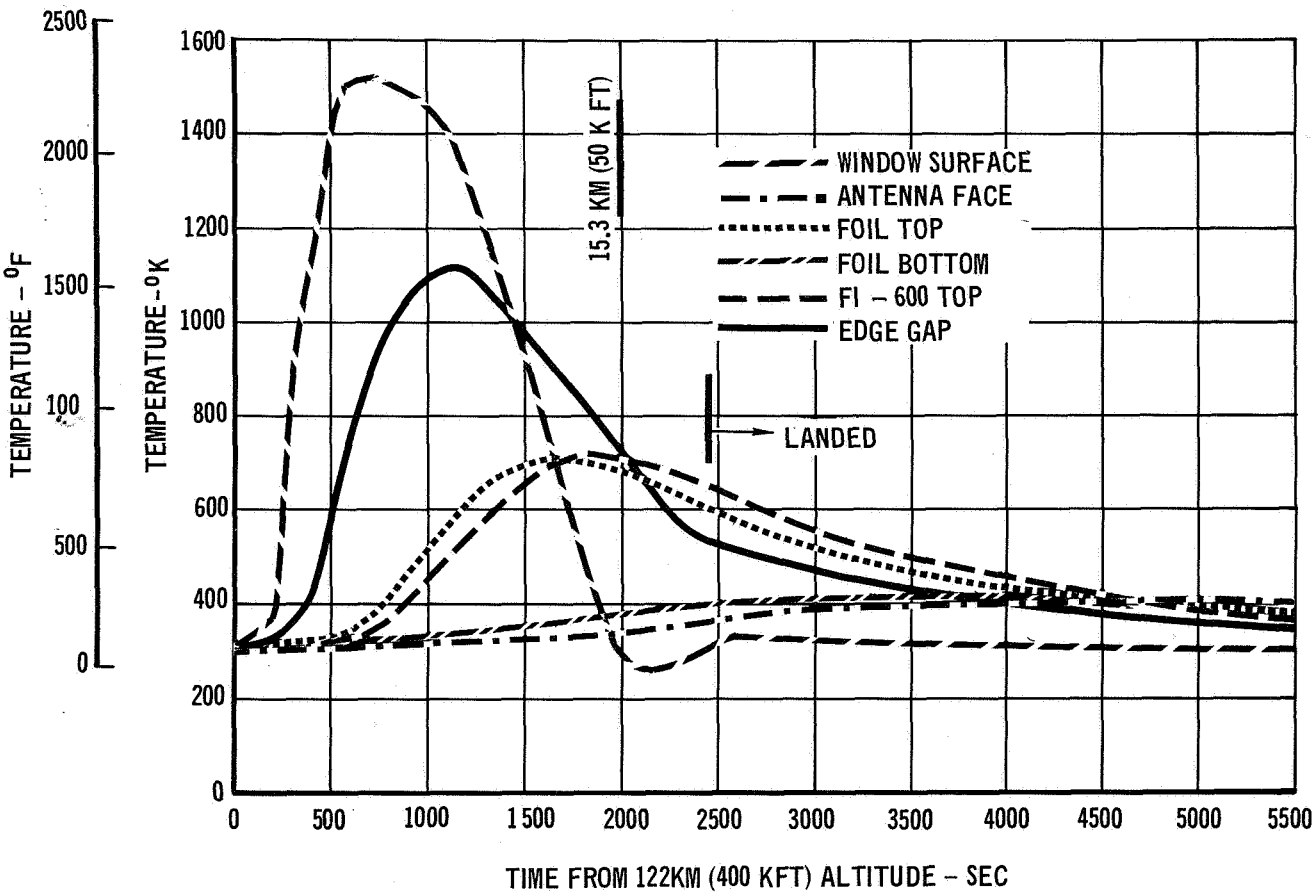

C-BAND HORN ANTENNA SYSTEM ENTRY THERMAL RESPONSE

Figure 97

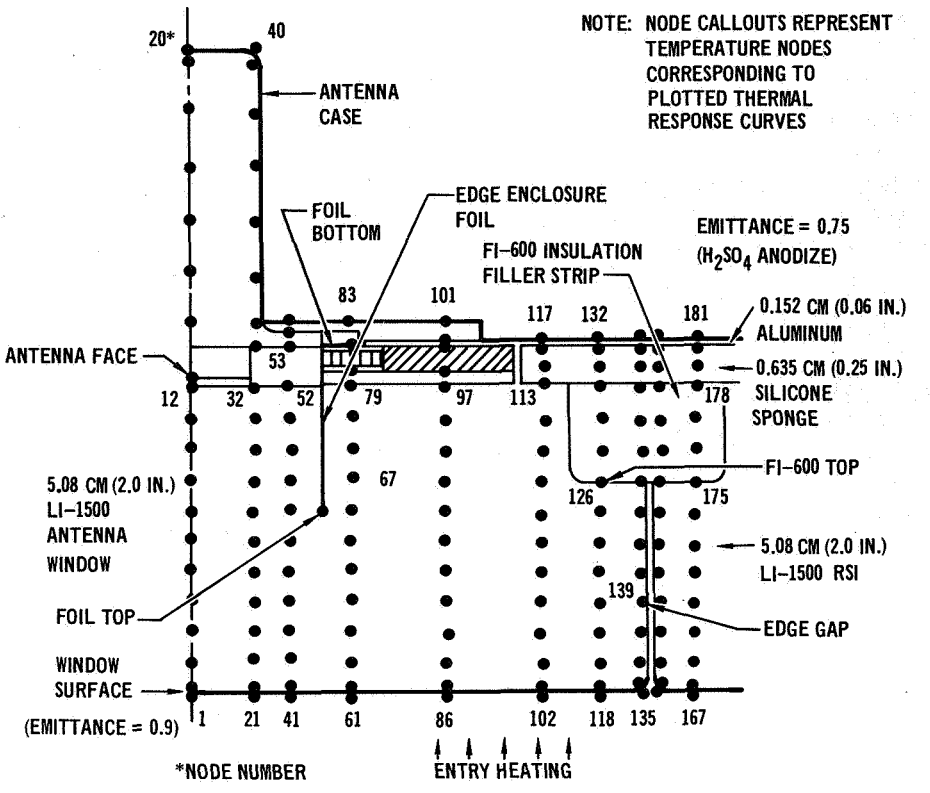

C-BAND SLOT ANTENNA SYSTEM THERMAL MODEL

Figure 98

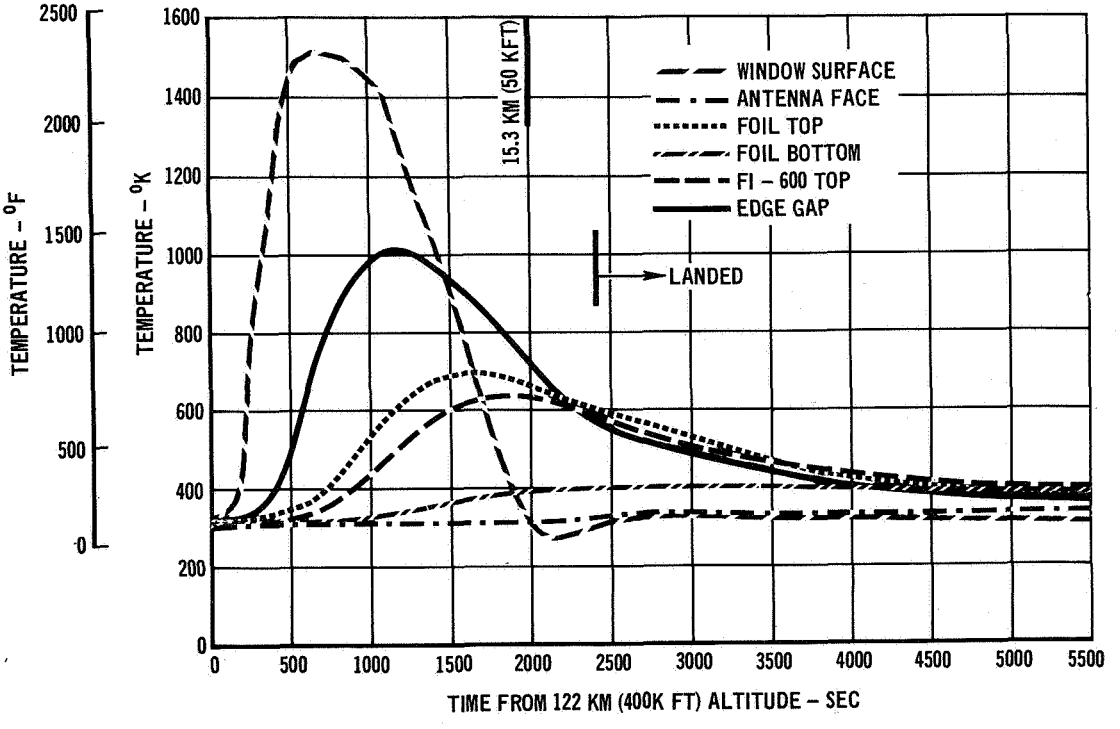

C-BAND SLOT ANTENNA SYSTEM ENTRY THERMAL RESPONSE

Figure 99

Strength Analysis

Standard methods of strength analysis were used to analyze and size components of the various antenna system designs. Material properties were taken either from MIL-HDBK-5B, if given, or Appendix A. Analyses are for antenna system designs illustrated in figures 85 through 88.

Structural load considerations. - The structural concept for each of the three antenna with RSI windows is basically the same. Collapsing pressure is exerted against the RSI external surface. The pressure is transferred to the sponge strain isolator by the RSI and, in turn, to the fiberglass honeycomb panel. Loads from the fiberglass honeycomb panel are transmitted by a mounting ring to the aluminum stringers. The stringers carry loads to the fuselage frames and the frames distribute the loads in the fuselage shell. Stringers were designed to withstand bending moments resulting from the external pressure as well as primary fuselage loads. The L-band multiple-layer antenna window is different than the RSI concepts in that the pressure load from the boron nitride is reacted around the perimeter of the window by a columbium enclosure ring. The columbium ring is fastened to the antenna support structure which is attached to the stringers. The stringers then distribute the loads in the same manner described for the RSI concept.

Analysis procedures. - Stresses acting on axisymmetrical elements were calculated using the computer program SAAS II described in reference 9. This is a finite element program which determines displacements, stresses, and strains in axisymmetric solids with orthotropic, temperature-dependent material properties under axisymmetric thermal and mechanical loads. Thermal stresses acting on nonaxisymmetrical elements were calculated using a MDC Computer Program, KBEB. This is a finite element program which uses a method of analysis consistent with classical beam bending theory to determine thermal stresses. Stresses acting on simple structure such as stringers, mounting clips, and bolts were manually calculated using classical procedures. The margin of safety, showing the strength in excess of that required by the 1.4 safety factor, was calculated for critical items.

L-band antenna system results. - The stresses in the L-band RSI window are essentially equivalent to those calculated for the C-band horn antenna window below. The L-band window is made up of four (4) RSI tiles each of which is approximately the same size as the C-band window. The tile size used for the L-band window is considered near optimum for the Orbiter RSI TPS as a result of design and testing of thermal protection systems.

Boron nitride window ascent mechanical stresses resulting from an ultimate external pressure of 73 100 N/m^2 (10.6 psi) and thermal stresses resulting from the window temperatures shown on table X are shown on figure 100. These stresses were calculated using the SAAS II computer program. The computer model is shown on figure 101.

TABLE X
TEMPERATURES – BORON NITRIDE (HD–0092) WINDOW

R CM (IN.)	Z CM (IN.)	T ^{o}K (^{o}F)	R CM (IN.)	Z CM (IN.)	T ^{o}K (^{o}F)
1.27 (0.50)	0.00 (0.00)	1446 (2143)	12.95 (5.10)	0.00 (0.00)	1439 (2131)
1.27 (0.50)	0.53 (0.21)	1406 (2071)	12.95 (5.10)	0.53 (0.21)	1398 (2056)
1.27 (0.50)	1.07 (0.42)	1390 (2043)	12.95 (5.10)	1.07 (0.42)	1382 (2028)
3.81 (1.50)	0.00 (0.00)	1446 (2143)	15.75 (6.20)	0.00 (0.00)	1385 (2033)
3.81 (1.50)	0.53 (0.21)	1406 (2071)	15.75 (6.20)	0.53 (0.21)	1342 (1956)
3.81 (1.50)	1.07 (0.42)	1390 (2043)	15.75 (6.20)	1.07 (0.42)	1323 (1921)
6.86 (2.70)	0.00 (0.00)	1446 (2143)	16.51 (6.50)	0.00 (0.00)	1371 (2008)
6.86 (2.70)	0.53 (0.21)	1406 (2071)	16.51 (6.50)	0.53 (0.21)	1328 (1931)
6.86 (2.70)	1.07 (0.42)	1390 (2043)	16.51 (6.50)	1.07 (0.42)	1298 (1876)
9.65 (3.80)	0.00 (0.00)	1445 (2141)	17.15 (6.75)	0.00 (0.00)	1344 (1959)
9.65 (3.80)	0.53 (0.21)	1404 (2068)	17.15 (6.75)	0.53 (0.21)	1301 (1882)
9.65 (3.80)	1.07 (0.42)	1389 (2041)	17.15 (6.75)	1.07 (0.42)	1295 (1872)

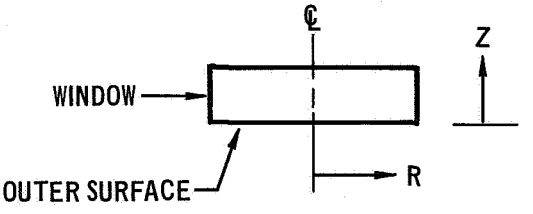

NOTES:
1. ENTRY TIME = 600 SEC
2. TEMPERATURES SHOWN ARE THOSE ENTERED IN COMPUTER PROGRAM TO CALCULATE THERMAL STRESSES SHOWN ON FIGURE 100

The maximum stress occurring during ascent (at room temperature) are at the center of the boron nitride window and are 2.33×10^7 N/m^2 (3385 psi) in both the radial and tangential directions. From Appendix A, the allowable flexural stress for this type of boron nitride, HD-0092, at room temperature is 4.13×10^7 N/m^2 (6000 psi). For this condition the margin of safety, MS, is obtained from the following expression.

$$MS = \left[1/(U_R^{1.7} + U_T^{1.7})^{1/1.7}\right] - 1$$

where

U_R = applied stress/allowable stress in the radial direction

U_T = applied stress/allowable stress in the tangential direction

For this case $U_R = U_T = (3385/6000)$, therefore, MS = 0.18. The margin of safety is higher for the entry condition and is, therefore, not shown.

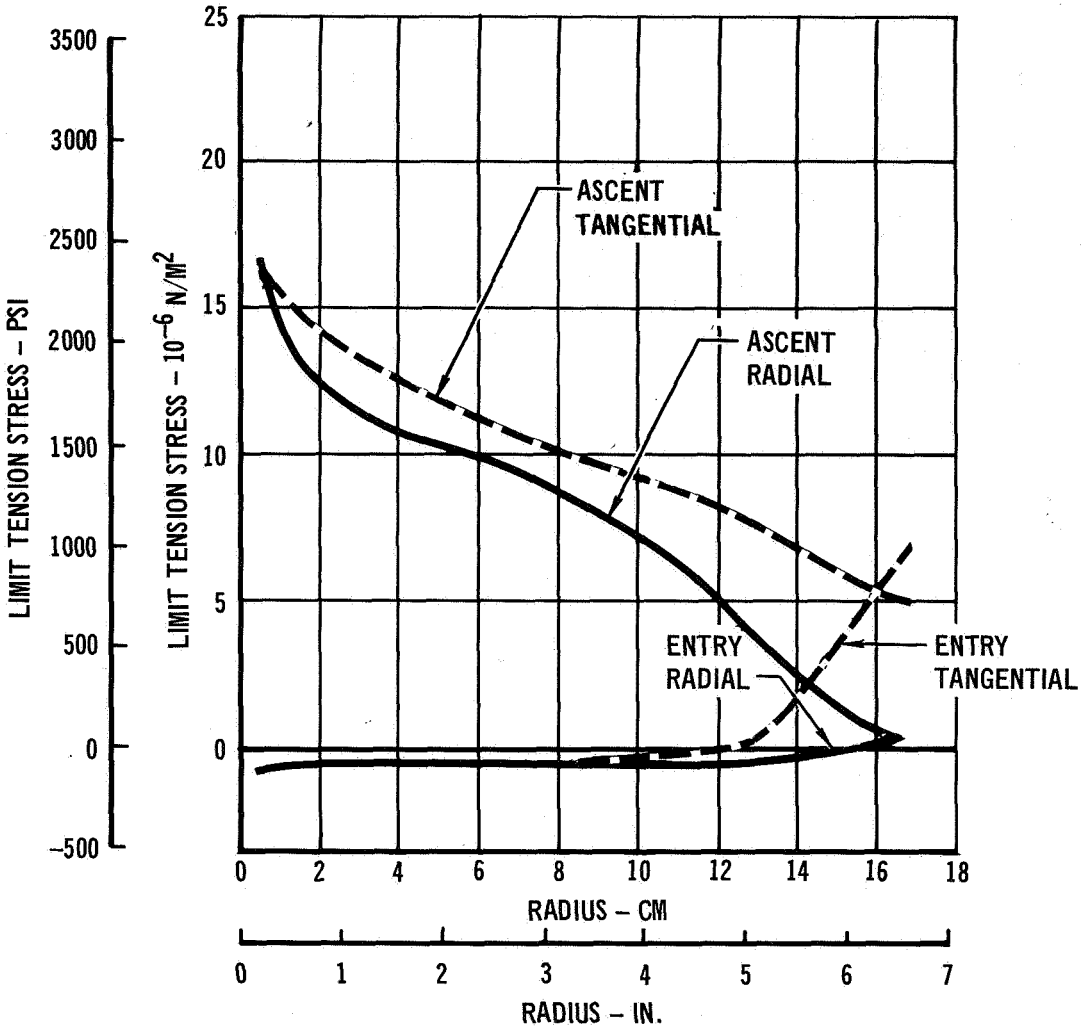

NOTES:

1. WINDOW DIMENSIONS:
   DIAMETER = 34.3 CM (13.5 IN.)
   THICKNESS = 1.065 CM (0.42 IN.)
2. ENTRY TIME = 600 SEC
3. ASCENT STRESSES SHOWN ARE AT INSIDE SURFACE. ENTRY STRESSES SHOWN ARE 0.585 CM (0.23 IN.) FROM INSIDE SURFACE
4. ASCENT STRESSES RESULT FROM 52,300 N/M^2 (7.55 PSI) PRESSURE LOAD. ENTRY STRESSES RESULT FROM TEMPERATURES SHOWN IN TABLE X

LIMIT THERMAL AND MECHANICAL STRESSES – BORON NITRIDE (HD–0092) WINDOW

Figure 100

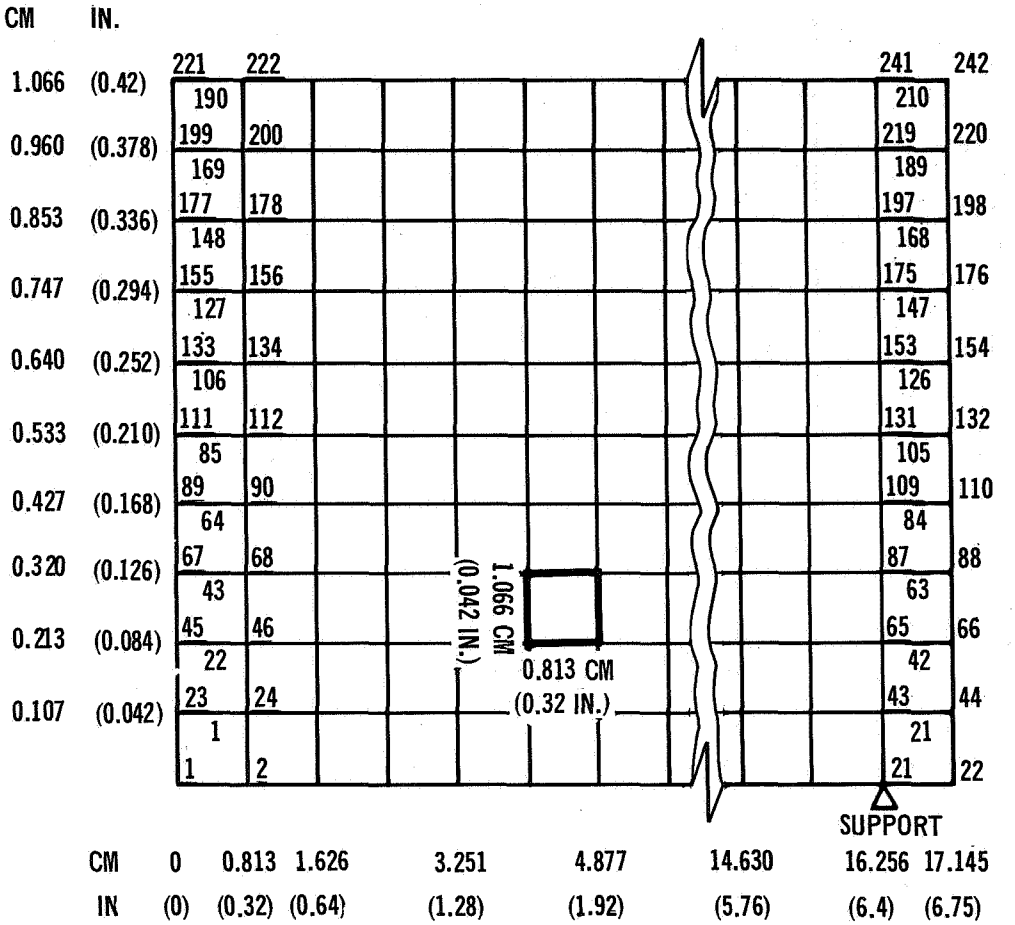

NOTES

1: ELEMENT NUMBERS ARE SHOWN AT MIDDLE OF ELEMENTS.
NODE NUMBERS ARE SHOWN AT CORNERS OF ELEMENTS

2. 34.29 CM (13.5 IN.) DIAMETER

3. 1.066 CM (0.42 IN.) THICK

COMPUTER MODEL – BORON NITRIDE (HD–0092) WINDOW

Figure 101

The thickness of a circular plate required to withstand a given pressure varies directly as the diameter. The boron nitride window analyzed was 34.3 cm (13.5 in.) in diameter and 1.065 cm (0.42 in.) thick. The thickness required for a window of any other diameter can be determined by multiplying the 1.065 cm (0.42 in.) thickness by the ratio of the new diameter to the 34.3 cm (13.5 in.) diameter.

Thermal stress in the columbium enclosure ring which supports the boron nitride window are of interest because this ring experiences a severe temperature gradient during entry. Ring temperatures and resulting thermal stresses existing 800 seconds after start of entry are shown on figure 102. The most critical stress is 5.8×10^7 N/m^2 (8410 psi) compression at 1420°K (2100°F).

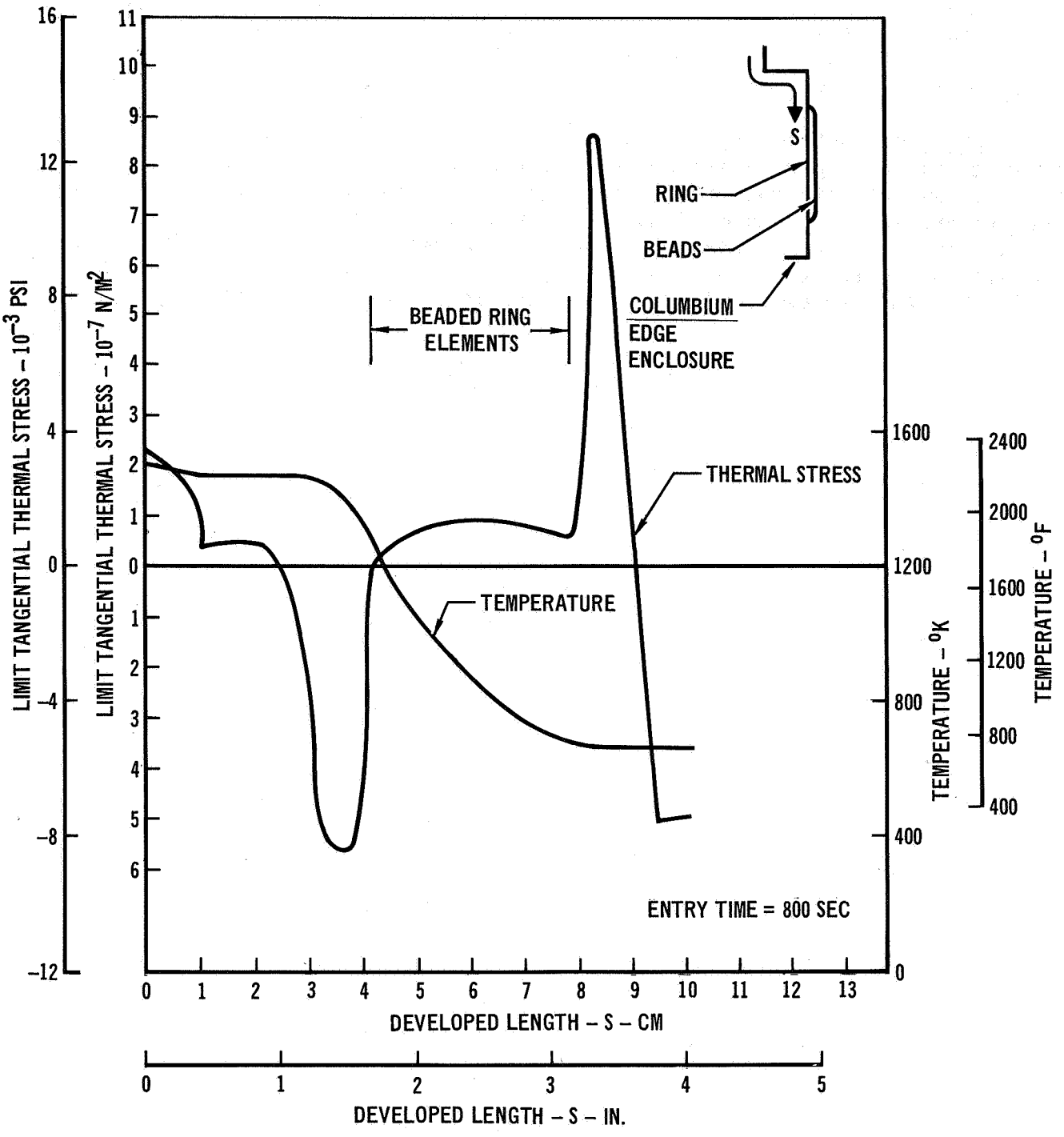

TEMPERATURES AND LIMIT THERMAL STRESSES – WINDOW EDGE ENCLOSURE FOR MULTIPLE-LAYER ANTENNA WINDOW DESIGN

Figure 102

This is well below the compression stress, 13.8 N/m^2 (20,000 psi), which would cause structural failure at this temperature. The computer model used to calculate the stresses is illustrated on figure 103. These stresses were calculated using the SAAS II Computer Program.

C-band horn antenna system results.- As a typical example, thermal stresses are shown for a composite section consisting of LI-1500 RSI, sponge strain isolator, and the fiberglass-honeycomb subpanel. The temperatures used for the analysis are shown on table XI and the stresses are shown on figure 104. The SAAS II computer program was used for this analysis. The computer model used is shown on figure 105. The maximum in plane tension stress in the RSI is 0.69×10^5 N/m^2 (10 psi). At this temperature the allowable in plane tension

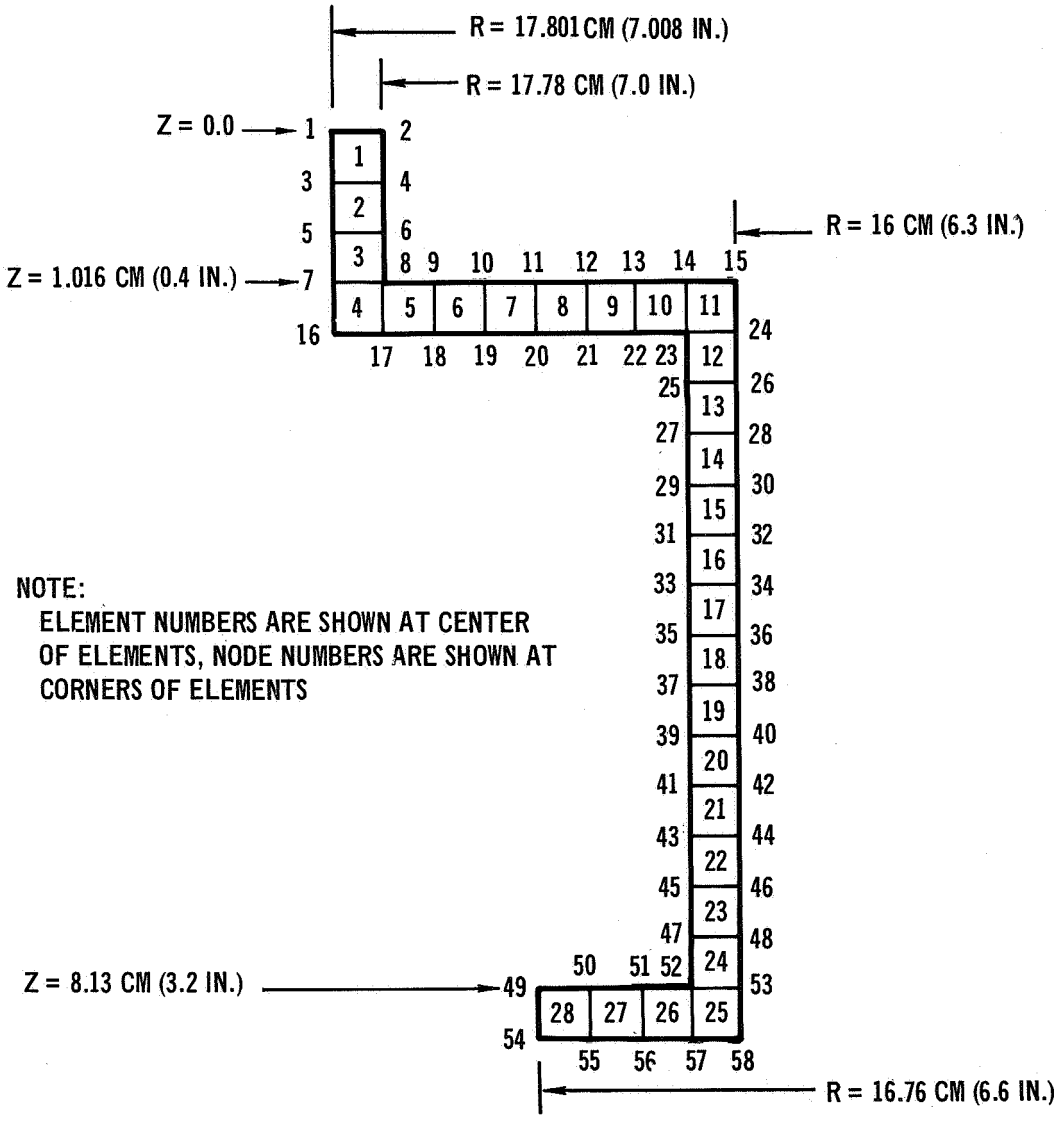

COMPUTER MODEL – WINDOW EDGE ENCLOSURE FOR MULTIPLE-LAYER ANTENNA WINDOW DESIGN

Figure 103

TABLE XI
TEMPERATURES – SINGLE-LAYER RSI ANTENNA WINDOW DESIGN

R CM (IN.)	Z CM (IN.)	T °K (°F)	R CM (IN.)	Z CM (IN.)	T °K (°F)	R CM (IN.)	Z CM (IN.)	T °K (°F)
1.49 (0.59)	5.72 (2.25)	1508 (2254)	6.10 (2.40)	3.18 (1.25)	378 (215)	7.32 (2.88)	4.70 (1.85)	923 (1201)
1.49 (0.59)	5.21 (2.05)	1257 (1802)	6.10 (2.40)	2.67 (1.05)	338 (149)	7.32 (2.88)	4.19 (1.65)	621 (659)
1.49 (0.59)	4.70 (1.85)	933 (1220)	6.10 (2.40)	2.16 (0.85)	323 (121)	7.32 (2.88)	3.68 (1.45)	449 (348)
1.49 (0.59)	4.19 (1.65)	634 (681)	6.10 (2.40)	1.65 (0.65)	316 (109)	7.32 (2.88)	3.18 (1.25)	357 (183)
1.49 (0.59)	3.68 (1.45)	459 (366)	6.10 (2.40)	1.15 (0.45)	313 (104)	7.32 (2.88)	2.67 (1.05)	339 (151)
1.49 (0.59)	3.18 (1.25)	375 (216)	6.10 (2.40)	0.64 (0.25)	312 (101)	7.32 (2.88)	2.29 (0.90)	331 (136)
1.49 (0.59)	2.67 (1.05)	338 (149)	6.10 (2.40	0.53 (0.21)	312 (101)	8.59 (3.38)	5.72 (2.25)	1508 (2254)
1.49 (0.59)	2.16 (0.85)	322 (120)	6.10 (2.40)	0.00 (0.00)	311 (100)	8.59 (3.38)	5.21 (2.05)	1264 (1816)
1.49 (0.59)	1.65 (0.65)	315 (107)	6.71 (2.64)	5.72 (2.25)	1508 (2254)	8.59 (3.38)	4.70 (1.85)	955 (1259)
1.49 (0.59)	1.15 (0.45)	313 (103)	6.71 (2.64)	5.21 (2.05)	1255 (1799)	8.59 (3.38)	4.19 (1.65)	658 (725)
1.49 (0.59)	0.64 (0.25)	312 (101)	6.71 (2.64)	4.70 (1.85)	928 (1211)	8.59 (3.38)	3.68 (1.45)	455 (359)
1.49 (0.59)	0.53 (0.21)	311 (100)	6.71 (2.64)	4.19 (1.65)	629 (672)	8.59 (3.38)	3.18 (1.25)	386 (235)
1.49 (0.59)	0.00 (0.00)	311 (100)	6.71 (2.64)	3.68 (1.45)	454 (358)	8.59 (3.38)	2.67 (1.05)	346 (164)
4.37 (1.72)	5.72 (2.25)	1508 (2254)	6.71 (2.64)	3.18 (1.25)	372 (210)	8.59 (3.38)	2.29 (0.90)	333 (139)
4.37 (1.72)	5.21 (2.05)	1256 (1801)	6.71 (2.64)	2.67 (1.05)	339 (151)	9.70 (3.82)	5.72 (2.25)	1508 (2254)
4.37 (1.72)	4.70 (1.85)	933 (1220)	6.71 (2.64)	2.16 (0.85)	325 (126)	9.70 (3.82)	5.21 (2.05)	1270 (1826)
4.37 (1.72)	4.19 (1.65)	634 (681)	6.71 (2.64)	1.65 (0.65)	335 (114)	9.70 (3.82)	4.70 (1.85)	992 (1326)
4.37 (1.72)	3.68 (1.45)	459 (366)	6.71 (2.64)	1.15 (0.45)	315 (107)	9.70 (3.82)	4.19 (1.65)	713 (823)
4.37 (1.72)	3.18 (1.25)	376 (217)	6.71 (2.64)	0.64 (0.25)	313 (103)	9.70 (3.82)	3.68 (1.45)	521 (479)
4.37 (1.72)	2.67 (1.05)	338 (149)	6.71 (2.64)	0.53 (0.21)	313 (103)	9.70 (3.82)	3.18 (1.25)	425 (306)
4.37 (1.72)	2.16 (0.85)	322 (120)	6.71 (2.64)	0.00 (0.00)	311 (100)	9.70 (3.82)	2.67 (1.05)	375 (216)
4.37 (1.72)	1.65 (0.65)	315 (107)	6.99 (2.75)	3.05 (1.20)	358 (184)	9.70 (3.82)	2.29 (0.90)	350 (171)
4.37 (1.72)	1.15 (0.45)	313 (103)	6.99 (2.75)	2.67 (1.05)	343 (157)	10.39 (4.09)	5.72 (2.25)	1507 (2253)
4.37 (1.72)	0.64 (0.25)	312 (101)	6.99 (2.75)	2.16 (0.85)	331 (136)	10.39 (4.09)	5.21 (2.05)	1223 (1742)
4.37 (1.72)	0.53 (0.21)	312 (101)	6.99 (2.75)	1.65 (0.65)	323 (122)	10.39 (4.09)	4.70 (1.85)	1080 (1484)
4.37 (1.72)	0.00 (0.00)	311 (100)	6.99 (2.75)	0.64 (0.45)	318 (112)	10.39 (4.09)	4.19 (1.65)	830 (1035)
6.10 (2.40)	5.72 (2.25)	1508 (2254)	6.99 (2.75)	0.53 (0.21)	314 (106)	10.39 (4.09)	3.68 (1.45)	619 (654)
6.10 (2.40)	5.21 (2.05)	1255 (1800)	6.99 (2.75)	0.00 (0.00)	312 (102)	10.39 (4.09)	3.18 (1.25)	515 (468)
6.10 (2.40)	4.70 (1.85)	932 (1217)	7.32 (2.88)	5.72 (2.25)	1508 (2255)	10.39 (4.09)	2.67 (1.05)	434 (321)
6.10 (2.40)	4.19 (1.65)	632 (677)	7.32 (2.88)	5.21 (2.05)	1253 (1795)	10.39 (4.09)	2.29 (0.90)	353 (176)
6.10 (2.40)	3.68 (1.45)	457 (363)						

NOTES:
1. ENTRY TIME = 800 SEC
2. TEMPERATURES SHOWN ARE THOSE ENTERED IN COMPUTER PROGRAM TO CALCULATE THERMAL STRESSES SHOWN ON FIGURE 104

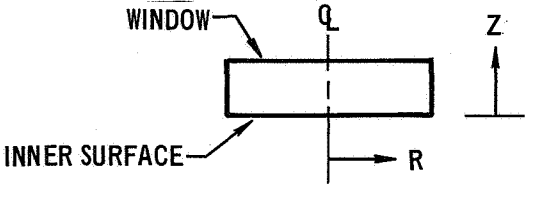

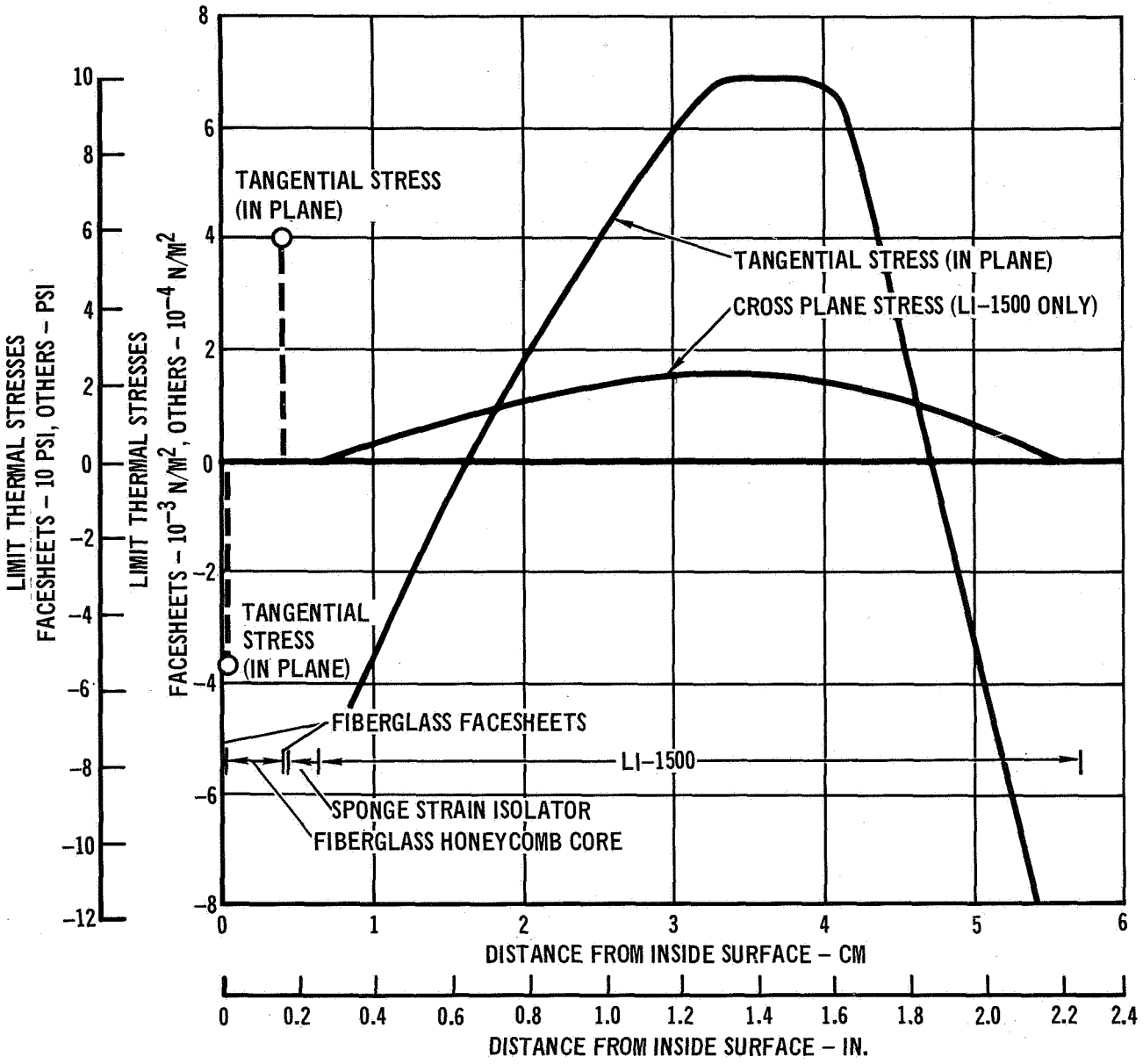

NOTES:

1. ENTRY TIME = 800 SEC
2. POSITIVE STRESSES ARE TENSION STRESSES.
3. SCALE IS DIFFERENT FOR FACESHEETS ONLY.
4. STRESSES IN FIBERGLASS HONEYCOMB CORE AND SPONGE STRAIN ISOLATOR WERE INSIGNIFICANT.
5. STRESSES RESULT FROM TEMPERATURES SHOWN IN TABLE XII.
6. STRESSES SHOWN OCCUR AT WINDOW CENTERLINE

LIMIT THERMAL STRESSES – SINGLE-LAYER RSI ANTENNA WINDOW DESIGN

Figure 104

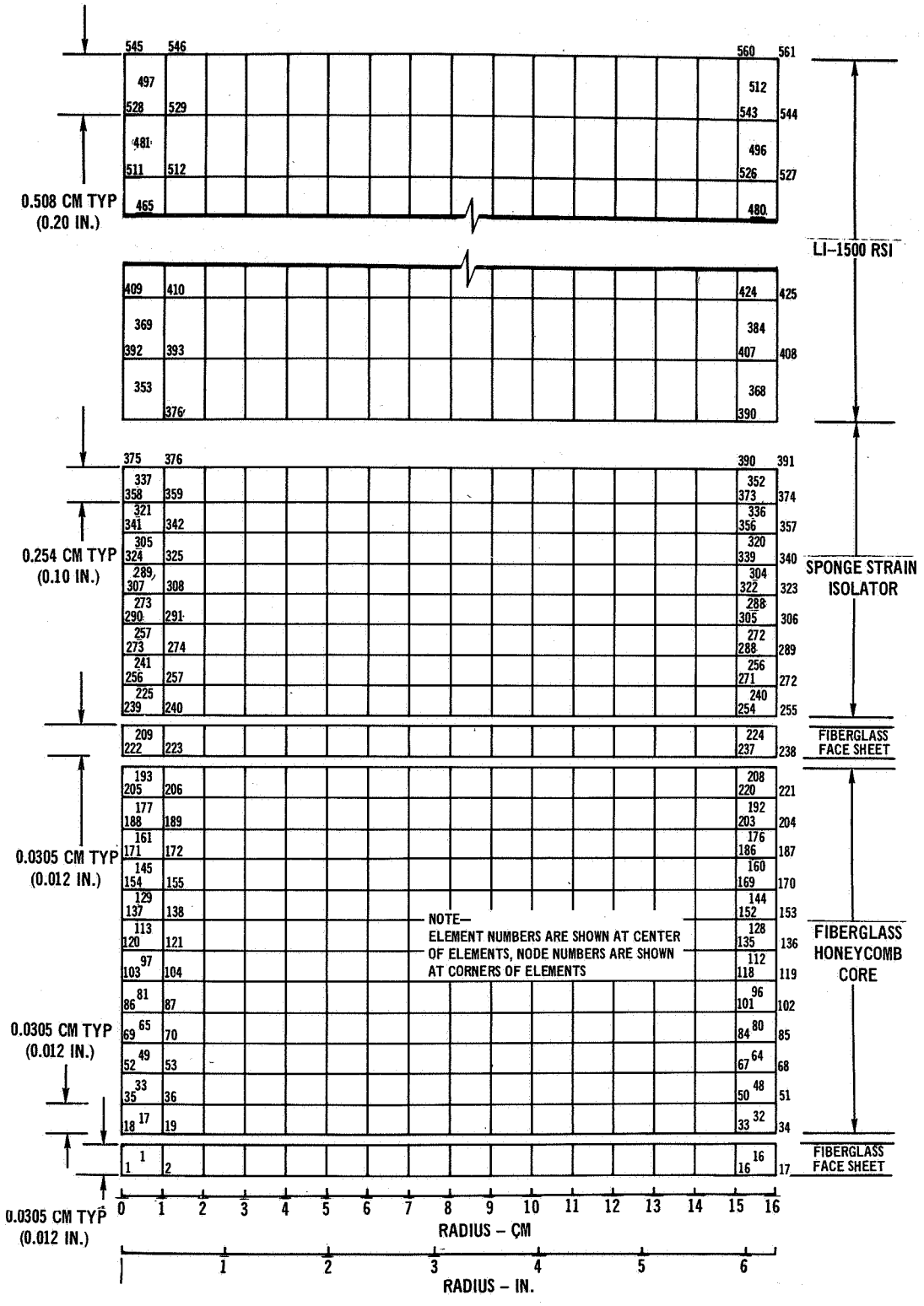

COMPUTER MODEL – SINGLE-LAYER RSI ANTENNA WINDOW DESIGN FOR C-BAND ANTENNA SYSTEM

Figure 105

stress is 9.62 x 10^5 N/m^2 (140 psi). The maximum cross plane tension stress is 0.137 x 10^5 N/m^2 (2 psi). The allowable cross plane tension stress is 1.24 x 10^5 N/m^2 (18 psi). It is concluded that the sponge strain isolator effectively isolates the RSI thermal strains.

C-band slot antenna system results. - The C-band linear slot antenna is similar in design to the C-band horn but smaller as shown by figure 88. Analysis for this antenna therefore was not required. The antenna fits between stringers spaced 10.16 cm (4.0 in.) apart. The only structural modifications required is the addition of a sill around the cutout in the skin. The sill has the capability of transferring skin loads around the cutout.

Fuselage stringers. - The fuselage stringers adjacent to the antennas were sized to withstand the design loads shown in the section on Strength Requirements. The minimum margin of safety was 0.29 for the ascent pressure loads applied to the C-band horn antenna system. The margin of safety is greater than that for the stringers in the L-band and C-band slot antenna system designs.

CONCLUSIONS AND RECOMMENDATIONS

Several conclusions can be reached from the results obtained during this study. They are:

a. Antenna systems consisting of off-the-shelf antennas thermally protected by RF windows can be designed for Space Shuttle Orbiter application.

b. The basic antenna temperature can be maintained at 422°K (300°F) without great complexity.

c. The use of RSI, particularly LI-1500, provides the simplest and most direct approach.

d. The dielectric constant and loss tangent of LI-1500 are low and change very little with temperature, therefore, the test results obtained at room temperature are expected to be equally valid at the high operating temperature.

e. A window edge enclosure may be used for pattern control for some antenna types.

f. The extension of a window edge enclosure into the RSI window material is limited by the heat sink capability at the point where the window edge enclosure attaches to the ground plane (or structure) around the antenna.

g. The multiple-layer window approach results in the need for a large heat sink because of the heat short from the antenna window retaining ring at the surface of the TPS to the ground plane (or structure) around the antenna.

h. The antenna window can be designed to provide easy access for installation or removal.

i. The reusability of the antenna system is limited primarily by external damage such as rain, or runway sand and gravel errosion.

j. Additional material development does not appear to be necessary to meet the high temperature requirements.

The work during this study also leads to several recommendations to further develop these designs:

a. One or more of these designs should be fabricated and subjected to complete environmental testing to evaluate the designs generated in this study (high temperature testing is currently being implemented for an S-band antenna design, which includes many of the design features developed during this contract, by McDonnell Douglas contract (NAS9-13004) to NASA Manned Space Center at Houston, Texas.

b. One or more of the off-the-shelf antennas applicable to these designs be subjected to the cold condition of space to determine what problems exist and the solutions to these problems.

c. One or more of these antenna systems should be fabricated and tested in a ground plane essentially the same size as the Space Shuttle Orbiter surface(s) to better assess the effects of surface wave excitation.

APPENDIX A

MATERIAL DESIGN PROPERTIES

The material properties given in tables XII through XIX were used in analyses performed on this program.

TABLE XII
REUSABLE SURFACE INSULATION (LI-1500)

DENSITY: 15.0 LB/FT^3

THERMAL CONDUCTIVITY:

CONDUCTIVITY (BTU/HR FT ^{0}R)

TEMPERATURE (^{0}F)	PRESSURE (LB/FT^2)				
	2.785	27.85	278.5	2116.	9000.
460	0.0142	0.0234	0.0267	0.0292	0.0292
760	0.0175	0.0258	0.0283	0.0308	0.0308
1160	0.0225	0.0292	0.0392	0.0433	0.0433
1860	0.0375	0.0500	0.0750	0.0834	0.0834
2460	0.0558	0.0850	0.1167	0.1300	0.0130
2960	0.0766	0.1125	0.1565	0.1740	0.1740
3460	0.1050	0.1470	0.2000	0.2220	0.2220

EMITTANCE:

TEMPERATURE (^{0}R)	EMITTANCE
532	0.9

SPECIFIC HEAT:

TEMPERATURE (^{0}R)	SPECIFIC HEAT (BTU/LB ^{0}R)
360	0.0716
540	0.1510
720	0.1980
900	0.2340
1000	0.2630
1260	0.2800
1440	0.2870
1800	0.2940
2160	0.3060
2520	0.3160
2960	0.3200

TABLE XIII
LOW DENSITY RESILIENT INSULATION (FI-600)

DENSITY: 6.00 LB/FT^3

THERMAL CONDUCTIVITY:

CONDUCTIVITY (BTU/HR FT ^{0}R)

TEMPERATURE (^{0}R)	PRESSURE (LB/FT^2)			
	0.278	27.8	2116.	9000.
200	0.00045	0.00245	0.0059	0.0059
400	0.0017	0.0068	0.0138	0.0138
600	0.00375	0.0112	0.0228	0.0228
980	0.00916	0.025	0.04	0.04
1460	0.0208	0.0408	0.069	0.0691
1960	0.035	0.0692	0.097	0.0967

EMITTANCE:

TEMPERATURE (^{0}R)	EMITTANCE
532	0.9

SPECIFIC HEAT:

TEMPERATURE (^{0}R)	SPECIFIC HEAT (BTU/LB ^{0}R)
360	0.0716
540	0.1510
720	0.1980
900	0.2340
1000	0.2630
1260	0.2800
1440	0.2870
1800	0.2940
2160	0.3060
2520	0.3160
2960	0.3200

TABLE XIV
SILICONE SPONGE (RL–524 TYPE S–105)

DENSITY:	20.0 LB/FT^3
THERMAL CONDUCTIVITY:	0.12 BTU/HR FT ^{0}R
SPECIFIC HEAT:	0.32 BTU/LB ^{0}R

TABLE XV
BORON NITRIDE (HD–0092)

DENSITY: 120 LB/FT^3

THERMAL CONDUCTIVITY:

TEMPERATURE (^{0}R)	CONDUCTIVITY (BTU/HR FT ^{0}R)
0	20.0
530	20.0
1460	18.6
1960	11.6
2460	10.2
2960	8.3

EMITTANCE:

TEMPERATURE (^{0}R)	EMITTANCE
0	0.93
1350	0.93
1710	0.90
1980	0.76
2520	0.70
2880	0.72
3150	0.69
3690	0.63
3870	0.63
4320	0.47
4500	0.43

SPECIFIC HEAT:

TEMPERATURE (^{0}R)	SPECIFIC HEAT (BTU/LB ^{0}R)
0	0.193
540	0.193
670	0.263
852	0.283
1032	0.324
1212	0.358
1392	0.389
1572	0.416
1752	0.441
1932	0.468
2960	0.468

NOTE: MULTIPLY K VALUES BY 0.5285 FOR THERMAL CONDUCTIVITY PERPENDICULAR TO MOLD LINE (PARALLEL TO PRESSING DIRECTION)

TABLE XVI
DYNAQUARTZ (JOHNS-MANVILLE)

DENSITY: 10.0 LB/FT^3

THERMAL CONDUCTIVITY:

CONDUCTIVITY (BTU/HR FT ^oR)

TEMPERATURE (^oR)	PRESSURE LB/FT^2						
	0.278	2.78	8.36	27.8	278.	836.	9000.
0	0.0183	0.0197	0.0233	0.0318	0.0465	0.0508	0.0508
1660	0.0216	0.0233	0.0275	0.0375	0.0559	0.0600	0.0600
1860	0.0242	0.0258	0.0300	0.0400	0.0617	0.0658	0.0667
2060	0.0292	0.0313	0.0350	0.0458	0.0683	0.0733	0.0750
2260	0.0350	0.0367	0.0417	0.0517	0.0759	0.0816	0.0830
2460	0.0417	0.0425	0.0467	0.0567	0.0833	0.0900	0.0917
2660	0.0492	0.0500	0.0541	0.0600	0.0933	0.1000	0.1025
2860	0.0592	0.0600	0.0642	0.0750	0.1041	0.1125	0.1150

EMITTANCE:

TEMPERATURE (^oR)	EMITTANCE
0	0.84
530	0.84
860	0.82
1260	0.70
1660	0.50
2060	0.44
2460	0.34
2860	0.27
5000	0.27

SPECIFIC HEAT:

TEMPERATURE (^oR)	SPECIFIC HEAT (BTU/LB ^oR)
0	0.170
530	0.170
860	0.230
1060	0.248
1260	0.260
1460	0.269
1660	0.277
1860	0.283
2060	0.288
2260	0.294
2460	0.298
2660	0.302
5000	0.302

TABLE XVII
LOAD BEARING INSULATION (MIN-K TYPE 1301)

DENSITY: 20.0 LB/FT^3

THERMAL CONDUCTIVITY:

TEMPERATURE (^{0}R)	CONDUCTIVITY (BTU/HR FT ^{0}R)
560	0.0150
1460	0.0225

SPECIFIC HEAT:

TEMPERATURE (^{0}R)	SPECIFIC HEAT (BTU/ LB ^{0}R)
500	0.180
660	0.202
860	0.220
1060	0.233
1260	0.246
1460	0.256
1660	0.262
1860	0.272
2060	0.274

TABLE XVIII
NICKEL BASE SUPERALLOY (INCONEL 702)

DENSITY: 525.6 LB/FT^3

THERMAL CONDUCTIVITY:

TEMPERATURE (^{0}R)	CONDUCTIVITY (BTU/HR FT ^{0}R)
460	6.2
660	7.1
860	8.2
1060	9.3
1260	10.6
1460	12.0
2460	19.0

SPECIFIC HEAT:

TEMPERATURE (^{0}R)	SPECIFIC HEAT (BTU/LB ^{0}R)
210	0.073
260	0.079
360	0.09
530	0.106
660	0.111
860	0.116
1060	0.121
1260	0.126
1460	0.132
1660	0.140
1860	0.145
2060	0.149
2460	0.155

TABLE XIX
MECHANICAL PROPERTIES

MATERIAL	TEMPERATURE (°F)	MODULUS OF ELASTICITY IN TENSION: IN PLANE (PSI)	MODULUS OF ELASTICITY IN TENSION: CROSS PLANE (PSI)	ν POISSON'S RATIO	SHEAR MODULUS (PSI)	COEFFICIENT OF THERMAL EXPANSION: IN PLANE IN/IN/°F	COEFFICIENT OF THERMAL EXPANSION: CROSS PLANE IN/IN/°F	ULTIMATE TENSILE STRESS: IN PLANE (PSI)	ULTIMATE TENSILE STRESS: CROSS PLANE (PSI)
L1-1500 RSI [i]	70	10^5	10^4	0.1 [f]	6600	3×10^{-7}	h	115	18
	2500	10^5	10^4	0.1	6600	3×10^{-7}		166	18
PHENOLIC FIBER-GLASS CLASS D SHEET [j] MIL-H-17 PAGE 4-100	70	3.2×10^6		0.2	0.835×10^6 [a]	4.5×10^{-6}	16×10^{-6}	40,000	
	150	3.14×10^6		0.2	0.82×10^6	4.5×10^{-6}	16×10^{-6}	37,750	
	200	3.04×10^6		0.2	0.792×10^6	4.5×10^{-6}	16×10^{-6}	36,300	
	300	2.7×10^6		0.2	0.703×10^6	4.5×10^{-6}	16×10^{-6}	33,700	
	400	2.3×10^6		0.2	0.60×10^6	4.5×10^{-6}	16×10^{-6}	30,000	
PHENOLIC [c] [k] FIBERGLASS HONEY-COMB AVERAGE OF L&W PROPERTIES	70	10,000 [b]		0.01	10,700 [a]				
	150	10,000		0.01	10,450				
	200	10,000		0.01	10,100				
	300	10,000		0.01	9,000				
	400	10,000		0.01	7,700				
S-105 SPONGE STRAIN ISOLATOR	70	60		0.01	30	2.35×10^{-4}		100	
	400	60		0.01	30	2.35×10^{-4}		100	
BORON NITRIDE GRADE HD-0092 [l]	70	7.0×10^6	12.3×10^6	0.1 [e]	5.6×10^6	0.0		6,000 [d]	
	752	7.0×10^6	12.3×10^6	0.1	5.6×10^6	1.33×10^{-7}		6,200	
	1472	7.0×10^6	12.3×10^6	0.1	5.6×10^6	3.4×10^{-7}		7,000	
	2192	7.0×10^6	12.3×10^6	0.1	5.6×10^6	5.5×10^{-7}		8,000	
	2912	7.0×10^6	12.3×10^6	0.1	5.6×10^6	8.57×10^{-7}		10,000	
COLUMBIUM	70	21×10^6 [m]		0.3	8.08×10^6	3.5×10^{-6}		64,000 [g]	
	500	20×10^6		0.3	7.7×10^6	4.0×10^{-6}		43,000	
	1000	19.5×10^6		0.3	7.5×10^6	4.4×10^{-6}		37,000	
	1500	19.0×10^6		0.3	7.3×10^6	4.6×10^{-6}		34,000	
	2000	18.0×10^6		0.3	6.92×10^6	4.8×10^{-6}		24,000	
	2500	15.5×10^6		0.3	5.97×10^6	5.11×10^{-6}		15,000	

NOTES:

a. VARIATION WITH TEMPERATURE DETERMINED BY MULTIPLYING ROOM TEMPERATURE VALUE BY THE RATIO OF THE E OF FIBER-GLASS SHEET AT TEMPERATURE TO E AT ROOM TEMPERATURE.

b. ARBITRARY VALUE

c. WHEN FIBERGLASS HONEYCOMB PROPERTIES ARE NOT SHOWN FIBERGLASS SHEET PROPERTIES WERE ENTERED IN THE COMPUTER PROGRAMS AS HONEYCOMB PROPERTIES.

d. FLEXURAL STRENGTH SHOWN

e. ESTIMATED BY CONSIDERING DATA FOR GRAPHITE

f. ESTIMATED BY CONSIDERING DATA FOR MDC RSI

g. YIELD STRENGTH SHOWN

h. WHERE CROSS-PLANE DATA IS NOT SHOWN IN-PLANE DATA WAS ENTERED IN THE COMPUTER PROGRAMS AS CROSS-PLANE DATA.

i. "EVALUATION OF NONMETALLIC THERMAL PROTECTION MATERIALS FOR THE MANNED SPACE SHUTTLE", VOLUME V, BATTELLE MEMORIAL INSTITUTE, DATED JUNE 1, 1972

j. MIL-HDBK-17A "PLASTICS FOR AEROSPACE VEHICLES, PART I, REINFORCED PRACTICE" DATED JANUARY 1971.

k. BROCHURE D "HONEYCOMB SANDWICH DESIGN DATA AND TEST METHODS" HEXCEL PRODUCTS INC.

l. BULLETIN NO. 442-209HD "NATIONAL BORN NITRIDE GRADE HD-0092 HOT PRESSED SHAPES" UNION CARBIDE CORPORATION

m. SCHMIDT, F.F., ET AL., "ENGINEERING PROPERTIES OF COLUMBIUM AND COLUMBIUM ALLOYS," REP. NO. DMIC 188, BATTELLE MEMORIAL INST, SEP. 1963

APPENDIX B

COMPUTED RADIATION PATTERNS

This appendix presents the results of radiation pattern calculations performed at the Langley Research Center. These patterns were computed for a C-band linear slot antenna in a 76.2 x 76.2 cm (30 x 30 in.) ground plane, figure 106, and with the ground plane covered with 5.08 cm (2 in.) thick dielectric material, figure 107. These results correspond to the results shown in figures 69 and 70 of the text for identical configurations.

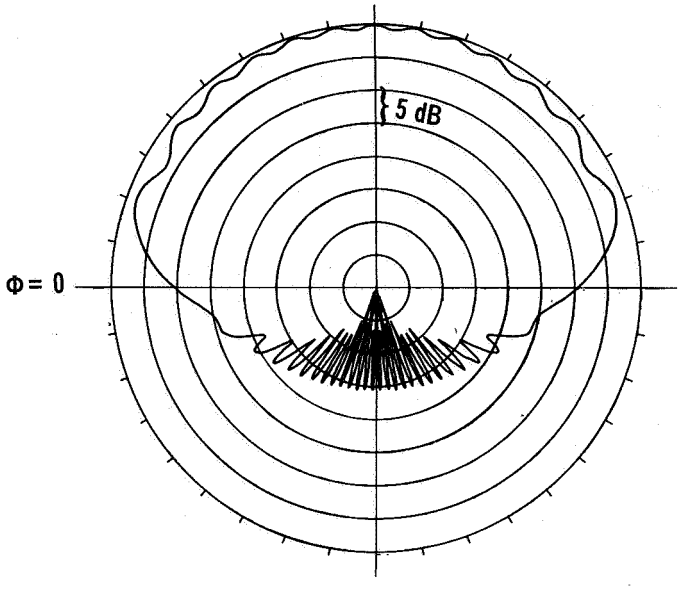

RECTANGULAR C-BAND WAVEGUIDE ON A FINITE GROUND PLANE

Figure 106

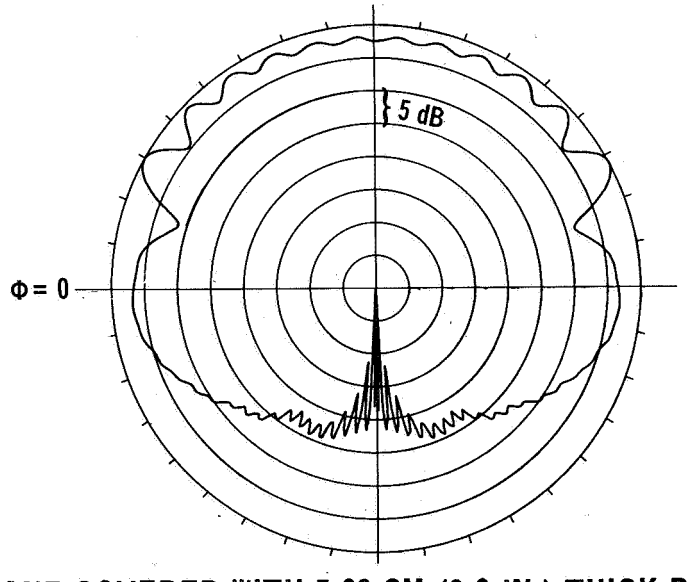

GROUND PLANE COVERED WITH 5.08 CM (2.0 IN.) THICK DIELECTRIC LAYER
(Dielectric Constant = 1.2, Loss Tangent = 0.002)

Figure 107

APPENDIX C

EQUATIONS FOR CALCULATING POWER TRANSMISSION THROUGH MULTIPLE LAYERS OF LOSSY DIELECTRIC

Plane wave transmission loss through N layers of a lossy dielectric may be calculated using several approaches (refs. 10 and 11). The equations used for the results given in the section on Antenna Window Transmission are given below.

(1) MODEL

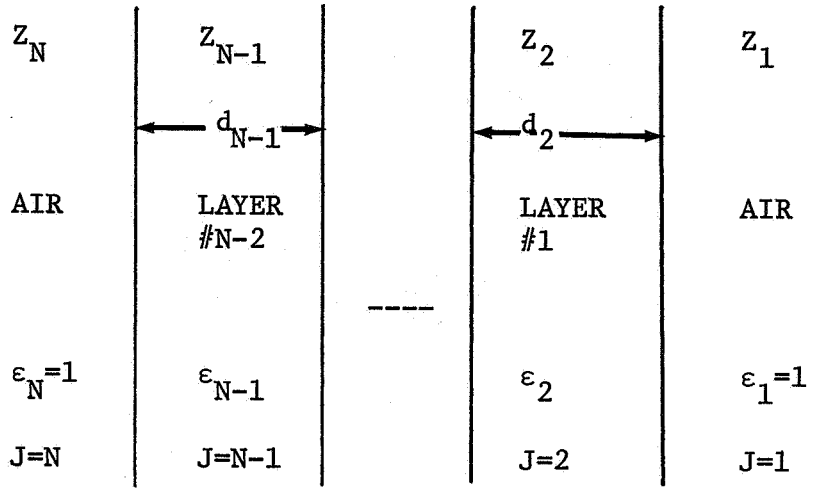

(2) SNELL's LAW

$$\theta_J = \arcsin \left[\sqrt{\varepsilon_1/\varepsilon'_J} \, (\sin \theta_1) \right]$$

where

θ_J = angle of propagation in dielectric sheet number J

θ_1 = angle of incidence

ε_1 = relative dielectric constant of air

ε'_J = relative dielectric constant of sheet number J

(3) WAVE IMPEDANCE

$$Z_J = \left(\frac{\mu_o}{\varepsilon_o}\right)^{1/2} \frac{1}{\sqrt{\varepsilon_J \cos \theta_J}} \quad \text{(for perpendicular polarization)}$$

$$Z_J = \left(\frac{\mu_o}{\varepsilon_o}\right)^{1/2} \frac{\cos \theta_J}{\sqrt{\varepsilon_J}} \quad \text{(for parallel polarization)}$$

where

Z_J = characteristic impedance of dielectric sheet number J.

μ_o = permeability of free space

ε_o = permittivity of free space

ε_J = complex dielectric constant ($\varepsilon_J = \varepsilon'_J (1 - j\tan \delta)$)

(4) PROPAGATION CONSTANT IN MEDIA

$$\gamma = \alpha + j\beta = j\omega\sqrt{\mu_o \varepsilon_o \varepsilon_J}$$

where

α = attenuation constant

β = phase constant

ω = angular frequency

(5) IMPEDANCE TRANSFORMATION

$$ZI_{J+1} = Z_J \frac{ZI_J \cosh \gamma d_J + Z_J \sinh \gamma d_J}{Z_J \cosh \gamma d_J + ZI_J \sinh \gamma d_J}$$

where

ZI_J = the equivalent impedance at the right boundary of dielectric sheet number J, which represents the load impedance for that sheet,

d_J = thickness of dielectric sheet number J.

Note that

$$ZI_2 = Z_1 = \frac{1}{\cos \theta_1}$$

(6) POWER TRANSMISSION COEFFICIENT

$$T = \left|\frac{E_{TRANSMITTED}}{E_{INCIDENT}}\right|^2 = \left|\frac{E_1}{E_{J=N}}\right|^2$$

where

N = TOTAL NUMBER of dielectric sheets (including air sheets)

E_1, E_J = voltage at left surface of dielectric sheet number J

At the left air-dielectric interface

$$\frac{E_N}{E_{N-1}} = \frac{1}{1 + \rho_N}$$

where

$$\rho_N = \frac{ZI_N - Z_N}{ZI_N + Z_N} \text{ (Note: } Z_N = Z_1 \text{ since sheet N is also air.)}$$

However,

$$\frac{E_{N-1}}{E_{N-2}} = \frac{1}{ZI_{N-1}} [ZI_{N-1} \cosh \gamma_{N-1} d_{N-1} + Z_{N-1} \sinh \gamma_{N-1} d_{N-1}],$$

and

$$\frac{E_2}{E_1} = \frac{1}{ZI_2} (ZI_2 \cosh \gamma_2 d_2 + Z_2 \sinh \gamma_2 d_2),$$

therefore,

$$\frac{E_N}{E_1} = \frac{E_N}{E_{N-1}} \quad \frac{E_{N-1}}{E_{N-2}} \quad - - - - \quad \frac{E_2}{E_1}$$

and

$$\frac{E_{INCIDENT}}{E_{TRANSMITTED}} = \frac{1}{1+\rho_N} \quad \frac{E_{N-1}}{E_{N-2}} \quad - - - - \quad \frac{E_2}{E_1}$$

REFERENCES

1. E. A. Kuhlman, "A Solution for the Space Shuttle High Temperature Antenna Problem," Proceedings of the Space Shuttle Integrated Electronics Conference, Vol. 2, May 11-13, 1971.

2. Development and Design Application of Rigidized Reusable Surface Insulation Thermal Protection System. Contract NAS 9-12854 Monthly Progress Report RDMA067 98207E457-12, October 1972.

3. Personal Communication from W. F. Croswell, NASA, Langley Research Center.

4. Personal Communication from C. R. Cockrell, NASA, Langley Research Center.

5. H. Jasik, Antenna Engineering Handbook, Chap. 32 (McGraw-Hill Book Company, New York, N. Y., 1961).

6. C. M. Knop, J. J. Meier, and O. K. Kim, "The Dielectric Clad Axial Slot Cylinder Antenna", Contract NAS1-6242, Andrew Corporation, July 1967, pp 47-49.

7. G. A. Deschamps, "Determination of Reflection Coefficients and Insertion Loss of a Wave-Guide Junction," Journal of Applied Physics, Vol. 24, No. 8 (August 1953).

8. Anon: Reference Data for Radio Engineers, Fifth ed., Chap. 24 (Howard W. Sams and Company, New York, N.Y., 1969).

9. R. M. Jones and J. G. Crose, "SAAS II Finite Element Stress Analysis of Axisymmetric Solids with Orthotropic, Temperature-Dependent Material Properties," Aerospace Report No. TR-0200 (54980)-1 (Air Force Report No. SAMSO-TR-68-455), San Bernadino Operations, The Aerospace Corporation, September, 1968.

10. R. E. Collins, Field Theory of Guided Waves, pp. 87-94 (McGraw-Hill Book Company, New York, N.Y., 1960).

11. G. P. Bein, "Plane Wave Transmission and Reflection Coefficients for Lossy Inhomogeneous Plasma," IEEE Transactions on Antennas and Propagation, July, 1966.

*U.S. GOVERNMENT PRINTING OFFICE: 1973-739-153/53

NATIONAL AERONAUTICS AND SPACE ADMINISTRATION
WASHINGTON, D.C. 20546

OFFICIAL BUSINESS
PENALTY FOR PRIVATE USE $300

SPECIAL FOURTH-CLASS RATE BOOK

POSTAGE AND FEES PAID
NATIONAL AERONAUTICS AND SPACE ADMINISTRATION
451

U.S.MAIL

POSTMASTER: If Undeliverable (Section 158 Postal Manual) Do Not Return

"The aeronautical and space activities of the United States shall be conducted so as to contribute . . . to the expansion of human knowledge of phenomena in the atmosphere and space. The Administration shall provide for the widest practicable and appropriate dissemination of information concerning its activities and the results thereof."

—NATIONAL AERONAUTICS AND SPACE ACT OF 1958

NASA SCIENTIFIC AND TECHNICAL PUBLICATIONS

TECHNICAL REPORTS: Scientific and technical information considered important, complete, and a lasting contribution to existing knowledge.

TECHNICAL NOTES: Information less broad in scope but nevertheless of importance as a contribution to existing knowledge.

TECHNICAL MEMORANDUMS: Information receiving limited distribution because of preliminary data, security classification, or other reasons. Also includes conference proceedings with either limited or unlimited distribution.

CONTRACTOR REPORTS: Scientific and technical information generated under a NASA contract or grant and considered an important contribution to existing knowledge.

TECHNICAL TRANSLATIONS: Information published in a foreign language considered to merit NASA distribution in English.

SPECIAL PUBLICATIONS: Information derived from or of value to NASA activities. Publications include final reports of major projects, monographs, data compilations, handbooks, sourcebooks, and special bibliographies.

TECHNOLOGY UTILIZATION PUBLICATIONS: Information on technology used by NASA that may be of particular interest in commercial and other non-aerospace applications. Publications include Tech Briefs, Technology Utilization Reports and Technology Surveys.

Details on the availability of these publications may be obtained from:

SCIENTIFIC AND TECHNICAL INFORMATION OFFICE

NATIONAL AERONAUTICS AND SPACE ADMINISTRATION

Washington, D.C. 20546